SANDIA REPORT
SAND2010-8200
Unlimited Release
January, 2011

Disposal Systems Evaluations and Tool Development – Engineered Barrier System (EBS) Evaluation

Prepared for
U.S. Department of Energy
Used Fuel Disposition Campaign

Carlos F. Jové Colón (SNL)

Florie A. Caporuscio, Schön S. Levy, Hongwu Xu (LANL)

James A. Blink, William G. Halsey, Thomas Buscheck,

Mark Sutton, M. A. Serrano de Caro, Thomas J. Wolery (LLNL)

Hui-Hai Liu, Jens Birkholzer, Carl I. Steefel, Jonny Rutqvist, Chin-Fu Tsang,

Eric Sonnenthal (LBNL)

Prepared by
Sandia National Laboratories
Albuquerque, New Mexico 87185-0836

Sandia National Laboratories is a multi-program laboratory managed and operated by Sandia Corporation, a wholly owned subsidiary of Lockheed Martin Corporation, for the U.S. Department of Energy's National Nuclear Security Administration under contract DE-AC04-94AL85000.

Issued by Sandia National Laboratories, operated for the United States Department of Energy by Sandia Corporation.

Available to DOE and DOE contractors from
U.S. Department of Energy
Office of Scientific and Technical Information
P.O. Box 62
Oak Ridge, TN 37831

Telephone: (865) 576-8401
Facsimile: (865) 576-5728
E-Mail: reports@adonis.osti.gov
Online ordering: http://www.osti.gov/bridge

Available to the public from
U.S. Department of Commerce
National Technical Information Service
5301 Shawnee Rd,
Alexandria, VA 22312
Telephone: (800) 553-6847
Facsimile: (703) 605-6900
E-Mail: orders@ntis.fedworld.gov
Online order: http://www.ntis.gov/help/ordermethods.aspx

SANDIA REPORT
SAND2010-8200
Unlimited Release
January, 2011

Disposal Systems Evaluations and Tool Development – Engineered Barrier System (EBS) Evaluation

Carlos F. Jové Colón (SNL)

Radiological Consequence Management and Response Technologies
Sandia National Laboratories
P. O. Box 5800 MS 0779
Albquerque, NM 87185

Additional Authors:

Florie A. Caporuscio, Schön S. Levy, Hongwu Xu (LANL)

James A. Blink, William G. Halsey, Thomas Buscheck,
Mark Sutton, M. A. Serrano de Caro, Thomas J. Wolery (LLNL)

Hui-Hai Liu, Jens Birkholzer, Carl I. Steefel, Jonny Rutqvist, Chin-Fu Tsang,
Eric Sonnenthal (LBNL)

This page is intentionally left blank

Executive Summary

Key components of the nuclear fuel cycle are short-term storage and long-term disposal of nuclear waste. The latter encompasses the immobilization of used nuclear fuel (UNF) and radioactive waste streams generated by various phases of the nuclear fuel cycle, and the safe and permanent disposition of these waste forms in geological repository environments. The engineered barrier system (EBS) plays a very important role in the long-term isolation of nuclear waste in geological repository environments. EBS concepts and their interactions with the natural barrier are inherently important to the long-term performance assessment of the safety case where nuclear waste disposition needs to be evaluated for time periods of up to one million years. Making the safety case needed in the decision-making process for the recommendation and the eventual embracement of a disposal system concept requires a multi-faceted integration of knowledge and evidence-gathering to demonstrate the required confidence level in a deep geological disposal site and to evaluate long-term repository performance.

The focus of this report is the following:

- Evaluation of EBS in long-term disposal systems in deep geologic environments with emphasis on the multi-barrier concept;
- Evaluation of key parameters in the characterization of EBS performance;
- Identification of key knowledge gaps and uncertainties;
- Evaluation of tools and modeling approaches for EBS processes and performance.

The above topics will be evaluated through the analysis of the following:

- Overview of EBS concepts for various NW disposal systems;
- Natural and man-made analogs, room chemistry, hydrochemistry of deep subsurface environments, and EBS material stability in near-field environments;
- Reactive Transport and Coupled Thermal-Hydrological-Mechanical-Chemical (THMC) processes in EBS;
- Thermal analysis toolkit, metallic barrier degradation mode survey, and development of a Disposal Systems Evaluation Framework (DSEF).

This report will focus on the multi-barrier concept of EBS and variants of this type which in essence is the most adopted concept by various repository programs. Empasis is given mainly to the evaluation of EBS materials and processes through the analysis of published studies in the scientific literature of past and existing repository research programs. Tool evaluations are also emphasized, particularly on THCM processes and chemical equilibria. Although being an increasingly important aspect of NW disposition, short-term or interim storage of NW will be briefly discussed but not to the extent of the EBS issues relevant to disposal systems in deep geologic environments. Interim storage will be discussed in the report *Evaluation of Storage Concepts FY10 Final Report* (Weiner et al. 2010).

This page is intentionally left blank

CONTENTS

FIGURES

TABLES

Acronyms

AFCI	Advanced Fuel Cycle Initiative
ANL	Argonne National Laboratory
ASCEM	Advanced Simulation Capability for Environmental Management
BBM	Barcelona Basic Model
BMT	Bench Mark Test
BRIE	Bentonite Rock Interaction Experiment
CBP	Cement Barrier Partnership
CEA	Commissariat à l'Énergie Atomique
CSNF	Commercial Spent Nuclear Fuel (CSNF)
COX	Callovo-Oxfordian formation
CRT	Canister Retrieval Test
DECOVALEX	DEvelopment of COupled Models and their VALidation against EXperiments
DIC	Dissolved Inorganic Carbon
DOE	Department of Energy
DSEF	Disposal Systems Evaluation Framework
EBR-II	Experimental Breeder Reactor II
EBS	Engineered Barrier System
EC	European Community
Echem	Electrochemical processing
EDZ	Excavated Disturbed Zone
EM	Environmental Management
EPA	Environmental Protection Agency
FC-R&D	Fuel Cycle Research and Development
FEBEX	Full-scale Engineered Barriers Experiment
FEP	Features, Events, and Processes
GNEP	Global Nuclear Energy Partnership
GTCC	Greater Than Class C
HTGR	High Temperature Gas Reactor
IAEA	International Atomic Energy Agency
INL	Idaho National Laboratory
IGSC	Integration Group for the Safety Case

IWP	Integrated Waste Package
LANL	Los Alamos National Laboratory
LILW	Low to Intermediate Level Radioactive Waste
LLNL	Lawrence Livermore National Laboratory
LLW	Low Level Waste
LTHLW	Lower Than High Level Waste
LWR	Light Water Reactor
MCM	Multi-Component Module
MIT	Massachusetts Institute of Technology
MOX	Mixed OXide fuel
NEA	Nuclear Energy Agency
NIF	National Ignition Facility
NW	Nuclear Waste
OECD	Organization for Economic Co-operation and Development
PA	Performance Assessment
SEM	Scanning Electron Microscopy
SNF	Spent Nuclear Fuel
SNL	Sandia National Laboratories
TBT	Thermal Bentonite Test
THM	Thermal-Hydrological-Mechanical
TM	Thermal-Mechanical
THMC	Thermal-Hydrological-Mechanical-Chemical
TSPA	Total System Performance Assessment
TSX	Tunnel Sealing Experiment
UFD	Used Fuel Disposition
UNF	Used Nuclear Fuel
UZ	Unsaturated Zone
WAC	Waste Acceptance Criteria
WIPP	Waste Isolation Pilot Plant
WP	Waste Package
XRD	X-ray Diffraction
YMP	Yucca Mountain Project

USED FUEL DISPOSITION CAMPAIGN/ DISPOSAL SYSTEMS EVALUATIONS AND TOOL DEVELOPMENT

1. Overview of EBS Concept Evaluation

1.1 Introduction

The long-standing need for short- and long-term disposition of nuclear waste (NW) originates from the continued accumulation of used nuclear fuel (UNF) and from the legacy of nuclear weapons production and decommissioning activities. Key components of the nuclear fuel cycle are storage and disposal of nuclear waste. The latter encompasses the immobilization of various radioactive waste streams generated by various phases of the nuclear fuel cycle, and the safe and permanent disposition of these waste forms in geological repository environments. The disposition of nuclear waste where the most hazardous are those with long-lived radionuclides such as UNF and vitrified waste forms needs to be safely contained, emplaced, and isolated far from the biosphere (Bennett et al., 2006). The engineered barrier system (EBS from hereon) plays a very important role in the long-term isolation of nuclear waste in geological repository environments. EBS concepts and their potential interactions with the natural barrier are inherently important to the long-term performance assessment of the safety case where nuclear waste disposition needs to be evaluated for time periods in the order of thousands of years. Making the safety case needed in the decision-making process for the recommendation and eventual embracement of a repository concept requires the multi-faceted integration of knowledge and evidence gathering to demonstrate the confidence level of a geological disposal site (Bennett et al., 2006). Another important component of the safety case is the post-closure safety assessment which involves the technical evaluations and the decisional process in knowledge gathering to improve and expand our understanding of long-term repository performance.

First, let us begin with the definition of the EBS based on the consensus achieved by many nations with active repository research programs and given by the Nuclear Energy Agency (NEA) Integration Group for the Safety Case (IGSC) EBS project:

"The "engineered barrier system" represents the man-made, engineered materials placed within a repository, including the waste form, waste canisters, buffer materials, backfill and seals. The "near-field" includes the EBS and those parts of the host rock in contact with or near the EBS, whose properties have been affected by the presence of the repository. The "far-field" represents the geosphere (and biosphere) beyond the near-field" (NEA OECD State-Of-The-Art Report, 2003).

There is a wide agreement with this definition for many repository programs but there are some exceptions, for example, in the Waste Isolation Pilot Plant (WIPP) repository programs in the USA where the waste package is not credited to be part of the EBS. Other repository programs such as that from Finland, Belgium, and Canada recommend extending the definition of EBS to the region that comprises some domains of the host-rock or the far-field in close proximity or in contact with the EBS. The reason to extend the EBS domain is due to the influence exerted on the properties of the far-field in the vicinity of the EBS, for example, the excavated disturbed zone (or EDZ) where thermal effects in the EBS can indeed affect transport phenomena in the host rock.

The focus of this report is the following:

- Evaluation of EBS in long-term disposal systems in deep geologic environments with emphasis on the multi-barrier concept;

- Evaluation of key parameters in the characterization of EBS performance;
- Identification of key knowledge gaps and uncertainties;
- Evaluation of tools and modeling approaches for EBS processes and performance.

The above topics will be evaluated through the analysis of the following:

- Overview of EBS concepts for various NW disposal systems (this section);
- Natural analogs and room chemistry (LANL, SNL);
- Reactive Transport and Coupled Thermal-Hydrological-Mechanical-Chemical (THMC) processes in EBS (LBNL);
- Development of a Disposal Systems Evaluation Framework (DSEF) and Thermal analysis (LLNL)

Most of the EBS concepts to be reviewed in this report are focused in the European, USA, and (to some extent) the Japanese repository programs where their efforts have been summarized in reports by the Nuclear Energy Agency (NEA) Organization for Economic Co-operation and Development (OECD) Integration Group for the Safety Case (IGSC) EBS project. Other important sources are reports produced by these NW repository research programs and the scientific literature.

The report will focus on the multi-barrier concept of EBS and variants of this type which in essence is the most adopted concept by various repository programs. This EBS concept is essentially the close integration of the waste package container and overpack with buffer/backfill materials. Figure 1.1-1 shows an example of the EBS for the Belgian repository concept showing the multi-barrier concept hosted in the Boom clay formation.

1.2 Interim Storage and Long-Term Waste Isolation

1.2.1 Interim Storage: Wet and Dry Short-Term Storage

Given the relatively large amounts of UNF accumulated from nuclear power plants in the USA and the current time needed to develop a long-term NW repository, interim storage is seriously considered as a central strategy for an economically viable and also flexible short-term solution for nuclear waste storage. There are two types of interim or short-term storage scenarios: wet and dry. Wet storage of nuclear waste is practiced in the form of storage water pools either on-site or off-site from reactor sites. According to Bunn et al. (2001), all operating nuclear power plants in the USA utilize storage water pools for storing the UNF and also for the process of cooling the fuel. In fact, about 90% of the UNF in interim storage produced by the world's nuclear reactors is stored in water pools and in some cases the storing time exceeds forty years without any significant safety incident (Bunn et al., 2001). These pools are made of reinforced concrete lined with stainless steel and coated with epoxy-based paints. The operation of these storage pools involves constant monitoring of water chemistry (borated water), any potential leakage, and the level of radioactivity being generated. According to Bunn et al. (2001), the most important safety issues are:

- Loss of pool water. It is important to make sure there is sufficient water to keep the UNF fully immersed in the pool and in contact with water. Also pool water leakage could translate into an important safety risk.

• Relative positioning of UNF elements. It is also important to make sure that spacing of UNF elements and neutron absorption is sufficient as to not induce a nuclear chain reaction in the pool. This is also important for the thermal load management of the UNF during cool down.

Examples of wet storage of UNF are the Olkiluoto interim storage site in Finland and the CLAB underground interim storage facility in Oskarshamn, Sweden. Figure 1.2.1-1 below show the storage water pools at the Clab underground facility in Sweden.

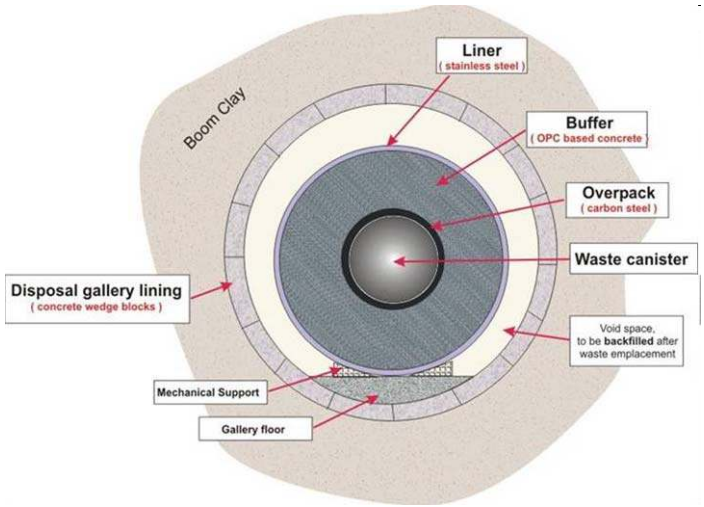

Figure 1.1-1 Multi-barrier concept for the Belgian radioactive waste repository concept (source: http://www.sck.be/en/Our-Research/Research-domains).

Figure 1.2.1-1 Storage water pools at the Clab underground facility, Sweden (source: www.skb.se/upload/publications/pdf/ClabEng.8.3.pdf).

After cooling down for several years (5-10 years depending on the UNF characteristics) in used fuel pools, the UNF can then be placed in dry storage facilities (Fig. 1.1-2). The UNF from the water pools is placed in metal casks or canisters that are drained, filled with an inert gas, and then sealed. The casks have a shell layered design and are made of steel, cast iron, and/or reinforced concrete to furnish shielding against radiation and also containment against any potential leakage. Prior to loading of the UNF into the cask, there are several factors to be considered in proceeding with dry

storage (Macfarlane, 2001): fuel burnup history, cooling history, initial ^{235}U enrichment, and fuel operating history. There are three types of dry storage concepts: dry cask, dry silo, and dry vault storage. Dry cask involves the placement of the storage cask onto a flat concrete pad whether inside or outside the building facility. Dry storage in a silo facility involves the placement of fuel into concrete cylinders lined with metal for shielding against radiation and radionuclide containment. Emplacement of the UNF in dry silo facilities can be either horizontal or vertical. Dry vault storage encompasses the placement of UNF into large cavities made of reinforced concrete having metal storage tubes capable of holding several fuel assemblies; all enclosed within a reinforced concrete building. The main safety issues with interim UNF dry storage are (after Bunn et al. 2001):

- Shielding against high levels of radiation. This is a concern for the safety of personnel involved in the monitoring and operation of the storage site.
- Release of radioactive material into the environment. Ensuring safe and robust containment of UNF is very important as to prevent potential releases under any potential failure scenario.

Integrity of the fuel cladding as a result of long-term thermal degradation has been a concern for dry storage where it could lead to a potential contamination risk. However, the general consensus with dry storage is that it is considered to be extremely safe. Dry storage is also considered a highly adaptable approach in terms of the type of fuels it can handle, flexible storage siting, and the amount stored fuel. Furthermore, it is also a cost-effective approach where most of the long-term costs (i.e., after fuel loading and emplacement) are mainly related to safety and security monitoring operations. In fact, overall costs of dry storage are less that those for wet interim storage.

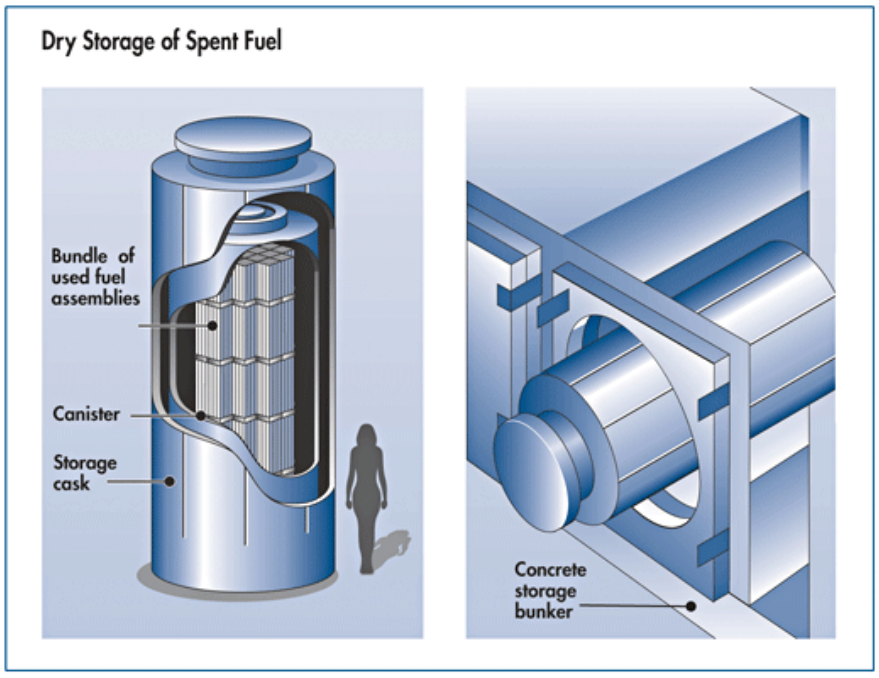

Figure 1.2.1-2 Dry storage of UNF: vertical storage cask (left) and horizontal vault type facility (right) (source: http://www.nrc.gov/waste/spent-fuel-storage/dry-cask-storage.html).

Although the definition of the EBS intrinsically applies to long-term of permanent isolation of nuclear waste, there is indeed an engineered barrier for interim storage concepts. Since storage of UNF in this type of facilities is only temporary, the regulations for waste management and

requirements for barrier containment are also different from those in deep geological repositories. Initial licensing of dry cask storage facilities is for 20 years but there have been studies aimed at extending this to much longer time periods (Eizinger et al. 1998; Bunn et al, 2001). Interim storage offers an economical, safe, and flexible option for UNF storage to the point that it should be considered as an important part of the nuclear fuel cycle. However, much of the resistance to this concept seems to be political and legal rather than technological where opposition to hosting such facilities at proposed locations proves to be a significant obstacle (Bunn et al. 2001).

As emphasized earlier, the focus of this report is the evaluation of EBS in deep geologic environments (as opposed to near-surface disposal) where by the nature of the waste hazard these are mainly restricted to host UNF and high-level radioactive waste (HLW). The only exception would be low to intermediate level nuclear waste (LILW) and will not be discussed in further except to briefly describe the types of EBS concepts adopted for the disposal of this type of waste. According to the IAEA report (2009) on the disposal of LILW (including that with long-lived radionuclides), some of the adopted options for near-surface (within the upper 30 meters of the land surface) disposal of LILW are landfill disposal, trench disposal, and engineered surface repositories (IAEA 2009). Landfill disposal is usually utilized to dispose very low level waste in many cases excluding long-lived radionuclides. This type of near-surface disposal doesn't require elaborated engineered barriers or sealing of the disposal site. Trench disposal is usually reserved for waste with higher radioactive activity. The waste is placed in an excavated compartment without any additional barriers surrounding the waste except for a top sealing cover to prevent water percolation. Engineered surface repositories are those of the vault type where engineered barriers are used to prevent interaction between water and waste. In this type of repository, the waste is placed in a concrete vault located in the excavated compartment and the barriers, including a top sealing cover, can have various types of configuration. Another form of near-surface waste containment is through the use of large underground storage tanks made of reinforced concrete and carbon steel liners that can accommodate large volumes of material (up to 1,000,000 gallons). An example of this is the Hanford tank farm in Washington, USA, hosting high-level waste from decommissioning activities.

1.2.2 Long-Term NW Isolation and the Multi-Barrier EBS Concept

Several geologic repositories setting for nuclear waste has been proposed since the 1970's and these can be divided according to host rock type, for example:

- Salt (e.g., WIPP (USA) and Morsleben (Germany); EBS: MgO backfill at WIPP).
- Granite, basalt, tuff (e.g., Yucca Mountain; EBS: drip-shield, invert).
- Clay, shale (e.g., Belgian repository concept; EBS: cementitious backfill and concrete buffer).

All of these types of host rocks provide a role in keeping water fluxes at minimum (McKinley 1997; Bennett et al. 2006). This is important for the immobilization capacity of the disposal as to prevent water-waste interaction; a process that is conducive of waste degradation and thus radionuclide transport beyond the confines of the near-field and the far-field domains towards the biosphere. In this regard, the EBS indeed plays a key role in ensuring containment of long-lived radionuclides for extended periods of time. The EBS concept is dependent on the host-rock type in the disposal environment, waste type, thermal load, cost, and safety margins assessed from a post-closure analyses and/or a performance assessment (PA) of the disposal system (Bennett et al. 2006; McKinley et al. 2006). Long-term processes (e.g., chemical, hydrological, thermal, mechanical) in the repository environment can exert significant changes to the EBS properties therefore affecting

the barrier performance of the entire disposal system. Key components and/or parameters that are key to EBS performance are:

- Container/overpack: permeability, corrosion rates, mechanical properties
- Unsaturated zone (UZ) repository interface: Percolation fluxes (gas and liquid); capillary barrier (Richards barrier).
- Waste form: leaching rates, radionuclide solubilities, durability, phase transformations with daughter ingrowth; thermo-mechanical properties, thermal load.
- Buffer/backfill: backfill saturation and swelling pressure, thermal conductivity, porosity and permeability, mechanical strength, long-term properties and alteration, buffer thickness and density, gas sorption capability, chemical stability.
- Seals (e.g., concrete): thermo-mechanical and hydraulic properties, long-term properties (hydration and setting), sorption, ion exchange, and solubility of cementitious materials, chemical stability.
- Aqueous and gas phase interactions: water and gas compositions, transport properties as a function of pressure and temperature, diffusion and advection, gas generation processes, chemical buffering.

Accurate understanding of all these EBS components and related processes under repository conditions are important to the PA of the disposal system. However, knowledge of all these processes at the relevant repository conditions (e.g., pressure, temperature) can be limited but in many cases these can be reasonably constrained.

It is worthwhile to also mention some of the key uncertainties related to these processes:

- Buffer/backfill emplacement methods: powder, pellets; costs and availability; hydration and mechanical properties.
- Long-term material properties performance: backfill/buffers physical and chemical stability; container corrosion, mechanical properties, and durability; host-rock: drift mechanical and chemical stability.
- Waste and waste matrix durability: waste form corrosion, release rates, secondary phases.
- Long-term buffer/backfill properties and interactions with fluids: chemical composition of fluids, gas transport, buffer/backfill alteration, bentonite-concrete interactions, aqueous and gas phase composition.

These uncertainties sometimes drive the complexities of proposed EBS concepts as to meet a high level of performance without compromising safety and quality assurance required for long-term isolation of nuclear waste. Even with all these potential uncertainties, the PA of EBS multi-barrier concepts has been developed since 1980 using models to represent various disposal environments. Stula et al. (1980), in a study sponsored by the Office of Nuclear Waste Isolation (ONWI) at that time, developed a PA model for a multi-barrier EBS surrounding a waste form package assembly in various host rock types that include salt, granite, basalt, and shale. Other subsequent studies evaluating various performance enhancement options of the EBS have been developed to address a larger number of processes with an enhanced level of model sophistication (see Balady, 1997). There are numerous reports on EBS performance investigations but these two reports are good examples of the investigated approaches and options to enhance performance.

The multi-barrier EBS concept has been widely adopted by several repository programs due in large part to the overall conceptual simplicity, cost-effectiveness, and long-term performance as an effective isolating barrier (see Fig. 1.1-1). Some EBS concepts, like that of Apted (1998), proposed a multi-barrier EBS concept referred as the Integrated Waste Package (IWP) where compacted buffer/backfill material is placed within the steel overpack. This EBS concept minimizes the use of EBS materials and costs while retaining the performance of current waste package designs for HLW. This level of design flexibility has prompted other levels of integration between EBS and waste package. McKinley et al. (2006) proposes a similar concept to that of Apted (1998) but with added level of complexity in the configuration of EBS components and type of materials. Their multi-barrier EBS concept called the Multi-Component Module (MCM) is similar to the IWP but having an optimized design that mainly entails the use of three backfill/buffer materials (bentonite clay, sand, and a mixture of both) configured in a layered manner to enhanced barrier capability. Figure 1.2.2-3 shows a schematic depiction of the MCM concept for the EBS after McKinley et al. (2006). This EBS concept is conceived as modular and can be prefabricated which brings certain advantages when it comes to handling and emplacement.

The main components of this multi-layered EBS concept are (after McKinley et al., 2006):

- The nuclear waste enclosed in a steel container/overpack.
- The sand layer is an interesting part of this concept since it is in immediate contact with the steel container and it has various barrier capabilities. The material could be sand having the integrity of a solid porous media but other synthetic materials with similar coarse grain size and mechanical properties could work as well. This sand layer could serve as a porous reservoir for gas generation also as a capillary barrier (Richards barrier) if the material meet this property.
- The bentonite layer can serve as a diffusion barrier for aqueous species in solution and also as a filter to immobilize colloidal phases and microbes.
- The sand/bentonite layer also serves as a diffusion barrier but the sand fraction also decreases the potential for bentonite erosion.
- The geotextile layer allows for homogenous wetting of the bentonite layer and serves as an additional protection against bentonite erosion.
- The outer steel shell is mainly for handling of the EBS module but it also provides an additional form of containment. This metal shell can also serve as a redox barrier where it could generate the appropriate chemical buffering conditions for retardation of some long-lived radionuclides whose solubilities are redox-sensitive.

McKinley et al. (2006) describe the many advantages if this EBS concept from the standpoint of anticipated processes in the long-term degradation of the barrier(s) and related mitigating effects on radionuclide migration in EBS failure scenarios. McKinley et al. (2006) also describes the modular versatility and flexibility of this EBS concept to accommodate multiple waste packages within the steel container overpack.

As noted previously, cost is an important driver behind the EBS multi-barrier concept where cost reduction is achieved through minimization of the use of EBS materials without compromising barrier performance (Apted, 1998). Moreover, the minimization of EBS materials and modular geometry also works in favor of ameliorating the logistics for waste emplacement in a subsurface environment whether vertical or horizontal disposal galleries are considered. For example, the

French repository concept has expressed a preference for horizontal disposal galleries instead of vertical ones for at least three reasons (Kursten et al. 2004):

- Performance is enhanced from technical and cost considerations;
- Volume of excavated clay is minimized;
- Requires a smaller underground area for construction of the disposal site.

All these reasons are mainly driven by operational/logistic aspects of waste disposition at the site. In salt repositories like the German and WIPP (USA) programs, the disposal rooms are much larger and backfill/buffer emplacement and sealing operations become relatively less demanding because the creeping salt becomes the long-term barrier. The proposed dimensions/geometry of the waste container/overpack can vary depending on waste characteristics and emplacement configuration; this can of course influence the waste emplacement logistics. However, many European repository programs have proposed dimensions of the waste container that in general do not seem to exceed ~1 m in diameter and ~4.6 m in length (Kursten et al. 2004). A general summary of some repository programs and their EBS components is given in Table 1.2.2-1.

1.3 Experimental Programs in EBS

Experimental programs in EBS and their findings are key in the understanding of EBS processes and performance. Many of studies have been conducted in underground laboratories such as Mont Terri Project (http://www.mont-terri.ch/) and the Grimsel Test Site (http://www.grimsel.com/) in Switzerland, and the HADES Underground Research laboratory (http://www.sckcen.be/en/Our-Research/Research-facilities/HADES-Underground-laboratory) in Belgium. For example, the FEBEX (Full-scale Engineered Barriers Experiment) at the Grimsel Test Site comprises various tests at the repository scale with the goal of testing the viability of the Spanish EBS multi-barrier concept and in the development of technologies for the study and monitoring of THMC processes in the EBS. The Section on Reactive Transport and Coupled THMC processes in EBS in this report describes the role and interactions with these experimental projects. This section also describes their importance in knowledge gathering for the modeling of THMC processes. The results of all these experimental activities related to EBS processes and performance will be reviewed to identify knowledge gaps and key findings that are critical to EBS performance.

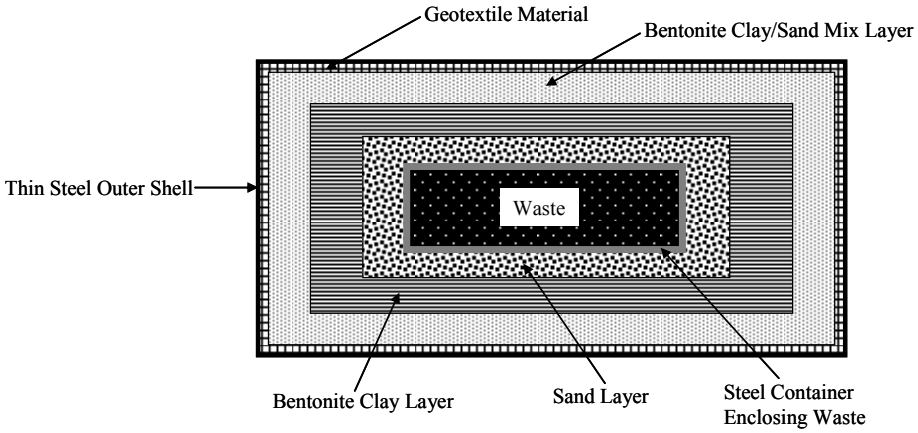

Figure 1.2.2-3 Schematic diagram of the MCM concept after McKinley et al. (2006).

1.4 Summary

This report will focus on the multi-barrier concept of EBS for long-term NW isolation and the primary processes affecting its performance. Emphasis is placed at important processes and effects that may occur at EBS components and interfaces, and THCM coupled processes in clay. Short-term or interim storage of NW is an important issue and will be discussed in more detail in the report *Evaluation of Storage Concepts FY10 Final Report* (Weiner et al. 2010).

Table 1.2.2-1 Examples of EBS Components in various repository programs (Source: OECD State-of-the-Art Report: EBS and the Safety of Deep Geological Repositories 2003, Table 3.1).

Country	Waste Type	Waste Matrix	Container/Overpack	Buffer/Backfill	Others
Belgium	HLW/Spent Fuel[(1)]	Borosilicate glass	304 stainless steel container, 316L stainless steel overpack	FoCa clay (Fourges-Cahaignes, France), 60% calcium bentonite, 35% quartz sand, 5% graphite	Disposal tube, tunnel lining
Canada	Spent fuel	UO_2	Carbon steel inner container with a copper outer shell	Buffers: bentonite or bentonite/sand buffer, Backfill: clay/crushed rock backfill	Tunnel and shaft seals
Finland	Spent Fuel	UO_2 (Not considered part of EBS)	Copper-iron	Bentonite buffer, backfill of compacted crushed rock and bentonite	Bentonite and concrete plugs
France	HLW (Type C)	Borosilicate glass	Stainless steel container, steel overpack	Optional bentonite buffer	Bentonite seals
Germany/ Morsleben	LLW, ILW and sealed sources	Not considered	Not considered	Salt concrete	Seals
Japan	HLW	Glass	Carbon steel overpack	Bentonite-sand mixture	Tunnel sealing plugs and grout
Spain	Spent Fuel	UO_2	Carbon steel/Bentonite	Bentonite	Concrete and bentonite seals
US (YMP)	Commercial Spent Fuel (CSNF), Defense Spent Fuel, HLW	Various Types: Fuel rods, Zircaloy cladding, borosilicate glass	316 stainless steel container; Alloy-22 outer barrier	None	Ti alloy drip shield, crushed rock invert
US (WIPP)	Transuranic Waste (TRU)	Various types	208L steel drums (Not part of the EBS)	MgO backfill	Concrete panel closures and shaft seals

(1) The Belgian repository EBS concept, as describe in the OECD report (2001), doesn't define waste type, waste matrix, and container/overpack for spent fuel waste.

1.5 References

Apted, M.J. (1998) "A models proposal: A robust, cost-effective design for high-level waste packages, Scientific Basis for Nuclear Waste Management XXI, Mat. Res. Soc. Symp. Proc. Vol. 506, p. 589-596.

Balady, M.A. (1997) "Engineered Barrier System performance requirements systems study report (Rev. 02)", TRW Environmental Safety Systems, Inc., Las Vegas, DOE/RW/00134-T31, 354p.

Bennett, D.G., Hooper, A.J., Voinis, S., and Umeki, H. (2006) "The Role of the Engineered Barrier System in Safety Cases for Geological Radioactive Waste Repositories: An NEA Initiative in Co-operation with the EC", Scientific Basis for Nuclear Waste Management XXIX, Mat. Res. Soc. Symp. Proc. Vol. 932, p. 43-52.

Bunn, M., Holdren, J.P., MacFarlane, A., Pickett, S.E., Suzuki, A., Suzuki, T., and Weeks, J. (2001) "Interim Storage of Spent Nuclear Fuel - A Safe, Flexible, and Cost-Effective Near-Term Approach to Spent Fuel Management", *A Joint Report from the Harvard University Project on Managing the Atom and the University of Tokyo Project on Sociotechnics of Nuclear Energy*, 127 pp.

Eizinger, R.E., McKinnon, M.A., and Machiels, A.J. (1999) "Extending Dry Storage Of Spent LWR Fuel For Up To 100 Years", Data Needs for Long-Term Dry Storage of LWR Fuel, EPRI TR-108757.

IAEA Nuclear Energy Series (2009) "Disposal Approaches for Long Lived Low and Intermediate Level Radioactive Waste", Report No. NW-T-1.20, 38 pp.

Kursten, B., Smailos, E., Azkarate, I., Werne, L., Smart, N.R., and Santarini, G. (2004) "COBECOMA State-of-the-art document on the COrrosion BEhaviour of COntainer Materials", Final Report, European Commission, 5th EURATOM Framework Programme 1998-2002, 299 pp.

Macfarlane, A. (2001) "Interim Storage of Spent Fuel in the United States", Annu. Rev. Energy Environ., Vol. 26, p.201–235.

McKinley, I.G. (1997) "Engineering for robustness: An approach to optimising HLW disposal concepts", Waste Management, Vol. 17, No. 1, pp. 1-8.

McKinley, I.G., Neall, F.B., Kawamura, H., and Umeki, H. (2006) "Geochemical optimisation of a disposal system for high-level radioactive waste", Journal of Geochemical Exploration, Vol. 90, p. 1–8.

OECD (2003) "Engineered Barrier Systems and the Safety of Deep Geological Repositories State-of-the-Art Report", Nuclear Energy Agency (NEA) Organization for Economic Co-operation and Development (OECD), 71 pp.

Stula, R.T., Albert, T.E., Kirstein, B.E., and Lester, D.H. (1980) "Systems Study on Engineered Barriers: Barrier Performance Analysis", Office of Nuclear Waste Isolation (ONWI), Report ONWI-211.

Weiner, R.F., Stockman, C.T., Ottinger Farnum, C., Sorenson, K.B., McConnell, P.E., Alsaed, A., Birk, S.M., Nutt, W.M., and Carter, J., (2010). "Evaluation of Storage Concepts – FY10 Final Report", Fuel Cycle Research and Development, U.S. Department of Energy (DOE), 37 pp.

Belgian Nuclear Research Centre, SCK·CEN, "Research Domains", Accessed April, 2010: http://www.sck.be/en/Our-Research/Research-domains

The Grimsel Test Site (GTS), Accessed April 2010: http://www.grimsel.com/

HADES Underground Research laboratory, Accessed in April 2010: http://www.sckcen.be/en/Our-Research/Research-facilities/HADES-Underground-laboratory

The Mont Terri Project, Accessed April 2010: http://www.mont-terri.ch/

SKB, Swedish Nuclear Fuel and Waste Management Company, "Clab: Central Interim Storage Facility for Spent Nuclear Fuel", Accessed April, 2010: www.skb.se/upload/publications/pdf/ClabEng.8.3.pdf

Nuclear Regulatory Commission (NRC), "Dry-Cask Storage", Accessed April 2010: http://www.nrc.gov/waste/spent-fuel-storage/dry-cask-storage.html

NATURAL ANALOGS AND DISPOSAL ROOM CHEMISTRY: MATERIALS AND MODELS

2. Applications of Natural Analogs to the Analysis of EBS

2.1 Introduction

The concept of geologic disposal of radioactive waste, to be acceptable to society, relies on demonstrations that long-term isolation from the biosphere can be maintained for periods of tens of thousands up to one million years. Processes operating on these time scales cannot be completely observed in laboratory or field experiments, and numerical simulations of these processes therefore cannot be fully validated. This issue can be partly addressed by geologic natural analog studies. Natural analogs are the preserved geologic records of chemical and physical processes that may be relevant to the processes that would occur in a radioactive-waste repository. The strength of natural analog studies lies in the opportunities they provide to observe natural hydrologic and geochemical processes that resemble the processes considered important for radioactive-waste containment over a time scale and at a level of complexity generally impossible to simulate under laboratory conditions (Chapman, McKinley, and Smellie, 1984).

In general, the simplest and most straightforward applications of natural analogs are for degradation of fuel or other materials and for near-field processes. Extending studies into the realm of far-field transport greatly increases the volume of subsurface environment to be characterized. It also leads to increased heterogeneity and uncertainty. In some cases, regional processes must be included as well.

This brief, preliminary overview identifies some of the potential advantages and disadvantages for a few of the best-known natural-analog sites. Attributes that may be advantages or disadvantages are of necessity oversimplified here. The potential for new analog sites relevant to redox fronts also is examined.

2.1.1 Oklo

Oklo, Okelobondo, and Bangombe, in Gabon, Africa, are economic uranium deposits about 1.97 billion years old (Smellie, 1995). These sites are the only known examples of ancient uranium deposits that experienced natural nuclear criticality and stable nuclear fission at a time when fissionable ^{235}U was more abundant than it is now. Uranium mineralization occurred within the basal series of sedimentary-basin deposits (the Franceville Basin) resting unconformably on plutonic-metamorphic basement rocks.

The uranium deposits developed through a series of stages. Uranium mineralization initially resulted from partial recrystallization of uraniferous conglomerate/sandstone placer deposits. These deposits were overlain by organic-rich black shales associated with limestones. When burial temperatures approached 150°C, the organic matter matured to form hydrocarbons. About 2.05 billion years ago, compaction and diagenesis of the sedimentary section partially remobilized the uranium due to the circulation of oxidizing waters through widespread percolation through fractures. When the oxidizing uraniferous waters came into contact with the reducing front of the organic matter, the uranium precipitated and was concentrated in the sandstone sediments beneath the shales and limestones. At Oklo, mineralization was concentrated in a sandstone layer a few meters thick. The role of organics at Oklo and other reactor sites deserves much attention. Nagy et al. (1991) studied the graphitic bituminous organic matter at the Oklo site where a significant fraction of the uraninite phase is retained. These authors conclude that the presence of this bituminous organic matter is key to the containment and immobilization of radionuclides in reactor zones rich in organic matter. As explained above, immobilization of the radionuclides is attributed to the interaction of U-bearing solutions with organic-rich liquids (e.g., liquid bitumen) causing reduction and precipitation of

uraninite in the reactor zone. Further heating of the organic phase along with solidification caused the formation of a graphitic-rich solid that serves as a containment medium for uraninite. The importance of this observation is to recognize the role of organic matter as a potential barrier material; not only as a containment phase but as a chemically active redox barrier. For example, the use of specific asphalt or bituminous materials in the form of seals could provide added redox barrier capabilities in a repository environment in addition to their well-known hydrophobic properties. Savary and Pagel (1997) study of the redox conditions at conditions at some of the natural reactors at the Oklo site suggest that the chemically reducing environment has been maintained for millions of years due to the presence of organic matter. However, their study also outlines the importance of radiolytic processes in affecting local redox conditions and retention capacity of radionuclides.

The reactor zones are about 1.97 billion years old, and fission persisted for perhaps one-half to one million years. Fission reaction temperatures were in the range of 160-350°C. Conditions necessary for controlled fission included are: 1) high uranium content; 2) low content of neutron-capturing nuclei such as boron and rare-earth elements; 3) the presence of light nuclei (neutron moderators) such as hydrogen in water; and 4) high concentration of fissionable ^{235}U. Criticality could have been achieved in locations where the UO_2 (uraninite) concentration exceeded 11% over a thickness of 2 m, perhaps in locations, such as faults, with increased porosity and more water available.

Present-day depths of the reactor zones vary from about 11-12 m to about 350 m below the surface. The more deep-seated sites may have been shielded from much groundwater interaction for long periods of geologic time. The shallower sites are now located within groundwater-alteration zones and are more likely to have been affected by recent low-temperature interactions.

2.1.1.1 Site Studies

The Gabon sites, and in particular the Oklo site, have been studied as natural reactors and as potential natural analogs for an underground nuclear waste repository since 1972. Oklo has been selected for this analysis because of the extensive characterization studies conducted for the natural reactors at this site. Major areas of study include earth science, isotope geochemistry, and reactor physics (IAEA, 1975, 1978). These studies have documented or modeled some of the physical conditions under which criticality occurred and established the mobility of elements at least qualitatively. The geochronology of major early events has been determined. Results generally indicate limited mobility of the reactor radionuclide products.

Oklo: Potential Advantages as a Natural Analog

- Due to the natural fission of ^{235}U, this site has the closest chemical match to used nuclear fuel, including fission products and their daughters, actinides and their daughters.
- The creation of fission products and the modification of uranium isotopic systematics by the natural reactor mean that evidence of transport could be documented despite the presence of uraniferous rocks beyond the reactor zones.
- Due to the natural fission, this site is suitable for investigation of radiolytic effects, including the generation of redox fronts.

- The evidence of radionuclide interactions with hydrocarbons and of the effects of heating on hydrocarbons provides opportunities to study potential advantages or disadvantages of carbon-containing materials. Moreover, this site provide evidence for the role of organics that provide the necessary redox conditions for U mineralization and radionuclide retention even for extended periods of time.
- Rock alteration around the natural reactors created halos of clay that could serve as analogs to backfill/buffer.
- The mineral uraninite in the deposits is very similar to spent-fuel mineralogy and composition.
- Site geology makes this a suitable analog for a repository in sedimentary rock.

Oklo: Potential Disadvantages as a Natural Analog

- Temperatures of fission reactions were higher than many planned repository-operating temperatures, so that data may serve only to place bounds on temperature-dependent processes.
- The great age of fission reaction means there is a lot of uncertainty about physical (temperature, hydrologic environment) and chemical conditions (e.g., Eh, pH) since that time.
- Economic pressures exist for continued mining and consequent loss of access to study areas and destruction of exposures.

2.1.2 Cigar Lake

The 1.3-billion-year-old Cigar Lake uranium deposit is located in northern Saskatchewan, Canada (Cramer, 1995). There is no evidence of nuclear criticality at this site, but the concentrations of uranium, locally as high as 50 to 55%, contribute to the creation of detectable radioactive isotopes by neutron capture, a process that is useful for documenting ground-water residence times and transport. At present, the deposit is located about 450 m below the ground surface. Figure 2.1.2-1 depicts a schematic cross-section of the Cigar Lake uranium deposit after Percival and Kodama (1989).

The uranium ore deposit near Cigar Lake is a narrow, elongated body at the base of a thick sandstone formation in the Athabasca Basin (Cramer, 1995). The sandstone rests unconformably upon the eroded and locally subsided surface of the Canadian Shield. A fault zone allowed deep formation waters access to the graphite-rich shield rocks beneath the sediments. Chemically reducing waters were produced by this interaction. At around 1.3 billion years ago, a hydrothermal event caused alteration, particularly around the subvertical graphite-rich fault zone. Results included: 1) local dissolution of quartz from the sandstone, leaving a clay-enriched zone, 2) local mixing of the uranium-bearing sediment waters with hotter reducing fluids rising along the fault zone, causing precipitation of uranium minerals and associated sulfides inside the clay-rich zone, and 3) local bleaching of the sandstone caused by the reduction of ferric to ferrous iron in a chimney-like zone rising around and above the deposit.

The hydrothermal temperatures at which the uranium deposit was formed were in the range of 150 to 220°C, and there were about three kilometers of sedimentary overburden. The ore body appears to have been subsequently unaffected except by a small event about 300 million years ago in which uranium was remobilized into small, isolated pockets in some of the steeply dipping fractures above and beneath the main ore body. Since that time, the deposit has been affected only by gradual uplift through erosion of the overlying sandstone.

2.1.2.1 Site Studies

The main source of information on site studies at Cigar Lake is the report, "Final report of the AECL/SKB Cigar Lake Analog Study" (Cramer and Smellie, 1994). The report contains the results of studies in the areas of geology, mineralogy and litho-geochemistry, ore mineralogy and geochemistry, hydrogeologic modeling, hydrogeochemistry, colloids, organics and microbiology, nuclear reaction product geochemistry, and performance-assessment-related modeling. These studies were undertaken prior to the onset of mining activities. One of the distinctive overall attributes of the Cigar Lake ore body is the absence of surficial radioactivity, an indicator of naturally excellent containment.

Cigar Lake: Potential Advantages as Natural Analog

- Natural analog for sandstone repository in saturated zone.
- Clay-rich zone surrounding the deposit is analog for backfill/buffer.
- Deep underground (450 m) workings provide access at repository-relevant depths.
- Documented excellent isolation of radioactive elements.
- Opportunity to study operational challenges and solutions in mining an underground facility in deep saturated sandstone.
- Radioisotopes created by neutron capture provide natural tracers for groundwater residence times and transport.
- Studies of uraninite alteration are applicable to waste-form degradation

Cigar Lake: Potential Disadvantages as Natural Analog

- Potential for new studies may be hampered by current mine flooding and plans for mining (*Uranium-Stocks.net*, 2009, *World Nuclear News*, 2010).

- The uranium deposits are of hydrothermal origin, and hydrothermal alteration has affected the surrounding rock, making it difficult in some cases to distinguish between effects of hydrothermal processes and effects of uranium/rock/groundwater interactions at lower temperatures.

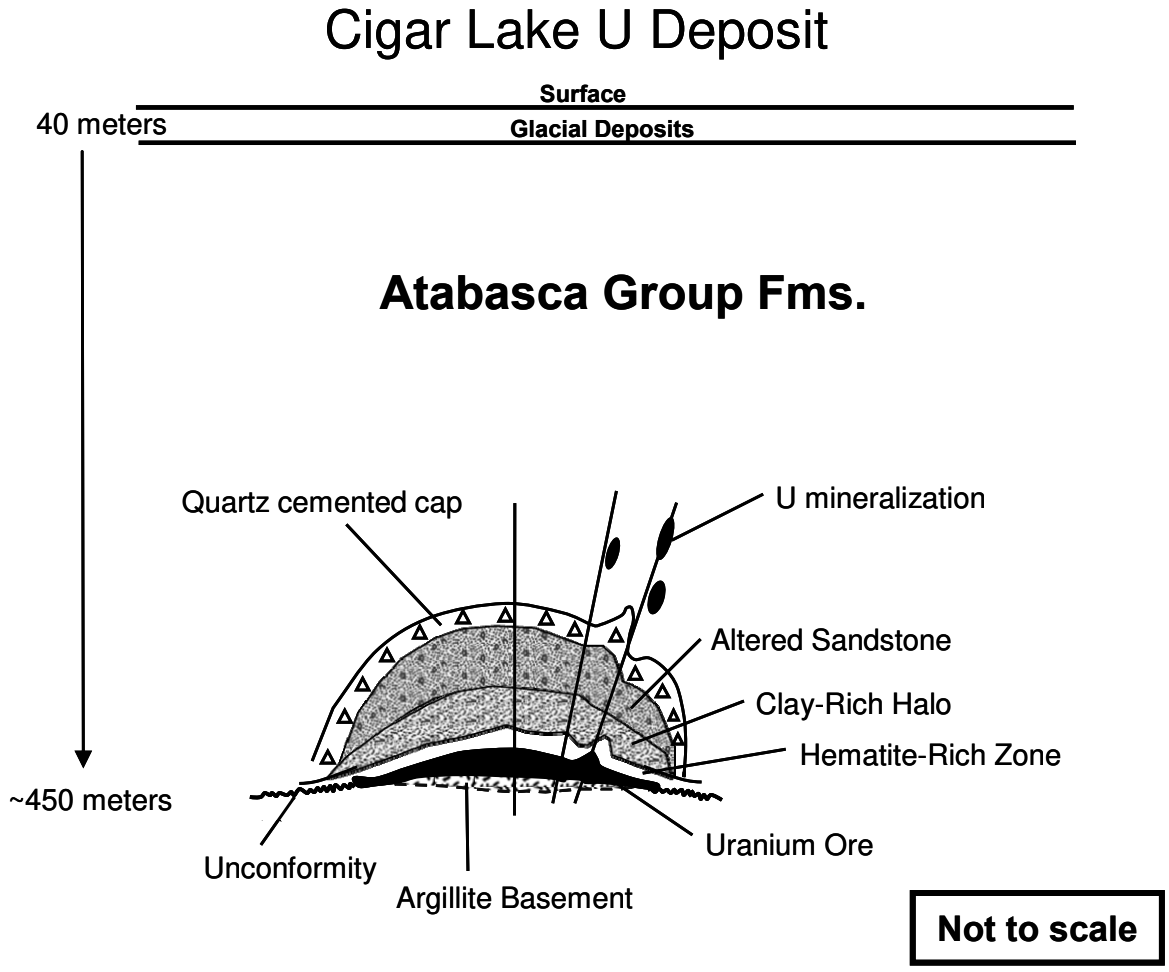

Figure 2.1.2-1 Simplified schematic cross section of the Cigar Lake U deposit (redrawn after Percival and Kodama, 1989).

2.1.3 Redox Front Analog Sites

Redox fronts, as the term applies to geohydrologic systems, are created at the boundary between two rock/groundwater systems with different oxidation environments (Miller et al., 2000). It is very likely that redox fronts would develop in the near- and far-fields of repositories of all designs. Even in a repository with natural reducing conditions, transient oxidizing zones in the near-field may be created by introduction of air over periods of decades or by waste-induced radiolysis of water.

Redox fronts in the far-field may form where oxidizing recharge water encounters deeper reducing water.

Natural analog sites for study of redox processes are pertinent as analogs of radionuclide transport and retardation. The greatest value of such sites would be as test cases to validate transport models. The sites generally are not applicable to issues such as waste-form degradation or engineered-barrier performance.

One of the best-known redox front natural-analog sites is Poços de Caldas in the state of Minas Gerais in central Brazil (McKinley, 1995). Two uranium/thorium/rare-earth-element mines – Morro do Ferro and Osamu Utsumi – were recognized as locations where redox fronts have influenced the mobility and distribution of uranium in the fractured phonolite host rock. Both the host rock and the uranium mineralization are of Late Cretaceous age (Schorscher and Shea, 1990). Hydrogeologic studies were performed at both of these sites. The goal was to collect sufficient information to test the conventional advective transport/radionuclide sorption models used in performance assessment. This effort was judged not successful because the hydrology was either too complex (unsaturated zone/oscillating water table at Morro do Ferro) or too disturbed (Osamu Utsumi) to be adequately characterized. It was possible to test, to some extent, the more detailed and limited process models that are used to support the abstraction process for simplified performance assessment models.

Another type of redox front uranium deposit that has been proposed as a potential natural analog is the roll-front deposit. These deposits are considered to be the products of a redox trap resulting from physical, chemical, or microbiological processes. Hydrogen-sulfide-rich zones, for example, precipitate uranium and other metals from solution because their solubility is sensitive to changes in Eh, pH, and sulfide concentration. Reduction and deposition of uranium is coupled to an oxidation reaction such as the conversion of ferrous to ferric iron that occurs when pyrite is replaced by goethite and/or hematite. There may be a decrease of organic material. These reactions often are catalyzed by anaerobic bacteria (Chapman, McKinley, and Smellie, 1984).

Roll-front uranium deposits are the products of moving redox fronts that are generated as oxidizing groundwater moves through permeable pathways, usually sandstone (bounded above and below by less permeable rock), from higher to lower hydraulic potential. The uranium source commonly is tuffaceous or granitic material in the sandstone. The roll front is a migrating reaction zone within the aquifer rock where oxidizing water reacts with local reducing rock-water-gas. Deposits of this type have been found in the southwestern United States, the Navajo Nation, the Colorado Plateau, and the Powder River Basin of Wyoming and Montana. Dimensions of such deposits range from a few meters to more than six kilometers. The deposits are mostly of Cretaceous or younger age, although older deposits are known.

Chapman, McKinley, and Smellie (1984) proposed the use of roll-front uranium deposits as natural analogs for redox processes in geologic waste repositories. The potential advantages listed below are from their report. Some of the potential disadvantages are inferred from Poços de Caldas studies undertaken after the 1984 report was published.

2.1.3.1 Roll Front Deposits: Potential Advantages and Disadvantages as Natural Analogs

- Original mineralization and subsequent modification typically occurred at temperatures below 100°C, and therefore are more applicable to low-temperature repository designs.
- Uranium-series disequilibrium measurements could be used to study the redox behavior of uranium and its daughters at ambient temperatures in the groundwaters and ore/host rock.
- Isotopic constraints could be used to bound the geologic time-scale for the migration speeds of redox fronts.
- Opportunity to study mineralogic alteration that accompanies the progression of the redox front through a porous medium.

Roll Front Deposits: Potential Disadvantages as Natural Analogs

- The hydrology of near-surface deposits shows considerable local variability, and is easily disturbed by mining or by natural groundwater-table fluctuations.
- Some deeper deposits have been disturbed by open-pit mining.
- Deeper deposits that have been developed as *in-situ* leach mines are disturbed and also are not available for direct observation and sampling.
- The organic matter that can play a major role in establishing the redox front in natural roll-front deposits has no equivalent in nuclear-waste repositories and is a potential complicating factor.

2.2 Summary (Natural Analogs)

The existing and potential natural analog sites described here represent only a small part of the spectrum of studied and potential sites. All sites are unique in a sense, but the Gabon fossil reactors are the only known example of self-sustained natural fission. Cigar Lake is not unique in terms of mode of occurrence of the uranium ore. However, it should be compared with additional sites in similar settings to ascertain whether the extremely good radionuclide containment is typical of this type of setting and to verify the contributing factors. Oklo and Cigar Lake are examples of analog sites that have features similar to a waste repository. Poços de Caldas and potential analog sites in uranium roll-front deposits are examples of sites that have or could be used to investigate redox fronts and transport/sorption models. The Oklo, Cigar Lake, and Poços de Caldas sites are of hydrothermal origin, whereas roll-front deposits form under ambient conditions. Roll-front deposits are attractive as potential natural analogs of redox fronts, but the development of these sites as open-pit or *in-situ* leach mines may limit the choice of sites for scientific characterization.

2.3 Disposal Room Chemistry

2.4 Introduction

Nuclear waste repository investigations can make salient use of phase equilibria studies to predict/control radionuclide solubility. Such studies can begin at the generic level and be performed iteratively through to license application, thus restricting unknown variables in room chemistry. Multiple modeling tools (EQ3/6, PHREEQC, Geochemist's Workbench) for solution-mineral-

equilibria and kinetics now exist and can be easily implemented along internally-consistent thermodynamic databases for a large set of solids, aqueous, and gas species. These basic studies can be used to predict formation of secondary mineral phases, solution chemistry in equilibrium with room conditions, and gas stabilization. This technique can be expanded to a variety of host rocks, waste form/packages and water chemistries and thus provide predictive chemical controls (i.e., backfill, removal of EBS components, tailored waste forms). Such studies will also point to knowledge gaps in thermodynamic databases, issues with kinetics (i.e., metastable phases), potential chemical component substitutions needed, and geochemical experiments needed for verification. Described below are examples of how such studies were used at salt repositories (Metz, et al., 2004, Brush, 2009), a case of a natural analog whose phase equilibria put constraints on repository waste form alteration mineralogy (Murphy, 2007), and a discussion of deep borehole room chemistry by the US Japan Waste Form Working Group (2010).

Another important aspect of disposal room chemistry is gas phase generation and transport in the disposal environment. Some of the key issues of gas phase process are (FORGE report, 2010):

- Flow and dilational mechanisms
- Long-term behavior of seals
- Preferential transport within the EDZ
- Gas transport in host-rock
- PA issues and treatment of long-term gas migration
- Gas generation/consumption/buffers: radiolysis, corrosion, and related rate processes
- EBS and seals: migration processes

According to the FORGE report (2010), many of these issues are being planned for future research investigations while others such as gas transport simulations in a NW repository have been already conducted for an EBS surrounding a copper canister (Cleall et al., 2006). The potential effects of gas phase chemistry on the redox state of EBS aqueous solutions and its influence on radionuclide transport will be also reviewed as part of the FY10 final progress report.

2.4.1 Salt Repository Room Chemistry

German studies – Metz et al. (2004) determined that $Mg(OH)_2$ would be best backfill to control CO_2 acidification at Asse. The Asse salt mine was used as a test site for radioactive waste disposal from 1967 to 1978 by the German government. Both low and intermediate radioactive waste forms (LILW) were emplaced, containing a total radionuclide inventory of 3×10^{15} Bq. It was expected that $MgCl_2$-rich brine (Q brine) would enter the emplacement rooms and react with the cemented waste products. Possible microbial degradation of organic waste components in $MgCl_2$-rich brine could produce significant quantities of CO_2, resulting in an acidification and consequently in an increase of element solubilities. The application of buffering backfill materials was discussed for closure of the mine. The potential selection of backfill materials was based on geochemical modeling taking into account the corrosion of the cemented LILW and degradation of organic waste components. The geochemical environment in the emplacement rooms was computed for the interaction of the relevant brine with the waste forms, the outcropping rock salt and potential backfill materials, *i.e.* Portland cement, crushed salt and a $Mg(OH)_2$-based backfill. In their study the solubilities of Am, Np, Pu, U, Th, Tc, Sr, Cs and I were modeled for each emplacement room.

Geochemical modeling lead to the conclusion that Portland cement, a $Mg(OH)_2$-based material and crushed salt can be used in different combinations as backfill materials. According to modeling results, $Mg(OH)_2$-based backfill material controlled the pH (7.9 – 9.0) and concentration of dissolved inorganic carbon (below 10^{-5} mol $(kgH_2O)^{-1}$) within ranges that are favorable with respect to actinide solubilities. Backfilling of a sufficient amount of an $Mg(OH)_2$-based material, provided favorable geochemical conditions with respect to radionuclide solubility. Since $Mg(OH)_2$ limits the dissolved inorganic carbon DIC concentration by formation of (Mg,Ca)-carbonates, it prevented acidification and carbonate complexation. Moreover, it provided a relatively uniform geochemical environment in the majority of emplacement rooms. A uniform geochemical environment would be of benefit for the performance assessment of the Asse salt mine, because it constraints the number of variability parameters.

WIPP Studies- Brush (2009) determined that MgO would be best backfill to control CO_2 acidification at WIPP. Prior to the decision to introduce a buffering backfill into WIPP, the room chemistry was virtually uncontrolled. CO_2 generation from microbial activity associated with organic degradation needed to be buffered to prevent acidification. Such acidification would have greatly increased the solubility of actinides in the repository. Brush (2009) reports that MgO mixed with ERDA-6 brine produces brucite ($Mg(OH)_2$), whereas the Generic Weep Brine (GWB) and MgO produces both brucite and an amorphous or crystalline Mg-OH-Cl-H_2O phase. In either scenario, CO_2 is buffered and pH is controlled near a value of 9. Furthermore, the average total inorganic carbon values for the two brines in approximately 0.4 mM. The modeling code used to determine the phase equilibria of the room chemistry was primarily EQ3/6, with BRAGFLO used to track CO_2 transport. This report successfully used phase equilibria studies to predict geochemical behavior in repository rooms that was later verified by experimental results, thereby satisfying regulatory requirements by the US EPA. In both cases (German and USA), computer models of phase equilibria provided strong evidence for final decisions.

2.4.2 Natural Analog Study- Nopal I, Pena Blanca, Mexico

Murphy (2007) was able to use equilibrium phase relations among uranyl minerals at Nopal I, Pena Blanca, Mexico to show uranophane stability over a broad range of realistic conditions and indicate that uranyl mineral variety reflects persistent chemical potential heterogeneity. This study was the outcome of years of research of the hydrothermal alteration of primary uraninite that produced secondary uranyl minerals at the site, which was recognized as a natural analog for the Yucca Mountain Project proposed HLW repository. By first determining field relations and petrographic textural relations, Murphy concluded that he would focus the phase equilibria study on (meta-) schoepite, becquerelite, soddyite, and uranophane because they are predominant secondary minerals at Nopal I. To look at phase relations at elevated temperatures, Murphy (2007) used the Van 't Hoff relation:

$$\ln K_T = \ln K_{298.15} - \left(\frac{\Delta H_r^\circ}{R}\right)\left(\frac{1}{T(K)} - \frac{1}{298.15}\right)$$

where K_T stands for the equilibrium constant at the temperature T in degrees K, ΔH_r° is the enthalpy of the dissolution reaction of the U phase, and R designates the gas constant. The important assumption in using this relation to extrapolate equilibrium constants to elevated temperatures is that ΔH_r° doesn't change appreciably with temperature. Murphy (2007) used this relation and parameter values therein to calculate equilibrium constants (enthalpy and free energy) from 25°C to 200°C.

The outcome of his work indicated uranophane stability increased with temperature at the expense of soddyite, and likewise, that becquerelite consumed (meta-) schoepite. Furthermore, the calculation indicates that uranophane is the most stable uranyl phase over a broad range of moderate to elevated silica activities coupled with near neutral to slightly alkaline pH and moderately low (and higher) Ca ion activity. Becquerelite stability is restricted to a narrow range of conditions at 25°C relative to other uranyl minerals, and stabilities of the Ca-free phases, metaschoepite and soddyite, are restricted to low Ca activities and/or acidic conditions at elevated temperatures. The existence of relict metaschoepite and soddyite in field samples speaks to kinetic delays in alteration reactions. Murphy (2007) concluded that uranophane would be the most stable secondary uranyl phase over a wide range of geochemical conditions similar to those at Yucca Mountain. A similar approach could be implemented to other types of equilibrium reactions, for example, those involving cementitious materials for which data at elevated temperatures are scarce.

2.4.3 Deep Boreholes – Selected waste forms

The US-Japan Joint Nuclear Action Plan Waste Management Working Group Phase I Report (March, 2010) provides both a brief summary of US and Japanese investigations concerning deep borehole disposal, along with selected other international research. It should be also noted that the Swedish Nuclear Fuel and Waste Management Company (SKB) have also conducted studies on deep boreholes for groundwater chemistry characterization (Laaksoharju et al., 1995) and another deep research drillhole study in central Germany to investigate the hydrogeology of deep-seated rock (Stober and Bucher, 2005). Concepts for deep borehole disposal date from the 1970s and earlier, and were further considered in the 1990s, with a report on Pu disposal by Los Alamos National Lab (1996). More recently, MIT (2003) provided a discussion on this disposal option in "The Future of Nuclear Power", and Sandia National Laboratories is presently investigating Deep Borehole options (Brady et al., 2009). In the American arena, two disposal concepts have been proposed, 1) a low and 2) a high temperature facility. The low temperature concept would have low waste concentrations such that heat released to the host rock is limited and helps to maintain a stable groundwater density stratification. The high temperature concept, in which the heat generated would partially melt the immediately surrounding rock, would purge the area around the boreholes of water and gas. As the waste cools, the rock would solidify into dry, newly crystallized rock.

As described in the US-Japan Phase I Report (2010) "Rather than relying on a combination of engineered and natural barriers to protect the public as does a mined geologic repository, deep boreholes rely on the natural conditions of the site as the only isolation barrier. However, in a high-temperature concept, the waste package must remain intact during the high-temperature stage. Lifetimes on the order of 10,000 years are required. Copper or noble metal alloys may be the only metallic materials that could survive the high temperatures and pressures for the requisite time. Mineral-based waste packages may be needed."

Since this disposal option relies primarily on the host rock as the isolation barrier, this is perhaps the best example of a simplified room chemistry. There would be very limited EBS materials involved, therefore there would be more restricted components. The waste form chemistry would most probably be restricted (i.e., Cs/Sr, Am only). Because deep boreholes rely on simple waste packages, crystalline rock types, and restricted water brine chemistry, phase equilibra studies would be ideal to predict which chemical interactions would be the driving forces for alteration. Potential reaction pathways to explore include 1) cement interaction with deep groundwater, 2) redox evaluation as to how elevated temperatures affect pH, and 3) variable grout, backfill, cement and asphalt plug

interaction with groundwater and waste package. These reaction pathways can be tested systematically with thermodynamically based phase equilibria studies and then verified with select hydrothermal experiments.

2.5 Hydrochemistry of Deep Crystalline Rocks for Borehole Disposal of Used Nuclear Fuel

2.5.1 Introduction

The concept of deep borehole disposal of used nuclear fuel typically invokes emplacement designs with minimal engineered barriers. Deep-disposal borehole systems in crystalline rock would rely on the expected favorable water chemistry, low host rock permeability, and slow groundwater movement to maintain isolation for hundreds of thousands to millions of years.

This section briefly summarizes concepts and state of knowledge relating to attributes of deep groundwater in crystalline rocks. Precambrian rocks in the Canadian and Fennoscandian Shield areas have undergone the most extensive hydrologic and geochemical characterization. Crystalline rock in other settings has been less thoroughly investigated, and a few examples are described here in a less comprehensive treatment.

2.5.2 Deep Groundwaters in Crystalline Rocks of the Shield Areas

2.5.2.1 Fracture and Matrix Fluids

The large contrast in hydraulic properties between fractures and the crystalline rock matrix affects the ways in which groundwater interacts with the rock. Free water collected from boreholes, such as the water samples with chemical analyses included in Table 2.5.1, essentially is only fracture water. Pore water, the water in the connected pore space of the rock matrix, can be collected for analysis only by extraction from rock core. Within the rock mass, pore water is accessible for diffusion-dominated interactions with groundwater circulating in nearby fractures of all sizes (Waber and Smellie, 2008).

Studies of pore waters and nearby fracture waters were undertaken at the Laxemar site in Sweden (Waber et al., 2009). The 1.8-billion-year-old bedrock of the Transcandinavian Igneous Belt, as exposed at Laxemar, includes Ävrö granite and quartz monzodiorite, with minor diorite. General conclusions include the following (Svensk Kärnbränslehantering AB, 2009):

- Pore waters are generally of a dilute Na-HCO_3 type, with Cl concentrations below 1,500 mg/L down to depths of 420 to 620 m. The associated stable-isotope signatures suggest a meteoric influence from climatic conditions similar to those prevailing today in all boreholes and, locally, from the Holocene temperature maximum.
- A steady-state situation between pore water and fracture groundwater for both Cl concentration and isotope signatures is established only in some locations to about 350 m depth, whereas transient states prevail for at least one of the natural tracers at intermediate levels. In this context, a steady-state situation means that pore waters and fracture groundwater have similar compositions and concentrations. Steady-state conditions in the shallow rock probably are attributable to the higher fracture abundance relative to deeper rock.
- Matrix diffusion was identified to occur over at least several decameters.

- In general, pore waters below about 350 m tend to be more dilute than nearby fracture waters, although intervals with the opposite pattern also exist.
- Cold-climate influence from the latest glaciation occurs in some porewater samples collected close to fractures down to depths of 350 to 500 m.
- A distinct change in chemical and isotopic composition of the pore water to a highly mineralized Na-Ca-SO_4 type is observed within intervals of about 430- to 530-m depths in some boreholes and 620 to 750 m in another hole. Associated fracture groundwaters could not be collected for comparison. The pore water signatures appear to have evolved before the last glacial maximum from fracture groundwater possibly influenced by freeze-out processes involving mirabilite formation and breakdown. Dissolution of old fracture gypsum during the last deglaciation, when glacial rebound may have reactivated sealed fracture systems of Paleozoic age, is a possible additional process contributing Ca and SO_4.
- In general terms, the pore water data indicate a change with increasing depth from waters of temperate meteoric origin, to glacial waters, and finally to saline waters (i.e., a progressive change from dilute Na-HCO_3 to a saline Na-Ca-Cl type) with a highly mineralized Na-Ca-SO_4 pore water observed within a narrow depth interval at intermediate depths.

2.5.2.2 Groundwater Compositional Changes with Depth

The most significant change that occurs in groundwater composition, especially for deeply circulating water, is the increase in salinity due to uptake of Na, Ca, and Cl ions (Gascoyne, 1997). These ions may be derived from primary residual magmatic fluids, deuteric fluids from high-temperature post-emplacement alteration, hydrothermal fluids from moderate-temperature metamorphic events, or incursions of low-temperature meteoric water, seawater, or brines. The large variation of chloride at shallow depths indicates advective groundwater flow and mixing of chemical compositions in the upper 300-500 m of rock. This condition changes to predominantly low- or no-flow conditions below this depth, where dissolved salts move mainly by diffusive rather than advective processes.

In most groundwater-recharge environments in crystalline rock across the shield area, the near-surface water typically is dilute, slightly alkaline (pH= 7 to 8), and Ca-(Na)-HCO_3 in composition (Gascoyne, 1997). As the groundwater moves to greater depths or travels farther along groundwater flow paths, it evolves to higher pH (8 to 9) and Na-(Ca)-HCO_3 water. Studies of fracture minerals in the plutons suggest a relationship between low-temperature mineralogy and groundwater composition (Gascoyne and Kamineni, 1994). Especially in mafic plutons, hydrolysis of plagioclase feldspars to liberate Na and Ca into solution, coupled with Ca loss by calcite precipitation and/or exchange for Na in clay minerals, are the main processes.

Calcium-dominated deep saline groundwaters are thought to have evolved over long periods of geologic time, as long as 10^9 years (Frape et al., 2003). These are dominantly pore fluids rather than fracture fluids. The pore fluids have the same $^{87}Sr/^{86}Sr$ ratios as the whole rock, which is rare in water-rock systems. This implies isotopic and possibly chemical equilibrium between fluid and rock, suggesting a very long residence time for the fluids.

The Lac du Bonnet groundwaters contain almost no H_2S, CH_4, H_2, or NO_3^- (Gascoyne, 1997). The major dissolved gases in groundwaters from the Fennoscandian Shield and the Laxemar-Simpevarp area, in approximate order of decreasing abundance, are N_2, CO_2, He, CH_4, Ar, H_2, and light

hydrocarbons (Svensk Kärnbränslehantering AB, 2009). Nitrogen and carbon dioxide are most common in the shallower groundwaters, and helium is most common in the deeper parts of the system. The available data indicate that the total gas content is less than would be expected in groundwaters of the area. However, many deep saline fluids in crystalline rock contain volumetrically significant amounts of hydrocarbon gas (Frape et al., 2003).

2.5.3 Groundwater Redox Conditions in Crystalline Rocks

The composition of groundwater in fractured crystalline rock and its state of redox potential changes as the groundwater flows from a recharge to a discharge environment (Gascoyne, 1997). The rate of consumption of dissolved oxygen and subsequent decrease in measured Eh potential is difficult to quantify for the natural groundwater environment because multiple competing reactions may occur simultaneously and because concentrations of reacting species, ratios of surface area to volume, and the influence of microbial catalysis all vary along the flow path.

2.5.3.1 Dissolved Oxygen

Studies of the rate of change of dissolved oxygen concentrations and measured Eh with depth were conducted in the URL/Lac du Bonnet granitic batholith (Gascoyne, 1997) at vertical depths from four to 240 m. Most samples had low dissolved O_2 concentrations even in the near surface. Dissolved-oxygen content dropped to 4 µg/L or less below about 60 m depth, with values of 0-0.5 µg/L at 240 m. The redox potential also shows a general trend of decreasing Eh with increasing depth, although the measurements range from +70 to –190 mV in all locations except one shallow piezometer (+200 mV) and in piezometers where H_2S was detected (about 200 mV).

At the Clara Mine in the Black Forest (Germany), dissolved oxygen is present at all measured depths to about 700 m (Bucher, Zhu, and Stober, 2009). Dissolved-oxygen contents of precipitation, surface waters, and springs are in the range of 10 to 13 mg/L. Groundwaters have values in the range of about 3 to 10 mg/L but show no clear pattern of change with depth. Bucher, Zhu, and Stober (2009) propose that atmospheric oxygen in underground tunnels contribute to mineral reactions; therefore, oxygen may be locally entering the groundwater and disturbing the natural distribution.

The most likely reaction controlling the consumption of dissolved oxygen in rapidly recharging groundwater is the microbially mediated oxidation of dissolved organic carbon. Surface waters generally contain sufficient dissolved organic carbon (DOC) to remove all dissolved oxygen, and data from the Canadian Shield environments support this observation. Gascoyne (1997) highlights the difficulty of documenting the persistence of this condition over periods of tens of thousands to millions of years. Conditions of reduced DOC input could exist in environments with little soil or vegetation and rapid recharge through fractures. Similar results obtained for groundwater inflow into the Hard Rock laboratory at Äspö, Sweden (Banwart et al., 1994), support a tentative conclusion that conditions leading to oxygen consumption at shallow depths are common and persistent.

Despite the apparent co-variation of dissolved oxygen and Eh with depth at Lac du Bonnet, Gascoyne (1997) concludes, along with other researchers, that measured Eh is not simply controlled by concentrations of dissolved oxygen in most groundwater. Eh is less than the values expected for a reversible equilibrium between oxygen and water (+700 to +800 mV).

2.5.3.2 Redox Reactions

Crystalline igneous and metamorphic rocks contain significant amounts of iron in iron silicates, part of which is in the reduced form, and in Fe-Ti oxides and iron sulfides. At depths where flow is through low-permeability fractures and pores, and where the rock/water ratio is higher, the Fe(II)-Fe(III) redox couple controls the Eh of groundwater in the Lac du Bonnet batholith (Gascoyne, 1997).

Sensitivity studies were conducted for naturally occurring redox reactions that may control oxygen ingress in the crystalline rocks of the Canadian Shield (Spiessl, MacQuarrie, and Mayer, 2008). Scenarios considered were based on simplified conceptual models that include a single vertical fracture, or a fracture zone, that extends from the ground surface to a depth of 500 m. Consistent with field observations, chlorite is present in the fracture and biotite and minor pyrite are present in the rock matrix. Results indicate that for the single-fracture case, the most influential factors controlling dissolved oxygen ingress are flow velocity in the fracture, fracture aperture, and the biotite reaction rate in the rock matrix. The most important parameters for the fracture-zone simulations are flow velocity in the individual fractures, partial pressure of oxygen in the recharge water, biotite reaction rate, and to a lesser degree the abundance and reactivity of chlorite in the fracture zone, and the fracture-zone width.

In some locations, oxygenated meteoric waters react with and oxidize sulfides in the subsurface (Frape et al., 2003). The more general case, in areas where sulfides are minor constituents of crystalline rocks, may be that sulfide oxidation has little effect on the water quality or Eh of groundwater. The loss of sulfate by bacterial reduction commonly is reported in many brackish and slightly saline groundwaters at depths of less than 500 m.

Table 2.5.1. Geochemistry of representative groundwater samples from shield sites

Location	Sample ID	Depth (m)	Water Type	TDS (mg/L)	Ca (mg/L)	Na mg/L	Mg (mg/L)	K (mg/L)	Sr (mg/L)	Cl (mg/L)	Br (mg/L)	SO_4 (mg/L)	HCO_3 (mg/L)
Finland													
Outokumpu	OKU551/90/1	427	Na-Cl	1,400	196	334	1	3.7	2.1	847	4		9
	OKU741	610	Ca-Cl	12,870	3,380	1,260	10	9.7	20.9	8,030	49	17	74
	OKU741	1,004	Ca-Na-Cl	28,120	5,730	2,940	998	34.3	40.5	18,100	120	20	93
Pori	POR-1	111	Na-Cl	2,690	272	669	12	1.0	5.8	1,510	6	74	139
	POR-1	201	Na-Cl	4,880	653	1,100	24	1.6	18.7	2,870	13	167	32
	Po-1	600	Ca-Cl	120,400	36,000	9,500	82	5.0	531.0	73,660	550	19	7
	PO1/87	470	Ca-Na-Cl	132,600	36,650	9,420	81	4.8	760.0	85,000	628	32	9
Ylifieska	YL1313/92	329	Na-Cl	460	54	95	41	3.9	1.4	129	1	4	129
	YL1313/90	511	Na-Ca-Mg-Cl	53,480	5,450	10,100	5,260	57.6	168.0	32,143	244	<1	54
	YL1313/88	539	Na-Ca-Mg-Cl	53,660	5,878	10,730	3,366	65.0	186.9	33,000	349	<1	70
	YL1313/92	521	Na-Ca-Mg-Cl	65,700	6,420	12,000	4,390	53.3	205.0	42,300	450		53
	YL1313/90	587	Na-Mg-Ca-Cl	82,870	8,550	16,000	5,230	96.3	276.0	52,030	625	<1	51
Enonkoski	ENONKOSKI 336	492	Na-Ca-Cl	11,720	1,220	2,616	720	23.0	75.4	6,895	78	<10	33
	La-375	419	Na-Ca-Mg-Cl	27,600	3,450	5,560	1,470	45.0	206.0	16,690	184	10	13
Juuka/Miihkali	MIIHK116	753	Ca-Na-Cl	34,280	8,050	5,190	1	42.0	33.7	20,500	177	202	78
	MIIHK116	490	Ca-Na-Cl	40,680	8,650	5,130	18	48.7	28.8	26,300	187	187	69
	Ju/Mi-114	920	Ca-Na-Cl	70,200	16,200	10,800	522	16.0	116.0	42,000	280	190	83
	MIIHK116	946	Na-Ca-Cl	134,140	16,700	38,600	228	520.0	156.0	78,700	507	514	189
	Ju/Mi-116	1,020	Na-Ca-Cl	166,200	17,000	48,000	230	600.0	188.0	99,500	490	45	146
Noormarkhu	R-43	575	Ca-Na-Cl	46,700	10,880	5,670	52	27.0	77.0	29,800	137	2	21
Mäntsälä	MHA1/92	100	$Ca-HCO_3$	100	13	10	4	3.0	0.1	4	0	24	65

Table 2.5.1. Geochemistry of representative groundwater samples from shield sites (continued)

Location	Sample ID	Depth (m)	Water Type	TDS (mg/L)	Ca (mg/L)	Na mg/L	Mg (mg/L)	K (mg/L)	Sr (mg/L)	Cl (mg/L)	Br (mg/L)	SO_4 (mg/L)	HCO_3 (mg/L)
	MHA2/91	207	Ca-HCO_3	200	27	11	7	2.5	0.2	3	0	19	125
	Mha-2	455	Ca-Mg-Na-SO_4	190	24	12	7	2.5	0.2	2		30	
	MHA1/92	850	Na-Ca-Cl	4,900	835	1,010	1	11.0	9.4	2,880	17	45	38
	Mha-2	855	Ca-Na-Cl	50,300	12,700	6,870	17	18.0	95.0	30,300	253		29
Oikiluoto	OL-KR1	750	Ca-Na-Cl	34,900	6,560	6,880	52	23.0	47.0	21,200	157		18
Tipasjarvi	TIP115/87	523	Ca-Na-Cl	12,510	3,612	893	2	14.0	14.8	7,700	51	57	75
Ruuki	PV11/87	298	Na-Ca-Cl	1,530	150	380	22	6.9	1.7	820	6	5	134
Kolari	KOL162	525	Na-SO_4	2,490	660	58	3	9.0	3.2	135	0	1,600	24
Palmottu	NP 357/90/3	242	Na-Cl-SO_4	800	37	229	8	3.2	0.3	251		196	62
	R348(P)	200	Na-SO_4	1,190	25	430	5	2.0	0.3	71	0	580	76
	NP 348,P200	165	Na-SO_4	1,460	27	462	5	3.0	0.3	66		838	60
	R385	403	Na-Cl	1,620	89	514	15	4.6	1.1	901	8	57	32
Sweden													
Aspo	KASO3-1566	129	Na-Ca-Cl	2,110	160	583	20	2.2	3.2	1,240	5	33	62
	KLX02-2934	1,155	Ca-Na-Cl	25,210	5,250	3,730	5	10.5	83.8	15,130	125	860	11
	KLX02-2931	1,345	Ca-Na-Cl	50,090	11,200	6,210	3	17.9	191.0	31,230	196	1,024	9
	KLX02-3038	1,385	Ca-Na-Cl	61,240	14,800	7,420	1	32.6	253.0	36,970	509	1,205	42
Stripa	V2(17-38)	436	Na-Ca-Cl-HCO_3	2,016	18	56	1	0.4		84		3	54
	V2-5(4419)	801	Na-Ca-Cl	300	34	47	0	0.3		190	2	4	16
	V2(69-4)	822	Na-Ca-Cl	790	109	181	0	0.5		440		46	9
	V2-4(850514)	814	Na-Ca-Cl	1,170	175	250	0	0.9		640	6	85	6
	V1(81WA203)	815	Na-Ca-Cl	1,203	172	277	0	1.2		630	7	102	9

Table 2.5.1. Geochemistry of representative groundwater samples from shield sites (continued)

Location	Sample ID	Depth (m)	Water Type	TDS (mg/L)	Ca (mg/L)	Na mg/L	Mg (mg/L)	K (mg/L)	Sr (mg/L)	Cl (mg/L)	Br (mg/L)	SO_4 (mg/L)	HCO_3 (mg/L)
Canada													
East Bull Lake	EBL-2	460	Na-Ca-Cl	2,060	228	570	2	1.1	1.5	1,237	3	11	
	EBL-4	429	Na-Ca-Cl	4,330	455	1,160	2	3.4	6.2	2,580	11	108	
Keweena	#6		Ca-Cl	164,400	47,500	13,200	7	70.0	223.0	102,171	829	368	26
Centennial URL	URL16-4-1	85	Na-HCO_3	340	35	52	9	3.5	0.4	18	0	37	184
	M10-1-7	50	Na-HCO_3	350	26	69	3	2.1	0.2	36	0	25	186
	M1A-3-7	265	Na-Cl	700	30	170	2	2.1	0.4	207	1	128	158
	WN3-90	90	Na-HCO_3	730	25	160	11	3.3	0.5	119	0	82	328
	URL15-1-4	125	Na-Cl	750	30	200	4	5.4	0.3	191	1	93	222
	M11-3-4	290	Na-Cl	1,840	145	440	10	2.8	1.5	590	2	380	276
	URL12-10-19	390	Na-Cl	2,410	156	735	3	2.6	2.3	1,246	3	217	52
	WN10-3-4	245	Na-Ca-Cl-SO_4	3,210	289	770	27	5.6	4.1	1,350	6	700	71
	URL12-13-21	605	Ca-Na-Cl-SO_4	4,900	1,070	530	25	10.2	7.7	2,454	12	776	32
	URL14-8	280	Ca-Na-Cl-SO_4	6,660	710	1,800	8	4.9	7.8	3,389	18	732	15
	M5A-1N8	340	Ca-Na-Cl	7,590	1,480	1,200	12	5.7	10.7	3,980	26	876	32
	M14-4-4	370	Ca-Na-Cl-SO_4	11,120	2,600	1,540	18	5.6	16.3	5,800	35	1,138	19
	WN4-13-20	650	Na-Ca-Cl-SO_4	20,110	2,687	4,890	26	10.5	39.8	11,091	33	1,393	15
	WN11-17-15	1.000	Na-Ca-Cl-SO_4	31,840	4,930	6,800	27	19.1	61.8	18,944	62	1,105	20
Matagami	R46	1,300	Ca-Cl	81,090	22,600	4,850	1,500	62.5	547.0	50,828	628	5	72
	R36	1,800	Ca-Cl	227,200	61,300	14,800	3,400	338.0	1,460.0	143,581	1,785	405	101
Norita	UN 249		Ca-Na-Cl	12,090	2,640	1,050	525	16.5	107.0	7,600	118	5	38
	4E-85 #1		Ca-Na-Cl	139,100	29,100	13,300	4,200	335.0	960.0	90,000	1,134	5	76

Table 2.5.1. Geochemistry of representative groundwater samples from shield sites (continued)

Location	Sample ID	Depth (m)	Water Type	TDS (mg/L)	Ca (mg/L)	Na mg/L	Mg (mg/L)	K (mg/L)	Sr (mg/L)	Cl (mg/L)	Br (mg/L)	SO_4 (mg/L)	HCO_3 (mg/L)
Sudbury	N3651	1,600	Ca-Cl	240,700	65,000	16,880	12	122.0	1,390.0	156,000	1,090	138	
	N3646A	1,600	Ca-Cl	249,100	63,800	18,900	78	430.0	1,580.0	162,700	1,250	223	58
	N3640a	1,500	Ca-Cl	250,360	63,800	18,500	24	371.0		166,200	1,200	265	
Thompson	T3-2000	610	Ca-Na-Cl	20,340	4,540	2,740	160	32.1	79.7	12,600	111	1	55
	2200-1	671	Ca-Na-Cl	22,490	4,840	2,930	233	92.6	98.3	13,700	115	444	28
	4000-3	1,220	Ca-Na-Cl	65,440	15,900	6,800	549	45.7	277.0	41,400	405	2	10
	4000-6	1,220	Ca-Na-Cl	101,400	26,800	8,670	637	59.9	558.0	63,800	793	2	15
	4000-5	1,220	Ca-Na-Cl	182,600	46,300	17,000	1,960	126.0	910.0	115,000	1,110	107	9
	4000-4	1,500	Ca-Na-Cl	324,500	64,000	45,000	5,100	199.0	1,080.0	207,000	1,760	284	19
Yellowknife	4500-2	1,372	Ca-Na-Cl	58,340	15,700	9,420	250	110.0	314.0	31,900	324	198	69
	4500-3	1,372	Ca-Na-Cl	63,140	12,900	10,900	268	111.0	671.0	37,100	358	746	28
	YK3464	1,372	Ca-Na-Cl	130,290	26,400	18,800	406	109.0	628.0	82,700	756	428	14
	YK2042	1,372	Ca-Na-Cl	172,900	39,300	21,700	820	164.0	910.0	109,000	935	54	
	4500-1c	1,372	Ca-Na-Cl	213,940	49,400	27,900	712	393.0	1,190.0	132,800	1,180	8	16
	4500-6C	1,372	Ca-Na-Cl	237,100	57,300	32,600	920	495.0	1,640.0	142,000	1,520	1	2

Table 2.5.1. Geochemistry of representative groundwater samples from shield sites (continued)

Location	Sample ID	Depth (m)	Water Type	TDS (mg/L)	Ca (mg/L)	Na mg/L	Mg (mg/L)	K (mg/L)	Sr (mg/L)	Cl (mg/L)	Br (mg/L)	SO_4 (mg/L)	HCO_3 (mg/L)
Russia													
Mir	N 82 [537]	600	Ca-Cl	242,820	46,417	4,025	9,853	4,432.0	882.0	173,338	4,712	38	
Udachnaya	Borehole 330	504	Ca-Cl-HCO_3	344,500	70,923	19,870	11,693	12,095.0	1,127.0	139,435	3,094		
Udachnaya	Borehole 310	834	Ca-Cl	364,020	94,723	5,066	15,306	17,678.0	1,600.0	212,280	5,637	38	
Mir	Borehole 28	500	Ca-Cl	369,540	86,041	11,294	13,870	7,574.0	1,791.0	158,918	3,816	100	
Trelyahskaya	Borehole 746	2,777	Ca-Cl	372,530	108,747	10,406	4,005	1,195.0	2,279.0	187,668	4,725	183	
Western Europe													
Leuggern	Le	1,643	Na-HCO_3-SO_4	1,050	9	295	0	8.8		125		263	273
Berghaupten	Berg	392	Na-Cl-HCO_3	1,860	24	568	4	14.8		447		276	452
Bad Säckingen	GW9-1/86	82	Na-Ca-Cl	3,500	314	1,041	30	81.7		1,761	5	115	525
Ohlsbach	Ohlsbach	59	Na-Cl	10,120	594	2,891	34	252.6	20.5	5,357	18	385	500
Schramberg	Schramb	505	Na-Cl-SO_4	10,680	368	3,205	57	63.0		3,318		3,206	381
Buehl	Bu	2,535	Na-Ca-Cl-SO_4	201,350	11,700	63,900	1,900	503.0	485.0	120,500	726	1,525	
UK													
Wheal Jane	WJ2	280	Na-Ca-Cl	7,550	995	1,620	23	100.0	16.8	4,460	17	189	24
Wheal Jane	WJ3	400	Na-Ca-Cl	9,930	1,300	2,090	13	132.0	23.0	6,090	19	114	54
South Crofty Mine	SC1	580	Na-Ca-Cl	15,250	1,840	3,520	55	153.0	30.0	9,280	35	129	60

Source: Frape et al. (2003) and references cited therein.

Redox interactions of sulfur-bearing minerals with organics related to both biotic and abiotic processes has been explored in the literature but rarely addressed from the standpoint of subsurface repository environments. For example, the treatment of gypsum ($CaSO_4 \bullet 2H_2O$) as an inert phase in a salt repository environment should be put into question and thus be evaluated in terms of redox processes. For example, let's consider the redox equilibria for the system Ca-Fe-SO_4-H_2O-H_2S. For reactions involving sulfate reducing bacteria (SRB), let's assume a potential set of reactions with strong relevance to microbial activity as envisioned in repository environments such as that for WIPP:

$$2\ CH_2O\ (org,\ Formaldehyde) + CaSO_4 \bullet 2H_2O + O_{2(g)} + 2\ H^+ = Ca^{++} + H_2S_{(aq)} + 2\ HCO_3^- + 4\ H_2O$$

$$Fe^{+++} + 1/2\ H_2O = Fe^{++} + 1/4\ O_{2(g)} + H^+$$

$$S^{--} + H^+ = HS^-$$

$$FeS(troillite) + H^+ = Fe^{++} + HS^-$$

$$HS^- + 2\ O_{2(g)} = H^+ + SO_4^{--}$$

$$H_2S_{(aq)} = H^+ + HS^-$$

$$CaCO_3 + H^+ = Ca^{++} + HCO_3^-$$

$$HCO_3^- = H^+ + CO_3^{--}$$

$$FeS_2(pyrite) + H_2O = Fe^{++} + 1/4\ H^+ + 1/4\ SO_4^{--} + 7/4\ HS^-$$

$$CaSO_4 \bullet 2H_2O = Ca^{++} + SO_4^{--} + 2\ H_2O$$

$$CaSO_4 \bullet 1/2H_2O = Ca^{++} + SO_4^{--} + 1/2\ H_2O$$

$$CaSO_4 = Ca^{++} + SO_4^{--}$$

$$FeOOH\ (goeth.) + 3\ H^+ = Fe^{+++} + 2\ H_2O$$

$$Fe(OH)_3 + 3\ H^+ = Fe^{+++} + 3\ H_2O$$

The above set of reactions should be an initial step in examining redox equilibria between organic and inorganic species for the system Ca-SO_4-Fe-CO_2-H_2O. This approach would also allow for the evaluation of the thermodynamic "drivers" involving potential abiotic redox buffering for this system.

2.5.3.3 Groundwater Redox State, Canister Corrosion, and Actinide Solubility

The interaction of groundwater with metallic barrier components can produce consumption of available O_2 in the EBS. Due to the large amount of iron anticipated to be present in the form of barrier materials, corrosion of iron-bearing phase may well exert a strong influence on dissolved $O_{2(aq)}$ (and therefore effective $O_{2(gas)}$ fugacity) in solutions contacting a corroding waste canister. This is based on recent experimental observations of simulated aqueous solution interactions with steel scale-model waste packages (Zarrabi et al. 2003, Ferriss et al. 2009). In the experiments of Ferris et al. (2009), few of the packages contained some amount of UO_2. The major corrosion products observed from the two year experiments are magnetite (Fe_3O_4) and maghemite (Fe_2O_3) with some akaganeite(β-$FeO_{1-2x}(OH)_{1+x}Cl_x$), lepidocrocite (γ-FeOOH), and hematite (Fe_2O_3). Their study also shows that the UO_2 phase did not show any significant extent of oxidative alteration concluding that sufficiently reduced conditions were maintained locally in the course of these experiments.

Figure 2.5.1 (Jové Colón and Finch, *in prep.*) shows the redox stability of iron-bearing phases as function of pH for common corrosion products of metallic materials such as steels providing a good representation of how an iron-dominated system could influence solution redox condition. This figure elucidates the strong agreement between predicted Eh-pH relations for the ferric-ferrous iron system and measured Eh-pH reported for the Pu solubility experiments given by Rai et al. (2001) and Neck et al. (2007). This observation suggests that if overall solution redox is controlled by equilibria with $Fe(OH)_3$-Fe^{2+} and/or $Fe(OH)_3$-"green rust", then the solution redox condition in contact with corroding canister or iron-bearing barrier material may closely corresponds to redox conditions observed in plutonium solubility experiments that are controlled by plutonium redox couples. Therefore, solution redox conditions might be strongly influenced or controlled by systems where iron-bearing phase predominate maintaining locally reduced conditions at EBS domains. Figure 2.5.1 also shows the solution redox of subsurface waters for three types of host-rock environments: salt, clay rock, and granite. The Eh-pH redox relations for solutions sampled in these environments indicate a consistently reduce state; a common feature of many deep subsurface waters. All these observations are indicative of the potential redox conditions of solutions confined to EBS environments and the plausible existence of "redox barriers" that could enhance the overall barrier capability of the EBS. Therefore, it is inherently important to evaluate the potential for these redox barriers and their capability to affect arrest radionuclide transport.

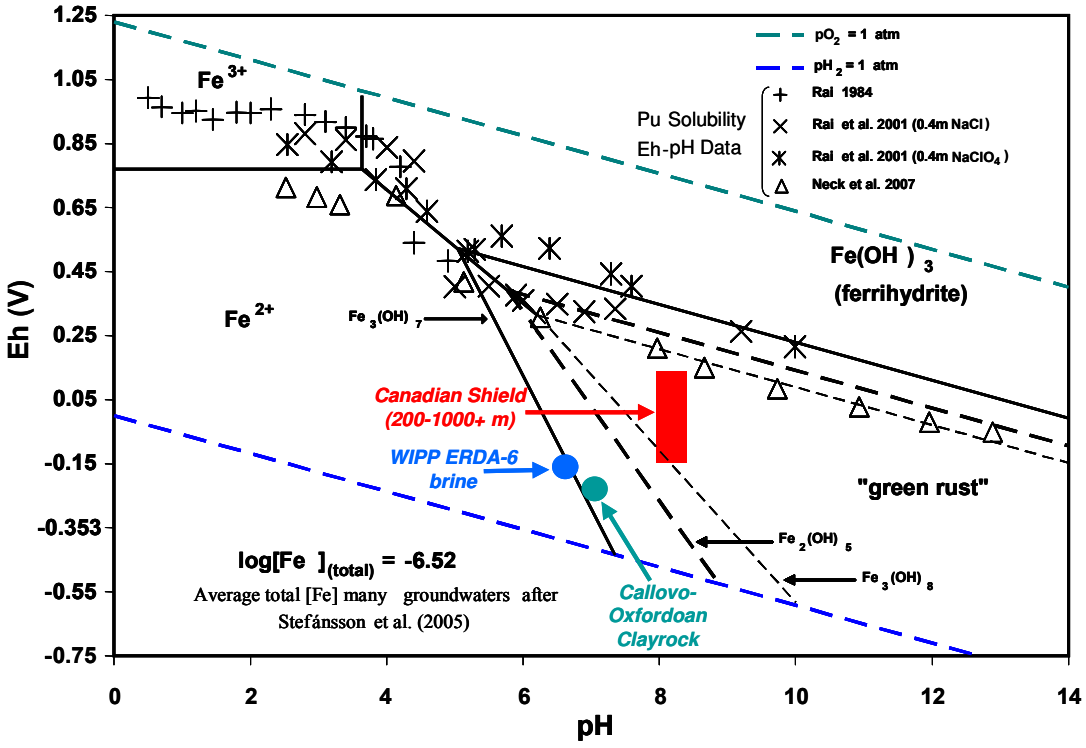

Figure 2.5.1. Plot of Eh versus pH relationships for the iron system with relevance to solution redox control for a corroding metallic barrier material (see text). Diagram was constructed using thermodynamic data from Bourrie et al, (1999, 2004) for "green rust" phases, YMP Pitzer thermodynamic database (Mariner, 2007) for ferrihydrite ($Fe(OH)_{3(s)}$), and ancillary data used obtained from the YMP thermodynamic database (Wolery and Jové-Colón, 2007), Robie et al. (1979), Stefansson et al. (2005), and Parker and Khodakovskii (1995). The Eh-pH data depicted in the diagram for the Canadian Shield waters, WIPP ERDA-6 brine, and Callovo-Oxfordian clayrock are from Gascoyne et al. (2004), D'Appolonia Consulting Engineers (1983), and Gaucher et al. (2009), respectively.

2.5.3.4 Uranium Content as an Indicator of Redox Potential

Concentrations of natural dissolved uranium are redox-sensitive indicators of groundwater movement (Gascoyne, 1997). The uranium concentration may be a useful indicator but not a controller of groundwater redox conditions in unmineralized crystalline-rock environments. Near-surface groundwater in granitic plutons of the Canadian Shield may have uranium concentrations >100 µg/L. The uranium content of groundwater in a gabbroic pluton is less than 5 µg/L. These results show that the uranium contents of the groundwater and the aquifer rock are related, and therefore interpretations of the range of values always should be considered as site-specific.

In the Lac du Bonnet batholith, shallow groundwater in overburden and bedrock contains the highest uranium concentrations (as much as 900 µg/L). Below depths of about 300 m, uranium concentrations are lower, generally <10 µg/L. The dominant factors controlling uranium content appear to be Eh and HCO_3^- concentrations (Betcher, Gascoyne, and Brown, 1988). Higher uranium concentrations are associated with more oxidizing, HCO_3^--rich groundwater. Prior to excavation of the URL, the uranium redox front had existed as a boundary at about 100 to 200 m below the surface.

2.5.3.5 Microbial Activity in the Deep Subsurface

Microbial consumption of oxygen and oxidation of dissolved organic matter has been documented as an important process at depths of less than one kilometer. At greater depths, microbial populations are not necessarily dependent on photosynthetically produced electron donors and acceptors (i.e., nutrients; Lin et al., 2006). The existence of microorganisms at depths greater than one kilometer is well established, but much remains unknown regarding the abundance and sustainability of these microbial communities. Lovley and Chapelle (1995) give a general summary of deep subsurface microbial processes. Chivian et al. (2008) provide a schematic illustration of microbial processes in a deep single-species ecosystem, including mineralogic reactions and the radioactive and radiolytic processes that contribute energy and nutrients. Pedersen (1996) provided a review of investigations of bacteria in deep crystalline bedrock and their potential importance for nuclear-waste disposal in underground repositories. This review summarizes abundances of bacteria predominantly in Swedish locations from the surface to depths of 1240 m. An investigation of a deeper bacterial occurrence that includes isotopic studies of water sources and ages is summarized below.

Studies of the indigenous microbial community were undertaken in the 2.7-billion-year-old Ventersdorp Supergroup metabasalt (South Africa; Lin et al., 2006). High-pressure water was sampled from a fracture intersected at 2.8 km below the land surface, part of an inferred three- to four-kilometer-deep fracture system. The initial water temperature was estimated to have been greater than 60ºC. One dominant microbial species, a thermophilic sulfate reducer belonging to the *Firmicutes* phylum, was identified in the samples. The measured cell density in the initial water sample, $5.1 \pm 0.5 \times 10^4$ cells/mL, did not distinguish between total and viable cells, but it is order-of-magnitude comparable to the maximum concentrations of viable sulfate-reducing bacteria reported by Pedersen (1996).

Metabolic processes of the *Firmicutes* bacteria are highly complex and incompletely understood, but the most thermodynamically productive redox reaction may be the reaction of hydrogen gas, hydrogen ion, and sulfate to produce hydrosulfide and water (Lin et al., 2006). Methanogenesis may occur through the reaction of hydrogen gas, hydrogen ion, and bicarbonate ion to form methane and water. Other metabolic reactants and products include formate and acetate. Light hydrocarbon molecules of inferred abiotic origin also are present.

Water properties measured on-site included temperature (>60ºC), pH (9.3), Eh (-330 mV), and dissolved oxygen (Lin et al., 2006). The dissolved-oxygen content of the initial sample was slightly above the detection limit of 1 μM (32 μg/L), but this might have been an artifact of the initial high flow rate given that subsequent samples had no detectable oxygen. The Na-Ca-Cl water contains 8580 μM (138 mg/L) methane.

Stable-isotope and noble-gas-isotope analyses were used to investigate sources and ages of the deep fracture water (Lin et al., 2006). Based on various models, the bulk age of the fracture water and its microbial community may be in the range of 3 to 25 million years. This model age represents either the true subsurface residence time or the mixing between an ancient saline and hydrogen- hydrocarbon-, and sulfate-rich hydrothermal fluid (0.8 to 2.5 billion years old) and paleometeoric water (3 to 4 million years old) that was moderately saline and poor in hydrogen, hydrocarbon, and sulfate. Sulfate in the ancient water may have been derived from pyrite oxidation (by radiolytically produced oxidants) and barite dissolution. As much as 70% of the initial sulfate in the water may have been removed as microbially precipitated pyrite. The nutrient budget seems to indicate that the deep crustal biosphere is energy-rich and capable of sustaining microbial communities indefinitely by geological processes.

There is some evidence that factors in addition to nutrient-supply rates may control the abundance of microbes in the deep subsurface. Kyle et al. (2008) found four distinct groups of bacteriophage viruses in groundwaters to depths of 450 m at the Äspö hard rock laboratory in Sweden. A predator-prey relationship may exist in deep groundwater, with active and growing microorganisms continuously predated by viruses to observed steady-state numbers in the range of 10^4 to 10^6 cells per milliliter.

2.5.3.6 Speculative Processes Involving Ancient Organic Matter

The Proterozoic (2.1 to 1.5 billion years; Lanev et al., 1987) rock section of the Kola SG-3 deep borehole, extending from the surface to a depth of 6842 m, contains mostly minute quantities of organic molecules (Karus et al., 1987). In the metamorphosed mafic to intermediate intrusive and extrusive rocks, the chloroform bitumen extract is dominated by oxygen-bearing phthalates (esters of aromatic dicarboxylic acids). These occurrences are attributed to the incomplete transformation of organic matter in an oxidizing environment and to the breakdown of organic matter in zones of high-temperature metamorphism accompanied by the production of free hydrogen and oxygen. This results in the formation of local areas characterized by an oxidizing environment favorable for the presence of phthalates (Karus et al., 1987). The timing of phthalate-producing processes is uncertain. Major metamorphism occurred in the period of 2.1 to 1.5 billion years ago, but additional alteration occurred as recently as ~ 600 million years ago (Lanev et al., 1987; Glagolev et al., 1987).

The contribution of preserved oxygen-bearing phthalates to existing groundwater chemistry in SG-3 is unknown. Waters from the upper 610 m were tested in a satellite well and found to be slightly reducing (Eh = -20 mV; Borevsky, Vartanyan, and Kulikov, 1987). The very low content of these molecules in Kola rocks, less than 0.2% (Karus et al., 1987), probably indicates only a minor potential to affect the Eh of groundwater.

2.5.3.7 Controls on pH

In shallow groundwaters, the pH commonly is controlled by carbonate equilibria. Bicarbonate enters the groundwater system as a result of the uptake of CO_2 from soil-zone gases and/or direct atmospheric inputs. Additional sources of bicarbonate can come from dissolution of carbonate minerals (Langmuir, 1971). High concentrations of CO_2 in some bicarbonate mineral waters of the Black Forest region (Central Europe) lead to pH values around 6. The source of the CO_2 is uncertain because δHe^3 data indicate a significant mantle contribution, but all other aspects of the mineral waters indicate a shallow reservoir depth and no connection to deep reservoirs (Stober and Bucher, 1999).

CO_2-rich recharge from surface water has initially low pH, typically around 6 but as low as 5 (Bucher, Zhu, and Stober, 2008). In deeper systems dominated by calcium-rich saline fluids, both carbonate-solubility constraints and silicate reactions act to remove bicarbonate ions as precipitated calcium- and magnesium-carbonates, often adjusting the pH to levels greater than 9 (Frape et al., 2003).

2.5.3.8 Natural Constituents as Tracers of Groundwater Movement

Although the deep crystalline-rock environment generally provides effective hydrologic isolation from the surface and shallow subsurface, pathways for upwelling and surface discharge of fluids from depth do exist. Preferential flow paths usually are combinations of structural elements such as faults and fracture zones. Depending on their orientations, faults and fracture zones may function as either recharge or discharge pathways. Structural pathways of much less than vertical dip, especially if they intersect the ground surface in upland areas, may support elevated hydraulic head leading to upward discharge where these pathways intersect high-angle faults or fracture zones. Hot springs are the most unambiguous manifestation of discharge from depth (e.g., Bucher, Zhang, and Stober, 2009). In the absence of hot springs, the existence of such flow paths may be hypothesized or confirmed based on combined data from surface geologic mapping, fluid and rock geochemistry, geophysical measurements, and subsurface investigations.

Subsurface excavations to a depth of 420 m and an array of 100 boreholes up to one kilometer deep at the Underground Research Laboratory in the Lac du Bonnet batholith provide access to groundwaters and subsurface expressions of fracture zones (elevation range approximately 300 to –100 masl; Frape et al., 2003). The large range in salinity between groundwaters near the surface and at a depth of 1,000 m is due mainly to increasing concentrations of sodium, calcium, and chlorine with depth. The compositional differences among fracture zones are an indication of the limited interconnectivity of these zones. In some locations, shallow groundwaters have a strong chloride signature that indicates upward movement and discharge of the deeper saline

groundwaters at the surface. These areas have localized discharge of helium gas, an additional and more sensitive indicator of groundwater discharge.

In the Black Forest region, the abundance of total dissolved solids can be an indicator of the source depth and a means to identify waters containing a component of upwelling, heavily mineralized fluid. Thermal waters sampled at depths of 2 to 505 m originated thousands of meters below the surface – calculated reservoir depths range from 2000 to 3400 m (Stober and Bucher, 1999). Non-thermal, low-TDS waters are present at depths to about 300 m. At depths of more than 300 m, the TDS is more than 1000 mg/kg, and at depths of more than 2000 to 3000 m TDS is greater than 5000 mg/kg. Within the regional population of wells is a subpopulation of wells less than about 500 m deep and with ostensibly non-thermal water, but with TDS well above 1000 mg/kg. Waters from these wells would merit additional analysis for geochemical signatures of an upwelling deep-water contribution.

Gorbatsevich, Ikorsky, and Zharikov (2010) investigated potential correlations of variations in helium-isotope ratios with changes in structure, anisotropy, and permeability in deep-seated rocks in the Kola Superdeep Borehole SG-3. These studies identified both a major fault and the contact between the Proterozoic and Archaean complexes as preferential flow paths for migration of deep fluids to the surface.

2.5.3.9 Long-Term Groundwater-Compositional Variations

An aspect of importance for the long-term geochemical stability of borehole disposal is the possibility that recharge waters may be enriched in dissolved oxygen during periods of glacial melt-water production (Spiessl, MacQuarrie, and Mayer, 2008). The potentially higher oxygen content of melt water during glacial periods, as much as three to five times higher than present-day interglacial recharge water, has been attributed to 1) the dissolution of air bubbles that are trapped in ice into glacial melt water; 2) the elevated pressure below the melting ice; and 3) a reduction in near-surface organic carbon as a result of soil erosion by glacial action and reduced photosynthesis. Increased oxygen input could result from increases in groundwater recharge rates as ice melting occurs beneath warm-based ice sheets in contact with exposed bedrock fractures.

2.5.4 Groundwaters in Younger Crystalline Rocks: Spain

Gómez et al. (2006) describe the hydrochemical characteristics of three former uranium-mine locations in the Central-Iberian Zone of the Hesperian Massif. The two locations in crystalline rock are 1) El Berrocal (Province of Toledo) and 2) Los Ratones mine in the Albalá Granitic Pluton (Cáceres Province).

El Berrocal is a 297 million-year-old (Pérez del Villar et al., 2003) altered granite pluton exposed at an altitude above 960 m. Groundwater recharge occurs at higher elevations and discharge at lower elevations. Quartz veins and major fractures are preferential flow zones. Groundwater samples come from 60- to 489-m depths. The Los Ratones mine is located in a concentrically zoned 302 million-year-old pluton at an altitude over 450 m. Both recharge and discharge occur within the extent of the pluton. Discharge is assumed

to occur along a broad, inclined fault zone. Groundwater was collected at depths from 24 to 469 m.

The water quality in both areas evolves from Ca-HCO_3 type near the surface to Na-Ca-HCO_3 types at intermediate depths and to Na-HCO_3 type at around the 465-m depth. The waters are dilute, with electrical conductivity values in the range of 100 to 700 µS/cm (Gómez et al., 2006). Equivalent total dissolved solids are 595 mg/L at Los Ratones and 227 mg/L at El Berrocal. Some waters from boreholes that intersect zones of uranium mineralization with sulfides have developed an Mg-Ca-SO_4 composition. These waters also tend to be relatively more concentrated.

Shallow and intermediate groundwaters at both sites have near-neutral pH (6.2 to 7.4), and the pH is buffered by calcite dissolution (Gómez et al., 2006). Deeper waters at Los Ratones, where complex carbonates [e.g., ankerite, $CaFe_{0.4}Mg_{0.6}(CO_3)_2$] are dissolving and cation exchange with smectites is occurring, become more alkaline (pH = 8.4).

All the waters from El Berrocal contain dissolved oxygen and have positive Eh values (Gómez et al., 2006). They are considered to be recharge waters in a transitional environment evolving toward isolation from the atmosphere. All groundwaters at Los Ratones have reducing Eh values and have dissolved-oxygen contents at or below 0.2 mg/L. Redox models for groundwaters related to the uranium deposit of Los Ratones have suggested that the Eh is maintained by arsenopyrite, pyrrhotite, and ferrihydrite equilibria.

Groundwaters shallower than 200-m depth at Los Ratones have tritium contents compatible with relatively short residence times in the flow system (Gómez et al., 2006) or the presence of a component less than 50 years old. Waters below 200 m have residence times greater than 60 years, based on tritium contents less than 0.7 tritium units. Fracture waters have carbon-14 ages ranging from 1.2×10^4 years at 200-m depth to 1.6×10^4 years at 500-m depths. Recharge temperatures, calculated from noble-gas concentrations and an assumed recharge elevation of 1,000 m, range from 11.3ºC at 60-m depth to 2.7ºC at 469-m depth.

2.5.5 Groundwater Geochemical Characteristics and Waste-Disposal Depth

Reducing and alkaline groundwater chemical conditions are most favorable to minimize corrosion of used-fuel containers and dissolution of used fuel. Canadian field studies indicate that groundwater at disposal-vault depths of 500 to 1,000 m in Shield rocks already are reducing and require no additional conditioning (Gascoyne, 1997). These favorable conditions exist, at least in part, because the deep groundwaters are old enough for surface-derived dissolved gases to have been consumed and for water-mineral reactions to approach equilibrium. In some areas, such as Laxemar, reducing conditions are present from the surface downward (Svensk Kärnbränslehantering AB, 2009). Obviously, long groundwater residence time is itself a favorable site attribute for waste isolation.

Deep groundwater geochemistry in younger crystalline rocks is expected to be more heterogeneous because these rocks are more likely to be in areas with significant topographic relief and complex patterns of groundwater recharge, transport, and discharge. Groundwaters in these settings may have shorter residence times allowing less modification of surface-derived constituents. The geochemical attributes of groundwater in such settings still could be acceptable for waste isolation, but more detailed characterization might be required. Additional compositional data for deep waters (> 500 m) from younger plutons that are not in geothermal areas will be needed to help develop site-selection criteria.

2.6 Review of Concrete and Metal Natural Analogs for Introduced Underground-Repository Materials

2.6.1 Introduction

Natural analog studies are often defined as investigations of natural environments or naturally occurring materials that provide information that may be applied to the underground nuclear-waste repository system. Included within the realm of natural analogs are investigations of man-made materials or artifacts that have remained for long periods of time in natural environments relevant to repository conditions (Miller and Chapman, 1995). General principles of natural-analog studies, including archaeological studies, are described by Chapman, McKinley, and Smellie (1984), Petit (1992), Miller et al. (2000), and in many other publications.

2.6.2 Concrete

Concrete in an underground nuclear-waste repository serves a direct function as a structural or sealing material in the engineered-barrier system. In addition, concrete may serve a designed or gratuitous function as a moderator of groundwater chemistry. Studies of archaeological and historical concretes have been undertaken to investigate the long-term mechanical durability and chemical stability of concretes as much as about 2000 years old. Unusual natural occurrences of minerals identical to those in concrete have provided an opportunity to characterize and model long-term mineral-water interactions. Neither natural nor archaeological materials are strictly equivalent to modern formulations, but studies of these materials are viewed as support for building confidence in predicting the performance of similar materials over hundreds of thousands of years.

2.6.2.1 Man-Made Concrete

The earliest well documented concrete technologies were invented by the Romans, although possible earlier uses are mentioned, for example, by Alexander (1995). The Romans had two basic formulations with different reactive ingredients. Both formulations contained slaked lime. Pozzolanic cement contained volcanic ash (pozzolana) that included easily soluble silica and alumina. *Opus signinum* contained crushed terra cotta or brick as sources of silica and alumina (Lancaster, 2008). Both formulations had so-called hydraulic properties, meaning that they would set up underwater. *Opus signinum* was used as a waterproofing material for cisterns and elements exposed to the weather. It was also generally used as a strengthening agent where pozzolana was not available.

Jull and Lees (1990) studied Roman concretes in Great Britain from Hadrian's Wall (circa 200 CE) and the Roman baths in London (circa 61 to 410 CE). Additional samples of Roman and Medieval concrete from Vicus Augustanus, southwest of Rome, Italy (*circa* first century CE and approximately 900-1100 CE). A sample of 19th century concrete at least 110 years old from Thomas More Street in London, taken from a concrete foundation in damp conditions, also was studied.

A sample from Hadrian's Wall contain calcium silicate hydrates (similar to constituents of modern concrete) in the innermost portion of the core, documenting that these compounds can persist for many hundreds of years. This observation is especially interesting because it is unclear that any sources of soluble silica and alumina were deliberately added to the cement mix. Silica and alumina may have been present in the limestone used to prepare the slaked lime. Jull and Lees (1990) note that the mortar and rubble core of Hadrian's Wall was placed in layers and that some layers are much better preserved than others, indicating that a high degree of workmanship also is required for durability. Calcium silicate hydrates also were observed in samples from Vicus Augustanus.

Most relative density and compressive strength determinations of Roman concretes were very low, and water absorption values very high, suggesting that the concretes contained many voids and generally were very weak (Jull and Lees, 1990). The only sample with a relatively high compressive strength was a waterproof bath lining from Vicus Augustanus. This sample contains both volcanic material and crushed burnt clay, such as brick or tile.

Determinations of pH showed that none of the Roman or Medieval concretes has maintained a very alkaline pH and therefore would not contribute to the long-term establishment of alkaline conditions favorable for immobilizing radioactive compounds such as plutonium (Jull and Lees, 1990). Only the relatively modern sample from Thomas More Street has maintained a pH of 10.4.

Rassineux, Petit, and Meunier (1989) studied mortars and concreted from Gallo-Roman thermal baths built in France in the first century CE. They found that the concrete matrices were composed mainly of calcium carbonate. Other phases included calcium aluminosilicates with compositions close to those of hydrogrossular and a hydrated calcium sulfoaluminate of the ettringite type. These minerals were formed only in concretes and mortars with crushed brick added. Their survival for about 1800 years attests to the durability of the minerals, which are essentially similar to minerals formed in modern concretes, so long as good preparation and installation practices were followed. Additional studies are summarized by Krupka and Serne (1998).

2.6.2.2 Geopolymers

A description of "geopolymers" should be introduced given their relevance to historical man-made types of concretes. The term "geopolymer" refers to a family of cementitious materials formed by subjecting aluminosilicate phases (e.g., kaolinite clay) to highly alkaline hydroxide (and/or silica-rich) solutions in order to form certain types of binder and concrete materials (Davidovits 1989, 1991, 2008; Duxson et al., 2007). The process

to form this type of materials involves gelation and polymerization of a silica-rich phase that generates a solid with remarkable cementitious properties. The term "geopolymer" has been used widely but other type of cementitious materials have very similar properties and fabrication methods such as alkali-activated cement, geocement, and hydroceramic (Russell et al., 2006; Duxson et al., 2007). Davidovits (1991, 1993) advanced the idea of ancient geopolymer concretes that are similar to the synthetic ones made today noting their remarkable durability and resistance to long-term natural weathering processes. There have been ideas for using "geopolymer" materials for nuclear waste encapsulation given the retention performance of this material (Hermann et al. 1999; Hanzlicek et al. 2006). However, like many other cementitious materials, most applications of geopolymers to radioactive waste disposal are focused on low- to intermediate level waste or for use in repository seal materials (Perera et al. 2007). This type of materials deserves consideration given their desirable properties for retention of hazardous metals and fabrication.

2.6.2.3 Salt-Saturated Concretes

Solutions concentrated in Na and Cl can be deleterious to cementitious materials, particularly in salt repository environments such as the WIPP. For this reason, the level of deterioration of the concrete phase is of particular interest to sites where long-term exposure to saline fluids is expected. Degradation of cements saline environments is characterized by loss of Ca and precipitation of Mg and sulfate-bearing phases which causes loss of strength in hardened concrete (Wakeley et al. 1993). To mitigate this deleterious effect on the cementitious phase, a salt-saturated form of concrete was developed to withstand rock salt repository environments. The development of such concrete was based on the enhancement in compatibility with the host rock to prevent chemical degradation in the form of cement dissolution and to minimize reduction of volume (e.g., induce expansiveness) after emplacement, thus preventing loss of cohesiveness (Wakeley, 1987). This type of cement has a composite nature made from a mixture of NaCl, sand/gravel mixtures, fly-ash, $CaSO_4 \cdot 0.5H_2O$, and Portland cement. Some work has been documented of this type of concrete as part of the WIPP repository project to investigate the leachability and reaction mechanism for cement deterioration (Wakeley, L.D., 1987).

2.6.2.4 Low-pH Concretes

Low-pH concretes refer to cementitious materials with the least amount of portlandite ($Ca(OH)_2$) as a binder (Dole and Mattus, 2007.) The low amount of soluble portlandite as a binder is replaced by a phase having a high silica content like silica fume or fly-ash to provide more resistance to potential deleterious interaction with groundwaters. For this reason, low-pH concretes have a good resistance to leachability even to water chemistries that may be aggressive to cement types containing a large fraction of Portland cement. Calvo et al. (2010) report the results of leaching experiments with cements having various levels of Ordinary Portland Cement (OPC) content. Their results show that the pore water chemistry for the cement mixture having the highest silica content shows the lowest pH. A decrease in pH for waters derived from reacted cementitious materials is considered beneficial in nuclear waste repository environments as to prevent deleterious EBS and waste form material degradation expected from strongly alkaline pore solutions. There is a need for a comprehensive compilation of leaching data for this

and other types of cements to then evaluate the leachate chemical characteristics for various cement compositions.

2.6.2.5 Natural Concrete Minerals

An unusual geologic occurrence at Maqarin, Jordan, provides an opportunity to study and model mineral-water interactions relevant to concrete interactions with the aqueous environment (Khoury et al., 1992; Alexander et al., 1992). This site appears to be unique in that the hyperalkaline groundwaters in the area are the product of leaching of an assemblage of natural cement minerals produced by high-temperature metamorphism of marls and limestones (Miller et al., 2000). The groundwater pH is buffered at 12.5 by abundant portlandite, $Ca(OH)_2$, in the source rock. In a younger part of the groundwater system, the water contains much higher concentrations of Na and K with a pH of 12.9, suggesting control by NaOH and KOH.

The conceptual model of the Maqarin system as a natural analog for concrete assumes that cement leachates rich in Na, K, and Ca flow outward from a repository, driven by the groundwater-flow system. As the plume begins to interact with the host rock, a complex sequence of reactions can occur, involving dissolution of aluminosilicate minerals in the rock and precipitation of calcium silicate hydrate compounds and, eventually, zeolites as the pH decreases and the aluminum concentration increases in the groundwater (Miller et al., 2000). Numerical models of this system continue to be developed and tested.

2.7 Metals

Metals will be present in the EBS as canisters and overpacks for vitrified high-level waste and spent fuel and as rock supports and reinforcements (Miller et al., 2000). In the post-closure repository environment, these metals will begin to corrode. Metal corrosion proceeds by a series of complex processes. As corrosion progresses, a metallic compound may be formed on the metal surface, although some metals (such as copper) may corrode under certain conditions without the formation of any compound at the surface. This layer of corrosion product may limit the flow of metal ions to solution, slowing the corrosion rate. This property is called passivity, and the formation of a passive film on the metal surface may slow down further corrosion. When a passivating layer is physically damaged or suffers chemical attack, then localized corrosion may occur. The processes of corrosion and passivation are discussed by Miller et al. (2000). Ancient archaeological metals of relevance for waste disposal include copper, bronze, iron, and iron alloys. Natural metallic objects include native copper and iron, metallic meteorites, and Fe-Ti oxides. The work by Johnson and Francis (1980) is an example of a comprehensive study of corrosion rates of archaeological artifacts and meteoritic iron. The artifacts exhibited similar corrosion rates of between 0.1 and 10 μm/year. Additional studies are described by Miller et al. (2000).

2.8 Discussion and Conclusions

Jull and Lees (1990) point out that concrete is a very complex material with a large number of variables potentially contributing to the relative durability of historic concretes. Many of these variables, such as the exact proportions and compositions of ingredients and the methods of preparation and installation, cannot be reconstructed with a high degree of confidence. They recommend that results of their studies should be used

to develop mixes for "Roman" concretes. These laboratory-made materials should be subjected to tests similar to those used to characterize the actual ancient concretes. This would give an insight into the behavior of young "Roman" concrete and would indicate whether the comparison between ancient and modern concretes is valid. Some university programs (e.g., MIT, 2002) are addressing these issues.

Miller et al. (2000) highlight the existence of relatively few *in situ* studies of concrete interactions with adjacent rock. This is a potential area for further study, but one that would require greater integration of archaeological and geochemical studies from the inception of investigation than has generally been the case.

In regard to metal archaeological analogs, Miller et al. (2000) stress the desirability of obtaining materials fresh from the interment environment rather than from museum collections. Collections of items, such as buried iron nail hoards, provide better opportunities to determine average corrosion rates without the bias of focusing on the best-preserved items and excluding the most heavily corroded material.

Modern archaeological projects are becoming increasingly involved in salvage investigations where the site will be destroyed or will not be preserved in an accessible form. Also, more investigations are located at more mundane, non-royal sites where concretes and metallic materials are less likely to be unique or to possess very high artistic or architectural merit. These recent developments may offer increased opportunities for collaborations between the archaeological and materials-science communities.

3. Cement, Clay, Sulfate, and Asphalt Stability in Near Field Environments

3.1 Cement chemistry

Cement chemistry plays an important role in industry. Applications to the nuclear fuel cycle have focused on reactor pools and containment for decades. However cement/concrete research for nuclear fuel disposal has focused on the application for Yucca Mountain specific unsaturated and low thermal load problems. Therefore LANL has undertaken to look at other research on cement/concrete to gauge useful information developed from international nuclear programs and industrial applications. Information was gathered on experimental work (lab and field scale), modeling efforts, thermodynamic calculations, analytical characterization of phases, and degradation phenomena.

Skibsted and Hall (2007) provided a review paper of analytical quantification instruments (X-ray and neutron diffraction, nuclear magnetic resonance, X-ray absorption and Raman Spectroscopy) for the characterization of cement minerals and their reaction products. The review article provided good information on various strengths and weaknesses of the techniques described above. There may be significant developments concerning the application of Raman Spectroscopy in the near future. The authors provided a very complete discussion of secondary mineral phases and nature of cement heterogeneity.

Glasser et.al. (2008) developed an excellent major review paper on cement degradation. Their discussion primarily centers on mechanisms of transport of ions, moisture and gases in degrading cement, and three chemical degradation phenomena (chloride, carbon dioxide, and sulfate). The sulfate attack from external sources resulting in the formation of ettringite and thaumasite are described. The article includes modeling efforts by the authors and review of other models. They conclude that the mineralogy of Portland cement is very sensitive to temperature and thermal cycling, especially during the early hydration period.

Extensive work has been done at the Grimsel site in Switzerland, involving laboratory and integrated field scale experiments, along with reactive transport modeling. Mader, et al. (2006) studied hyperalkaline fluid (from degraded concrete) transport in fractured rock at Grimsel site. In their study a hypersaline solution (K-Na-Ca-OH; pH 13.4) representing an early leachate of Portland cement degradation, was injected into shear zone. This was done both at a lab and field scale. Fluid transported and deposited calcite in veins over short distances, allowing for self sealing. Their work resulted in a long term field experiment, which was well thought out, provided a good data set which can be used for further experiments. Furthermore, the authors described their test equipment information in detail. The results of the study are as follows; 1) fluids are very reactive and cause significant dissolution and precipitation, changing flow field, 2) high pH plume is possible from cement, 3) self sealing of flow paths observed in both experiments, 4) results are transferable between experiments.

An earlier article by Soler and Mader (2005) described reactive transport calculations produced using kinetic rate laws for mineral reactions. The mineral reaction rates taken from literature experimental results, not the tests at Grimsel. Both diffusion and advection solution transport taken into account in model (GIMRT). However the experimental data and model did not match well. Furthermore, the authors did not identify secondary mineral phases formed. Therefore these two factors did not provide a model that was convincing. Once the field data from Mader, et al. (2006) was included, their overall transport model was much more convincing.

Two peer review articles focusing on radionuclide leaching from cement waste forms are very useful. The first article by Kienzler (2000) described experimental leaching of radionuclides from cement waste forms (Morsleben repository site in Germany in saline brines) over 19 year period. The authors focused their work on determining pore volumes of cement and relation to water/cement ratio of waste forms. They included a fairly good data base for EQ3/6 concerning Cs, U, Np. However, their model only “loosely correlates” to experimental data, and the authors call for more work on Pitzer parameters for U, Np, Al and Si species and solids. The second article by Schuessler, et.al. (2001) focused on the influence of buffer materials such as MgO / CaO and clays on the sloubilities of Am, Np, Pu, and U. The analysis was performed on low level cemented waste forms in contact with $MgCl_2$ saturated salt brine (Q brine). The resulting actinide solubility was modeled in the German salt repository with two buffers (MgO only, MgO and Clay). The final results determined that; 1) MgO may limit CO_3^{--} concentration and thus, actinide carbonate complexation. 2) smectite dissolution lowers pH and therefore may increase actinide solubilities.

Pfingstein (2002) used simplified experiments and modeling (MCOTAC) to discuss self sealing of fractures by calcite precipitation. The purpose is to look at the effects of cement degradation and secondary mineral precipitation. He presents an early attempt at thermodynamic-based modeling effort. The modeling primarily charts an advection-dispersion and diffusion system. The model presented neglects the effect of kinetics, host rock composition, rock heterogeneities, and metastable phases. Furthermore, near field geometry, structure and geochemistry is rudimentary in the model. Conclusions of the paper stated that research is needed in the following areas; 1) relevant repository scenarios: 2) expand and improve existing thermodynamic data, 3) metastable phase retention, and 4) relevant experiments

Matschei et.al. (2007) produced a review paper on the thermodynamic properties of cement hydrates in the system $CaO–Al_2O_3–SiO_2–CaSO_4–CaCO_3–H_2O$. Their focus was to produce a database for commonly-encountered cement substances including C–S–H, $Ca(OH)_2$, selected AFm, Aft, and hydrogarnet compositions as well as solid solutions. The data were obtained for the most part from experiment and many of the predicted reactions were confirmed by focused experiments. The temperature-dependence of the thermodynamic data for the above phases, determined partly from experiment and partly from thermodynamic estimations, is also tabulated in the range 1 °C to 99 °C. The new database enables the ultimate hydrate mineralogy to be calculated from chemistry: most solid assemblages, the persistence of C–S–H apart, correspond closely to equilibrium conditions. The development of a thermodynamic approach also enables a fresh look at how mineralogical changes occur in response to environmentally-conditioned reactions. From their modeling endeavors, the authors were able to determine that depending on the bulk chemistry of the overall system, calcite, ettringite, and/or hydrogarnet may be stable at low temperatures. They believe that kinetics may hamper the formation of these phases in many instances.

3.2 Thermodynamic Data and Modeling of Cement Phases

The thermodynamic database developed for the Yucca Mountain Project (YMP) contains 42 cementitious materials plus other associated phases (see Wolery and Jové-Colón, 2007). Cementitious materials are a fundamental part of many EBS concepts whether in the form of backfill/buffer or seal material. Therefore, cementitious materials also constitute an important part of the EBS chemical environment. A general review of the literature on the chemical modeling of cementitious phases provides the basis for investigating the effects of solution interactions with these materials in the EBS. The use of thermodynamic modeling to evaluate chemical equilibria between cement phases, aqueous solutions, and gases has been advanced as a powerful tool for modeling these interactions (Gartner and Jennings 1987; Reardon 1990; Matschei et al. 2007).

Cementitious materials are compositionally complex phases. The compilation of thermodynamic and solubility data was restricted to cement phases for which either solubility and/or thermodynamic data are well-constrained, even for the common cement phases. For example, thermodynamic data for some cement phases are given by their pure end-member compositions. Still, for the purpose of establishing the groundwork for a modeling framework for cementitious materials these data are useful even with all inherent limitations on data availability, uncertainties, and compositional variability present in cement phases.

The cement phases and selected thermodynamic data in this YMP thermodynamic data compilation are given in Table 3.2.1. The sources reviewed in this compilation effort (Taylor 1990; Reardon 1992; Bruton et al. 1993; Atkins et al. 1992; Neall 1996; Batchelor and Wu 1993; Sarkar et al. 1982; Atkins et al. 1993; Shaw et al. 2000; Glasser et al. 1987; Damidot et al. 1994; Bennett et al. 1992; Babushkin et al. 1985; Greenberg and Chang 1965; Fujii and Kondo 1983; Harvie et al. 1984; MacPhee et al. 1989; Berner 1987, 1990; Greenberg and Moller 1989; Perkins and Palmer 1999, Matschei et al., 2007). Some of these sources also include previous modeling studies from U.S. and international nuclear waste research programs. The cement phases listed in Table 3.2.1 are considered common to the hydration of Portland cements and are generally limited to the Ca-Al-Si-S-Mg-H_2O system. In some cases, the phase naming is consistent with the nomenclature used for cement phases (see Taylor 1990). Perkins and Palmer (2000) reports a log K value at 25°C for the reaction $CaCrO_4(aq) = Ca^{2+} + CrO_4^{2-}$ (log K = –2.77) consistent with the solubility data for Cr-ettringite given in that source and it's also included in the YMP thermodynamic database (Wolery and Jové-Colón, 2007). Other phases associated with cementitious materials are also included in the thermodynamic database with log K values up to 300°C: gypsum, wollastonite, brucite, portlandite, lime, ferrite-Mg, ferrite-Ca, ferrite-Cu, ferrite-dicalcium, sepiolite, gibbsite, anhydrite, and periclase. The only exception is for the minerals gypsum and sepiolite where the log K values are only given up to 300°C. Data for the calcium silicate hydrate (CSH) cement phase are from Fujii and Kondo (1983). Thermodynamic data for supporting aqueous species in all cement reactions are given in Wolery and Jové-Colón (2007).

The evaluation of thermodynamic data for cement phases described in Wolery and Jové-Colón (2007) was to a large extent based on the data obtained in the thermodynamic compilation of Babushkin et al. (1985). Evaluation of thermodynamic data parameters was performed by cross-check of data values for several cement minerals and these were found to be the either the same or in good agreement with the tabulated data. The compilation by Sarkar et al. (1982) provides thermodynamic data from various sources in the literature. These authors evaluated and selected the best values for heats of formation, standard entropies, and free energies of formation for calcium silicates, aluminates, and ferrites including data for other cement phases including CSH gel and Friedl salt. Sarkar et al. (1982) determined that the best thermodynamic data source for many cementitious phases is a data compilation volume translated from Russian entitled *Thermodynamics of Silicates*. The revised version of this book was published in English in 1985 as Babushkin et al. (1985). Heat capacity data for most of the cement phases were extracted from Babushkin et al. (1985). The exception is the phase CSH for where the heat capacity values were estimated $C_p°$ data for portlandite, alpha-quartz, and H_2O (see Wolery and Jové-Colón 2007). Also, the heat capacity data for $CaCl_2(cr)$ was used to extend the log K values for CSH and Friedl salt phases to elevated temperatures. The extrapolation method of the log K values as a function of temperature assumes an approximation of the cement heat capacity based on the heat capacity values of the stoichiometric constituent oxides, hydroxides, and salts to form the cementitious phase (Helgeson et al. 1978). This approximation is considered reasonable, however, further refinement of the solubility constants as a function of temperature are needed to better constrain these extrapolated values. The the Maier-Kelly equation defined by Johnson et

al. (1992) for the standard hea0074 capacity $C_p°$(cal/mol K) is used here for the extrapolation of this parameter as a function of temperature:

$$C_p^\circ = a + bT + \frac{c}{T^2}$$

where T is temperature in degrees Kelvin. The coefficients a, b, and c in the above equations corresponds to those listed in Table 3.2.2. Wolery and Jové-Colón (2007) provide more details on the estimation methodology for the retrieval of thermodynamic parameter data of cementitious phases. Table 3.2.2 provide a partial list of thermodynamic data for cement phases taken from Wolery and Jové-Colón (2007). Only the data developed for the YMP thermodynamic database was included in this table.

3.2.1 Cement Leaching Modeling Test Case: Preliminary Results

One of the purposes of the thermodynamic modeling and chemical equilibria is to provide a predictive tool for the evolution of water chemistries reacting with cementitious materials and the resulting secondary phases from such interaction. As a preliminary test, a reaction path calculation using the computer code EQ3/6 (Version 8.0; Wolery and Jarek, 2003) and the YMP thermodynamic database were conducted to compare results with those obtained in long-term (~9.5 years) Ordinary Portland Cement (OPC) leaching experiments described by Kienzler et al. (2000) and Metz et al. (2004). This comparison is to a large extent qualititative since the EQ3/6 code results are time-independent. However, the main purpose is to provide a *quantitative* comparison of the Ca and S composition trends of the leachate solutions observed for the time span of these experiments. It should be noted that Metz et al (2004) conducted a similar trend analysis but with a different thermodynamic database and a different version of the EQ3/6 code. The reacting solution composition corresponds to that for the Q-brine which is essentially a concentrated $MgCl_2$ brine (Kienzler et al. 2000). Activity coefficient corrections for the concentrated $MgCl_2$ brine are achieved through the use of the Pitzer approach which is implemented in the EQ3/6 code using parameter values from the Pitzer database developed for the YMP (see Appendix I of Mariner, 2007). EQ3/6 code runs in a reaction path mode can be described as irreversible mass transfer equilibrium calculations progressing as a series of discrete steps where reactant is added to the solution (similar to a titration process) and the extent of reactant mass converted to reaction products is measured by the reaction progress variable (ξ). Figs. 3.2.1a and 3.2.1b show the EQ3/6 code results plotted as a function of the reaction progress variable (ξ). As depicted in these two figures, there is a good agreement between the overall total Ca and S concentration evolution trend of the brine given by the code calculations and that observed in the experiments. The reaction path trend curves are defined by an assemblage of saturated or equilibrium solids denoted by the curve labels. The ‘kinks’ in the curves correspond to a change in the equilibrium mineral assemblage or the appearance of saturated solids along the reaction path. These type of calculation involved some caveats and assumptions in the form of solid phase suppressions. Justification for suppressing solids from forming in the computed reaction path is mainly based on considerations of common alteration products observed in cement degradation. For example, the phases dolomite, talc, and anhydrite were suppressed on the basis of temperature considerations for the known stability regimes of these phases. Various EQ3/6 code runs were conducted to test the sensitivity of these imposed solid suppressions on the resulting compositional trends indicating that their effect is relatively

minimal relative to the overall experimental data. Another assumption is the use 25°C as the temperature for the code calculations even when the experiments being compared in this exercise were conducted at 40°C. The justification for this is that some solid phase thermodynamic data is only available at 25°C. Still, exploratory code runs were conducted at 40°C and the effect of temperature in this case was also minimal on the overall compositional evolution of the brine phase.

It should be emphasized that these are preliminary results and this effort is still on-going in evaluating these leaching data and cement phase solubilities. Work is planned to assess the following:

- Expanding the list of cementitious phases currently in the YMP thermodynamic database for which adequate data is available.

- Conduct a comprehensive evaluation of existing thermodynamic data for cement phases against other sets of data. This effort could translate in data updates and/or refinements.

- Create catalog of test cases and benchmark problems for predicted thermodynamic properties and solubilities of cement phases. This could be, for example, in the form of predicted solubilities versus experimental data as function of temperature.

- Expand thermodynamic modeling methologies to include C-S-H cement solid solutions between $Ca(OH)_2$ and SiO_2 to capture the large range of Ca/Si ratios for the compositional variability exemplified by hydrated cement mixtures. Examples of such thermodynamic modeling approaches are given by Sugiyama and Fujita (2006) and Carey and Lichtner (2007).

- Establish synergies with other research programs such as the Cementitious Barriers Partnership (CBP) which is sponsored by DOE-EM.

Table 3.2.1. Sources of Data for Common Cementitious Phases (after Wolery and Jové-Colón, 2007)

Cement Phase	Taylor 1990	Reardon 1992	Bruton et al. 1993	Atkins et al. 1992	Neall 1996	Batchelor and Wu 1993	Sarkar et al. 1982	Atkins et al. 1993	Harvie et al. 1984	Bennett et al. 1992	Matschei et al. 2007	Included in YMP Database[d]?
Afwillite	X		X				X	X				Y
Allite (C_3S)	X	X					X				X	Y
Anhydrite	X	X							X		X	Y
Bellite (C_2S)	X	X					X				X	Y
Brucite	X	X		X					X			Y
$C_{12}A_7$	X						X					Y
C_2AH_8	X					X	X				X	Y
C_3A	X	X					X				X	Y
C_3AH_6											X	N
C_4AF	X	X									X	Y
C_4AH_{13}	X	X		X		X	X	X			X	Y
C_4AH_{19}	X						X					Y
CA	X						X					Y
CA_2	X						X					Y
CAH_{10}	X						X				X	Y
C-S-H[a]	X	X		X	X	X	X	X		X	X	Y
Ettringite	X	X		X	X	X	X	X			X	Y
Ferrite-Ca	X						X					Y
Ferrite-Dicalcium	X						X					Y
Foshagite			X				X					Y
Friedl Salt[b]	X					X	X	X				Y
Gehlenite Hydrate[c]	X			X				X		X		25[d]
Gibbsite	X	X		X							X	Y
Gismondine-Na								X				25[d]
Gismondine-Ca								X				25[d]
Gypsum	X			X					X		X	Y
Gyrolite	X		X				X					Y
Hillebrandite	X		X				X					Y
Hydrogarnet	X	X		X	X		X	X		X	X	Y
Hydrotalcite[e]	X	X		X	X			X		X		25[d]
Jennite[a]	X							X			X	Y
Monocarboaluminate		X				X		X			X	25[d]

Table 3.2.1. Sources of Data for Common Cementitious Phases (Wolery and Jové-Colón, 2007) (Cont.)

Cement Phase	Taylor 1990	Reardon 1992	Bruton et al. 1993	Atkins et al. 1992	Neall 1996	Batchelor and Wu 1993	Sarkar et al. 1982	Atkins et al. 1993	Harvie et al. 1984	Bennett et al. 1992	Matschei et al. 2007	Included in YMP Database?
Monosulphate	X	X		X		X	X	X			X[j]	Y
Nekoite			X									N
Okenite			X				X					Y
Periclase	X	X										Y
Plombierite[f]	X		X				X					Y
Portlandite	X	X		X	X				X		X	Y
Reyerite			X									N
Riversideite[g]			X				X					Y
Syngenite	X	X				X			X			25[d]
Thaumasite	X											N
Tobermorite-1.1nm[h]	X		X	X			X	X			X	Y
Truscottite	X		X									N
Xonotlite	X		X				X					Y
$CaSO_4 \cdot 0.5H_2O$ (beta)												Y
Hemicarboaluminate											X	25[d]
Tricarboaluminate[i]											X	N

[a] C-S-H can be a solid solution. Note that Glasser et al. (1987, p. 338) indicates that Portland cement generally hydrates to give a C-S-H composition with a Ca/Si ratio close to 1.7. Matschei et al. (2007) provides data for two types of C-S-H phases: jennite-type (Ca/Si=1.67) and tobermorite-type (Ca/Si=0.83). The C-S-H phase included in the YMP database closely resembles the Ca/Si ration of a jennite-type cement.

[b] Often listed as $C_3AlCaCl_2 \cdot 10H_2O$ or called calcium chloroaluminate hydrate (Taylor 1990). The reported name for this phase in the cement literature is "Friedel's salt," not "Friedl Salt."

[c] Also known as strätlingite (Taylor 1990; Matschei et al. (2007)).

[d] The annotation "25" indicates 25°C data only. "Y" signifies "yes" and "N" corresponds to "no".

[e] Hydrotalcite referred to here is the formulation of Bennett et al. (1992), not the natural hydrotalcite mineral with a formula of $(Mg_{0.75}Al_{0.25}[OH]_2)][(CO_3)_{0.125}(H_2O)_{0.5}$.

[f] 1.4 nm tobermorite is also known as plombierite (Shaw et al. 2000, p. 143).

[g] 9 nm tobermorite is known as riversideite (Shaw et al. 2000, p. 143).

[h] This is commonly referred to as "normal" tobermorite or tobermorite 11Å.

[i] Never reported to occur in cement pastes exposed to intensive carbonation (Damidot et al. 1994, p. 563).

[j] Reported in Matschei et al. (2007) as monosulfoaluminate.

NOTE: Listing includes minerals used in modeling studies. For the cement phase nomenclature, the letter "A" stands for Al_2O_3, "C" for CaO, "S" for SiO_2, and "H" for H_2O components in the cement. The work of Matschei et al. (2007) was not evaluated for cementitious phases included in the YMP thermodynamic database (Jové-Colón, 2007). This work is currently in the process of examining the work Matschei et al. (2007) for evaluation, refinement, and expansion of the YMP thermodynamic database for cement phases.

Table 3.2.2 Thermodynamic Properties of Calcium Silicates and Aluminates in the YMP thermodynamic database (modified after Wolery and Jové-Colón, 2007)

					Heat Capacity Coefficients[a]		
Solid Phase	**Formula**	**$\Delta G°_f$ (cal/mol)**	**$\Delta H°_f$ (cal/mol)**	**$S°_{298}$ (cal/mol)**	**a (cal/mol-K)**	**b × 10^3 (cal/mol-K^2)**	**c × 10^{-5} (cal-K/mol)**
Allite (C_3S)	$3CaO·SiO_2$	-665470	-700430	40.3	49.85	8.62	-10.15
$C_{12}A_7$	$12CaO·7Al_2O_3$	-4410000	-4640160	249.7	301.96	65.5	-55.3
C_2AH_8	$2CaO·Al_2O_3·8H_2O$	-1151540	-1299200	106.4	68.38	153.45	-
C_3A	$3CaO·Al_2O_3$	-808400	-851000	49.1	62.28	4.58	-12.1
C_4AF	$4CaO·Al_2O_3·Fe_2O_3$	-1144000	-1214200	78	89.49	17.4	-
C_4AH_{13}	$4CaO·Al_2O_3·13H_2O$	-1756170	-1988000	171.6	109.6	242.19	-
C_4AH_{19}	$4CaO·Al_2O3·19H_2O$	-2096330	-2411000	228	122.36	394	-
CA	$CaO·Al_2O_3$	-527700	-556180	27.3	36.01	9.98	-7.96
CA_2	$CaO·2Al_2O_3$	-907100	-957060	42.5	66.09	5.48	-17.8
CAH_{10}	$CaO·Al_2O_3·10H_2O$	-1103700	-1271400	116.1	67.85	182.46	-
C-S-H (1.7)	$1.7Ca(OH)_2SiO_2{:}0.917H_2O$	-628585.1	-690726.6	47.8	46.54	9.27	-1.35
Afwillite	$Ca_3Si_2O_4(OH)_6$	-1052950	-1143200	74.6	81.54	45.1	-14.7
Bellite (C_2S)	$2CaO·SiO_2$	-524190	-551740	30.5	36.25	8.83	-7.24
Ettringite	$3CaO·Al_2O_3·3CaSO_4·32H_2O$	-3634260	-4201320	417.6	208	740.93	-
Cr-ettringite	$Ca_6Al_2\ (CrO_4)_3(OH)_{12}·26H_2O$	-3616395.8	-4141969.4	-	-	-	-
Foshagite	$Ca_4Si_3O_9(OH)_2·0.5H_2O$	-1347900	-1439900	78.95	87.95	3.95	-13.5
Friedl Salt	$CaCl_2·3CaO·16H_2O$	-	-1833000	-	-	-	-
Gismondine-Na	$Na_2Al_2Si_2O_8•4H_2O$	-1179160	-	-	-	-	-
Gismondine-Ca	$CaAl_2Si_2O_8•4H_2O$	-1187450	-	-	-	-	-
Gyrolite	$Ca_2Si_3O_7(OH)_2·1.5H_2O$	-1085650	-1175850	64	79.47	36.3	-17.6
Hillebrandite	$Ca_2SiO_3(OH)_2·0.17H_2O$	-592900	-637150	38.4	41.4	22.4	-7.4
Hydrogarnet	$3CaO·Al_2O_3·6H_2O$	-1198400	-1326000	96.7	68.91	127.17	-
Monosulphate	$3CaO·Al_2O_3·CaSO_4·12H_2O$	-1859140	-2096440	178.6	113.71	246.84	-
Okenite	$CaSi_2O_4(OH)_2·H_2O$	-686400	-750300	40.9	44.81	18.7	-10.4
Plombierite	$5CaO·6SiO_2·10.5H_2O$	-2647300	-2911250	193.15	132.2	270	-
Portlandite	$Ca(OH)_2$	-214739.5	-	-	101.79	18.0	–1.74
Riversideite	$Ca_5H_2(SiO_3)_6·2H_2O$	-2215000	-2375000	122.65	143.55	74.7	-20.8
Tobermorite	$5CaO·6SiO_2·5.5H_2O$	-2361450	-2556300	146.15	110.6	189	-
Xonotlite	$Ca_6[Si_6O_{17}](OH)_2$	-2259400	-2396700	121.3	132.25	65.2	-18.4

Sources: Babushkin et al. 1985, Appendix 1.
Cr-ettringite data, which are for 25°C, are from Perkins and Palmer 2000.
CSH(1.7) data is from Fujii and Kondo 1983.
Portlandite data are from Barin and Platzki (1995).
Gismondine (Na, Ca) data is from Atkins et al. (1993).

[a] Heat capacity coefficients refer to those for the $C_p°$ equation defined in Section 3.2.

NOTE: The nomenclature for cement phases is as follows: letter "A" stands for Al_2O_3, "C" for CaO, "S" for SiO_2, and "H" for H_2O components in the cement.

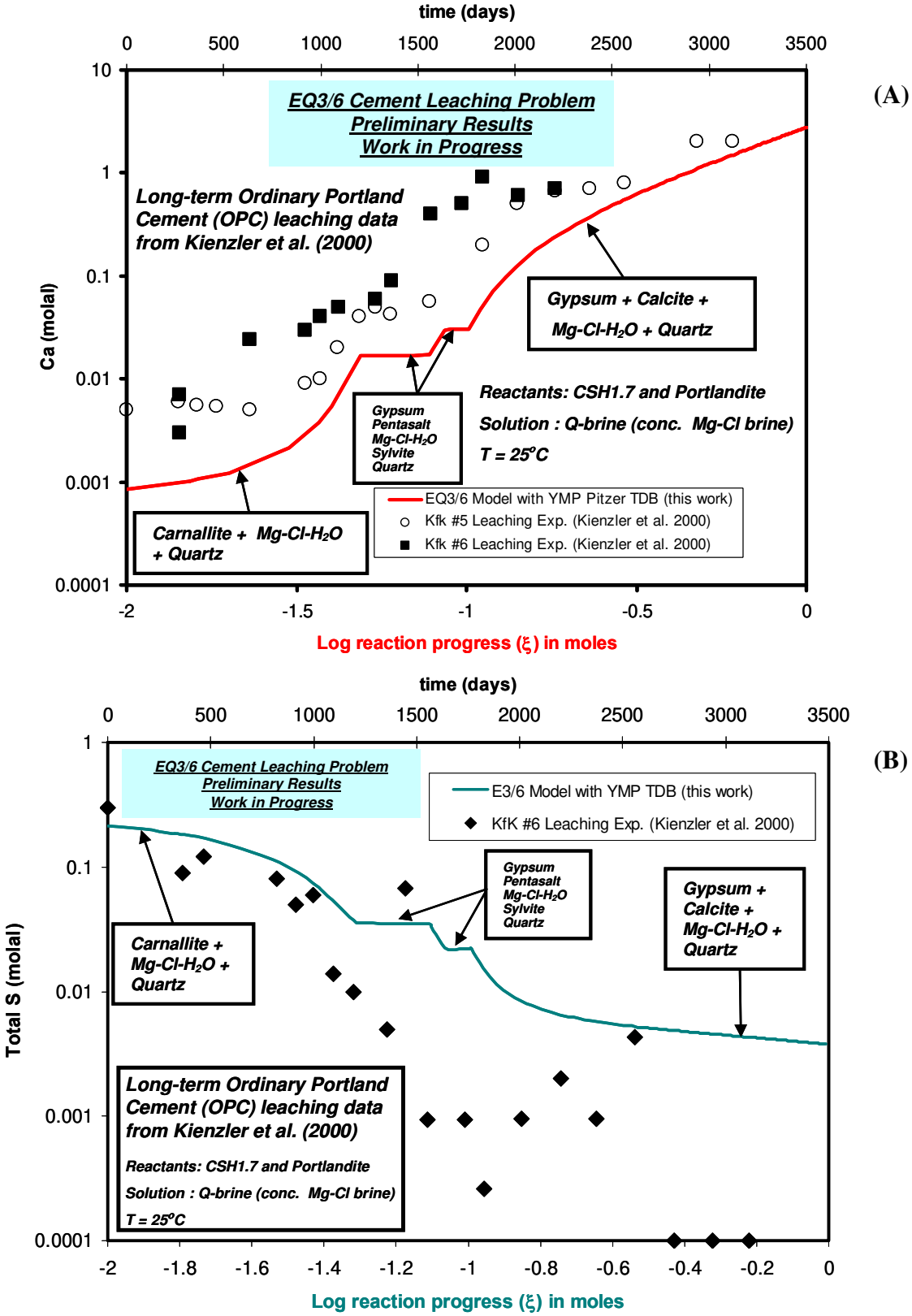

Figure 3.2.1. EQ3/6 results for the leaching of Ordinary Portland Cement (OPC). Symbols denote experimental data from Kienzler et al. (2000) for total concentrations of (A) calcium and (B) sulfur. See text for explanation.

3.2.2 Summary – Cement chemistry

Many different experiments concerning cement stability and leaching have been conducted by industry and international programs for nuclear waste disposal. Of the various experiments performed, very few examples scale up well from bench top. The retrieval of thermodynamic data for cementitious materials and its use with modeling tools has proven very useful in evaluating a wide range of problems on cement phase stability.
The following research is needed in the following areas;

- Relevant repository scenarios(pressure, temperature, brine, associated EBS materials, Redox) as dictated by the Used Fuel Campaign
- Expand and improve existing thermodynamic data,
- Phase equilibria studies on metastable phase retention and the role of kinetics, and
- Relevant experiments using suitable materials (and complex associations) at repository conditions

3.3 Clay Partial Dehydration and Stability

3.3.1 Introduction

Many minerals such as clay and gypsum contain water in the form of water molecule and/or hydroxyl. Clays, in particular, are present in significant amounts in many rocks surrounding potential geological repositories and are very important EBS buffer/backfill materials. When these minerals are heated above their dehydration/dehydroxylation points, due to radiation decay and any other heat sources, they decompose into water (liquid or vapor) and other minerals (typically denser phases). This process will release water to the neighboring environments. It may also reduce the volumes of the minerals, thereby causing changes in host rock strength, porosity and permeability. These processes may affect groundwater flow and thus related radionuclide transport. The extents of these effects may vary considerably, depending on the type of hydrous mineral, its dehydration/dehydroxylation temperature, its content in the host rock, the rock's location (both relative to the waste loadings and its depth) and thermal profile (as a function of time) of the repository.

3.3.2 Background and Significance

Clay dehydration is a step function that involves large and sudden volume changes that are related to release of water with the loss of water layers. Described below is a case study of Yucca Mountain (YM) (Bish 1988), in which clay minerals (especially smectites) are of primary concern.

Smectites are abundant (up to 50%) in the smectite- and zeolite-rich zone immediately beneath the Topopah Spring Member, the waste host rocks in the YM repository. Smectites are important in a repository environment as their volumes, water contents and stability can be affected by even small variations in temperature and partial water pressure, thereby resulting in changes in water amount in the environment and potentially in the host rock strength, porosity and permeability. In a repository, emplacement of waste will increase temperature and thus will change the water vapor pressure, especially

in a closed system. Since in such a geological system, the partial water pressure is typically lower than the total pressure, dehydration of smectites might occur below the boiling point of water (Koster van Groos and Guggenheim 1986). Different behaviors are expected depending on whether the rocks are unsaturated or saturated. Previous modeling studies (e.g., Travis and Nuttall 1987) on the thermal history of the Topopah Spring Member with waste loadings indicate that significantly elevated temperatures can be maintained for up to 1000 years. The zone within 20 m of the repository may be heated to temperatures > 100 °C. Moreover, an area of reduced water saturation will surround waste canisters, which in turn will be surrounded by a small volume of increased saturation that levels off to ambient saturation conditions. In the reduced saturation area, water pressures will be > 1 atm and temperatures > 100 ˚C. Hence, it was important to consider the effects of elevated temperatures and variable water vapor pressure on dehydration behavior and stability of smectites in the YM repository.

The thermal behavior of smectites may involve in several phenomena: (1) reversible collapse/expansion of the smectite layers due to loss/gain of interlayer water at water vapor pressures < 1 atm; (2) irreversible collapse of the smectite layers due to loss of interlayer water and migration of interlayer cations into the layers; (3) irreversible reduction of the osmotic swelling capacity of smectites in a steam atmosphere; and (4) inhomogeneous transformation of smectites into interstratified illites/smectites at temperatures > 300 °C. Of these four types of thermal reactions, reversible collapse and collapse in a steam environment probably play more important roles in a repository environment.

The amounts of water lost during dehydration but before dehydroxylation may vary considerably depending on the type of smectite (El-Barawy et al. 1986). Monovalent-cation smectites can be completely dehydrated at 100°C and 1 atm, whereas divalent- and trivalent-cation smectites may retain their interlayer water up to about 175°C. Smectites may contain > 30 wt% water in a saturated atmosphere, and much of this water can be lost at low temperatures with low heating rates. Therefore, smectites can be an important source of water in a repository, which affects groundwater amount and flow properties and thus the radionuclide transport.

Colten (1986) performed experimental runs on Na saturated montmorillonite in contact with NaCl solutions at temperatures as high as 200^{o}C and hydraulic pressures as high as 456 bar. Results of the experiments indicate that increased hydraulic pressure appears to favor hydration, as does decreasing salinity. Since there were no basal spacing changes with temperatures up to 200^{o}C the author concluded that the Na-smectite probably exists as a two water layer complex under diagenetic conditions. These results may have implications for clay phase transformations in potential salt repositories.
Wu et al. (1997) determined partial dehydration in Ca- and Mg-montmorillonite at pressures from the H_2O liquid-vapor boundary to about 10 Kb. Mg-montmorillonite partially dehydrates at 200-250 ^{o}C, while the Ca-montmorillonite partially dehydrates in the range of 260-350 ^{o}C, with a slight increase for increasing pressure. Furthermore, the authors were able to rehydrate the phases at the same temperature as dehydration.

Vidal and Dubacq (2009) provided thermodynamic modeling of clay dehydration and their chemical evolution with regard to temperature, pressure and water activity. This

excellent paper compares their model to a multitude of low temperature experiments in a number of chemical systems. The model closely coincides with the experimental work indicating smectites with divalent interlayer cations are calculated to contain more water than smectite with monovalent cations at the same activity of H_2O and temperature. The model also reaffirms the fact that clay dehydration is a step function that involves large and sudden volume changes that are related to release of water with the loss of water layers. The authors also expand the mineral stability fields (boundary conditions) under which they test their model into the realm of micas, glaucophane, and chlorite. This thermodynamic model show great promise in the ability to predict clay stability and sequential dehydration into a variety of scenarios. Vidal and Dubacq (2009) conclude that additional experiments at high pressures and temperatures are required to confirm the apparent inconsistencies between their model and the few available high-pressure experimental data

3.3.3 Summary – Clays

Regarding the importance of this effect, they may vary depending on the type of hydrous mineral, its dehydration/dehydroxylation temperature, its content in the host rock/packing material, the rock's location (both relative to the waste loadings and its depth) and thermal profile (as a function of time) of the repository.

Powder XRD is a common but yet powerful technique for identification and structural characterization of clay minerals. The behavior of a clay mineral (e.g., smectite) as a function of water vapor pressure is depicted by relating its basal (001) spacing to water vapor pressure, as represented by relative humidity. These data show the strong link between water vapor pressure and the basal spacing of clay minerals. Clay minerals tend to depredate under hydrothermal conditions. P – T phase diagrams of hydrous minerals are essential for predicting and evaluating their stability, i.e., their dehydration/rehydration reactions, at high temperature variable pressure conditions. Environmental SEM imaging provides complementary measurements for water sensitivity of clay-containing rocks (Montesa et al. 2004).

Data that are especially useful in assessing the potential importance of these reactions include:

- X-ray diffraction (XRD) data – variations of the basal spacings as a function of vapor pressure for various smectites as well as other clay minerals,
- Degradation of clay minerals as a function of temperature and water/clay ratio,
- Rehydration hysteresis needs further study over the spectrum of clay chemical species.
- Experiments at high pressures and temperatures are required to confirm the apparent inconsistencies between the model of Vidal and Dubacq (2009) and the few available high-pressure experimental data
- Pressure (P)-temperature (T) diagrams showing the dehydration reactions of hydrous minerals, such as Na-, K-, and Ca-smectites,
- Environmental scanning electron microscopy (SEM) data of water sensitivity of rocks containing clay minerals.

3.4 Sulfate Stability

The present TRU waste repository at WIPP in Carlsbad NM deals primarily with TRU waste that has low thermal output. Although not specifically called out in the WIPP FEP document, the WIPP Waste Acceptance Criteria (DOE-Carlsbad Field Office, 2010) constrains the heat load in the panels to less than a 4°C increase. Exothermic reactions at WIPP (i.e., cement hydration) would increase temperatures by about 35°C, but would be localized and transient in nature. If the US decides to develop a salt repository (either bedded or dome) questions must be answered concerning waste forms with high thermal output. As a part of enabling options to support a Modified Open or Full Recycle Nuclear Fuel Cycle, it will be crucial to determine physical properties of mineral phases that are susceptible to dehydration such as the gypsum phase transition to anhydrite. Gypsum ($CaSO_4 \cdot 2H_2O$) converts to anhydrite ($CaSO_4$) in evaporite beds between 100 and 140 ^oC . In that 40°C gap is hemihydrate, a metastable but kinetically favored phase (Shcherban and Shirokikh, 1971). The gypsum – anhydrite phase transition creates a large water release (21% wt. loss) and volume reduction (~40%) for the dehydration reaction at 25^{o}C. Blount and Dickson (1973) calculated the 4-phase invariant point equilibrium of gypsum, anhydrite, simple H_2O solution and vapor at 56 C +/- 3 C and 124 +/- 9 torr.

$$CaSO_4 \cdot 2H_2O = CaSO_4 + 2H_2O$$
Gypsum Anhydrite + Water

The amount of water released during the phase transition is 18.1 cc/mol. The molecular volume of gypsum is 74.4 cc/mol (Smyth and Bish , 1988), while the anhydrite molecular volume is significantly smaller at 46.1 cc/mol. This is due the release of structural water. Therefore, the dehydration of gypsum to anhydrite may cause significant water available for transport, and the volume reduction between hydrous and anhydrous solids (about -40%) may create fracture transport venues.

Because of discrepancies in experimental data concerning the temperature of the phase transition from gypsum to anhydrite, and kinetic effects pertaining to metastable phases, a vigorous experimental campaign should be developed. Along with geochemical modeling and thermodynamic constraints, the phase transition from gypsum to anhydrite should be mapped out in potential repository P–T space. The high pressure experimental lab at LANL is critically suited to perform such experiments in cold seal assemblies at potential repository maximum temperatures (350°C) and lithostatic pressures (600 bars).

With the full data set in hand as a verification tool, one could then limit heat loading in vicinity of large gypsum beds to prevent the change to anhydrite, allowing for enhanced stability of the site. In addition, the data set would enhance the ability to characterize site specific thermo-mechanical properties.

3.5 Asphalt Interaction with EBS Components

Asphalt is well characterized for its mechanical properties as sealant, especially in salt repositories such as the WIPP site. The material is thought to be useful in its ability to flow plastically and seal porous media cracks in disturned excavation zones. Hansen and Knowles (2000) in an article on the design of a shaft seal system for WIPP suggest asphalt as a component in the seal. However, they assume the environment will be

benign, both devoid of ultraviolet light and in a reducing atmosphere. Furthermore, temperatures are constrained to be low for the WIPP repository by the waste acceptance criteria. They would assure that microbial degradation would not occur by the addition of lime. Roffey and Norqvist (1991) studied the biodegradation of bitumen that would be used to encapsulate low and intermediate radioactive waste in certain Swedish repository designs. In their experiments, they found that both aerobic and anaerobic degradation of bitumen occurred, equivalent to 0.6 – 1.5 μmoles CO_2 / month per mg bitumen and 1.1 – 1.5 μmoles CO_2/month per mg bitumen, respectively. Such microbial activity would also decrease the pH so that hydrogen evolving corrosion would occur.

There seems to be an assumption that by engineering design asphalt would be stable in most US repositories. However there does not seem to be a systematic characterization of organic volatility at high temperatures for multiple repository scenarios. In particular, asphalt degradation and potential acid generation may cause certain concrete compositions to fail early. There is great potential for experiments to provide validation and verification of how asphalt sealants would interact with other EBS components. Such experiments could first be bounded by phase equilibria studies investigating EBS materials interacting with enriched CO_2 environments.

3.6 References

Alexander, W. R., (1995). "Natural Cements: How can they help us safely dispose of radioactive waste?" *Radwaste Magazine*, 5, 62-69.

Alexander, W. R., Dayal, R., Eagleson, K., Eikenberg, J., Hamilton, E., Linklater, C. M., McKinley, I. G., and Tweed, C. J., (1992). "A natural analogue of high pH cement pore waters from the Maqarin area of northern Jordan. II: results of predictive geochemical calculations," *Journal of Geochemical Exploration*, 46, 133-146.

Atkins, M.; Bennett, D.; Dawes, A.; Glasser, F.; Kindness, A.; and Read, D. (1992) "A thermodynamic model for blended cements". *DOE/HMIP/RR/92/005*. London, England: Department of the Environment.

Atkins, M.; Glasser, F.P.; Moroni, L.P.; and Jack, J.J. (1993) "Thermodynamic modelling of blended cements at elevated temperatures (50-90°C)." *DOE/HMIP/RR/94/011*. Aberdeen, United Kingdom: Aberdeen University.

Babushkin, V.I.; Matveyev, G.M.; and Mchedlov-Petrossyan, O.P. (1985) "Thermodynamics of silicates." Mchedlov-Petrossyan, O.P., ed. Berlin, Germany: Springer-Verlag.

Banwart, S., Gustafsson, E., Laaksoharju, M., Nilsson, A.-C., Tullborg, E.-L., and Wallin, B., (1994). "Large-scale intrusion of shallow water into a vertical fracture zone in crystalline bedrock: Initial hydrochemical perturbation during tunnel construction at the Äspö Hard Rock Laboratory, southeastern Sweden," *Water Resources Research*, 30, 1747-1763.

Betcher, R.N., Gascoyne, M., and Brown, D. (1988) "Uranium in groundwaters of southeastern Manitoba, Canada," *Canadian Journal of Earth Science*, 25, 2089-2103.

Barin, I. and Platzki, G. (1995). Thermochemical Data of Pure Substances. 3rd Edition. Two volumes. New York, New York: VCH Publishers.

Batchelor, B. and Wu, K. (1993). "Effects of equilibrium chemistry on leaching of contaminants from stabilized/solidified wastes." Chapter 9 of *Chemistry and Microstructure of Solidified Waste Forms*. Spence, R.D., ed. Boca Raton, Florida: Lewis Publishers.

Bennett, D.G.; Read, D.; Atkins, M.; and Glasser, F.P. (1992). "A thermodynamic model for blended cements. II: Cement hydrate phases; thermodynamic values and modelling studies." *Journal of Nuclear Materials*, 190, 315-325.

Berner, U.R. (1987) "Modeling porewater chemistry in hydrated Portland cement." *Scientific Basis for Nuclear Waste Management X*, Symposium held December 1-4, 1986, Boston, Massachusetts. Bates, J.K. and Seefeldt, W.B., eds. 84, 319-330.

Berner, U. (1990) "A Thermodynamic description of the evolution of pore water chemistry and uranium speciation during the degradation of cement." *PSI-Bericht 62*. Wurenlingen und Villigen, Switzerland: Paul Scherrer Institut.

Bish, D.L. "Smectite dehydration and stability: Applications to radioactive waste isolation at Yucca Mountain, Nevada," Los Alamos National Laboratory report LA-11023-MS. (1988)

Blount, C.W., and Dickson, F.W. (1973). "Gypsum-anhydrite equilibria in systems $CaSO_4$-H_2O and $CaCO_4$-NaCl-H_2O." *American Mineralogist*, 58, 323-331

Bourrie, G., Trolard, F., Genin, J.M.R., Jaffrezic, A., Maitre, V., and Abdelmoula M. 1999. "Iron control by equilibria between hydroxy-Green Rusts and solutions in hydromorphic soils." Geochimica Cosmochimica Acta, 63(19-20), 3417-3427.

Bourrie, G., Trolard, F., Genin, J.M.R., Jaffrezic, A., Maitre, V., and Abdelmoula M. 1999. "Iron control by equilibria between hydroxy-Green Rusts and solutions in hydromorphic soils." *Geochimica Cosmochimica Acta*, 63(19-20), 3417-3427.

Borevsky, L. V., Vartanyan, G. S., and Kulikov, T. B., (1987). "Hydrogeological Essay," in *The Superdeep Well of the Kola Peninsula*, Y. A. Kozlovsky, Editor-in-Chief, Springer-Verlag, Berlin, 271-287.

Brady, P.V., Arnold, B.W., Freeze, G.A., Swift, P.N., Bauer, S.J., Kanney, J.L., Rechard, R.P., and Stein, J.S. "Deep borehole disposal of high-level radioactive Waste.", SAND2009-4401, Sandia National Laboratories, Albuquerque, NM, 74p. (2009)

Brush, L., (2009). "Appendix MgO-2009 Magnesium oxide as an engineered barrier. As part of Title 40 CRF 191 Subparts B and C Compliance Recertification Application for the Waste Isolation Pilot Plant". DOE/WIPP-09-3424, 108pp.

Bruton, C.J.; Meike, A.; Viani, B.E.; Martin, S.; and Phillips, B.L. (1993). "Thermodynamic and structural characteristics of cement minerals at elevated temperature." *Proceedings of the Topical Meeting on Site Characterization and Model Validation, FOCUS '93, September 26-29, 1993, Las Vegas, Nevada.* 150-156.

Bucher, K., Zhu, Y., and Stober, I., (2008)."Groundwater in fractured crystalline rocks, the Clara mine, Black Forest (Germany)," *International Journal of Earth Science*, 98, 1727-1739.

Bucher, K., Zhang, L., and Stober, I., (2009). "A hot spring in granite of the Western Tianshan, China." *Applied Geochemistry*, 24, 402-410.

Calvo, J. L. G., Hidalgo, A., Alonso, C., and Luco, L.F., (2010). "Development of low-pH cementitious materials for HLRW repositories Resistance against ground waters aggression." *Cement and Concrete Research*, 40(8), 1290-1297.

Carey, J.W. and Lichtner, P.C., (2007). "Calcium silicate hydrate (C-S-H) solid solution model applied to cement degradation using the continuum reactive transport model FLOTRAN.". In *Transport Properties and Concrete Quality: Materials Science of Concrete*, Mobasher, B. and Skalny, J., eds, Special Volume, 73-106. American Ceramic Society; John Wiley & Sons, Inc.

Chapman , N. A., McKinley, I.G., and Smellie, J. A. T. (1984) "The potential of natural analogues in assessing systems for deep disposal of high-level radioactive waste." *Swedish Nuclear Fuel and Waste Management Co (SKB)*, Technical Report 84-16.

Chivian, D., Brodie, E. L., Alm, E. J., Culley, D. E., Dehal, P. S., DeSantis, T. Z., Gihring, T. M., Lapidus, A., Lin, L.-H., Lowry, S. R., Moser, D. P., Richardson, P. M., Southam, G., Wanger, G., Pratt, L. M., Andersen, G. L., Hazen, T. C., Brockman, F. J., Arkin, A. P., and Onstott, T. C. (2008). "Environmental Genomics Reveals a Single-Species Ecosystem Deep Within Earth," *Science*, 322, 275-278.

Cleall, P., Melhuish, T., and Thomas, H. (2006) "Modelling the three-dimensional behaviour of a prototype nuclear waste repository", *Engineering Geology*, 85(1), 212-220.

Cramer, J. (1995) "Cigar Lake: A natural example of long-term isolation of uranium." *Radwaste Magazine*, 36-40.

Colten, V.A. (1986) "Hydration states of smectite in NaCl brines at elevated pressures and temperatures." *Clays Clay Miner.*, 34(4), 385-389.

Cramer, J. and Smellie, J., eds. (1994) "Final report of the AECL/SKB Cigar Lake Analog Study." *Swedish Nuclear Fuel and Waste Management Co (SKB)*, Technical Report 94-04.

D'Appolonia Consulting Engineers, Inc. "Brine reservoirs in the Castile Formation Waste Isolation Pilot Plant (WIPP) project, Southeastern New Mexico." Westinghouse Electric Corporation – Waste Isolation Division Carlsbad, NM., report TME 3153. (1983)

Damidot, D.; Stronach, S.; Kindness, A.; Atkins, M.; and Glasser, F.P. (1994). "Thermodynamic investigation of the CaO-Al2O_3-$CaCO_3$-H_2O closed system at 25ºC and influence of Na_2O." *Cement and Concrete Research*, 24(3), 563-572.

Davidovits, J. (1989) "Geopolymers and geopolymeric materials", *Journal of Thermal Analysis*, 35, 429-441.

Davidovits, J., (1991). "Geopolymers – inorganic polymeric new materials", *Journal of Thermal Analysis*, 37, 1633-1656.

Davidovits, J. (1993) "Are modern cements better than ancient cements?", *Structural Survey*, 2(2), 124-129.

Davidovits, J. (2008) "Geopolymer – Chemistry and Applications", *Geopolymer Institute*, 592 pp.

DOE Fuel Cycle Research & Development (March, 2010) Information Basis for Developing Comprehensive Waste Management System - The US-Japan Joint Nuclear Action Plan Waste Management Working Group Phase I Report. In Press, 108 pp.

Department of Energy (DOE), Carlsbad Field Office, Transuranic Waste Acceptance Criteria for the Waste Isolation Pilot Plant – Rev. 6.5, U.S., DOE/WIPP-02-3122, 106 pp.

Dole, L.R. and Mattus, C.H., (2007) "Low pH concrete for use in the US High-Level Waste repository: Part I Overview." *3rd Workshop on R&D on Low-pH cement for a Geological Repository*, Paris, France, June 13 -14.

Duxson, P., Fernandez-Jimenez, A., Provis, J.L., Lukey, G.C., Palomo, A., and Van Devender, J.S.J., (2007). "Geopolymer technology: the current state of the art." *J. Mater. Sci.*, 42, 2917–2933.

El-Barawy, K.A., Girgis, B.S., and Felix, N.S. (1986) "Thermal treatment of some pure smectites," *Thermochimica Acta*, 98, 181-189.

Frape, S. K., Blyth, A., Blomqvist, R., McNutt, R. H., and Gascoyne, M., (2003). "Deep fluids in the continents: II. Crystalline rocks," in *Treatise on Geochemistry, Volume 5*, J. I. Drever, ed., Elsevier, 541-580.

Ferriss, E.D.A., Helean, K.B., Bryan, C.R., Brady, P.V., Ewing, R.C, (2009). "UO_2 corrosion in an iron waste package." *Journal of Nuclear Materials*, 384, 130–139.

FORGE (Fate of Repository Gases) "Summary of gas generation and migration – current state-of-the-art", Euratom 7th Framework project, FORGE Report D 1.2 Ver1.0, 84 pp. (2010)

Fujii, K. and Kondo, W. (1983). "Estimation of thermochemical data for calcium silicate hydrate (C-S-H)." *Journal of the American Ceramic Society*, 66(12), C220-C221.

Gartner, E.M. and Jennings, H.M. (1987) "Thermodynamics of calcium silicate hydrates and their solutions." *Journal of the American Ceramic Society*, 70(10), 743-749.

Gascoyne, M. and Kamineni, D.C. (1994) "The Hydrogeochemistry of fractured plutonic rocks in the Canadian shield," *Applied Hydrogeology*, 2, 43-49.

Gascoyne, M. (1997) "Evolution of redox conditions and groundwater composition in recharge-discharge environments on the Canadian shield." *Hydrogeology Journal*, 5, 4-18.

Gascoyne, M. (2004) "Hydrogeochemistry, groundwater ages and sources of salts in a granitic batholith on the Canadian Shield, southeastern Manitoba." *Applied Geochemistry*, 19, 519–560.

Gaucher, E.C., Tournassat, C., Pearson, F.J., Blanc, P., Crouzet, C., Lerouge, C., and Altmann, S. (2009). "A robust model for pore-water chemistry of clayrock." *Geochimica et Cosmochimica Acta*, 73, 6470–6487.

Glagolev, A. A., Kazansky, V. I., Prokhorov, K. V., Rusinov, V. L., Maslennikov, V. A., Voronovsky, S. N., and Ovchinnikov, L. N., "Zonality and Age of Metamorphism," in *The Superdeep Well of the Kola Peninsula*, Y. A. Kozlovsky, Editor-in-Chief (Springer-Verlag, Berlin, 166-198. (1987)

Glasser, F. P.; Lachowski; E. E., and MacPhee, D. E. (1987) "Compositional Model for Calcium Silicate Hydrate (C-S-H) Gels, Their Solubilities, and Free Energies of Formation." *Journal of the American Ceramic Society*, 70(7), 481-485.

Glasser, F.P., Marchand, J., Samson, E., (2008). "Durability of concrete – degradation phenomena involving detrimental chemical reactions." *Cement and Concrete Research*, 38(2), 226-246.

Gómez, P., Turrero, M. J., Garralón, A., Peña, J., Buil, B., de la Cruz, B., Sánchez, M., Sánchez. D. M., Quejido, A., Bajos, C., and Sánchez, L. (2006) "Hydrogeochemical characteristics of deep groundwaters of the Hesperian Massif (Spain)." *Journal of Iberian Geology*, **32**, 113-131.

Gorbatsevich, F.F., Ikorsky, S. V., and Zharikov, A. V., (2010). "Structure and permeability of deep-seated rocks in the Kola superdeep borehole section (SG-3)." *Acta Geodynamica et Geomaterialia*, **7**, 145-152.

Greenberg, S.A. and Chang, T.N. (1965). "Investigation of the colloidal hydrated calcium silicates. II. solubility relationships in the calcium oxide-silica-water System at 25°C." *Journal of Physical Chemistry*, 69(1), 182-188.

Greenberg, J.P. and Moller, N. (1989). "The prediction of mineral solubilities in natural waters: A chemical equilibrium model for the Na-K-Ca-Cl-SO_4-H_2O system to high concentration from 0 to 250°C." *Geochimica et Cosmochimica Acta*, 53, 2503–2518.

Hansen, F.D. and Knowles, M.K., (2000.) "Design and analysis of a shaft seal system for the Waste Isolation Pilot Plant." *Reliability Eng. And Sys. Safety*, 69, 87-98.

Hanzlicek, T., Steinerova, M., and Straka, P. (2006) "Radioactive metal isotopes stabilized in a geopolymer matrix: determination of a leaching extract by a radiotracer method", *J. Am. Ceram. Soc.*, 89(11), 3541–3543.

Harvie, C.E.; Moller, N.; and Weare, J.H. (1984) "The Prediction of Mineral Solubilities in Natural Waters: The Na-K-Mg-Ca-H-Cl-SO_4-OH-HCO_3-CO_3-CO_2-H_2O System to High Ionic Strengths at 25°C." *Geochimica et Cosmochimica Acta*, 48(4), 723-751.

Helgeson, H.C.; Delany, J.M.; Nesbitt, H.W.; and Bird, D.K. 1978. "Summary and Critique of the Thermodynamic Properties of Rock Forming Minerals." *Amer. Jour. Sci.,* 278-A. New Haven, Connecticut: Yale University, Kline Geology Laboratory, 229 pp.

Hermann, E., Kunze, C., Gatzweiler, R., Kießig, G., Davidovits, J. (1999) "Solidification of various radioactive residues by Geopolymere® with special emphasis on long-term stability", Géopolymère '99 Proceedings, www.geopolymer.org.

IAEA "*The Oklo Phenomenon, Proceedings of a symposium on the Oklo Phenomenon organized by the International Atomic Energy Agency in Co-operation with the French Atomic Energy Commission and the Government of the Republic of Gabon and held in Libreville, Gabon from 23 to 27 June 1975"*, International Atomic Energy Agency, Vienna, Austria. (1975).

IAEA "*Natural Fission Reactors, Proceedings of a Meeting of the Technical Committee on Natural Fission Reactors organized by the International Atomic Energy Agency in co-operation with the French Atomic Energy Commission and held in Paris from 19 to 21 December 1977*", International Atomic Energy Agency, Vienna, Austria. (1978).

Johnson, A. B. and Francis, B. "Durability of metals from archaeological objects, metal meteorites, and native metals," Battelle Pacific Northwest Laboratory Report PNL-3198. (1980)

Johnson, J.W.; Oelkers, E.H.; and Helgeson, H.C. (1992). "SUPCRT92: A software package for calculating the standard molal thermodynamic properties of minerals, gases, aqueous species, and reactions from 1 to 5000 Bar and 0 to 1000°C." *Computers & Geosciences,* 18(7), 899-947.

Jové Colón and Finch, *in prep.* "Evaluation of data used to support the adjusted Eh model for calculating dissolved-concentration limits for plutonium", Sandia National Laboratories, Albuquerque, NM.

Jull, S. P. and Lees, T. P. "Studies of historic concrete: Final report," Commission of the European Communities Nuclear Science and Technology Report EUR 12972. (1990)

Karus, E. W., Nartikoyev, V. D., Bartashevich, O. V., Gigashvili, G. M., Ikorsky, S. V., Pavlova, M. A., Petersilje, I. A., and Pisarnitskaya, T. F. (1987) "Gases and organic matter," in *The Superdeep Well of the Kola Peninsula*, Y. A. Kozlovsky, Editor-in-Chief (Springer-Verlag, Berlin, 1987), 243-270.

Khoury, H. N., Salameh, E., Clark, I. D., Fritz, P., Bajjali, W., Milodowski, A. E., Cave, M. R., and Alexander, W. R. (1992) "A natural analogue of high pH cement pore waters from the Maqarin area of northern Jordan. I: introduction to the site," *Journal of Geochemical Exploration*, 46, 117-132.

Kienzler, B., Vejmelka, P., Herbert, H.J., Meyer, H., Althenhein-Haese, C. (2000) "Long-term leaching experiments of full-scale cemented waste forms: Experiments and modeling." *Nuclear Technology*, 129, 101-118.

Koster van Groos, A. F. and Guggenheim, S. (1986) "Dehydration of K-exchanged montmorillonite at elevated temperatures and pressures," *Clays Clay Miner.*, 34, 281-286.

Krupka, K. M. and Serne, R. J. "Effects on radionuclide concentrations by cement/ground-water interactions in support of performance assessment of low-level radioactive waste disposal facilities," U.S. Nuclear Regulatory Commission, Division of Waste Management, Office of Nuclear Material Safety and Safeguards, Report NUREG/CR-6377 (May 1998).

Kyle, J. E., Eydal, H. S. C., Ferris, F. G., and Pedersen, K. (2008) "Viruses in granitic groundwater from 69 to 450 m depth of the Äspö hard rock laboratory, Sweden," *The ISME Journal*, **2**, 571-574.

Laaksoharju, M., Smellie, J., Nilsson, A.-C., and Skarman, C. "Groundwater sampling and chemical characterisation of the Laxemar deep borehole KLX02", *Swedish Nuclear Fuel and Waste Management Co (SKB)*, Technical Report 95-05, 74 pp. (1995)

Lancaster, L., (2008). "Roman Engineering and Construction," in *The Oxford Handbook of Engineering and Technology in the Classical World,* Oxford University Press, Inc, New York, 260-261.

Lanev, V. S., Nalivkina, E. B., Vakhrusheva, V. V., Golenkina, E. A., Rusanov, M. S., Smirnov, Y. P., Suslova, S. N., Duk, G. G., Koltsova, T. V., Maslennikov, V. A., Timofeev, B. V., and Zaslavsky, V. G., (1987). "Geological section of the well", in *The Superdeep Well of the Kola Peninsula*, Y. A. Kozlovsky, Editor-in-Chief (Springer-Verlag, Berlin, 1987), 40-73.

Langmuir, D., (1971) "The geochemistry of some carbonate ground waters in central Pennsylvania," *Geochimica et Cosmochimica Acta*, 35, 1023-1045.

Lin, L.-H., Wang, P.-L., Rumble, D., Lippmann-Pipke, J., Boice, E., Pratt, L. M., Sherwood Lollar, B., Brodie, E. L., Hazen, T. C., Andersen, G. L., DeSantis, T. Z., Moser, D. P., Kershaw, D., and Onstott, T. C. (2006) "Long-term sustainability of a high-energy, low-diversity crustal Biome," *Science*, 314, 479-482. Supporting online material at www.sciencemag.org/cgi/content/full/314/5798/479/DC1.

Los Alamos National Laboratory "Disposition of excess weapon plutonium in deep boreholes, site selection handbook. Los Alamos National Laboratory, LA-13168-MS. (1996)

MacPhee, D.E.; Luke, K.; Glasser, F.P.; and Lachowski, E.E. (1989). "Solubility and aging of calcium silicate hydrates in alkaline solutions at 25ºC." *Journal of the American Ceramic Society,* 72(4), 646-654.

Mader, U.K., Fierz, T., Frieg, B., et al. (2006) "Interaction of hyperalkaline fluid with fractured rock: Field and laboratory experiments of the HPF project (Grimsel Test Site, Switzerland)." *Journal of Geochemical Exploration*, 90(1-2), 68-94**.**

Miller, B. and Chapman, N. (1995) "Postcards from the past: Archaeological and industrial analogs for deep repository materials," *Radwaste Magazine*, 2(1), 32-42.

Miller, W., Alexander, R., Chapman, N., McKinley, I., and Smellie, J. (2000) "*Geological Disposal of Radioactive Wastes and Natural Analogues: Lessons from Nature and Archaeology"*, Pergamon-Burlington, 126-142.

Lovley, D. R. and Chapelle, F. H, (1995). "Deep subsurface microbial processes," *Reviews of Geophysics*, 33, 365-381.

McKinley, I. G., (1995). "Poços de Caldas: Testing models of radionuclide transport processes," *Radwaste Magazine*, 2(4), 34-38.

Mariner, P.E. "In-Drift Precipitates/Salts Model", ANL-EBS-MD-000045 (Rev.03), Sandia National Laboratories, Albuquerque, NM. (2007)

Matschei, T., Lothenbach, B., and Glasser, F.P. (2007). "Thermodynamic properties of Portland cement hydrates in the system CaO-Al_2O_3-SiO_2-$CaSO_4$-$CaCO_3$-H_2O." *Cement and Concrete Research*, 37(10), 1379-1410.

Metz, V., Schussler, W., Kienzler, B., and Fanghanel, Th. (2004) "Geochemically derived non-gaseous radionuclide source term for the Asse salt mine – assessment for the use of a $Mg(OH)_2$ – based backfill material". *Radiochimica. Acta*, 92, 819-825.

Miller, W., Alexander, R., Chapman, N., McKinley, I., and Smellie, J. (2000) "*Geological Disposal of Radioactive Wastes and Natural Analogues"* (Pergamon, Burlington).

MIT (2003) The future of Nuclear Power, An Interdisciplinary MIT Study. Massachusetts Institute of Technology, 180 pp.

Murphy, W.M., (2007). "Hydrothermal phase relations among uranyl minerals at the Nopal I analog site. *Mater. Res. Soc. Symp. Proc.*, 985, Materials Research Society. p. 6.

Nagy, B., F. Gauthierlafaye, et al. (1991). "Organic-matter and containment of uranium and fissiogenic isotopes at the Oklo natural reactors." *Nature*, 354(6353), 472-475.

Neall, F.B. (1996). "Modelling the long-term chemical evolution of cement-groundwater systems." *Scientific Basis for Nuclear Waste Management XIX, Symposium held November 27-December 1, 1995, Boston, Massachusetts.* Murphy, W.M. and Knecht, D.A., eds. 412, 483-490. Pittsburgh, Pennsylvania: Materials Research Society.

Neck, V., Altmaier, M., Seibert, A., Yun, J.I., Marquardt, C.M., and Fanghanel, T. (2007). "Solubility and redox reactions of Pu(IV) hydrous oxide: Evidence for the formation of $PuO_{2+x(s,\,hyd)}$. *Radiochimica Acta*, 95(4), 193-207.

Parker, V.B. and Khodakovskii, I.L. (1995). "Thermodynamic properties of the aqueous ions (2+ and 3+) of iron and the key compounds of iron." *Journal of Physical and Chemical Reference Data*, 24(5), 1699-1745.

Pedersen, K. (1996). "Investigations of subterranean bacteria in deep crystalline bedrock and their importance for the disposal of nuclear waste," *Canadian Journal of Microbiology*, 42, 382-391.

Percival, J.B. and Kodama, H. (1989) "Sudoite from Cigar Lake, Sakatchewan" *The Canadian Mineralogist*, 27(4), 633-641.

Perera, D., Vance, E., Kiyama, S., Aly, Z., and Yee, P., (2007). "Geopolymers as candidates for the immobilisation of low- and intermediate-level waste", *Mater. Res. Soc. Symp. Proc.*, 985, 361-366.

Pérez del Villar, L., Reyes, E., Delgado, A., Núñez, R., Pelayo, M., and Cózar, J. S., (2003). "Argillization processes at the El Berrocal analogue granitic system (Spain): mineralogy, isotopic study and implications for the performance assessment of radwaste geological disposal." *Chemical Geology*, 193, 273-293.

Perkins, R.B. and Palmer, C.D. (1999) "Solubility of Ettringite ($Ca_6[Al(OH)_6]_2(SO_4)_3 \cdot 26H_2O$) at 5–75°C." *Geochimica et Cosmochimica Acta,* 63(13/14), 1969-1980.

Petit, J.-C., (1992). "Natural analogues for the design and performance assessment of radioactive waste forms: a review." *Journal of Geochemical Exploration* **46**, p. 1-33.

Pfingsten, W. (2002) "Experimental and modeling indications for self-sealing of a cementitious low- and intermediate-level waste repository by calcite precipitation." *Nuclear Technology,* 140, 63-82.

Rai, D., Moore, D.A., Felmy, A.R., Choppin, G.R., and Moore, R.C. (2001). "Thermodynamics of the PuO_2^+-Na^+-OH^--Cl^--ClO_4^--H_2O System: Use of NpO_2^+ Pitzer Parameters for PuO_2^+." *Radiochimica Acta*, 89(8), 491-498.

Rassineux, F., Petit, J.-C., and Meunier, A. (1989) "Ancient analogues of modern cement: Calcium hydrosilicates in mortars and concretes from Gallo-Roman thermal baths of western France." *Communications of the American Ceramic Society*, 72, 1026-1032.

Reardon, E.J. (1990) "An ion interaction model for the determination of chemical equilibria in cement water systems." *Cement and Concrete Research*, 20, 175-192.

Reardon, E.J. (1992) "Problems and approaches to the prediction of the chemical composition in Cement/Water Systems." *Waste Management,* 12, 221-239.

Robie, R.A., Hemingway, B.S., and Fisher, J.R. 1979. "Thermodynamic properties of minerals and related substances at 298.15 K and 1 Bar (10^5 Pascals) pressure and at higher temperatures. U.S. Geological Survey Bulletin 1452, Washington, D.C.: U.S. Government Printing Office.

Roffey,R. and Norqvist,A. (1991). "Biodegradation of bitumen used for nuclear waste disposal." *Cellular and Molecular Life Sci.*, 47(6), 539-542.

Russell, R.L., Schweiger, M.J., Westsik Jr., J.H., Hrma, P.R., Smith, D.E., Gallegos, A.B., Telander, M.R., and Pitman, S.G. "Low temperature waste immobilization testing", PNNL-16052 (Rev. 1), Pacific Northwest National Laboratory, Richland, WA. (2006)

Sarkar, A.K., Barnes, M.W., and Roy, D.M. "Longevity of borehole and shaft sealing materials: Thermodynamic properties of cements and related phases applied to repository sealing.", ONWI-201. Columbus, Ohio: Battelle Memorial Institute, Office of Nuclear Waste Isolation. (1982)

Savary, V. and Pagel, M. (1997) "The effects of water radiolysis on local redox conditions in the Oklo, Gabon, natural fission reactors 10 and 16." *Geochimica et Cosmochimica Acta,* 61(21), 4479-4494.

Schorscher ,H. D. and Shea, M. E. "The regional geology, mineralogy, and geochemistry of the Poços de Caldas alkaline caldera complex, Minas Gerais, Brazil," *Swedish Nuclear Fuel and Waste Management Co (SKB)*, Technical Report 90-10. (1991)

Schuessler, W., Kienzler, B., Wilhelm, S., Neck, V., and Kim, J.I., (2001) "Modeling of near feld actinide concentrations in radioactive waste repositories in salt formations: Effect of buffer materials." *Mat. Res. Soc. Symp. Proc.* 663, Materials Research Society

Shcherban, J.P., and Shirokikh, I.N. (1971) "Thermodynamic and experimental data on Stability of gypsum, hennhydrate, and anhydrite under hydrothermal conditions." *Int. Geology Review*, 13(11), 1671-1673.

Shaw, S., Henderson, C.M.B., and Komanschek, B.U. (2000) "Dehydration/recrystallization mechanisms, energetics, and kinetics of hydrated calcium silicate minerals: An in situ TGA/DSC and Synchrotron Radiation SAXS/WAXS Study." *Chemical Geology,* 167, (1-2), 141-159.

Skibsted, J., and Hall, C. (2007) "Characterization of cement minerals, cements and their reaction products at the atomic and nano scale." *Cement and Concrete Research*, 38, 205-225**.**

Smellie , J. (1995) "The Fossil Nuclear Reactors of Oklo, Gabon," *Radwaste Magazine*, 21, 18-27.

Smyth, J.R., and Bish, D. (1988). "*Crystal Structures and Cation Sites of the Rock-Forming Minerals*" Allen & Unwin.

Soler, J.M., Mader, U. (2005) "Interaction between hyperalkaline fluids and rocks hosting repositories for radioactive waste: Reactive transport simulations." *Nuclear Science and Engineering*, 151, 128-133.

Spiessl, S. M., MacQuarrie, K. T. B., and Mayer, K. U. (2008) "Identification of key parameters controlling dissolved oxygen migration and attenuation in fractured crystalline rocks," *Journal of Contaminant Hydrology*, 95, 141-153.

Stefánsson, A.; Anórsson, S.; and Sveinbjörnsdóttir, A.E. (2005). "Redox reactions and potentials in natural waters at disequilibrium." *Chemical Geology*, Vol. 221(3-4), p. 289-311

Stober, I. and Bucher, K. (1999) "Deep groundwater in the crystalline basement of the Black Forest region," *Applied Geochemistry* 14, 237-254.

Stober, I. and Bucher, K. (2005) "The upper continental crust, an aquifer and its fluid: hydaulic and chemical data from 4 km depth in fractured crystalline basement rocks at the KTB test site", *Geofluids*, Vol. 5, 8–19.

Sugiyama, D. and Fujita, T. (2006) "A thermodynamic model of dissolution and precipitation of calcium silicate hydrates", *Cement and Concrete Research* 36, 227-237.

Swedish Nuclear Waste Management Co. (SKB), "Site description of Laxemar at completion of the site investigation phase." *Swedish Nuclear Waste Management Co. (SKB)*, Technical Report TR-09-11. (December 2009)

Taylor, H.F.W. (1990). "*Cement Chemistry*" San Diego, California: Academic Press Limited.

Travis, B.J. and H.E. Nuttall "Two-dimensional numerical simulation of geochemical transport in Yucca Mountain," Los Alamos National Laboratory report, LA-10532-MS. (1987)

Vidal, O., and Dubacq, B. (2009). "Thermodynamic modelling of clay dehydration, stability and compositional evolution with temperature, pressure and H_2O activity." *Geochim. Cosmo. Acta.,* V73, p. 6544-6564.

Waber, H. N. and Smellie, J. A. T., (2008). "Characterisation of porewater in crystalline rocks." *Applied Geochemistry* **23**, p. 1834-1861.

Waber, H. N., Gimmi, T., deHaller, A., and Smellie, J. A. T. (2009) "Porewater in the rock matrix: Site descriptive modelling SDM-Site Laxemar." *Swedish Nuclear Waste Management Co. (SKB)*, Report R-08-112. (May 2009)

Wakeley, L.D., (1987). "Optimizing workability and expansion of a salt-saturated concrete.", Cement and Concrete Research, Vol. 17, p. 723-733.

Wakeley, L.D., Poole, T.S., Ernzen, J.J., and Neeley, B.D. (1993) "Salt saturated mass concrete under chemical attack.", in *High Performance Concrete in Severe Environments (SP-140)*, P. Zia (ed), American Concrete Institute, 239-267.

Wolery, T.J. and Jarek, R.L. "SoftwareUser's Manual – EQ3/6 Version 8.0". Software Document Number: 10813-UM-80-00, US Department of Energy, Office of Civilian Radioactive Waste Management, Office of Repository Development, 1261 Town Center Drive, Las Vegas, NV 89144. (2003)

Wolery, T.J. and Jové-Colón, C.F. "Qualification of Thermodynamic Data for Geochemical Modeling of Mineral–Water Interactions in Dilute Systems", ANL-WIS-GS-000003 (Rev.01), Sandia National Laboratories, Albuquerque, NM. (2007)

Wu, T.C., Bassett, W.A., Huang, W.L., Guggenheim, S., and Koster van Groos, A.F. (1997) "Montmorillonite under high H_2O pressure; stability of hydrate phases, rehydration hysteresis, and the effect of interlayer cations." *American Mineralogist*, 82, 69-78.

Zarrabi, K.; McMillan, S.; Elkonz, S.; and Cizdziel, J. "Corrosion and mass transport processes in carbon steel miniature waste packages." Document TR-03-003, Rev. 0. Task 34. Las Vegas, Nevada: University of Nevada, Las Vegas. (2003)

"Cameco completes draining of Cigar Lake." *World Nuclear News*, 12 February 2010 (available URL: http://www.world-nuclear-news.org/ENF-Cameco_completes_draining_of_Cigar_Lake-1202104.html)

"Cameco Corporation: No Production in 2011 for Cigar Lake!" *Uranium-stocks.net*, 16 February 2009 (available URL: http://www.uranium-stocks.net/cameco-corporation-no-production-in-2011-for-cigar-lake/)

Massachusetts Institute of Technology (MIT), "Module: Building Bricks and Monumental Glue," http://web.mit.edu/materialculture/www/monumentalglue.html (2002).

REACTIVE TRANSPORT AND COUPLED THERMAL-HYDROLOGICAL-MECHANICAL-CHEMICAL (THMC) PROCESSES IN ENGINEERING BARRIER SYSTEMS (EBS)

4. THMC Processes in EBS

4.1 Introduction

Geological repositories for disposal of high-level nuclear wastes generally rely on a multi-barrier system to isolate radioactive wastes from the biosphere. The multi-barrier system typically consists of a natural barrier system, including repository host rock and its surrounding subsurface environment, and an engineering barrier system (EBS). As described in the first chapter, the EBS represents man-made, engineered materials placed within a repository, including the waste form, waste canisters, buffer materials, backfill, and seals (OECD, 2003). EBS plays a significant role in the containment and long-term retardation of radionuclide release. It is also involved in complex thermal, hydrogeological, mechanical, chemical and biological processes, such as heat release due to radionuclide decay, multiphase flow (including gas release due to canister corrosion), swelling of buffer materials, radionuclide diffusive transport, waste dissolution and chemical reactions. All these processes are related to each other. Therefore, an in-depth understanding of these coupled processes is critical for the performance assessment (PA) for EBS and the entire repository. The current focus by the LBNL group is on (1) thermal-hydraulic-mechanical-chemical (THMC) processes in buffer materials (bentonite) and (2) diffusive transport in EBS associated with clay host rock, with a long-term goal to develop a full understanding of (and needed modeling capabilities to simulate) impacts of coupled processes on radionuclide transport in different components of EBS, as well as the interaction between near-field host rock (e.g., clay) and EBS and how they effect radionuclide release. In this part of the final report, specifically Section 4.2, summarizes progress on the literature review for THMC processes and reactive-diffusive radionuclide transport in bentonite. The literature review provides a picture of the state-of-the-art of the relevant research areas addressed by LBNL. This will also include a brief review of the current-state of TM modeling for salt. Section 4.3 documents the current modeling tools, available at LBNL, for the simulation of EBS processes. This may be important for identifying future modeling activities within the UFD campaign EBS process evaluation utilizing these modeling capabilities and to identify needs for future EBS modeling development. Section 4.4 presents the results of geomechanical modeling using the Barcelona Basic Model (BBM) constitutive relationship for thermo-elasto-plastic media such as bentonite and an update on reactive-diffusive transport modeling approaches through bentonite in the EBS. Section 4.5 discusses identified knowledge gaps and technical issues as well as short- and long-term R&D plans.

4.2 Literature Review

This section summarizes LBNL's current literature-review results in two focus areas: (1) THMC processes within EBS buffer materials to better understand bentonite behavior and stability, and (2) diffusive transport within bentonite to better understand radionuclide release into the natural system. The literature review intends to provide a comprehensive picture of the current status of research activities in the two areas, and to help identify the relevant technical issues and gaps of interest to the UFD campaign that require resolution in future studies. While the literature review, as a major task for FY10, is not completed yet, this section also documents remaining literature-review activities. The completed literature review will be part of the FY10 final progress report. A list of

technical issues and gaps (identified based on the current literature-review results) is provided in Section 4.5.1.

4.2.1 THMC Processes in Buffer Material (Bentonite)

For the EBS buffer material (bentonite) literature review, we have developed a list of key recent references related to THMC processes, mainly with papers published over the last five years. This reference list is given as an appendix to this report. (Some of these references are cited in this subsection.)
In addition to these references, there are also considerable activities on EBS in a number of on-going international collaborative projects. These include:

- DECOVALEX-2011 project
- THERESA project, sponsored by European Community (EC)
- TIMODAZ project, sponsored by EC
- EBS Task Force, sponsored by SKB, which includes the BRIE task (BRIE stands for Bentonite-Rock Interaction Experiment)

The above are all international cooperative projects, involving participation of most of the countries active in this field. Some of these projects include very valuable data sets from major multi-year field experiments. Available information from these international projects will also be reviewed. Some of these projects include data from major field experiments. To access these data, there may be a need for DOE to become a participant in these projects. Participating in one or more of these projects is an effective way for US researchers to be brought to the forefront of international EBS research activities.

The main component of the EBS, used in a number of countries, is bentonite, a clay with a high content of smectite minerals having properties very suitable for isolating radioactive waste canisters (Alonso and Ledesma, 2005; Pusch 2006; Pusch and Yong, 2006). It has a very low hydraulic conductivity and very low anion diffusion capacity, and a low transport capacity for positive-charged radionuclides. Thus, it can serve as a good buffer around waste canisters. Mechanically, its high swelling potential makes possible self-sealing of openings within the EBS system and of gaps between the bentonite with the rock and with the radioactive waste canister. Its thermal conductivity is adequate to conduct heat away from the canister, so that the canister can be maintained at a temperature 100°C or below. Furthermore, it has good colloid and microbial filtration capability. With these properties, a bentonite buffer generally is expected to fulfill the following functions:

- To limit the canister corrosion rate by minimizing groundwater access
- To conduct heat away from the canister
- To provide a mechanical buffer between the rock and the canister and to keep the canister in place in the deposition hole
- To reduce the potential for microbial activity
- To act as a medium that allows mainly solute diffusion and provide for large sorptive surfaces to retard any released radionuclides

There are three phases in the evolution of the bentonite buffer in a radioactive waste repository. The first phase is the installation and initial water intake of the buffer over a period of 0 to 100 years, dependent on repository design. The second phase is dominated

by heat input from the waste canister with a significant temperate gradient that is changing, with the temperature going through an increase and then decrease to ambient over a period of 100 to 1000 years. The third phase is a period with tectonic or glacial processes under ambient or reduced temperature conditions from 1000 to a million years.

When a bentonite buffer is installed around waste canisters in a repository, it is initially partially saturated with water. Water intake is a slow process because of the very low permeability of the bentonite and the surrounding crystalline or argillaceous rock. Flow through crystalline rock is mainly through fractures, which controls the rate and locations of incoming water for saturating the bentonite, such that bentonite wetting and swelling could well be uneven over its interface with the rock, resulting in uneven swelling pressure. For argillaceous rock, fracture flow is potentially less significant and wetting of the bentonite could be controlled by inflow from the rock matrix. Further, if the incoming flow from the rock is high, the bentonite will uptake the water under a positive pressure. However if the incoming flow is low, the uptake of water from the bentonite will create a negative pressure, which will dehydrate the rock in the immediate neighborhood.

Next, the heat released from radioactive waste begins to heat up the near field of the bentonite-rock system. Processes involved in the evolution of the bentonite buffer include thermally induced distribution of initial pore water in the clay during the early thermal phases (Nguyen et al., 2009; Tong et al., 2009; Gens et al., 2009; Thomas et al., 2009). On the outer part of the bentonite buffer, there is uptake of water from the rock-water interface, with potential swelling of bentonite in this region. On the inner part of the bentonite buffer, next to the heat-releasing waste canister, there is a decrease of moisture content (dissication) with potential shrinkage. Over time, the expansion of the bentonite as it is being hydrated may displace the position of the waste canister enveloped in it, as well as the position of the buffer-backfill interface. Chemically within the bentonite buffer, there may be dissolution of buffer minerals and precipitation of chemical compounds (Castellanos, et al., 2008; Guimaraes et al., 2009; Seetharam et al., 2006).

Major physical processes related to long-term stability of the buffer bentonite are erodability, colloidal transport and filtering, and microbiological filtering (Birgesson et al., 2009). Major chemical processes that may affect the chemical stability of the buffer bentonite after water saturation include dissolution and precipitation, conversion of smectite in the buffer to nonexpansive mineral forms, and cementation by precipitated complexes (Pusch and Yong, 2006).

Five areas of concern in recent studies of the bentonite buffer have been discussed by the research community. The first is the buffer hydration process and timing. The second is the thermo-hydro-mechanical (THM) processes involved in bentonite behavior. The third is the issue of homogenization, gaps and bentonite pellets, and the fourth area is piping and erosion. Finally the fifth is chemical and mineralogical interactions. These are briefly discussed below.

The hydration process is important for understanding the evolution of the waste repository and plays a significant role in the maximum temperature experienced by the canister (Tong et al., 2009). Also, if hydration is slow, it may influence the chemical state of the buffer. A particular issue of interest is the effect of uneven water wetting on

the bentonite buffer from water coming from individual fractures in the rock surrounding the buffer. It is also related to the question, what is the best way to understand and model the rock buffer interface? This question is being addressed in a new proposed project called BRIE (Bentonite Rock Interaction Experiment) being planned at the Äspö Hard Rock Laboratory in Sweden (see below). One problem to be investigated in this project is whether there is a need to develop special hydromechanical properties for the interface between bentonite and rock.

Concerning the understanding of THM processes in the bentonite, it has been noted that for some experiments, the models tend to overpredict the rate of hydration. This may be caused either by inaccuracies in parameter values, or by a faulty conceptual model of the THM processes. Some proposed additional phenomena (Cleall et al., 2007; Li et al., 2009) that could be included in our understanding and modelling of the buffer include (a) the effect of microstructural evolution (Sanchez et al., 2005) (b) the existence of different states of water in the bentonite, (c) the existence of a threshold hydraulic gradient for water flow and (d) thermo-osmosis (Zheng and Samper (2008); Zheng et al., 2010). A proper inclusion of relevant THM processes, together with thermodynamical constraints, is needed for extrapolation of bentonite behavior over a long time frame.

The buffer emplacement around waste canisters involves the use of bentonite blocks, which typically have gaps between individual blocks and between blocks and the rock. These gaps are often filled with bentonite pellets and pellet-powder mixture (Dixon et al., 2008). A concern that then arises is whether and how homogenization of bentonite density will take place. Here, homogenization refers to a process whereby all gaps are filled by the swelling and deforming bentonite blocks and pellets. A related question is, how well understood are the potential irreversible effects in large swelling and compression cycles? It is not expected that complete homogenization will be attained even if the buffer were of the same material, since the effects of swelling and compression cycles are expected to be irreversible. To have a proper study of this issue, THM models that include large strain formulations are needed.

The fourth area of concern is piping and erosion of the bentonite buffer (Birgersson et al., 2009; Birgersson and Karnland, 2009), which may cause significant mass loss during initial stages of the repository existence and during glaciation periods. In particular, water flow through the bentonite pellet fillings will cause bentonite erosion. The extent of pellet erosion depends on salinity, water flow rate, and granularity. Empirical erosion models and computer codes have been developed to evaluate the process and to suggest criteria, for example, on the maximum flow rate in order to limit the erosion potential. The flow rate may possibly be controlled by grouting or emplacement of plugs in the repository system.

Concerning chemical and mineralogical interaction in the bentonite buffer, a number of mineral reactions have been considered: (a) dissolution and precipitation of minerals, (b) ion-exchange such as from Na to Ca, (c) illitization and dissolution. The potential for release of colloids due to ion exchange, as well as the potential for diffusive transport of ions through the bentonite, needs to be evaluated. Furthermore, the possible chemical impact on THM processes leading to irreversible effects needs to be studied. To consider this possibility, multicomponent reactive transport models for repository environments

are being developed (Kimura et al., 2010; Seetharam et al., 2007, 2009; Guimaraes, et al., 2006, 2007; Xie, et al., 2004; 2006). A major development during the last few years is the re-establishment of the "chemical view" of bentonite (Birgersson and Karnland, 2009). This basic approach is primarily based on the ion equilibrium between an external solution and the bentonite interlayer pore-water, and has been demonstrated to explain the diffusional behavior of bentonite. Moreover, it provides a basic coupling between the chemistry and the hydromechanical processes. This approach should probably be important to consider for clay rock as well.

The above discussion is on the main component of the EBS, that is the bentonite. For a waste repository in clay formation, in addition to the buffer (which may be a bentonite-sand mixture, compacted pellets or clay from the site itself), there is also the concrete lining and steel support, forming part of the EBS system. Three major areas of knowledge gaps concerning the EBS in a clay repository have been identified (EC, 2010; Tsang et al., 2010): They are:

- Hydric condition, during the early stages before backfill and closure, between the tunnel air humidity and rock moisture conditions in the presence of the lining. This condition could well not be in equilibrium;

- Chemically interaction between the lining and steel support with the clay, modifying the clay properties,

- Over time, lining and steel support will degrade with potential release of gases, and thus gas transport through the EBS system and how the clay expands to fill the space of the degraded components are also problems of concern.

4.2.1.1 A Summary of Three Major International Activities and Suggested Needs for Further Research

In this section we shall describe three major on-going or recent research activities related to EBS-bentonite buffer and summarize the needs for further research identified by these projects:

1. The THERESA and TIMODAZ Projects
2. Äspö Hard Rock Laboratory EBS Studies and the BRIE Project
3. The DECOVALEX Project

4.2.1.2 The THERESA and TIMODAZ Projects

Within the European Commission (EC) Sixth Euratom Research and Training Framework Programme (FP6) on nuclear energy (EC, 2007) are two projects: the THERESA and TIMODAZ projects. Both are focused on coupled thermo-hydro-mechanical-chemical (THMC) processes in the near-field of a radioactive waste repository. Work has been done by a consortium of European research organizations over a four-year period and is planned to conclude about 2010 (EC, 2010)

The THERESA project is coordinated by the Royal Institute of Technology in Sweden and involves research organizations in seven countries: Sweden, Germany, The Netherlands, Spain, United Kingdom, Finland, and France. The project aims to develop scientific understanding, new approaches and methodologies for evaluating coupled THMC processes in the near-field, and to study their impact on performance assessment, repository design and construction, and post-closure monitoring of a waste repository. The project focuses on rock salt for the host rock, buffer materials (for crystalline rock repositories) and the buffer-rock interface.

Of particular interest is Work Package 4 (WP4) of this project, which focuses on modeling of coupled THM and THMC processes in buffer (mainly bentonite) and buffer-rock interfaces. The Centre International de Métodes Numeriés en Enginyeria (CIMNE) of Spain is the coordinator of this Work Package with participation of Cardiff University and Quintessa of UK, Posiva and Marintel of Finland and Institut de Radioprotection et de Sûreté Nucléaire (IRSN) of France. One of the main tasks within this Work Package is the study and modeling of the full-scale Canister Retrieval Test (CRT) at SKB's Äspö Hard Rock Laboratory.

The goal of CRT was to demonstrate readiness for recovering emplaced waste canisters in a full-scale (8m high, 1.65m diameter) deposition hole in crystalline rock with bentonite as buffer material. Canister and bentonite blocks were emplaced in 2000 and the hole was sealed with a plug. Then the heater in the canister was turned on and an artificial water supply was used to saturate the buffer. The saturation phase lasted for five years, until 2006. Over these years, continuous measurements of the wetting process, temperature, stresses and strains were conducted. In January 2006, the canister retrieval phase started with the canister successfully retrieved in May 2006. Bentonite from the deposition hole was then retrieved for laboratory testing. Data on mechanical strength, swelling pressure, hydraulic conductivity and chemical/mineralogical constitution of the bentonite over the experimental periods are becoming available.

The TIMODAZ project is coordinated by the Studie Centrum voor Kernenergie Centre Detude de L'Energie Nucleaire (SCK-CEN), Belgium, through the EURIDICE expertise group, with participation from research organizations of eight countries, Belgium, France, Switzerland, Germany, The Netherlands, Spain, Czech Republic, and United Kingdom. The rock type of interest in this project is clay, with three types being investigated: Boom clay found at the Belgium underground Research Laboratory HADES, Opalinus Clay existing at the Swiss Mont Terri Rock Laboratory; and the Callovo-Oxfordian argillite at the French Underground Research Laboratory at Bure. The approach is to conduct laboratory experiments, field tests and numerical modeling on coupled THMC processes in the near field. Here the near field is not only the buffer (e.g. bentonite, compacted pellets, cementitious materials) and the lining and steel support, but also the potential damaged zone in the near-field clay rock.

The THERESA and TIMODAZ projects held a joint Conference in Luxemberg, September 29-October 1, 2009 to review the progress and accomplishments from both projects (EC, 2010). At the conference, a working group on bentonite buffer was convened and discussed the state-of-the-art and open issues which are summarized in the last section. The group also came up with a table summarizing the processes in the buffer

materials, their relevance to performance assessment (PA) and the need for further research (Åkesson, 2010). This is shown as Table 4.2.1-1 below.

Table 4.2.1-1. Summary of processes, their relevance, and the need for further research (after Åkesson, 2010)

Processes	Relevance for PA	Need for experimental data	Need for code development	Need for development of conceptual models
Barrier hydration	Moderate.	Yes	If models can not predict new experiments	If models can not predict new experiments
Homogenization	Yes. Remaining heterogeneities should be limited	Yes	Yes	Yes
Piping and erosion	Yes. Significant mass loss should be avoided	Yes	Yes	Yes
Enrichment of groundwater substances	Yes, short term effects	No	Yes	No
Accessory mineral dissolution/precipitation	Yes, longer term effects	Yes	Yes	Yes
Montmorillonite surface reactions, Ion-exchange	Yes	No (Yes)	Yes	No (Yes)
Montmorillonite alteration illitization/dissolution	Yes	Yes	Yes	Yes
Colloid release in Na-montmorillonite	Yes	Yes	Yes	No
High salinity	Yes	No (Yes)	Yes	No
Diffusive transport	Yes	No (Yes)	Yes	No (Yes)

In addition to the THERESA and TIMODAZ projects, the European Commission FP6 program also supported the ESDRED (Engineering Studies and Demonstrations of Repository Design) project, coordinated by ANDRA, France with participation from nine countries; France, Finland, Spain, Switzerland, Sweden, Belgium, The Netherlands, Germany, and United Kingdom. Within this project, which lasted from 2004 to 2009, EBS for the different rock types have been studied, (Bock et al., 2008 Rothfuchs et al., 2007).

4.2.1.3 Äspö Hard Rock Laboratory EBS Studies and the BRIE Project

The Äspö Hard Rock Laboratory (HRL) operated by the Swedish Nuclear Fuel and Waste Management Company (SKB) has been the underground research facility for many aspects of nuclear waste disposal since 1995. While much of the work at the Laboratory is done to meet the needs of SKB, a substantial amount of activities are conducted as international cooperation. These international collaborative projects are

coordinated by the Äspö International Joint Committee, currently composed of representatives from SKB (Sweden), ANDRA (France), BMWi (Germany), CRIEPI (Japan), JAEA (Japan), NWMO (Canada), and Posiva (Finland).

A substantial number of large scale field experiments and supporting activities are conducted at Äspö HRL in the area of engineered barrier system. The goal is to develop, test and demonstrate EBS methods and procedures under realistic conditions and at appropriate scales. In a recent progress report (SKB, 2009) the following on-going experiments and activities are listed.

- *Prototype Repository:* Demonstration of the integrated function of the repository and testing of predicted models, based on study of six deposition boreholes.
- *Long Term Test of Buffer Material (LOT Experiment):* Data for validation of models and hypotheses concerning physical properties of bentonite buffer material and related processes in microbiology, radionuclide transport, copper corrosion and gas transport.
- *Alternative Buffer Materials:* Study of alternative clay materials potentially useful as buffer.
- *Backfill and Plug Test:* Study of a drift backfilled with a mixture of bentonite and crushed rock.
- *Canister Retrieval Test:* Demonstration of canister retrieval after surrounding bentonite buffer is fully saturated, with detailed monitoring of the wetting process, temperature, stresses and strains.
- *Temperature Buffer Test:* Study of THM behavior of buffer with temperature around and above 100°C during water saturation process.
- *KBS-3 Method with Horizontal Emplacement:* Developing methods for canister horizontal emplacement in a tunnel.
- *Large Scale Gas Injection Test:* Gas injection in a full scale KBS-3 deposition hole, with monitoring of full hydraulic behavior.
- *Sealing Test of Tunnel at Great Depth:* Testing of silica gel being a useful grout at water pressures prevailing at repository level.
- *In Situ Corrosion Testing of Miniature Canisters:* Study of corrosion processes inside a failed canister.
- *Cleaning and Sealing of Investigational Boreholes:* Identification and demonstration of best available techniques.
- *Task Force on EBS.*

The last activity, Task Force on EBS, is an international collaborative effort involving eight countries; Sweden, France, Germany, Japan, Switzerland, Finland, Canada and Czech Republic. Work is focused on THM modelling of processes during water transfer between buffer, backfill and near-field rock and on gas transport in saturated buffer. It was initiated in 2004 and the group has been meeting twice a year, the last being in Barcelona in May 2010. During this meeting, new issues were considered for future studies in the next phase of the Task Force. They are homogenization, erosion, gaps and interfaces, and effects of rock shear, as well as sensitivity studies and understanding of the relationship between simulation variables and performance results. These may be considered as open areas of research needing further investigation.

Concerning the particular topic of gaps and interfaces, a new task has been initiated called Bentonite Rock Interaction Experiment (BRIE). This task has the goal of understanding water exchange across bentonite rock interfaces, better prediction of bentonite wetting process, better characterization methods, and establishment of deposition hole criteria. Modelling is made in advance of an in-parallel field experiment, thus allowing for a blind prediction to analyze effects of different conceptual models. The experiment, BRIE, is divided into two parts: Part I concerning selection and characterization of a test site within the Äspö HRl and one or two central boreholes, and Part II concerning bentonite deposition, monitoring of physical and chemical changes, and extraction of the bentonite buffer. Work on this test is at the beginning stage.

4.2.1.4 The DECOVALEX Project

The DECOVALEX project is an international project initiated in 1992 to study the coupled THM processes around a nuclear waste repository (Tsang et al., 2009). The development of the research field of coupled THM processes including both modelling and laboratory or field experiments over the last 18 years has been very much influenced by this project. Over this time period, about 10 countries have participated in the collaborative research. The latest phase DECOVAKEX-2011 will conclude in 2011. The phase prior to this, named DECOVALEX-THMC, had a task to study coupled THM effects in the near field, including those on the bentonite buffer.

This task (Nguyen et al., 2009, Chijimatsu et al., 2009) was coordinated by Canada Nuclear Safety Commission with participation from Sweden, Japan, Finland, and Canada. First, bentonite models were calibrated against results from laboratory experiments on bentonite. These are swelling pressure tests, water uptake tests, thermal gradient tests, (Börgesson and Hernelind, 1999) and the CEA mock-up THM test (Gatabin and Billaud, 2005).

After the calibration studies, THM analysis was conducted to evaluate the near field behavior of the repository and their implication on the performance of a hypothetical repository. The scenario is based on a Canadian case study with the repository situated at a depth of 650 m in a stable crystalline rock of the Canadian Shield. Canisters are placed according to a horizontal borehole emplacement method with the gap between the canisters and rock filled with a bentonite buffer material. Factors of concern in the study include temperature rise, damage zone determination, change in permeability, resaturation of the bentonite buffer, swelling pressure and perturbation in the hydraulic

head distribution. These are calculated and studied for three phases: Excavation and waste emplacement (years 0-30), observation and monitoring (years 30-100), and post-closure period (years 100 to 1000 and more).

Results show that the permeability of the excavated damaged zone (EDZ) of the rock mass around the emplacement borehole could play a major role in the THM behavior in the near field. Thus an important open research area needing further study is the EDZ-EBS interaction. For sparsely fractured rock without EDZ, the bentonite is predicted to fully resaturate within a few decades, while for intact rock, full saturation might take more than 10,000 years. Temperature in all cases remain below 100°C. The predicted maximum total stress on the bentonite (MX-80 bentonite has been used in the study) could exceed 15 MPa which is the design pressure for the waste canister, when the rock mass is sparsely fractured. This result needs further research to confirm and to consider the implication.

4.2.2 Reactive-Diffusive Transport in the EBS

This subsection summarizes the literature review of reactive-diffusive transport in the EBS buffer materials, which is relevant for understanding the release and fate of radionuclide release into the natural system. Compacted bentonite has been proposed as backfill material in many of the European repositories, because of its very low permeability (Kim et al., 1993; Muurinen, 1994; Pusch, 2001; Molera and Eriksen, 2002; Bourg et al., 2003) and its strong sorptive properties (Eriksen et al., 1999; Ochs et al., 2001), both of which will limit the release of radionuclides. The low permeability of bentonite is largely due to the fact that it contains a high percentage of Na-montmorillonite, a clay that swells in water. The very low permeability of the compacted bentonite implies that transport of radionuclides away from the waste forms will be almost exclusively by molecular diffusion, with effective diffusivities far below that in water (Madsen, 1998; Ochs et al., 2001; Bourg et al., 2007). (This of course may change in the presence of advective pathways in the bentonite, which may result from insufficient homogenization, THMC-related fracturing, erosion, long-term degradation, etc. This is why THMC studies in Section 2 are so important.) Effective diffusivities for the compacted bentonite are very low as a result of its low porosity and the nanometer scale of the pores in the compacted clay. In much of the compacted bentonite, the pores are so small (<1 nanometer) that the electrical double layers balancing the charge of the bentonite (typically negative at circumneutral pH) overlap, thus potentially excluding anions altogether, or creating a deficiency in them with the Diffuse Double Layer balancing the surface mineral charge (Bourg et al, 2003; Bourg et al, 2006; Leroy et al, 2006; Gonçalvès et al, 2007).

Three types of water presence are recognized in compacted bentonite (Bourg et al, 2003; Wersin et al, 2004):

1. Interlayer water (φ_{IL}) with only water and cations within the Tetrahedral-Octahedral-Tetrahedral (TOT) layers of the montmorillonite. Here, the cations balance the fixed charge of the TOT layers;

2. Diffuse double layer (φ_{DDL}) containing cations and anions, but with an excess of ions (normally cations) to balance the charge of the clay surface;

3. Bulk or free pore water (φ_B), which is charge balanced.

The proportions of each kind of water depend on the compaction of the bentonite, but also the ionic strength through its effect on the width of the Diffuse Double Layer. In addition, the nature of cation affects the swelling and therefore the interlayer spacing.

Similar effects are also observed in clay-rich (20-40% typically) rocks that may be located in the near-field environment, although in this case the percentage of interlayer water may not be as significant. Examples are the Callovo-Oxfordian (COX) formation considered as a host rock for the French high level waste repository (Leroy et al., 2007; Appelo et al., 2008; Jougnot et al., 2009), or the Opalinus Clay under investigation in Switzerland (Appelo and Wersin, 2007). In experimental studies, it is common to observe the effects of anion exclusion, which in a diffusive regime is reflected by a late arrival (or release) of the negatively charged ions relative to neutral species (Bazer-Bachi et al., 2007 Melkior et al., 2007).

4.2.2.1 Formulation for Montmorillonite Interlayer Water

The volume of interlayer water has been measured as a function of the degree of compaction as reflected in the dry density (Muurinen, 2007). Strictly speaking, these results apply to montmorillonite with a large number of montmorillonite unit cells stacked on top of each other, since the interlayer porosity goes to zero as the grains become disperse. It was noted by Kosaki (1998) that a transition from 3 to 2 layer hydrates (corresponding to d001 spacing of 1.88 and 1.56 nm) occurred as the dry density increased from 1300 to 1600 kg/m^3. This led Muurinen et al. (2007) to propose an increase in interlayer spacing (in units of meters):

$$d_{IL} = 1.41\times10^{-9} - 4.9\times10^{-13}\rho_{dry}\,. \qquad (4.2\text{-}1)$$

Bourg et al (2006) placed the transition between three and two-layer hydrates between 1420 and 1570 kg/m^3. The interlayer spacing also decreases with increasing NaCl concentration, leading to the suggestion (Kozaki, 2008) of an osmotic effect:

$$d_{IL} = 1.41\times10^{-9} - 4.9\times10^{-13}\rho_{dry} + \gamma_{IL}(m_B - 0.2) \qquad (4.2\text{-}2)$$

where γ_{IL} is a coefficient (normally negative) and m_B is the molality of the NaCl in the bulk water. The porosity of the interlayer then becomes:

$$\phi_{IL} = d_{IL}\, A_{planar,\mathrm{int}} \Big/ 2\, w_{mont}\rho_{dry} \qquad (4.2\text{-}3)$$

where $A_{planar,int}$ is the surface area of the montmorillonite sheets stacked together (i.e., the internal surface area). Bourg et al. (2003) suggested a simpler linear relationship given by:

$$\phi_{IL} \approx 0.16\rho_{dry} \qquad (4.2\text{-}4)$$

They further suggested that the effective diffusion coefficient, D^*, is given by:

$$D^* = \frac{D_{free}(1-0.55\rho_{dry})}{\tau^2} \qquad (4.2\text{-}5)$$

where τ^2 is the tortuosity and D_{free} is the diffusion coefficient in pure water. This suggested that free water disappeared from a compacted bentonite once the dry density reached a value of about 1800 kg/m^3, in good agreement with the results of Kim et al (1993). However, Bourg et al. (2006) suggested a model that took into account the change from three- to two-hydrate layers at about 1450 kg/m^3, which resulted in a nonlinear dependence of the interlayer porosity on dry density.

4.2.2.2 Formulation for Diffuse Double Layer

A rigorous model for the diffuse layer could be derived from the combination of several equations, including the Poisson equation that describes the distribution of electrical potential, φ, in water:

$$\frac{\partial^2 \varphi}{\partial x^2} = -\frac{\rho_z}{\varepsilon}, \tag{4.2-6}$$

where ε is the permittivity and ρ_z is the volumetric charge density given by:

$$\rho_z = e\sum_i z_i C_i \,, \tag{4.2-7}$$

where e is the elementary charge of an ion, z_i is the charge of the ion, and C_i is its concentration. The Boltzmann distribution gives an expression for the concentration $\overline{C_i(x)}$ in the diffuse layer:

$$\overline{C_i(x)} = C_i \exp\left(\frac{-z_i e\varphi(x)}{k_B T}\right), \tag{4.2-8}$$

where C_i is here the concentration in the bulk solution, k_B is the Boltzmann constant, and T is the absolute temperature. Combining Equations 4.2-6 through 4.2-8 yields the Poisson-Boltzmann equation:

$$\frac{\partial^2 \varphi}{\partial x^2} = \frac{-e}{\varepsilon}\sum_i z_i C_i \exp\left(\frac{-z_i e\varphi(x)}{k_B T}\right) \tag{4.2-9}$$

which can be solved exactly for various simple formulations (e.g., the Gouy-Chapman model). For an arbitrary multicomponent system, Equation 9 needs to solved numerically together with the diffusion equations for the various species. Note that Equation 4.2-9 predicts an exponentially decaying electrical potential that will tend to zero with distance from the charged surface (Figure 4.2.2.2-1).

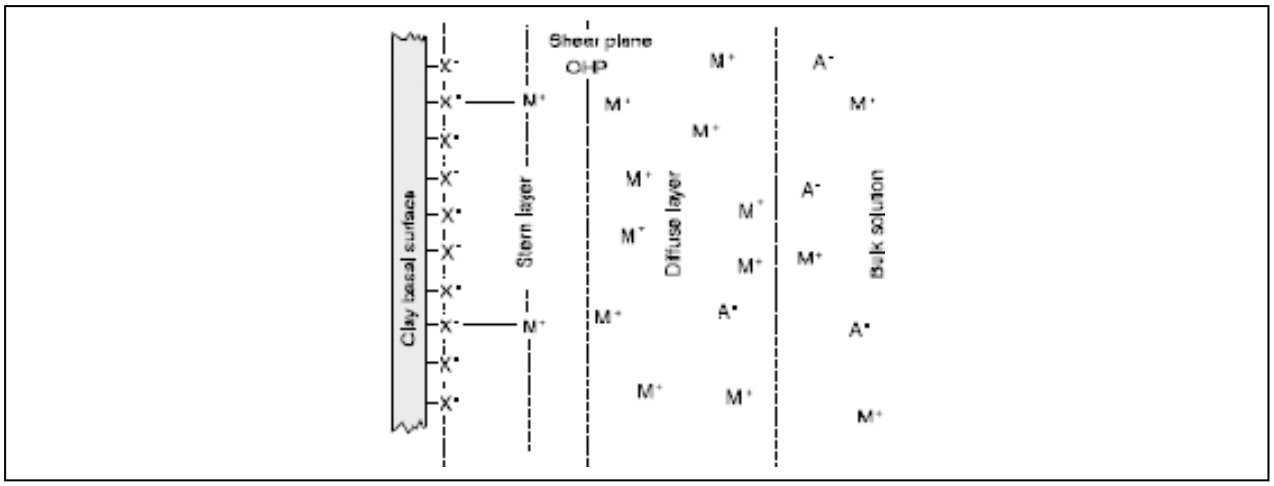

Figure 4.2.2.2-1 Schematic of the diffuse layer adjacent to a charged mineral surface. The counter-ions in the Stern Layer are calculated from a surface complexation model (either non-electrostatic or electrostatic) and is considered to be fixed, that is, inside of the shear plane. The diffuse layer, in contrast, is a swarm of mobile counter-ions that balance the charge of the mineral surface. Modified after Leroy et al., 2007.

Solving the full Poisson-Boltzmann equation is possible, but not normally very practical in the context of larger scale problems, since the scale of the diffuse layer is on the order of nanometers. Therefore, it is more practical to adopt an approach that treats porous medium as consisting of the three kinds of porosity corresponding to the kinds of water described above for compacted bentonite. For the Diffuse Double Layer, then, this involves defining a mean potential for the diffuse layer, the thickness of which will depend on the ionic strength of the solution. Its volume is given by the total surface area of charged mineral multiplied by the diffuse layer thickness:

$$\phi_{DDL} = A_{ext}\tau_{DDL}w_{mont}\rho_{dry} \qquad (4.2\text{-}10)$$

where A_{ext} is the external surface area of the montmorillonite, τ_{DDL} is the thickness of the diffuse layer, w_{mont} is the weight fraction of montmorillonite in the bentonite, and ρ_{dry} is the dry density of the compacted bentonite. At 25°C, the thickness of the diffuse layer can be approximated by the Debye length (κ^{-1}, the distance over which the potential in the diffuse layer drops by e);

$$\tau_{DDL} \cong \kappa^{-1} = \frac{3.04\times10^{-10}}{\sqrt{I}}, \qquad (4.2\text{-}11)$$

where I is the ionic strength (Stumm, 1992). In some cases, the diffuse layers may overlap, resulting in a smaller volume for the total diffuse layer per unit volume of porous medium.

Computationally, the diffuse layer balances the charge on the mineral surface itself, that is, Stern layer at the interface between the minerals and the pore water. The composition of the Stern layer is normally calculated with a surface complexation model which may be either an electrostatic model (the Diffuse Double Layer Model of Dzombak and

Morel, 1990, or potentially a Triple Layer Model, Leroy et al, 2007) or a non-electrostatic surface complexation model (Davis and Kent, 1990). The Stern Layer calculation includes a surface potential as an independent unknown if an electrostatic model is used. For the non-electrostatic case, only a set of secondary (non-component) surface complexes linearly related to the primary species in the bulk solution through mass action equations need to be calculated. The inclusion of an explicit diffuse layer, however, requires the introduction of a mean electrical potential for this volume as an independent unknown. This new unknown is solved through a charge balance equation and other relationships described further below.

4.2.2.3 Donnan Equilibrium Model

Several treatments of an explicit diffuse layer calculation based on a Donnan Equilibrium assumption have been presented in the literature (Wersin et al., 2004; Appelo et al., 2007; Leroy et al., 2007; Appelo et al., 2008). Typically, this involves an assumption that a Donnan Equilibrium condition applies, which equates the chemical potentials of the species in the diffuse layer and the bulk solution. Writing equations for the chemical potentials of the species *i* in the macroporosity (superscript "B") and microporosity (superscript "MP") respectively, we have:

$$\mu_i^B = \mu_i^{B,0} + k_B T \ln a_i^B \qquad (4.2\text{-}12)$$

$$\mu_i^{DDL} = \mu_i^{DDL,0} + k_B T \ln a_i^{DDL} + q_i \varphi_m \qquad (4.2\text{-}13)$$

where the superscript *0* (first term on the right hand side) refers to the chemical potential at the reference state, a_i are the species activities, q_i, is the charge of an ion (the elementary charge of a particle, e, multiplied by the valence of the ion, z_i), k_B is the Boltzmann constant, and φ_m is the mean electrical potential in the diffuse layer. The condition of Donnan Equilibrium implies that:

$$\mu_i^{DDL} = \mu_i^B \qquad (4.2\text{-}14)$$

$$\mu_i^{DDL,0} = \mu_i^{B,0}. \qquad (4.2\text{-}15)$$

Combining Equations 4.2-12, 4.2-13, 4.2-14, and 4.2-15 gives the Boltzmann distribution for the ion activities in the diffuse layer:

$$a_i^{DDL} = a_i^B \exp\left(\frac{-z_i e \varphi_m}{k_B T}\right). \qquad (4.2\text{-}16)$$

If the activity coefficients for the ions are assumed to be the same in the diffuse layer and the bulk water (probably not strictly true, but we would need a much more sophisticated model to improve on this assumption), then one can use Equation 4.2-16 to calculate concentrations in the diffuse layer as well:

$$C_i^{DDL} = C_i^B \exp\left(\frac{-z_i e \varphi_m}{k_B T}\right) \qquad (4.2\text{-}17)$$

Note that from Equation 4.2-17 it is possible to calculate all of the concentrations in the diffuse layer once its mean potential is determined numerically. The mean potential of the diffuse layer can be calculated with an additional charge balance equation:

$$\phi^{DDL}\sum_i z_i C_i^{DDL} = Q^{SL} \qquad (4.2\text{-}18)$$

where Q^{SL} is the total charge in the Stern Layer calculated with the surface complexation model, ϕ^{DDL} is again the volume of the diffuse layer, and C_i^{DDL} is the concentration in mol m^{-3}. The left hand side of Equation 4.2-18 gives a volumetric charge density in units of charge equivalents per unit volume porous medium. The surface charge is given by

$$Q^{SL} = \sum_k^{Ns} z_k \Gamma_k \qquad (4.2\text{-}19)$$

where Γ_k is the concentration in units of moles sorbed species per unit volume porous medium and z_k is the valence of the surface complex. By combining the Boltzmann equation (Eqn. 4.2-17), and the charge balance Equation 4.2-18, it is possible to calculate the mean potential of the diffuse layer, φ_m, along with the total concentrations of the primary species partitioned between the mineral surfaces (the Stern Layer), the diffuse layer, and the bulk solution. Since Equation 4.2-17 provides an algebraic relationship between the primary species in the bulk water and diffuse layer, it is not necessary to introduce the primary species in the diffuse layer as independent unknowns. In contrast, a kinetic treatment of the exchange between the two domains would require that the primary species in the diffuse layer be considered as independent unknowns. The total dissolved mass of a species, T_i, in units of moles per unit volume porous medium is calculated from:

$$T_i = \phi^B S_L C_i^B + \phi^{DDL} C_i^{DDL} \qquad (4.2\text{-}20)$$

where we have not included any contribution from mass in the clay interlayers as part of the dissolved total. Here the term S_L refers to the liquid saturation, which is assumed to be one in the case of the diffuse layer. The accumulation term for species *i* is then given by:

$$\frac{\partial}{\partial t}\left[\phi^B S_L C_i^B + \phi^{DDL} C_i^{DDL} + \Gamma_i + \phi^B S_G C_i^G\right] \qquad (4.2\text{-}21)$$

where Γ_i is the sorbed mass and C_i^G is the concentration of species *i* in the gas phase if present, and S_G is the gas saturation. This formulation treats the mass of species *i* in mineral phases as a separate pool that is kinetically controlled. Note that this approach conserves mass of component *i* over the entire porous medium, that is, mass is dynamically partitioned between the various pools (bulk solution, diffuse layer, surface complexes, etc.).

4.2.2.4 Diffusive Transport

Different transport operators are applied to each of the terms in Equation 4.2-21, including advection, dispersion and species-specific diffusion for the aqueous phase residing in the bulk water, species-specific diffusion for ions in the diffuse layer, and both advection and diffusion for the gas phase if present. Conceptually this means that within in any one grid cell there may be as many as three coexisting continua: 1) bulk water, 2) diffuse double layer, and 3) interlayer water/porosity. These continua can be assumed to be at equilibrium, in which case a single primary variable can be used to describe all of

them for a given element, or they can be treated kinetically, in which case primary independent unknowns are required for each of the porosity domains. In the case where equilibrium is assumed between the three (or two) domains, the transfer of mass between them is assumed to be instantaneous, implying that diffusion-controlled exchange between the two is not considered. However, diffusion within each continuum is possible (along with advection in the macroporosity), which requires that diffusion coefficients are provided separately for each of the continua. The model then calculates gradients within each continuum to determine the diffusive flux. The diffusive flux, J_i, in the case of the microporosity is given by (Steefel and Maher, 2009):

$$J_i^{MP} = -\phi^{MP} D_i^{MP} \frac{\partial C_i^{MP}}{\partial x} + \frac{t_i^{MP}}{z_i} \phi^{MP} \sum_j z_j D_j^{MP} \frac{\partial C_j^{MP}}{\partial x} \qquad (4.2\text{-}22)$$

where D_i^{MP} is the species-specific diffusion coefficient for the microporosity and t_i^{MP} is the transference number, or the fraction of the current carried by any one ion, for the microporosity given by:

$$t_i = \frac{z_i^2 u_i^{MP} C_i^{MP}}{\sum_j z_j^2 u_j^{MP} C_j^{MP}} \qquad (4.2\text{-}23)$$

In this expression, u_i refers to the mobility of ion i in the microporosity. A similar expression applies to species-specific, multicomponent diffusion in the macroporosity (Steefel and Maher, 2009).

4.2.2.5 Limitations to the Model

There is currently some interest in the community in being able to describe the slow release of ions or contaminants from low conductivity zones via diffusion. This kinetic behavior, which is frequently observed in both laboratory experiments and field tests, involves a diffusive transfer that is by definition non-equilibrium, driven as it is by gradients in chemical potential. With the assumption of a Donnan Equilibrium between the Diffuse Double Layer and the bulk or free water, however, no such chemical potential gradients can exist, since the chemical potentials in the two domains are assumed equal in this case. While diffusion-controlled kinetic release from "immobile" domains is relatively easy to model when no electrostatic effects are important (as the hydrologic community has discovered), the problem is far more difficult when electrical potential effects on chemical potentials (or ion activities) are included. A full treatment in this case requires solving the multicomponent diffusion equation along with the Poisson-Boltzman equation (Equation 9) at the nanometer scale. While this is possible, there are difficulties in upscaling the results when larger length scales (e.g., a laboratory column or larger) are considered.

It is likely that the activity coefficients for ions in the bulk solution and the diffuse layer are not the same. This follows from the fact that there is evidence for a change in the dielectric constant of water immediately adjacent to the charged mineral surface. The changes in activity coefficients would further change the counter-ion concentrations in the diffuse layer. Since the chemical potentials and activities are assumed the same in the bulk solution and the diffuse layer, no difference in the stability of either aqueous

complex, surface complexes, or minerals occur between the two domains. While the Donnan Equilibrium assumption means that important chemical changes in the immediate vicinity of the mineral surface are likely not captured, significantly more sophisticated modeling approaches would be needed to improve on this assumption.

4.3 The Current Modeling Capabilities at LBNL

This section provides a review of current LBNL modeling capabilities available for studying coupled THMC processes and reactive transport in EBS buffer materials. This review intends to help plan UFD EBS-group modeling activities with the current existing capabilities and also to help identify needs to improve these capabilities for future research activities.

4.3.1 Modeling Tools for Coupled THM processes

For the past decade, LBNL has been active in the development and application of coupled thermal-hydrological-mechanical (THM) modeling of bentonite-clay and rock systems associated with geological disposal of used nuclear fuel. As part of this effort, LBNL has since 1992 been involved as a research team in the international collaborative project DECOVALEX (Development of COupled Models and their VALidation against EXperiments in nuclear waste isolation). The modeling of THM processes in expansive (swelling) clay used as a buffer in most current disposal concepts in Europe, Asia and Canada, has been conducted using LBNL's **ROCMAS** finite element code. More recently, through the work within the Yucca Mountain Project, LBNL has developed an alternative model called **TOUGH-FLAC**, which is based on linking LBNL's TOUGH family multiphase flow codes to the commercial FLAC^{3D} geomechanical code. The development of the ROCMAS and TOUGH-FLAC has always been driven by needs for solving field-scale, multiyear *in situ* experiments of EBS and rock systems, including

1) The Kamaishi Mine heater test, Japan
2) The FEBEX *in situ* experiment at the Grimsel Test Site, Switzerland
3) The Drift Scale Test at Yucca Mountain, Nevada
4) The Tunnel Sealing Experiment (TSX) at URL Canada
5) The French Tournemire site in indurated clay.

A large number of Bench Mark Tests (BMTs) have been simulated, focusing on long-term coupled THM processes, both in the near field and EBS of multiple-barrier nuclear waste repositories and in the surrounding rocks. These cases include ROCMAS and TOUGH-FLAC modeling of:

1) The Japanese H12 repository design with vertical deposition holes.
2) The proposed high-level nuclear waste repository in Sweden for the KBS-3 concept.
3) The Canadian conceptual design for a repository in granite with horizontal deposition tunnels.
4) The Spanish EBS system emplaced in granite with horizontal deposition tunnels.

Moreover, a large number of laboratory experiments have been simulated for model validation as well as for calibration of coupled THM properties of bentonite-sand mixtures.

In the past year, LBNL has implemented the Barcelona Basic Model (BBM) into TOUGH-FLAC for rigorous modeling of thermo-elasto-plastic behavior of unsaturated soils. The BBM can describe a large number of typical features of the mechanical behavior of unsaturated soils, including wetting-induced swelling or collapse strains depending on the magnitude of applied stress, the increase of shear strength and apparent preconsolidation stress with suction. The BBM's implementation into TOUGH-FLAC is currently being tested and was applied to model the last case of the Spanish EBS system mentioned above. In this section, we first present the two modeling tools, ROCMAS and TOUGH-FLAC, and thereafter we demonstrate the application of ROCMAS and TOUGH-FLAC to the proposed high-level nuclear waste repository in Sweden.

4.3.2 The ROCMAS Code

The ROCMAS code (ROCk Mass Analysis Scheme) is a finite-element code for analysis of coupled THM processes in saturated-unsaturated fractured porous media. It has been gradually developed and extended since the early 1980s, headed by J. Noorishad at the LBNL. A hydromechanical formulation for fractured rock, based on Biot's general effective stress theory (Biot, 1941), was first developed, and a nonisothermal version of ROCMAS was presented in Noorishad et al., (1984). While at the time numerical models existed for coupled THM processes in porous media, the ROCMAS code was probably the first for fractured rocks, to include discrete fractures with non-linear coupled hydraulic and geomechanical behavior. The formulation was further extended from fully saturated to partially saturated media by Noorishad and Tsang (1996) and thereafter in Rutqvist et al. (2001), completing the formulation regarding the heat equation and effects of grain compressibility implemented into a full three-dimensional version.

In ROCMAS, the formulation of coupled thermo-hydroelasticity in terms of Biot's theory of consolidation (Biot, 1941) is extended to partially saturated media through Philip and de Vries' (1957) theory for heat and moisture flow in soil. In this theory, three phases (solid, liquid, and gas) are present. However, it is assumed that the gas pressure P_g is constant and equal to atmospheric pressure throughout the porous medium. As a consequence, vapor transport occurs only through molecular diffusion driven by a gradient in vapor concentration (density), while advection of vapor with bulk gas flow is neglected. The vapor density in the medium is governed by Kelvin's relation, assuming thermodynamic equilibrium for pore liquid in contact with its vapor, and phase transitions occur as evaporation-condensation processes. During heat transfer, coexisting fluid and solid components are assumed to be in local thermal equilibrium (i.e., locally they are at the same temperature). The mechanical behavior of the porous media consists of the gas, liquid and solid-matter responses to local pressure and the overall material (skeleton) response to effective stresses. Fractures are treated as a "porous medium" separate from the rock matrix and would be discretely defined by special fracture elements in a finite-element mesh. Therefore, the basic balance equations are the same for rock matrix and fracture materials, while some of the constitutive relations differ. With this approach and these assumptions, three balance equations—water mass balance, energy conservation and linear momentum balance—and a number of constitutive relations are required for a full description of the THM state. The ROCMAS code

includes various versions of constitutive geomechanical models for solid rocks, soils and discrete fractures including (Noorishad and Tsang, 1996):

- Linear elastic solid
- Associated and non-associated strain softening/hardening elastoplastic continuum
- Sandler/DeMaggio cap plasticity
- Oriented plasticity
- Compressible, dilating and strain softening elasto-plastic joints
- No tension continuum

The cap plasticity model may be applied to unconsolidated clay to model pore-collapse in addition to shear failure. However, for the EBS it must be extended to capture basic geomechanical behavior of unsaturated soil including saturation dependent strength and stiffness. A better option might be the Barcelona Basic Model that has been implemented in TOUGH-FLAC.

4.3.3 The TOUGH-FLAC Simulator

The TOUGH-FLAC was developed as a pragmatic approach for modeling coupled multiphase flow, heat transport and geomechanics, by linking the two established codes TOUGH2 and FLAC^{3D} (Rutqvist et al., 2002). In this approach, TOUGH2 (Pruess et al., 1999) is used for solving multiphase flow and heat transport equations, whereas FLAC^{3D} (Itasca, 2009) is used for solving geomechanical stress-strain equations. The TOUGH-FLAC simulator was originally developed for analysis of coupled THM processes associated with the Yucca Mountain Project. The FLAC^{3D} code was selected for the coupling to TOUGH2, because it is a well-established commercial code that has been extensively tested and verified. The two codes are sequentially coupled, but a TOUGH-FLAC simulation runs seamlessly. A great advantage with the adopted approach is that both codes are continuously developed and widely used in both academia and industry.

The simulator has been applied to study coupled geomechanical aspects under multiphase flow conditions for a wide range of applications, including nuclear waste disposal, CO_2 sequestration, geothermal energy extraction, naturally occurring CO_2 upwelling with surface deformations, and gas production from hydrate-bearing unconsolidated sediments. These applications have been accompanied with exploratory code developments. The most significant new development is a revised architecture compared to the earlier attempts, enabling a more rigorous and tight coupling procedure with improved computational efficiency. This development occurred when coupling the newly released TOUGH+ code to FLAC3D for the analysis of the geomechanical performance of hydrate-bearing unconsolidated sediments (Rutqvist and Moridis, 2009).

For analysis of coupled THM problems, the TOUGH2 and FLAC^{3D} are executed on compatible numerical grids and linked through a coupled THM model (Figure 4.3.3-1) with coupling functions serving to pass relevant information between the field equations that are solved in respective code. Depending on the problem and specific porous media (e.g., fractured rock, unsaturated clay, or hydrate-bearing sediments), a number of coupling functions have been developed.

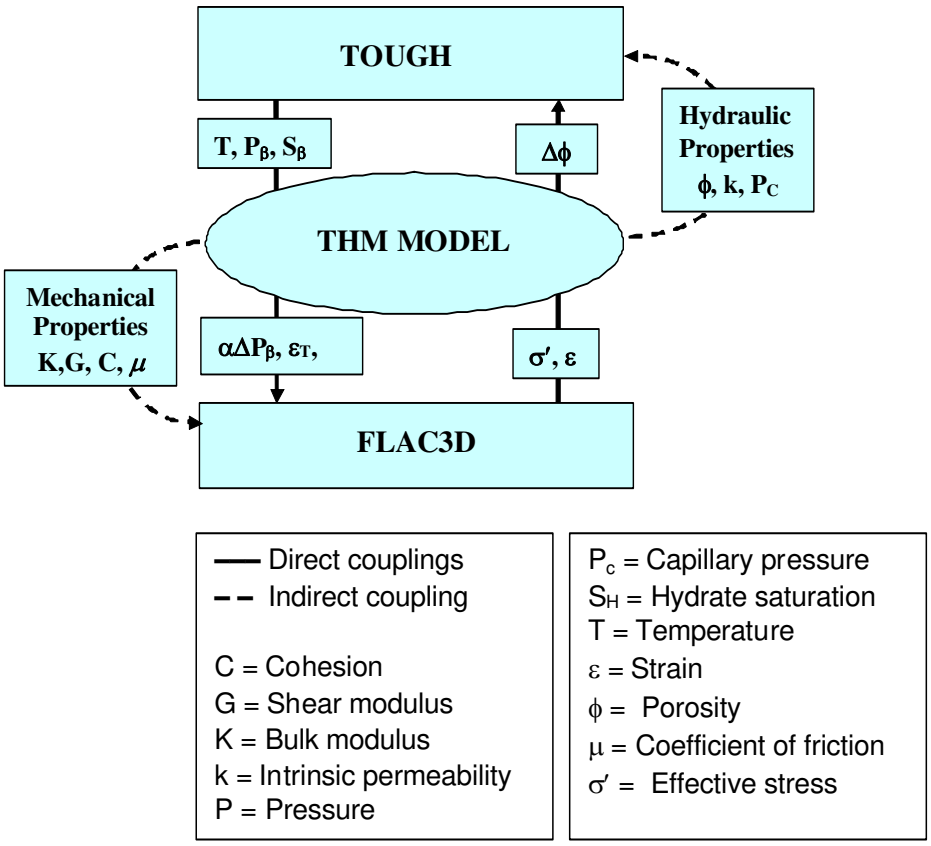

Figure 4.3.3-1 Schematic of linking TOUGH family code such as TOUGH+ and TOUGH2 with FLAC^{3D} for a coupled THM simulation.

In FLAC^{3D}, the basic explicit dynamic calculation iterates between solving the equation of motion and the stress-strain constitutive equation using a sufficiently small time step to assure numerical stability. In one time step, the equation of motion is first invoked to calculate new velocities based on previous velocities and forces. The nodal velocities are then used to derive new strain rates and stress, which in turn are used to update the force vector. The final solution is reached (using a damped solution) when the body is in equilibrium or in steady-state flow (plastic flow), and the out of balance force goes to zero.

A large number of constitutive geomechanical models are readily available in FLAC^{3D}, for both solid and interface elements, including:

- Elastic, isotropic, orthotropic, and transversely anisotropic
- Strain hardening/softening Mohr-Coulomb plasticity
- Ubiquitous joint (anisotropic) strain-hardening/softening bi-linear plasticity
- Double-yield plasticity
- Modified Cam-Clay
- Various creep models

The modified Cam-Clay may be applied to soft clay under saturated conditions. This model has been extended by the LBNL to the Barcelona Basic Model for thermo-elasto-plastic behavior of unsaturated soils (Rutqvist et al., 2009c). This type of model was recently applied by the group at the University of Cataluña, Barcelona, Spain, for modeling the thermo-elasto-plastic behavior of the compacted bentonite at the FEBEX *in situ* experiment. Thus, it is a contemporary model for the coupled geomechanical behavior of compacted bentonite-sand mixtures associated with nuclear waste respositories. The various anisotropic elastic and plastic models are suitable for modeling of shale.

In Figure 4.3.3-1, the data exchanges between TOUGH and FLAC^{3D} are illustrated with arrows going through the central THM model. The arrow on the right-hand side of Figure 3.3.3-1 shows the transmission of the effective stress σ' and strain ε (that are computed in FLAC^{3D}) to TOUGH for calculation of the updated porosity ϕ and the corresponding porosity change $\Delta\phi$. This mechanically induced $\Delta\phi$ has an immediate effect on fluid flow behavior. For example, if a change in σ' and ε causes ϕ to decrease, the pore pressure is expected to rise, especially if the permeability is low.

For porous deformable media, two models for mechanically induced porosity changes are implemented in the most recent version linking FLAC^{3D} to TOUGH+

(i) A poroelastic model (based on the approach proposed by Settari and Mourits (1998) that considers macroscopic stress/strain changes and grain deformability

(ii) An empirical model (proposed by Rutqvist and Tsang, 2002) that describes a nonlinear change in porosity as a function of the effective mean stress

The $\Delta\phi$ computed from either of these models is used to estimate changes in k by means of empirical equations. The updated ϕ and k values are in turn used to estimate changes in the hydraulic and wettability properties of the porous medium (i.e., aqueous- and gas-phase relative permeabilities k_{rA} and k_{rG}, and capillary pressure P_c) by employing appropriate scaling equations. For fractured media, a similar exponential empirical model has been applied to correct permeability for changes in the stress field (e.g., Rutqvist et al., 2002).

The arrow on the left side of Figure 4.3.3-1 depicts the flow of data obtained from TOUGH (namely the pressure P, temperature T, and phase saturations S_β) to FLAC^{3D} for processing and estimation of their impact on the effective stress $\alpha\Delta P_\beta$ (α being Biot's effective stress parameter), as well as on thermal and swelling strains (ε_T and ε_{sw}, respectively). Capabilities for modeling of moisture swelling and geomechanical behavior of unsaturated soil has recently been implemented into TOUGH-FLAC. In this model, the swelling can either be introduced as a function of phase saturation or as a function of suction (or capillary pressure, P_c) using the Barcelona Basic Model for elastoplastic behavior of unsaturated soils (Rutqvist et al., 2009c).

Additionally, changes in P, T, and S_β may also result in changes in other mechanical properties listed in Figure 3.3.3-1. These include the bulk modulus K, the shear modulus G, the cohesion C, and the coefficient of internal friction μ. For example, in the case of hydrate-bearing sediment, geomechanical properties change as a function of solid-phase

saturations, i.e., hydrate and ice saturations (S_H and S_I, respectively). In the case of unsaturated soil, the bulk modulus and friction angle is a function of suction.

4.3.4 Comparison of ROCMAS and TOUGH-FLAC to Other THM codes

A steadily growing interest in coupled THM phenomena in geological media has encouraged development of many computer codes at various levels of sophistication. Among those recently applied in the field of rock mechanics are THAMES (Ohnishi and Kobayashi, 1996), MOTIF (Guvanasen and Chan, 1995), FRACON (Nguyen, 1996), FEHM (Bower and Zyvoloski, 1997), GeoSys/Rockflow, (Kolditz et al. 2003), FRT-THM, (Liu et al. 2006), FRIP (Pine and Cundall, 1985), FRACture (Kohl and Hopkirk, 1995) and GEOCRACK (Swenson et al. 1997). The first four of these have been applied mostly in the field of geological disposal of nuclear waste, while the last three have been applied to the field of hot-dry-rock geothermal energy. There are also a few commercially available codes that have been applied to study these phenomena. The most frequently applied in soil and rock mechanics are ABAQUS (Börgesson, 1996), a finite-element code; FLAC (Israelsson, 1996a), a finite-difference code; and UDEC (Israelsson, 1996b), a discrete-element code.

Some of the above mentioned codes have also (like ROCMAS) been adapted for analysis of THM processes in variably saturated media (e.g., FRACON, FLAC, ABAQUS). At the same time, other codes have emerged from the field of soil mechanics. One of these is COMPASS (Thomas et al., 1998), which simulates two-phase (gas and liquid) in partially saturated soil, coupled with heat transport and mechanical responses. The mechanical behavior in COMPASS is governed either by a state surface approach or the more recent BBM. Another code in this group is CODE-BRIGHT (Olivella et al. 1994), which originally was developed for nonisothermal multiphase flow of brine and gas in saline media. This code has recently been adapted and applied to engineered clay barrier systems having similar characteristics to COMPASS, with two-phase flow for transport of moisture and heat coupled with mechanical responses using the state-surface approach (Gens et al. 1998) or the BBM thermo-elasto-plastic model that has recently been implemented in TOUGH-FLAC.

A number of simulators have also been developed focusing on oil and gas reservoir engineering, including commercial finite-element packages such as VISAGE (Koutsabeloulis, 1998), GMC-STARS, and a number of academic codes. TOUGH-FLAC is in the class of coupled simulators that is built upon coupling of a reservoir simulator to a geomechanical code. It is a delicate operation to correctly change the porosity of the reservoir simulator upon a change in stress or strain in the mechanical code. The ideas of Settari and Mourits (1998) have been implemented in TOUGH-FLAC coupling as one alternative poro-elastic model. The correct poro-elastic consideration is important when comparing simulation results to that of fully coupled poro-elastic finite element models of the Biot type. However, as described by Settari and Mourits (1998), in practice it is more important to consider the nonlinear stress-dependent effects on porosity and permeability over the range of stress expected in a problem. Such properties may be derived directly from laboratory data and fitted to theoretical or empirical functions (e.g., Liu et al., 2009) or by calibration to field experiments (e.g., Rutqvist et al., 2008).

In summary, it can be concluded that a large number of simulators have been developed for the analysis of coupled THM processes over the past 30 years. The ROCMAS code and TOUGH-FLAC are two different types of simulators that complement each other, have been extensively applied, and yet have the flexibilities for modifications and future improvements, such as linkage to TOUGHREACT for fully coupled THMC processes. When evaluating the capabilities of a code it is important to look at how it has been applied. The next section presents on example application of the ROCMAS and TOUGH-FLAC simulators related to nuclear waste isolation and EBS.

4.3.5 Modeling of the Proposed Swedish High Level Waste Repository

This example is part of LBNL's review of the Swedish Nuclear Fuel and Waste Management (SKB) program on coupled THM processes within the recent SR-Can project. SR-Can is SKB's preliminary assessment of long-term safety for a KBS-3 nuclear waste repository, and is a preparation stage for the SR-Site assessment, the report that will be used in SKB's application for a final repository. In this case the ROCMAS and TOUGH-FLAC codes were applied to analyze coupled THM processes at the two candidate sites, Forsmark and Laxemar, using data defined in SKB's site description models for respective sites. LBNL conducted a review and model analysis to address issues related to near-field behavior, such as buffer resaturation and the evolution of the excavation-disturbed zone, as well as far-field behavior, such as stress induced changes in hydrologic properties. The complete work is reported in Rutqvist and Tsang (2008). Here we focus on one example, related to the buffer/backfill/rock interaction for two alternative backfill options.

Figure 4.3.5-2 presents the model geometry representing one deposition hole and tunnel at the center of the repository. The model dimensions are different for Forsmark and Laxemar alternative, according to SKB's design that depends on site-specific conditions such as geology and *in situ* stress conditions. In 2009, the Forsmark site was selected by the SKB as the site for the SR-Site assessment.

Figure 4.3.5-3 presents the main difference in the backfill properties between the 30/70-mixture and Friedland Clay options considered in this case. One important issue identified in LBNL's modeling was that the initial suction pressure in the Friedland Clay was slightly higher than in bentonite buffer and much higher than in the rock. The high suction pressure in the Friedland Clay results in a strong potential for desaturation of the rock and even the possibility for suction of water from the buffer into the overlying backfill (Figures 4.3.5-4 and 4.3.5-5).

In the case of a very low rock permeability of $1x10^{-20}$ m^2, there is a strong desaturation of the rock surrounding the backfill and buffer, and total resaturation time for the two different backfill alternative varies between 20,000 to 40,000 years (Figure 4.3.5-5). Moreover, in the case of Friedland Clay, water would tend to be sucked from the buffer into the backfill rather than the reverse. The slow resaturation of the buffer implies that no substantial swelling pressure can develop before the thermal stress peak occurs at about 100 years. A lack of swelling pressure can have severe consequences for the development of rock failure and the EDZ around the deposition holes.

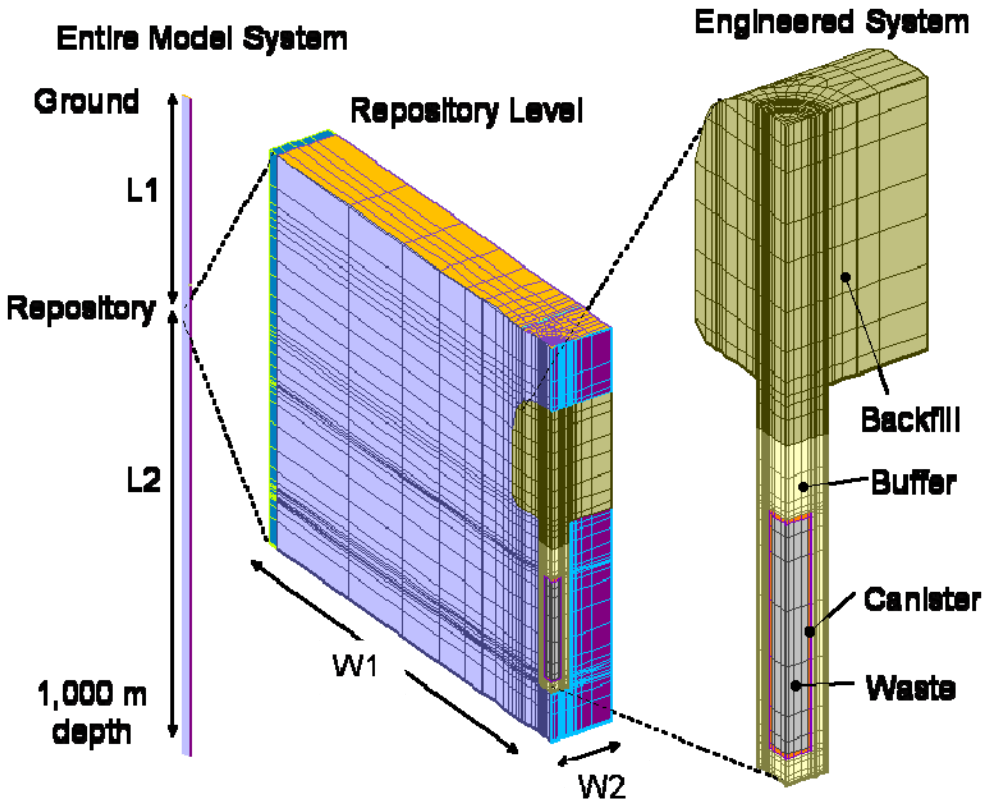

	Depth of repository, L1 (m)	Distance to bottom, L2 (m)	Half tunnel spacing, W1 (m)	Half canister spacing, W2 (m)
Laxemar	500 m	1,000 m	40/2 = 20	7.2/2 = 3.6
Forsmark	400 m	1,000 m	40/2 = 20	6/3 = 3

Figure 4.3.5-2. Quarter symmetric finite element model for coupled THM simulations of KBS-3V repositories at Forsmark and Laxemar.

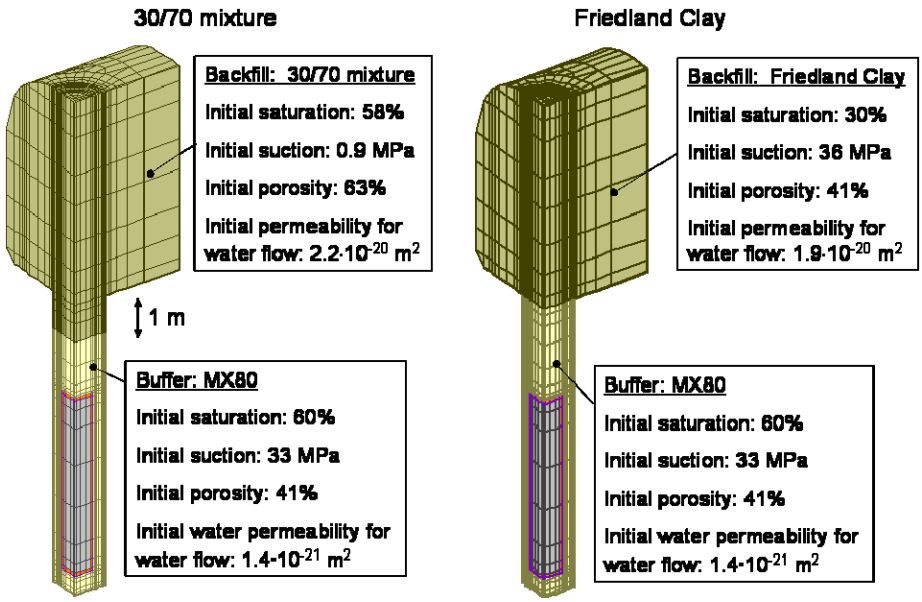

(a) (b)

Figure 4.3.5-3 Comparison of material properties and initial conditions for two alternative backfill materials: (a) 30/70 bentonite-rock mixture and (b) Friedland Clay.

(a) (b)

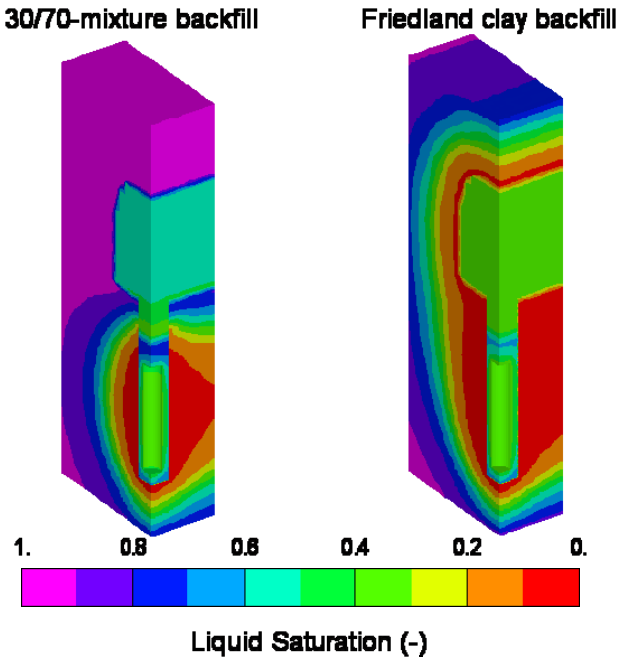

Figure 4.3.5-4 Variation backfill properties when rock permeability is low (k = 1×10^{-20} m^2): Distribution of liquid saturation 1,000 years after emplacement for a repository located at Forsmark when the tunnels are backfilled with (a) 30/70-mixture and (b) Friedland Clay.

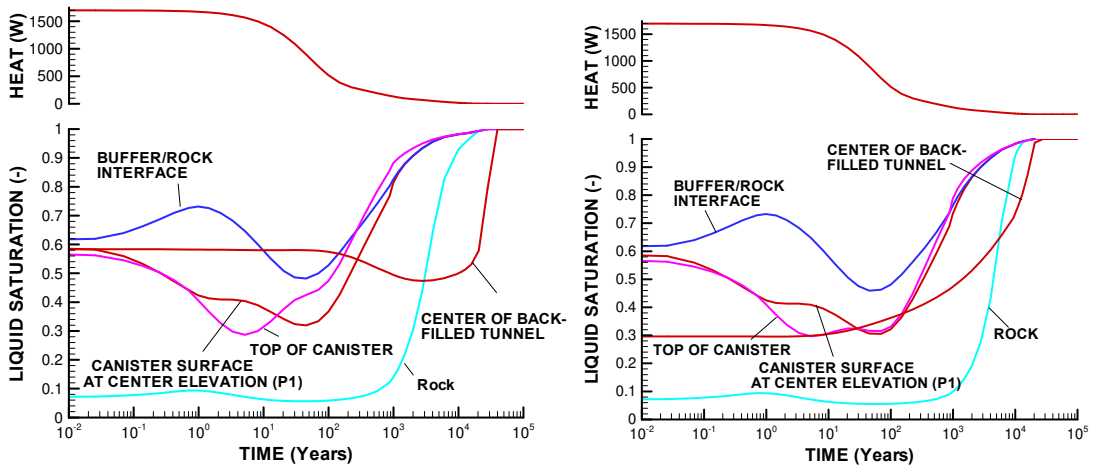

Figure 4.3.5-5 Variation of backfill properties when rock permeability is low (k = 1×10^{-20} m^2): Evolution of saturation at a repository located at Forsmark when the tunnels are backfilled with (a) 30/70-mixture and (b) Friedland Clay.

4.3.6 Modeling Tools for Reactive Transport

Two modeling tools, CrunchFlow and TOUGHREACT, are available at LBNL for modeling reactive transport processes. This subsection briefly reviews these two modeling tools.

4.3.6.1 CrunchFlow Code for Diffuse Double Layer Transport

Currently, the capability exists for modeling of solute partitioning into an explicit diffuse double layer and associated diffusion within this layer using the code CrunchFlow. No such capability presently exists for calculation of diffusion in interlayer porosity, although this is not seen as a serious obstacle. In the code CrunchFlow, which has had capabilities for multicomponent diffusion since 2002 (see Giambalvo et al, 2002), the option for calculation of an explicit diffuse double layer has been recently added. To do so, the mean electrical potential of the diffuse layer is added as an independent unknown, which is determiined in conjunction with the other primary variables by solving a charge balance equation for the diffuse layer balancing the mineral surface charge present in the Stern Layer. Since a Donnan Equilibrium condition is assumed, the concentrations of species in the diffuse layer are dependent variables algebraically linked to the primary species in the bulk water through the Boltzmann equation (Equation 17 in Section 4.2.2.3). Exchange between the diffuse double layer and the bulk water, therefore, is considered as instantaneous in this formulation. Species-specific diffusion with electrochemical migration (multi-component diffusion) is considered in both domains (diffuse layer and bulk water). An example simulation showing the slower diffusion of the anion chloride out of a clay-rich rock as a result of its partial exclusion in the diffuse double layer is shown in Figure 4.3.6-1.

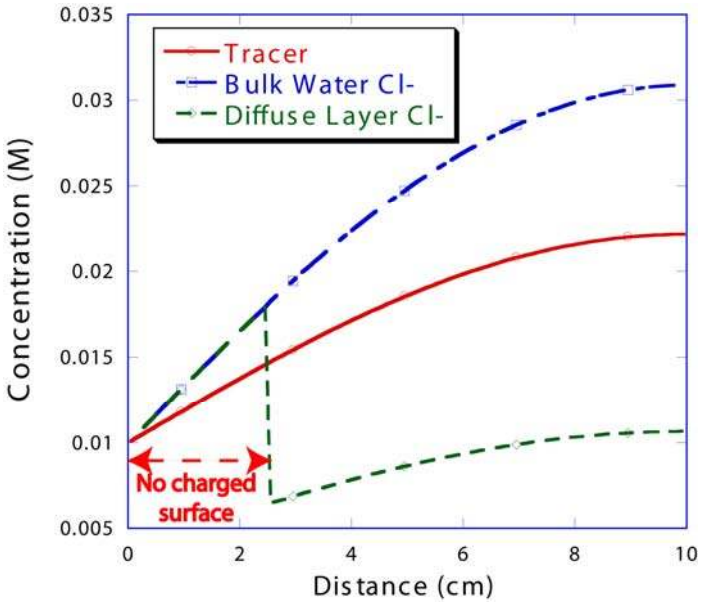

Figure 4.3.6-1 Spatial profile for the uncharged tracer and chloride in both the bulk water and diffuse layer where the charged illite surfaces result in anion exclusion. No charged surfaces within 1.5 cm of X = 0, which produces a discontinuity in the diffuse layer profile at this position. Calculation using CrunchFlow.

4.3.6.2 TOUGHREACT Code

Coupled modeling of subsurface multiphase fluid and heat flow, solute transport, and chemical reactions can be applied to many geologic systems and environmental problems, including geothermal systems, diagenetic and weathering processes, nuclear waste emplacement, acid mine drainage remediation, contaminant transport, and groundwater quality. TOUGHREACT has been developed as a comprehensive non-isothermal multi-component reactive fluid flow and geochemical transport simulator to investigate these and other problems (Xu et al., 2008). A number of subsurface thermo-physical-chemical processes are considered under various thermohydrological and geochemical conditions of pressure, temperature, water saturation, and ionic strength. TOUGHREACT can be applied to one-, two- or three-dimensional porous and fractured media with physical and chemical heterogeneity. The code can accommodate any number of chemical species present in liquid, gas and solid phases. A variety of equilibrium chemical reactions are considered, such as aqueous complexation, gas dissolution/exsolution, and cation exchange. Mineral dissolution/precipitation can take place subject to either local equilibrium or kinetic controls, with coupling to changes in porosity and permeability and capillary pressure in unsaturated systems. Chemical components can also be treated by linear adsorption and radioactive decay.

The first version of the non-isothermal reactive geochemical transport code TOUGHREACT was developed (Xu and Pruess, 1998) by introducing reactive geochemistry into the framework of the existing multi-phase fluid and heat flow code TOUGH2 (Pruess, 1991). TOUGHREACT was further enhanced with the addition of (1) treatment of mineral-water-gas reactive-transport under boiling conditions, (2) an improved HKF activity model for aqueous species, (3) gas species diffusion coefficients

calculated as a function of pressure, temperature, and molecular properties, (4) mineral reactive surface area formulations for fractured and porous media, and (5) porosity, permeability, and capillary pressure changes owing to mineral precipitation/dissolution. Subsequently, TOUGH2 V2 was released with additional EOS modules and features (Pruess et al., 1999 which was incorporated into the present version of TOUGHREACT (Xu et al., 2006).

4.3.6.3 Major Processes Treated by TOUGHREACT

The major processes for fluid and heat flow are: (1) fluid flow in both liquid and gas phases occurs under pressure, viscous, and gravity forces; (2) interactions between flowing phases are represented by characteristic curves (relative permeability and capillary pressure); (3) heat flow by conduction and convection, and (4) diffusion of water vapor and air. Thermophysical and geochemical properties are calculated as a function of temperature, such as fluid (gas and liquid) density and viscosity, and thermodynamic and kinetic data for mineral-water-gas reactions. Transport of aqueous and gaseous species by advection and molecular diffusion are considered in both liquid and gas phases. Depending on the computer memory and CPU performance, any number of chemical species in the liquid, gas and solid phases can be accommodated. Aqueous complexation, acid-base, redox, gas dissolution/exsolution, and cation exchange are considered under the local equilibrium assumption. Mineral dissolution and precipitation can proceed either subject to local equilibrium or kinetic conditions. Linear adsorption and decay can be included.

4.3.6.4 Governing Equations

The primary governing equations for multiphase fluid and heat flow, and chemical transport have the same structure, derived from the principle of mass (or energy) conservation. These equations are presented in Xu et al. (2008). Expressions for non-isothermal multiphase flow are given in Pruess (1987) and Pruess et al. (1999). The transport equations are written in terms of total dissolved concentrations of chemical components, which are concentrations of the basis species plus their associated aqueous secondary species (Yeh and Tripathi, 1991; Steefel and Lasaga, 1994; Walter and others, 1994; Lichtner, 1996; and Xu and Pruess, 2001). If kinetically-controlled reactions occur between aqueous species, then additional ordinary differential equations need to be solved to link the total concentrations of the primary species with the evolving concentrations of the secondary species (Steefel and MacQuarrie, 1996). Kinetically-controlled reactions between aqueous species are not considered in the present version. Slow aqueous phase reactions are common in the case of redox reactions and will be addressed in future development. Advection and diffusion processes are considered for both the aqueous and gaseous species. Aqueous species diffusion coefficients are assumed to be the same. Gaseous species, having a neutral valence, can have differing diffusion coefficients calculated as a function of T, P, molecular weight, and molecular diameter. The local chemical interactions in the transport equations are represented by reaction source/sink terms.

The primary governing equations must be complemented with constitutive local relationships that express all parameters as functions of fundamental thermophysical and chemical variables. The equations for chemical reactions are presented in Xu et al., (2008). Mass conservation in the closed chemical system is written in terms of basis

(component) species. The species distribution must be governed by the total concentrations of the components. The oxygen is used for formulating redox reactions by attributing the oxidizing potential to the dissolved oxygen (Nordstrom and Muñoz, 1986; Wolery, 1992). In contrast to the free electron in the hypothetical electron approach (Yeh and Tripathi, 1991), oxygen can be present and can be transported in natural subsurface flow systems. The formulation for cation exchange is similar to that of Appelo and Postma (1993). For kinetically-controlled mineral dissolution and precipitation, a general form of rate law (Lasaga, 1984; Steefel and Lasaga, 1994; Palandri and Kharaka, 2004) is used (Xu et al., 2008). Thermodynamic and kinetic data are functions of temperature.

Temporal changes in porosity, permeability, and unsaturated hydrologic properties owing to mineral dissolution and precipitation can modify fluid flow. This feedback between transport and chemistry can be important (e.g., Raffensperger, 1996; Dobson et al., 2003), and can be treated by TOUGHREACT. Changes in porosity during the simulation are calculated from changes in mineral volume fractions. The porosity-permeability correlation in geologic media can be complex, depending on several factors, such as pore size distribution, pore shapes, connectivity (Verma and Pruess, 1988), and crystal morphology. Several porosity-permeability and fracture aperture-permeability relationships are included in the model (Xu et al., 2008). The code can also be set to monitor changes in porosity and permeability during the simulation without considering their effects on fluid flow. In unsaturated systems, capillary pressure can be modified via permeability and porosity changes using Leverett scaling (based on Slider, 1976).

4.3.6.5 Application of TOUGHREACT to Bentonite-Filled EBS

This problem simulates water-rock interactions around nuclear waste packages emplaced in granitic host rock with bentonite backfill (Sonnenthal, 2008). This problem is based on data from the Swedish and Japanese nuclear waste programs, and was set up as a benchmark for the DECOVALEX-THMC project (Sonnenthal, 2008). Because this benchmark problem was intended for simulations using various codes of various levels of complexity, it was set up in a very simplified manner (e.g., reactions under local equilibrium, no ion exchange). Therefore, this problem should not be taken as an accurate representation of a nuclear waste repository. Nevertheless, this problem illustrates typical coupled thermal-hydrological-chemical processes that could occur in the EBS around nuclear waste packages as influenced by the very different near-field mineralogy and water chemistry. These processes include a heat pulse from the waste package (from radioactive decay), rewetting of the bentonite, a temporary decrease in the liquid saturation in the granite near the granite/bentonite interface, and chemical reactions in the granite near the interface (e.g., plagioclase alteration to clay with reduction in porosity). In comparison to other test problems, the dominant mode of transport is diffusion of aqueous species.

In this problem, the heat load results in temperature at the canister-bentonite interface climbing to a maximum near 95°C after about 10 years, then dropping back to about 55°C after 100 years. A porosity decrease of about 4% is computed in the granite at the bentonite-granite interface after 1000 years mostly from the dissolution of albite. Minerals precipitating near the interface include Na-montmorillonite, K-feldspar, quartz and calcite. Figure 4.4.2.3-2 shows the two-dimensional unstructured mesh for the TOUGHREACT simulations.

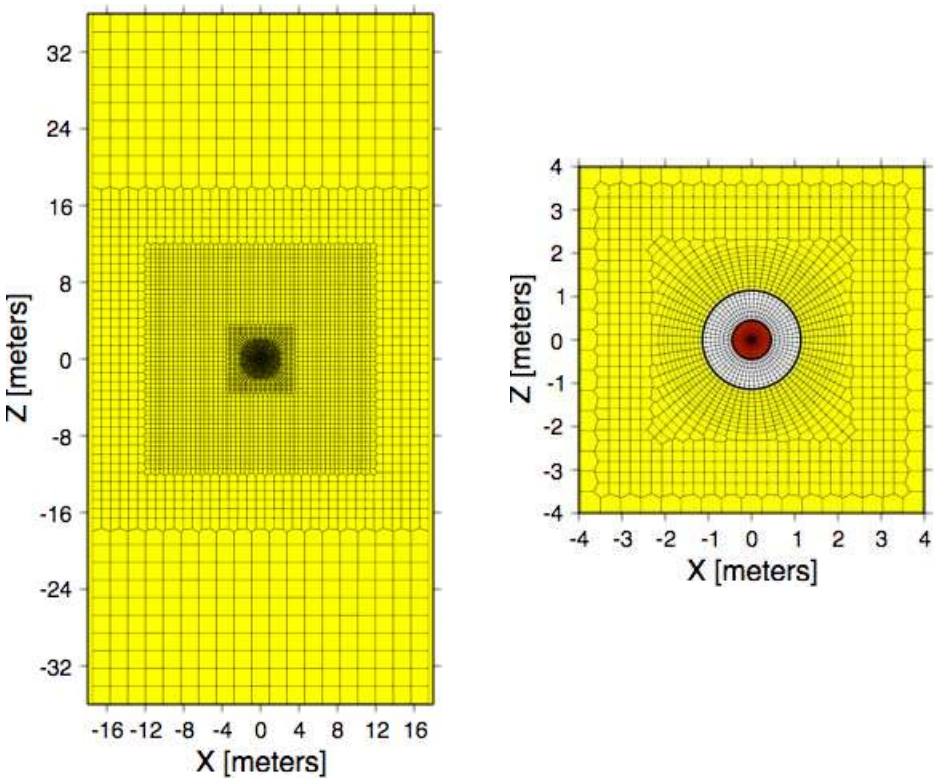

Figure 4.4.2.3-2. Two-dimensional numerical integral finite difference unstructured mesh for the TOUGHREACT simulations (left) and enlargement of drift mesh (right) showing waste canister (red), bentonite buffer (white), and drift wall boundary. Mesh extends 500 m above and below the drift center, and 17.5 m to each side.

Initially, there are small changes in the abundances of some minerals in the bentonite, owing to initial disequilibrium. The minor initial effects are overwhelmed by the heat- and transport-induced changes. By 1000 years, albite dissolution and quartz+calcite precipitation in the granite are evident (Figure 4.4.2.3-3). At this time, K-feldspar and calcite are dissolving in the bentonite near the margin of the granite, but were precipitated earlier in the hotter zone adjacent to the canister. The complex interplay of diffusion across the contact and the strong temperature gradients result in sharp changes in mineral dissolution/precipitation behavior traversing from the granite to the canister. Na-montmorillonite in the bentonite shows increased stability adjacent to the canister and also precipitates as a new secondary phase in the granite, but has dissolved in the bentonite at the margins of the drift.

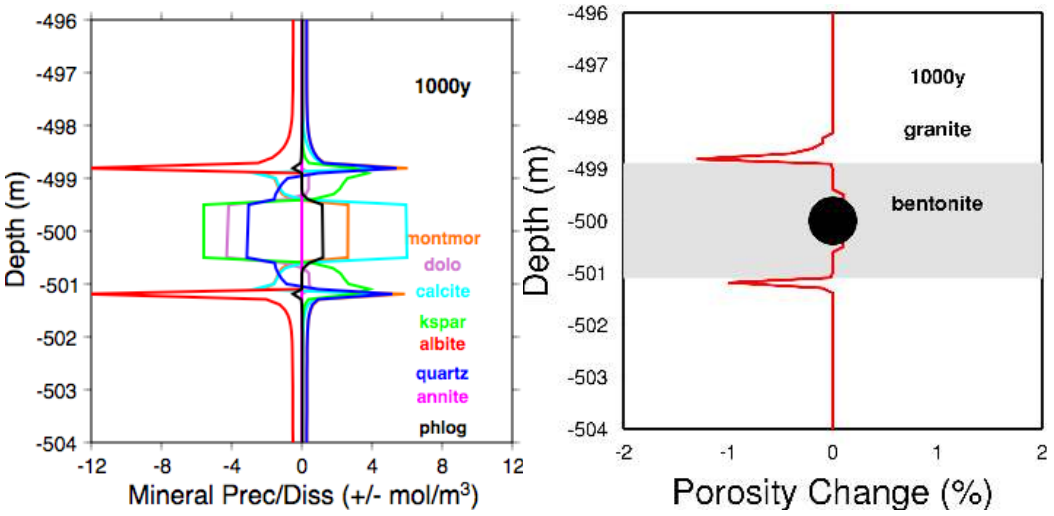

Figure 4.4.2.3-3 Mineralogical (left) and porosity (right) changes in bentonite and near-field granitic rock.

4.4 Modeling Results

In this section, modeling results are presented for THM studies implementing and testing the Barcelona Basic Model (BBM) for thermo-elasto-plastic behavior in bentonite and for an update on reactive-diffusive transport model approaches for radionuclide diffusion in bentonite.

4.4.1 Implementation and Testing of the Barcelona Basic Model

This section presents implementation and testing of the Barcelona Basic Model (BBM) into TOUGH-FLAC for modeling of mechanical behavior of unsaturated soils, including bentonite-sand mixtures for use a buffer material associated disposal of spent nuclear fuel. The BBM is a geomechanical constitutive model for capturing the elasto-plastic behavior of unsaturated soils. The model was first developed and presented in the early 1990s as an extension of the Modified Cam Clay (MCC) model to unsaturated soil conditions (Alonso et al., 1990). The model can describe many typical features of unsaturated-soil mechanical behavior, including wetting-induced swelling or collapse strains, depending on the magnitude of applied stress, as well as the increase in shear strength and apparent preconsolidation stress with suction (Gens et al., 2006).

The BBM is the most advanced and accepted constitutive model used for modeling of bentonite-buffer behavior in the various European and Japanese nuclear waste programs. For example, the BBM was recently successfully applied to model the coupled thermal-hydrological-mechanical (THM) behavior of an unsaturated bentonite clay associated with the FEBEX in situ heater test at the Grimsel Test Site, Switzerland (Gens et al., 2009). The BBM has also been applied to other types of bentonite-sand mixtures such as MX-80, considered as an option for an isolating buffer in the Swedish KBS-3 repository concept (Kristensson and Åkesson, 2008a).

In the following subsections, we first present the relevant equations of the thermo-elasto-plastic BBM, its relationship to the MCC, and how it is implemented into TOUGH-FLAC. This is followed by the description and results of a number of simulation tests to

verify the implementation of the BBM in comparison to published modeling, experimental, and laboratory data on THM behavior in unsaturated soils. Finally, we test and demonstrate the use of TOUGH-FLAC with BBM for a problem related to geological disposal of nuclear waste, involving the coupled THM performance of a bentonite back-filled nuclear waste deposition tunnel.

4.4.2 BBM Equations and implementation procedure

We implemented a thermo-elasto-plastic version of the BBM in which the soil strength depends on both suction and temperature, and includes features for expansive (swelling) clay (Gens, 1995). Figure 4.4.2-1 presents the three-dimensional yield surface in p'-q-s space and p'-q-T space, where p' is net mean stress (i.e., total stress minus gas-phase pressure), q is deviatoric stress (or shear stress), s is suction, and T is temperature (Gens, 1995). Under water-saturated conditions (s = 0), the yield surface corresponds to the MCC ellipse (Roscoe and Burgland, 1968), and the size of the elastic domain increases as suction increases. The rate of increase, represented by the loading-collapse (LC) curve, is one of the fundamental characteristics of the BBM (Gens et al., 2006). Moreover, in the thermo-elasto-plastic version of the BBM, the size of the yield surface decreases with temperature (Figure 4.4.2-1). We implemented the BBM into TOUGH-FLAC by (1) extending an existing MCC module within the framework of the FLAC^{3D} User Defined Model (UDM) capability, and (2) adding computational routines for suction-dependent strains and net stress in unsaturated soils.

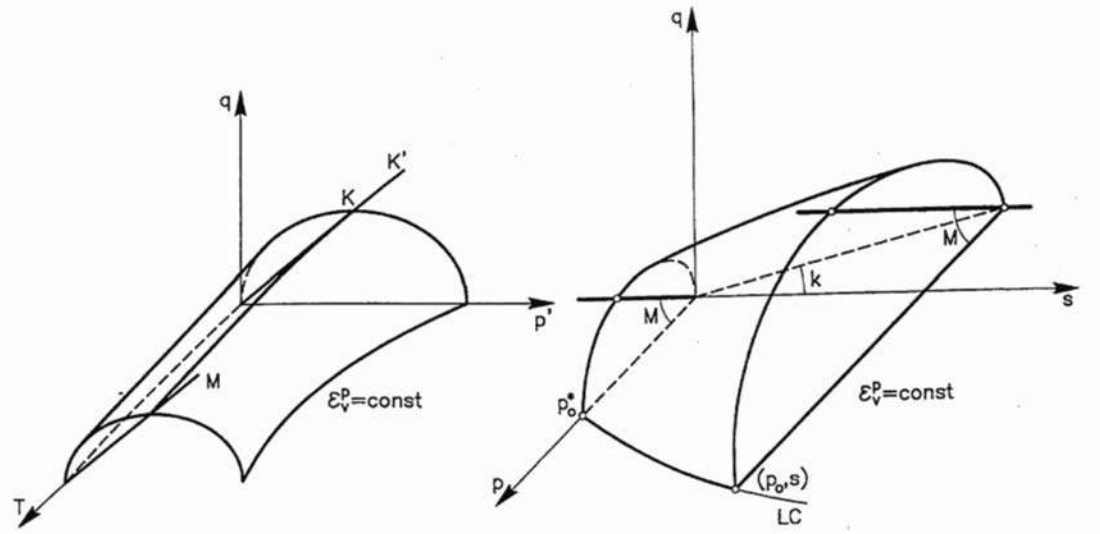

Figure 4.4.2-1. Three-dimensional representation of the yield surface in the thermo-elasto-plastic BBM (after Gens, 1995).

Stress State

The conventional (Terzaghi) effective stress that can be expressed as

$$\boldsymbol{\sigma}' = \boldsymbol{\sigma} - p^{\phi}\mathbf{I} \tag{4.4-1}$$

where σ' and σ are, respectively, the effective and total stress tensors (positive for compression), p^{ϕ} is pore pressure, and I is the identity tensor. The stress state can be divided into a hydrostatic part (1/3)trace(σ')I = p'I and deviatoric part s = σ' - p'I, where p' is the effective mean pressure (or effective mean stress) that can be expressed explicitly as:

$$p' = p - p^{\phi} = \frac{1}{3}(\sigma_1 + \sigma_2 + \sigma_3) - p^{\phi} \tag{4.4-2}$$

where p is total mean pressure (total mean stress), and σ_1, σ_2, and σ_3 are principal compressive stresses. The conventional effective mean stress is used for water saturated conditions in the original MCC model (Roscoe and Burgland, 1968) as well as in the FLAC^{3D} implementation of MCC (Itasca, 2009). In the BBM, however, under unsaturated conditions, the strains are related to changes in two independent stress variables, namely the net mean stress for which

$$p' = p - p^{g} \tag{4.4-3}$$

and suction, s, is defined as

$$s = p^{g} - p^{l} \tag{4.4-4}$$

where p^g and p^l are gas- and liquid-phase pressures.

The deviatoric (von Mises) stress, q, is defined as:

$$q = \sqrt{3J_2} = \sqrt{3\frac{1}{2}\mathbf{s}\cdot\mathbf{s}} = \sqrt{\frac{(\sigma_1' - \sigma_2')^2 + (\sigma_2' - \sigma_3')^2 + (\sigma_1' - \sigma_3')^2}{2}} \tag{4.4-5}$$

where J_2 is the second invariant of the effective deviatoric-stress tensor, s.

For the implementation of the BBM into TOUGH-FLAC, both suction and gas pressure are needed. We calculated s from the TOUGH capillary pressure, which in turn is calculated from gas- and liquid-phase pressures according to Equation (4.4-4). Moreover, in TOUGH-FLAC, the concept of net mean stress for unsaturated soils is implemented by transferring the maximum of the gas- or liquid-phase pressure from TOUGH to FLAC^{3D} according to

$$p^{\phi} = MAX(p^{l}, p^{g}) \tag{4.4-6}$$

This approach enables simulation of both saturated and unsaturated soils. Under single-fluid phase conditions, the first primary variable is p^g for single gas phase or p^l for single liquid phase. For two fluid phase conditions, the primary variable is gas pressure, which is greater than the liquid pressure. As a result, for fully liquid saturated conditions, the conventional effective stress applies according to Equation (4.4-2), whereas for unsaturated conditions, the mechanical behavior depends on the two stress variables net, stress and suction, defined in Equations (4.4-3) and (4.4-4).

Strains due to Stress, Temperature and Suction

The strain tensor can—similarly to the stress tensor—be expressed as the sum of a hydrostatic part (1/3)trace(ε)I=(1/3)ε_vI and deviatoric part e = ε - (1/3)ε_vI, where ε_v is the volumetric strain associated with change in net mean stress, p', and can be explicitly expressed as

$$\varepsilon_v = \left(\varepsilon_1 + \varepsilon_2 + \varepsilon_3\right) \tag{4.4-7}$$

where ε_1, ε_2, and ε_3 are principal strains.

An equivalent deviatoric strain, associated with distortion and changes in deviatoric stress q, may be defined as

$$\varepsilon_q = \frac{2}{3}\sqrt{3J_2'} = \frac{2}{3}\sqrt{3\frac{1}{2}\mathbf{e}\cdot\mathbf{e}} = \frac{2}{\sqrt{6}}\sqrt{\left(\varepsilon_1-\varepsilon_2\right)^2+\left(\varepsilon_2-\varepsilon_3\right)^2+\left(\varepsilon_3-\varepsilon_1\right)^2} \tag{4.4-8}$$

where J'_2 stands for stands for the second invariant of the deviatoric-strain tensor **e**.

For nonisothermal behavior of unsaturated soils, we may partition the total incremental strain into elastic, plastic, suction, and thermal strains:

$$\mathrm{d}\boldsymbol{\varepsilon} = \mathrm{d}\boldsymbol{\varepsilon}^{\mathrm{e}} + \mathrm{d}\boldsymbol{\varepsilon}^{\mathrm{p}} + \mathrm{d}\boldsymbol{\varepsilon}^{\mathrm{s}} + \mathrm{d}\boldsymbol{\varepsilon}^{\mathrm{T}} \tag{4.4-9}$$

where the suction strain corresponds to the hydraulic strain term suggested by Kristensson and Åkesson (2008a) and represents the strain associated with changes in suction. Each of these strain types are described in the following subsections.

Elastic Strain

The mechanical volumetric elastic strain increment is associated with changes in net mean stress dp' according to

$$\mathrm{d}\varepsilon_v^e = \frac{1}{K}\mathrm{d}p' \tag{4.4-10}$$

where the bulk modulus K is defined as

$$K = \frac{(1+e)p'}{\kappa_{ps}(s)} \tag{4.4-11}$$

in which the compressibility function $\kappa_{PS}(s)$ is defined as

$$\kappa_{ps}(s) = \kappa_{ps0}\left[1 + s\alpha_{ps}\right] \tag{4.4-12}$$

The deviatoric elastic strain increment is defined as

$$d\varepsilon_q^e = \frac{1}{3G}dq \tag{4.4-13}$$

where G may be obtained using a constant Poisson's ratio ν in

$$G = \frac{3(1-2\upsilon)}{2(1+\upsilon)}K \tag{4.4-14}$$

Thus, the equations for elastic mechanical strain indicate the dependency of bulk modulus on suction (and hence fluid saturation) in which dry clay can be significantly stiffer than water-saturated clay.

In the current FLAC^{3D} MCC implementation, there is the option of either inputting a constant υ and calculate G from Equation (4.4-14) or using a constant G and calculating υ from Equation (4.4-14). When implementing the BBM, this approach can be readily extended into unsaturated conditions, in which K is governed by Equation (4.4-11).

Plastic Strain

The temperature- and suction-dependent loading collapse (LC) yield surface (Figure 4.4-1) bounds the elastic region according to

$$f_{LC} = \frac{q^2}{g_y(\theta)^2} - \frac{M^2}{g_y(\theta=0)^2}\left(p' + p_s(s,T)\right)\left(p_0(s,T)\right) - p' = 0 \qquad (4.4\text{-}15)$$

where θ is the Lode's angle, and the function $g_y(\theta)$ describes the shape of the yield surface in the deviatoric plane (Kristensson and Åkesson, 2008b). M is the constant slope of the critical state line (Figure 4.4.2-1), whereas

$$p_s(s,T) = p_{s0} + k_s s \exp[-\rho_s \Delta T] \qquad (4.4\text{-}16)$$

represents the increases in cohesion with suction and temperature change $\Delta T = T - T_0$, where k_s and ρ_s are empirical material constants.

In Equation (4.4-15), the function

$$p_0(s,T) = p^c\left(\frac{p^*_{0T}(T)}{p^c}\right)^{[\lambda_{Ps0}-\kappa_{Ps0}]/[\lambda_{Ps}-\kappa_{Ps0}]} \qquad (4.4\text{-}17)$$

is the net mean yield stress (or apparent pre-consolidation stress) at current suction and temperature, where

$$p^*_{0T}(T) = p^*_0 + 2\left(\alpha_1 \Delta T + \alpha_3 \Delta T|\Delta T|\right) \qquad (4.4\text{-}18)$$

is the temperature-dependent net mean yield stress (or pre-consolidation stress) at full saturation and

$$\lambda_{PS}(s) = \lambda_{PS0}\left((1-r_\lambda)\exp(-\beta_\lambda s) + r_\lambda\right) \qquad (4.4\text{-}19)$$

is a compressibility parameter in virgin soil states at suction s. λ_{Ps} determines the shape of the LC yield surface, which increases in size with suction, whereas the temperature-dependent pre-consolidation stress $p^*_{0T}(T)$ results in a reduction of the yield surface with temperature (Figure 4.4-1).

When the stress state is on the yield surface, the plastic strains are obtained from the plastic flow rule

$$\mathrm{d}\varepsilon^P_P = \mathrm{d}\Lambda \frac{\partial g}{\partial p'} \qquad (4.4\text{-}20a)$$

$$\mathrm{d}\varepsilon_q^P = \mathrm{d}\Lambda \frac{\partial g}{\partial q} \tag{4.4-20b}$$

where $d\Lambda$ is the plastic multiplier obtained from the consistency condition $df_{LC} = 0$, and g_{LC} is the plastic potential defined by

$$g_{LC} = \frac{\alpha_a q^2}{g_y(\theta)^2} - \frac{M^2}{g_y(\theta = 0)^2}\left(p' + p_s(s,T)\right)\left(p_0\left(p_0^*, s\right)\right) - p' \tag{4.4-21}$$

where α_a is a parameter that gives rise to the nonassociative model, i.e. $g_{LC} \neq f_{LC}$.

In the implementation of the BBM in FLAC^{3D}, substantial extensions of existing MCC equations must be implemented and programmed for calculating the mechanical plastic strain. These extensions include considering the saturation and temperature dependency of many parameters in Equations (4.4-15) to (4.4-21) that define the shape of the LC yield surface, as well as extension to nonassociative plasticity.

Thermal Strain

Thermally induced strains are purely volumetric:

$$\mathrm{d}\varepsilon_v^T = \left(\alpha_0 + 2\alpha_2 \Delta T\right)\mathrm{d}T \tag{4.4-22}$$

where α_0 and α_2 are material parameters defining the temperature-dependent volumetric thermal expansion coefficient. Equation (4.4-22) is implemented as a simple extension of the existing thermal strain capability in FLAC^{3D}.

Suction Strain

In analogy with thermally induced strains, the suction strain is purely volumetric:

$$d\varepsilon_v^s = \frac{1}{K^s} ds \tag{4.4-23}$$

in which we (similarly to Kristensson and Åkesson, 2008b) define K^s to be the suction bulk modulus

$$K^s = \frac{(1+e)(s + p_{atm})}{\kappa_{sp}(p', s)} \tag{4.4-24}$$

where κ_{SP} is a compressibility parameter for suction induced strain defined as

$$\kappa_{sp}(p', s) = \kappa_{sp0}\left(1 + \alpha_{sp} \ln \frac{p'}{P_{ref}}\right)\exp(\alpha_{ss} s) \tag{4.4-25}$$

Suction strain was added to TOUGH-FLAC in an analogous manner to treatment of thermal strain in FLAC^{3D}, by adding an equivalent mean stress increment according to

$$dp^s = K d\varepsilon_v^s = \frac{K}{K^s} ds \tag{4.4-26}$$

This is implemented in FLAC^{3D} by adding increments to the normal stresses:

$$d\sigma_{xx}^{s} = \frac{K^{m}}{K^{s}} ds \tag{4.4-27a}$$

$$d\sigma_{yy}^{s} = \frac{K}{K^{s}} ds \tag{4.4-27b}$$

$$d\sigma_{zz}^{s} = \frac{K}{K^{s}} ds \tag{4.4-27c}$$

Both K and K^s are dependent on suction and mean net stress, according to Equations (4.4-11) and (4.4-24), and are calculated within the new FLAC^{3D} BBM module, whereas the stress increments are added in a separate routine using FISH, which is a programming capability attached to FLAC^{3D} (Itasca, 2009).

Evolution of specific volume

In the existing FLAC^{3D} implementation of the MCC model, the evolution parameter is the specific volume v, defined as,

$$v = \frac{V}{V^{s}} \tag{4.4-28}$$

where V^s is the volume of solid particles contained in a volume, V, of soil. The incremental relation between volumetric strain and specific volume is

$$\mathrm{d}\varepsilon_{v} = \frac{\mathrm{d}v}{v} \tag{4.4-29}$$

and an updated specific volume for a new step, $i + 1$, is calculated according to

$$v^{i+1} = v^{i}\left(1 - \mathrm{d}\varepsilon_{v}\right) \tag{4.4-30}$$

The initial value for specific volume v_i is dependent on the initial net mean stress and is calculated from

$$v_{i} = v^{c} - \lambda_{ps} \ln\left(\frac{p_{0T}^{*}}{p^{c}}\right) + \kappa_{PS} \ln\left(\frac{p_{0T}^{*}}{p_{i}'}\right) \tag{4.4.-31}$$

where v^c is a material input value of the specific volume at the reference net mean stress p^c.

From the evolution of the specific volume, porosity, ϕ, and void ratio, e, are evaluated as

$$\phi = \frac{V^{\phi}}{V} = \frac{v-1}{v} \tag{4.4.-32}$$

$$e = \frac{V^{\phi}}{V^{s}} = v - 1 \tag{4.4.-33}$$

where V^{ϕ} is the pore volume. When implementing the BBM into TOUGH-FLAC, these concepts are readily expanded into the unsaturated soil domain.

4.4.3 TOUGH-FLAC BBM module and input data

The thermo-elasto-plastic BBM was programmed in C++ and invoked into FLAC^{3D} according to the UDM capability available in FLAC^{3D}. The new C++ routine was compiled as a DLL file (dynamic link library) that can be loaded into FLAC^{3D} whenever needed. In a TOUGH-FLAC implementation of the BBM, we also developed a few FISH routines, such as one for calculating suction strain.

The extension of the MCC model to unsaturated media and nonisothermal conditions adds to the complexity and the number of input parameters required. Five parameters are required to define the MCC model, and seven additional parameters are required for the BBM model. In the thermo-elasto-plastic version of the BBM implemented in this study, the failure surface also depends on the temperature, and total of twenty-one material parameters are possible. Discussions on how to determine these parameters from laboratory experiments are given in Alonso et al. (1990) and Gens (1995), and more recently in Kriststensson and Åkesson (2008a). Frequently, the number of laboratory tests may be sparse, and some parameters may therefore be determined by model calibration. Kristensson and Åkesson (2008b) developed numerical tools in a Mathcad environment for a quick assessment of BBM parameters from laboratory experiments.

4.4.4 Simulation Test to Verify the BBM Implementation

A number of simulation tests were conducted to verify the implementation of the thermo-elasto-plastic BBM within the FLAC^{3D} UDM framework. These included basic tests at saturated conditions for the standard FLAC^{3D} MCC model (Itasca, 2009), and tests under unsaturated conditions of the BBM using published literature data. Table 4.4.4-1 summarizes a few examples of the small-scale simulation tests. AGJ1 and AGJ2 simulation tests examples enable comparison to analytical results of Alonso et al. (1990), whereas the K&Å1, K&Å2 and K&Å3 provide comparison to both independent model simulations and actual experimental data on MX-80 bentonite reported in Kristensson and Åkesson (2008a). The key simulation results from four of these tests are presented in Figure 4.4.4-1, as described in the second column of Table 4.4.4-1. One of the experiments, the K&Å1, is presented in more detail because it shows important loading and unloading behavior, including nonassociative plasticity.

The K&Å1 test example involves a laboratory compression test at constant suction with comparison to experimental data of MX-80 bentonite, as presented by Kristensson and Åkesson (2008b, c). This test was conducted in an oedometer, consisting of a steel ring around a sample subjected to humidified air through filters on both sides (Kristensson and Åkesson, 2008c; Duek, 2007). Pistons and force transducers were placed axially above the sample and radially through the steel ring, allowing for measurements of both axial and radial stresses.

Kristensson and Åkesson (2008b) studied this experiment, evaluated the BBM parameters using their Mathcad tool and presented simulation results using the CODE_BRIGHT finite element code with BBM. In our model, we directly adopt the material parameter developed and used by Kristensson and Åkesson (2008b), because our main interest is to use these data to conduct a detailed code-to-code verification of the TOUGH-FLAC BBM implementation.

The laboratory experiment by Duek (2007) was conducted by first loading the sample with axial compressive stress from 0.18 MPa to 19.77 MPa, and subsequently unloading the sample to 1.0 MPa. The loading and unloading was performed under a constant confining compressive stress of 2.97 MPa and a constant suction of 28 MPa. Both the experimental and numerical results show a significant irreversible volumetric deformation as a result of plastic collapsing soils (Figure 4.4.4-2). Kristensson and Åkesson (2008b) evaluated the parameters, first determining elastic parameters at relatively low stress and then defining the yield surface and plastic model parameters. This included a pre-consolidation pressure tuned to 7.7 MPa and λ_{ps0} to 0.101. Finally, the nonassociativity parameter α_a was calibrated to 0.72, to match the evolution of the radial stress during the unloading (Kristensson and Åkesson, 2008b). Figure 4.4.4-3 shows that for the input parameters listed in Table 4.4.4-2—including the nonassociativity parameter α_a set to 0.72—an excellent agreement is achieved between TOUGH-FLAC simulation results and independent model data published in Kristensson and Åkesson (2008a). To illustrate the effect of the nonassociative plasticity, we also present the results of an alternative simulation using associative plasticity (α_a = 1.0). Using associative plasticity (α_a = 1.0) the simulation results deviates more significantly from the experimentally q-vs-p' and radial stress evolution. Thus, it is important to consider nonassociative plasticity to replicate the stress-strain behavior observed in the laboratory for this type of material, which necessitated our implementation of nonassociative plasticity.

Table 4.4.4-1. Description of a few of the simulation tests that have been conducted to verify the BBM implementation in TOUGH-FLAC.

Test and source	Description and Results
AGJ1 Swelling and collapse at increasing confining stress (Case 1 in Alonso et al., 1990).	Involves three different loading paths for inducing volumetric deformation by wetting at increasing confining stress (Figure 4.1-2a). In all three cases loading collapse is induced by the movements of the LC curve from its initial position LCi. TOUGH-FLAC results in Figure 4.1-2a agree with analytical results presented in Figure 4.1-11 of Alonso et al. (1990).
AGJ2 Swelling and collapse at alternate load paths (Case 2 in Alonso et al., 1990).	Volumetric deformation is induced along three alternate paths of mechanical loading and suction (Figure 4.1-2b). The different combinations of wetting and loading induce either expansion or collapse, but the final volumetric deformation is the same at the final position F. TOUGH-FLAC results in Figure 4.1-2b agree with analytical results presented in Figure 12 of Alonso et al. (1990).
K&Å1 Compression of MX-80 (Section 5.1 in Kristensson and Åkesson, 2008b).	A compression test with axial loading in steps followed by two unloading steps. The experiment provides the evolution of axial and the radial stresses as well as the void ratio. The TOUGH-FLAC modeling of this experiment is described in more detail in Section 4 and Figure 4.1-3.
K&Å2 Swelling of MX-80 under constant axial load (Section 5.2 in Kristensson and Åkesson, 2008b).	A swelling test subjected to a constant axial stress level. Wetting with associated suction decrease induces an increase in void ratio and compressive radial stress (Figure 2c). TOUGH-FLAC results are in agreement with modeling results and experimental data presented in Kristensson and Åkesson, (2008b).
K&Å3 Triaxial compression and shear of MX-80 (Section 5.3 in Kristensson and Åkesson, 2008b).	A triaxial experiment performed by applying an increasing axial strain to a test sample, while monitoring triaxial stress state and displacements (Figure 4.1-2d). TOUGH-FLAC results are in agreement with modeling results and experimental data presented in Kristensson and Åkesson, (2008b).

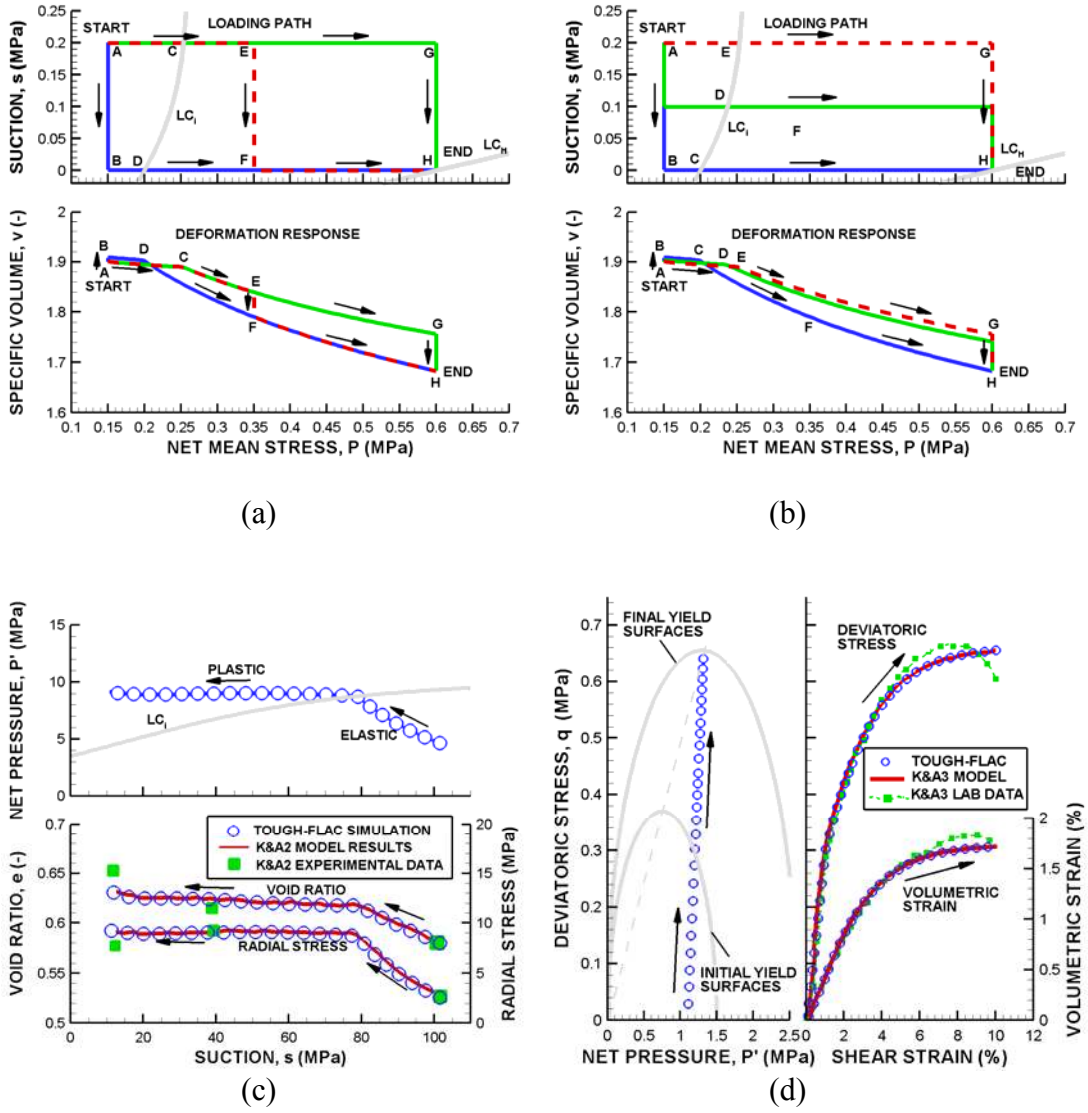

Figure 4.4.4-1. Result of simulation tests to verify the BBM implementation within the UDM capability of FLAC^{3D}: (a) Swelling and collapse at increasing confining stress (AGJ1), (b) swelling and collapse at alternate load paths (AGJ2), (c) swelling of MX-80 under constant axial load (K&Å2), (d) triaxial compression and shear of MX-80 (K&Å3).

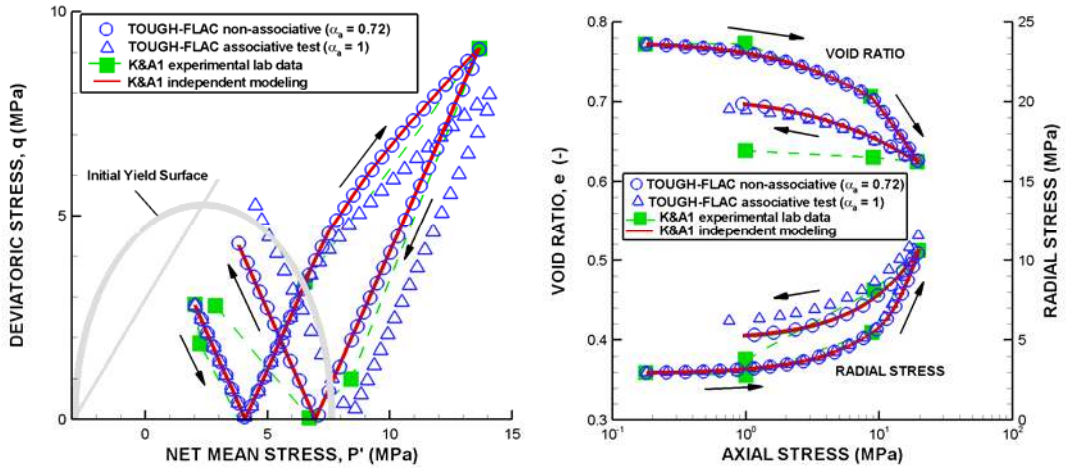

Figure 4.4.4-2. Comparison of TOUGH-FLAC with BBM simulation resultsl with experimental and modeling results presented in Kristensson and Åkesson (2008b) for MX-80 bentonite.

4.4.5 Simulation Tests Using TOUGH-FLAC with BBM and Swelling

The interaction of the TOUGH-FLAC simulator with the newly implemented thermo-elasto-plastic BBM and suction strain capability were tested using two example problems:

1) A laboratory swelling stress experiment.

2) A bentonite-backfilled horizontal nuclear waste emplacement tunnel.

The two examples are simulated using two options:

A) A linear elastic (LE) swelling model using a swelling strain that is linearly dependent on saturation changes.

B) A full BBM simulation with suction-dependent swelling.

The use of the LE swelling model example enabled a comparison of simulated results to simple analytical calculations to verify the implemented routines for TOUGH-FLAC modeling of suction strain, whereas modeling of the full BBM provides a check and demonstration of the applicability of the entire TOUGH-FLAC and BBM system. Table 4.4.5-1 lists thermal and hydraulic properties of the bentonite, which were derived in a previous study from experimental data or by model calibration (Rutqvist and Tsang, 2004; Alonso et al. 2005) for the modeling of the FEBEX in situ experiment. For the LE swelling model, only a few mechanical input parameters were needed (as described in Section 4.4.2). The input parameters for the BBM simulations were extracted from Gens et al. (2009) and represent BBM material parameters derived specifically for the bentonite buffer at the FEBEX experiment (Table 4.4.4-2, last column).

Table 4.4.4-2. Thermo-elasto-plastic BBM input parameters for simulation tests.

Parameter	AGJ1	AGJ2	K&Å1	K&Å2	K&Å3	FEBEX
κ_{PS0} (-)	0.02	0.02	0.057	0.06	0.1	0.05
κ_{SP0} (-)	0.008	0.008	0	0.3	0	0.25
G (MPa)	10	10	NA	NA	NA	NA
ν (-)	NA	NA	0.224	0.2	0.3	0.4
α_{SS} (-)	0	0	0	0	0	0
α_{PS} (MPa^{-1})	0	0	0	0	0	-0.003
α_{SP} (-)	0	0	0	0	0	-0.161
P_{ref} (MPa)	0.1	0.1	0	0.1	0	0.5
α_0 ($°C^{-1}$)	0	0	0	0	0	1.5E-4
α_2 ($°C^{-1}$)	0	0	0	0	0	0
λ_{PS0} (-)	0.2	0.2	0.101	0.9	0.135	0.15
R_λ (-)	0.75	0.75	0	0.75	0	0.925
β_λ (MPa^{-1})	12.5	12.5	0	0.03	0	0.1
ρ_s ($°C^{-1}$)	0	0	0	0	0	0
k_s (-)	0.6	0.6	0.1	0.1	0.1	0.1
P_{S0} (MPa)	0	0	0	0	0	0
P^C (MPa)	0.1	0.1	0.1	0.2	0.1	0.5
M (-)	1	1	1	1	0.5	1
α_a (-)	0.4	0.4	0.72	1	0.5	0.53
v_λ (-)	2.033	2.033	2.140	4.173	2.135	1.937
P^*_0 (MPa)	0.2	0.6	7.7	3.5	1.5	12.0

Table 4.4.5-1. Thermal and hydraulic material parameters for the FEBEX buffer material used in the numerical modeling of swelling experiment and multiple barrier repository.

Parameter	Value/Function
Initial dry density, ρ_d [kg/m^3]	$1.6 \cdot 10^3$
Initial porosity, ϕ [-]	0.41
Saturated permeability, k [m^2]	$2.0 \cdot 10^{-21}$
Relative permeability, k_r [-]	$k_{rl} = S_l^3$
Van Genuchten's (1980) parameter, P_{VG} [MPa]	30
Van Genuchten's (1980) parameter, λ_{VG} [-]	0.32
Thermal expansion, β [1/°C]	$1.5 \cdot 10^{-4}$
Dry specific heat, C_s [J/kg·°C]	$c_s = 1.38T + 732.5$
Thermal conductivity, λ_m [W/m·°C]	$\lambda_m = 1.28 - \frac{0.71}{1 + e^{(S_l - 0.65)/0.1}}$
Effective molecular diffusion coefficient, D_v [m^2/s]	$D_v = 2.16e-5 \times \tau \times \phi \times S_g \left(\frac{T_{abs}}{273.8} \right)^{1.8}$
Mass flow times tortuousity factor, τ [-]	0.8

4.4.6 TOUGH-FLAC Simulation of a Laboratory Swelling Stress Experiment

Swelling pressure tests are conducted on fully confined samples wetted to full saturation. In this case, the experiments were conducted on bentonite material used in the FEBEX in situ experiment and part of the international collaborative project DECOVALEX (Alonso et al., 2005). For a dry density of 1.6 g/cm^3 and 65% initial saturation, a swelling pressure of about 5 to 6 MPa developed at full saturation in the swelling experiments (Alsonso et al. 2005).

For the LE swelling model, the model input parameters can be determined analytically to achieve a desired maximum swelling stress of 5 MPa. In such a case, the bentonite is assumed to behave elastically, with a volumetric swelling and a swelling stress that depends on the changes in water saturation, ΔS_l, according to:

$$\Delta\sigma'_{sw} = 3K\Delta\varepsilon_{sw} = K\Delta S_l \beta_{sw} \qquad (4.4\text{-}34)$$

where $\Delta\sigma'_{sw}$ is the induced swelling stress (an effective stress), K is the bulk modulus, and β_{sw} is a moisture swelling coefficient. For an average bulk modulus of 20 MPa, the appropriate moisture swelling coefficient can be calculated using Equation (4.4-34) as:

$$\beta_{sw} = \frac{\Delta\sigma'_{sw}}{3K\Delta S_l} = \frac{5\cdot 10^6}{3\cdot 20\cdot 10^6\cdot 0.35} = 0.238 \qquad (4.4\text{-}35)$$

The swelling stress experiments is simulated using a 3D 20×20×20 mm model with 20 elements in the vertical direction (Figure 4.4.6-1). The model boundaries are fixed for displacement normal to the boundaries, which means that the model is fully confined from a mechanical viewpoint. The model is also hydraulically confined (no flow across boundaries) except at the bottom (water inlet) where a fully saturated condition and a slightly elevated pressure are applied. The simulation is conducted for about 10 days under isothermal conditions at a temperature of 25°C. Figure 4.4.6-1 shows a plot of the saturation distribution after about 4 days.

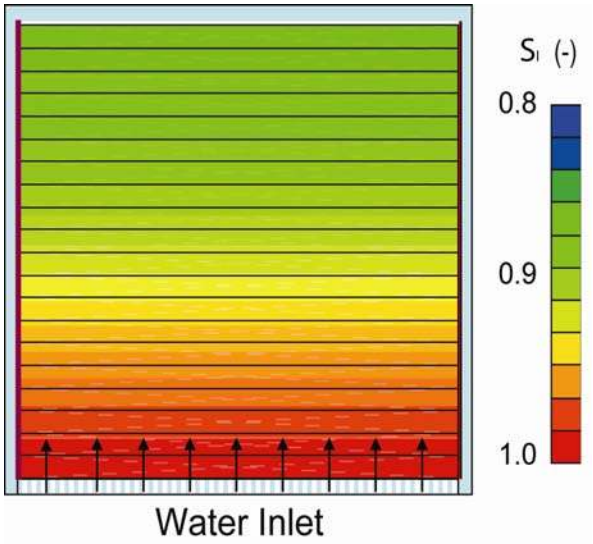

Figure 4.4.6-1. TOUGH-FLAC model of a swelling stress experiment and results of liquid saturation after 4 days of water infiltration.

In the simulation, the soil sample becomes practically fully saturated in about 10 days (Figure 4.4.6-2a). The compressive stress increases proportionally to the saturation, but does achieve a maximum value of about 5.56 MPa, higher than the expected 5 MPa (Figure 4.4.6-2b). The reason for a higher-than-expected stress is that gas is trapped in a hydraulically confined model, and gas pressure increases by about 0.5 MPa (from 0.1 to maximum 0.6 MPa), creating an additional poro-elastic stress increase of about 0.5 MPa (Figure 4.4.6-2b). The effect of gas pressure on stress can be eliminated by setting Biot's constant to zero ($\alpha_B = 0$). In such a case, the final stress is 5.12 MPa, i.e., exactly 5 MPa above the initial stress of 0.12 MPa (Figure 4.4.6-2b). This shows that the implemented routines for suction strain in TOUGH-FLAC work as intended.

The full BBM model simulation results in a swelling stress of 5.35 MPa, which is in agreement with experimental data and similar to the final swelling stress of the LE swelling model (Figure 4.4.6-2b). However, a significant difference exists in the time evolution of stress in the results from the full BBM compared to those of the LE swelling model. The time evolution achieved in the case of the full BBM is the most realistic,

because it accurately relates the volumetric change to changes in suction, in which most of the swelling takes place at high saturation values. In the case of the LE swelling model, the swelling is linearly related to saturation changes, but may be calibrated to achieve the correct final swelling pressure.

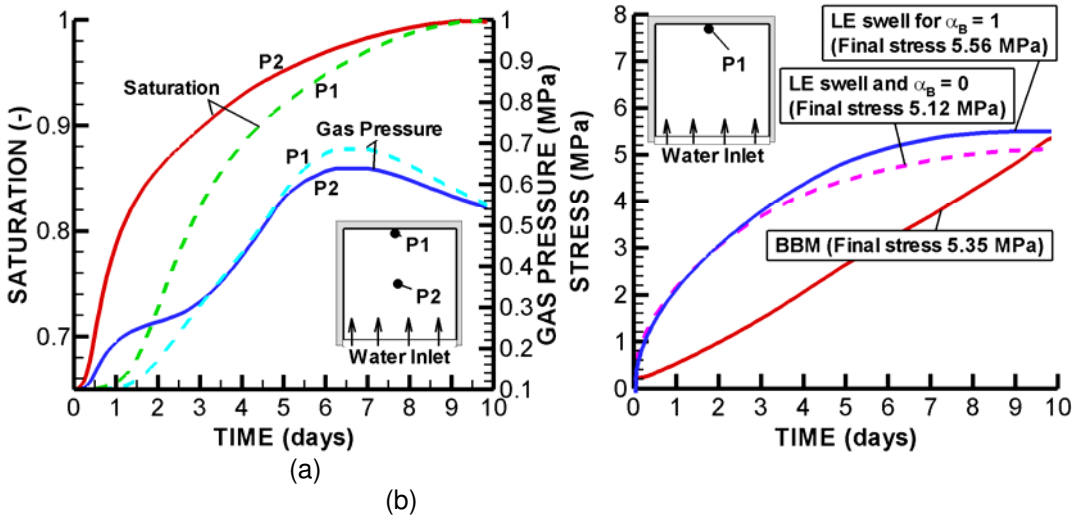

Figure 4.4.6-5. TOUHG-FLAC modeling of numerical swelling test: Simulated time evolution of (a) saturation and gas pressure at P1 and P2, and (b) stress at P1 for LE swelling model and BBM.

4.4.7 TOUGH-FLAC Simulation of a Bentonite-Backfilled Nuclear Waste Emplacement Tunnel

This modeling example is taken from the international DECOVALEX project involving a horizontal nuclear waste emplacement tunnel at 500 m depth (Rutqvist et al., 2008b, 2009). Here, we present new model simulations of this example using TOUGH-FLAC to check and demonstrate the applicability of this coupled modeling approach to a problem involving complex, multimedia (canister, bentonite, rock) coupled THM interactions. The model simulation was conducted in a nonisothermal mode with a time-dependent heat power input over 100,000 years of simulation time (Figure 4.4.7-1). In this study we focus on the coupled THM behavior of the buffer, whereas the surrounding rock mass and its hydraulic and thermal properties affect the temperature and fluid pressure evolution. In this simulation, the rock permeability is sufficiently high ($k = 1\times10^{-17}$ m^2) so as to avoid suction-induced desaturation of the rock that could otherwise significantly affect the buffer resaturation (e.g., Rutqvist et al., 2005). The overall temperature evolution is controlled by the thermal decay function, assumed tunnel spacing (Figure 4.4.7-1), and rock-mass thermal properties. The rock thermal conductivity is set to 3 W/m°C, whereas the heat capacity is determined from a specific heat constant equal to 900 J/kg·°C, a 1% rock porosity, and a bulk density of 2700 kg/m^3 (Rutqvist et al., 2008b). A direct code-to-code comparison of simulation results is provided using results from an independent numerical analysis with the finite element code ROCMAS (Rutqvist et al., 2001).

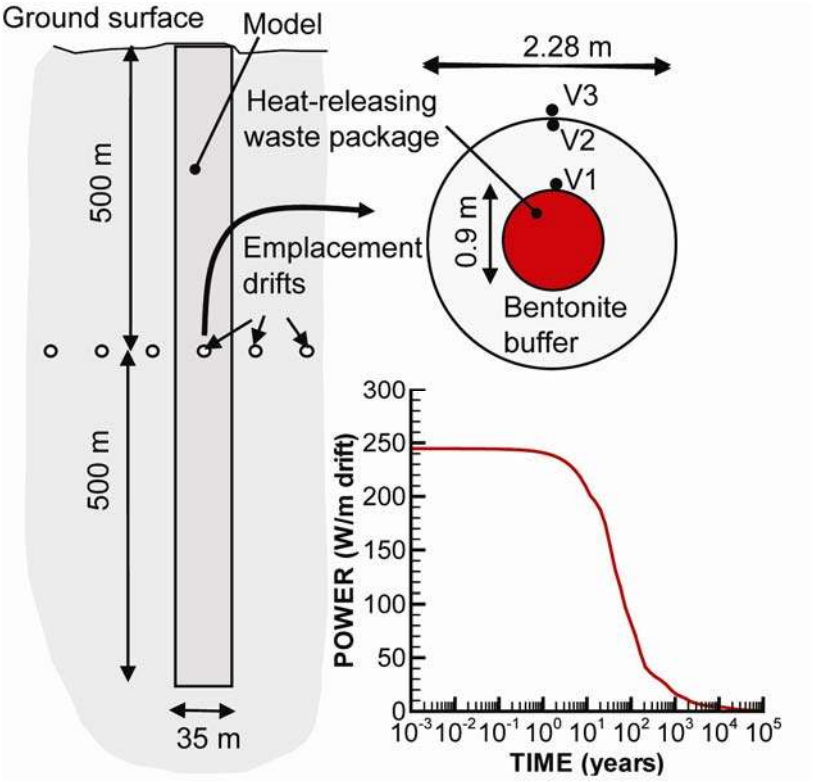

Figure 4.4.7-1. Model domain for a TOUGH-FLAC test example of a bentonite back-filled horizontal emplacement drift at 500 m depth (Rutqvist et al., 2009d).

Figure 4.4.7-2 presents the calculated evolution of temperature, saturation, fluid pressure, and stress within the buffer. The figure shows a good agreement between the simulation results of the TOUGH-FLAC and ROCMAS codes. The slight disagreement that can be observed in Figure 4.4.7-2 can be attributed to differences in the modeling approach. Indeed, ROCMAS is a finite element code for fully coupled THM analysis under single phase, unsaturated flow conditions, whereas TOUGH-FLAC is based on the sequential coupling of a finite volume fluid flow code to a finite difference geomechanical code, but with full multiphase flow capability—see Wang et al., (2010), for a recent discussion on single-versus-multiphase fluid flow modeling approaches for this type of problem). The results in Figure 4.4.7-2 are also in general agreement with simulation results of other numerical models for the same DECOVALEX bench-mark test presented in Rutqvist et al. (2008b, 2009d).

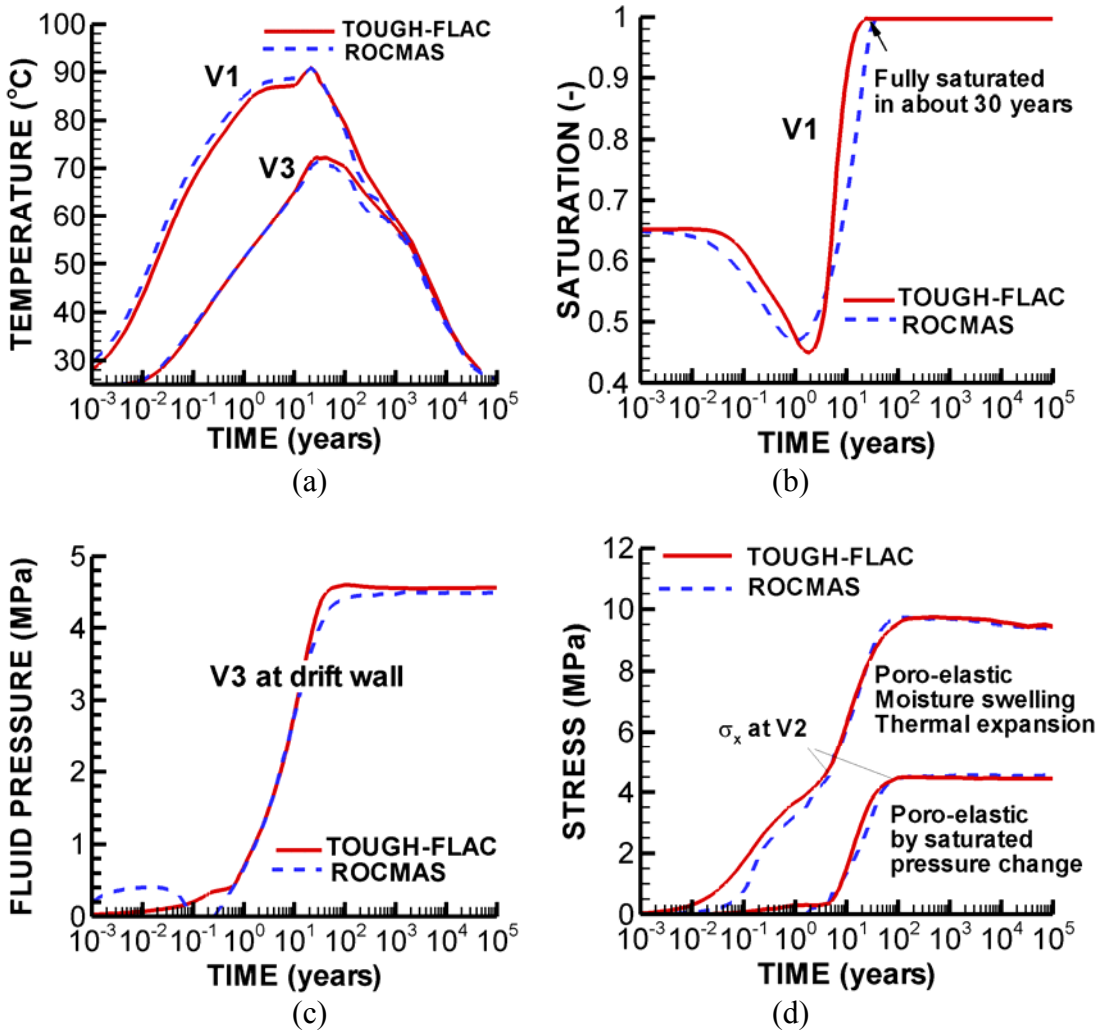

Figure 4.4.7-2. Simulated evolution of THM processes in the buffer: (a) temperature at V1 and V3, (b) liquid saturation at V1, (c) fluid pressure at V3, and (d) total radial stress (σ_x) at V2.

Figure 4.4.7-2d is of utmost interest here because it shows the evolution of stress as a result of three sources: (1) swelling stress caused by saturation changes, (2) poro-elastic stress from fluid pressure changes under saturated conditions, and (3) thermal stress. The poro-elastic stress resulting from the restoration of fluid pressure accounts for about 4.5 MPa of total stress. Indeed, this contribution is proportional to the evolution of fluid pressure in Figure 4.4.7-2c. The swelling caused by saturation changes amounts to about 5 MPa, leading to a total stress change of 9.5 MPa. The contribution to the total buffer stress from the thermal expansion is about 0.4 MPa at the thermal peak. This is reasonable considering the magnitudes of temperature increase $\Delta T \approx$ 55°C, a bulk modulus K = 20 MPa, and thermal expansion coefficient of $\alpha_T = 1.5\times10^{-4}$ °C^{-1}.

Figure 4.4.7-3 and 4.4.7-4 present the geomechanical results for TOUGH-FLAC simulations employing the thermo-elasto-plastic BBM with the material parameters representing the bentonite buffer taken from Gens et al. (2009), used for modeling of the FEBEX in situ heater experiment. Figure 4.4,2-3a shows that the stress evolution is

relatively uniform within the buffer; the stress evolution near the canister (point V1) follows the stress evolution near the rock wall (point V2). The stresses at V1 and V2 increase and peak at about 8 to 9.5 MPa, but then decrease to about 6.5 to 7.5 MPa towards the end of the simulation. A stress peak of about 9.5 MPa could be expected as a result of the combined effect of swelling and pressure restoration, consistent with the results of the linear swelling model in Figure 4.4.7-2d. The relatively strong reduction in stress towards 100,000 years in Figure 4.4.7-3a is a result of cooling shrinkage at the time when the buffer has become relatively stiff. Indeed, Figure 4.4.7-3a also shows that the bulk modulus increases with stress and is affected by suction changes. The initial bulk modulus is about 2 MPa and peaks at about 200 MPa (0.2 GPa), i.e., a 100-fold increase in stiffness.

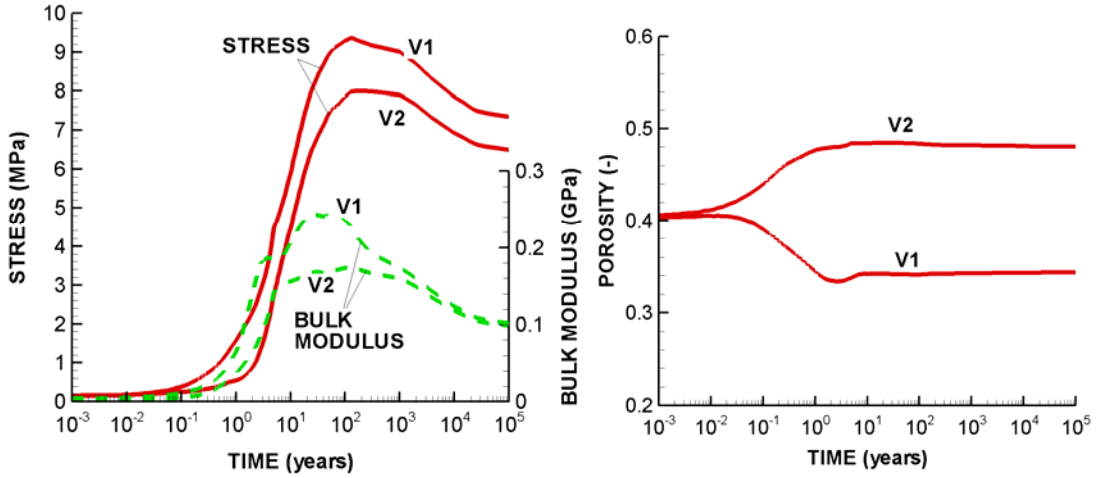

Figure 4.1-8. Simulated evolution of THM processes in the buffer when using the BBM: (a) tangential stress and bulk modulus, and (b) porosity for point V1 and V2 located within the buffer.

Figure 4.4.7-3b shows the evolution of porosity. A nonuniform porosity evolution can be observed with decreasing porosity at the canister (point V1) and increasing porosity at the rock wall (point V2). The porosity decreases near the canister as a result of drying and suction, which tends to contract the buffer. Meanwhile, the porosity increases near the buffer-rock interface as a result of wetting, which tends to expand the buffer. Interestingly, the porosity change occurring during the first few years never recovers even after full saturation and restoration of fluid pressure. The porosity does not recover because the buffer becomes stiff with the stress increases occurring after the first few years.

Figure 4.4.7-4 shows that at the end of the simulation, a nonuniform dry density is obtained that is consistent with the nonuniform porosity distribution. The nonuniformity of the buffer density is a result of the complex nonlinear elastic behavior and interactions of the outer and inner parts of the buffer. This is an eye-opening result, one which warrants further detailed studies and confirmation with independent models that are out of the scope of this paper. However, we conclude from this study that the mechanical

evolution of the buffer is far more complex than what could be captured with the LE swelling model. The BBM implementation into TOUGH-FLAC provides a practical tool for a more realistic and rigorous analysis of the mechanical behavior associated with bentonite back-filled nuclear waste repository tunnels.

.

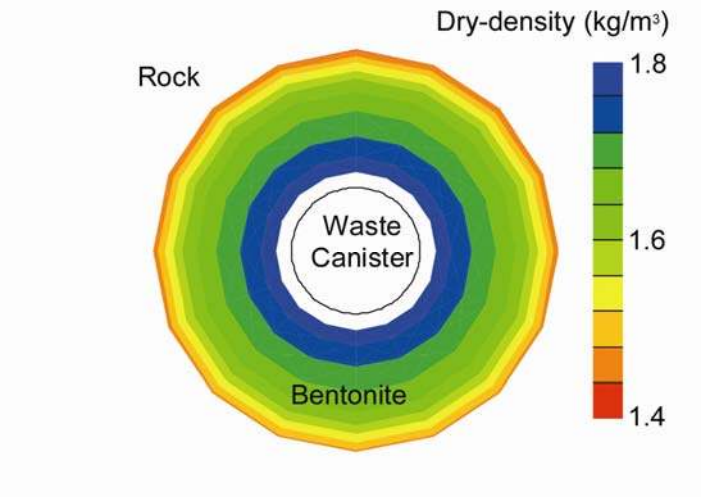

Figure 4.4.7-4. Calculated distribution dry-density in the buffer after full resaturation and restoration of ambient pressure and temperature (at 100,000 years) showing a relatively high density near the canister and a relatively low density near the rock wall.

4.4.8 Simulation of a Generic Repository in Clay Host Rock

This section presents the initial results of the simulation of coupled THM processes in the EBS and host rock for high-level radioactive waste repository in clay formations. It is our intent to investigate the coupled THM behavior for a range of clay host rocks, including plastic clay and indurated more brittle claystone. In our first base case simulation scenario we will use clay host rock properties derived from the Opalinus clay stone at Mont Terri, Switzerland (Table 4.4.8-1), and will use a repository design and EBS with emplacement into horizontal tunnels that are back-filled with bentonite-based swelling clays as a protective buffer. We adopt the heat load developed for the Generic Disposal System Environment (GDSE) within the UFD for Pressurized Water Reactor (PWR) used nuclear fuel. The first step in this analysis is to design the repository in terms of spacing between emplacement tunnels and individual waste packages along the tunnels, to achieve a distributed heat load that would meet criteria for desired maximum temperature.

4.4.8.1 The Repository Design and Heat Load

We chose a repository design similar to the one considered in Swiss nuclear waste disposal program for a repository in Opalinus Clay. We assume that the drift is located at a depth of 500 m and the top boundary located at the ground surface. The heat load for individual emplacement tunnels and their spacing are designed by a constraint of a maximum temperature of 100 ºC max in the contact between the canister and the bentonite. In repository designs with bentonite-backfilled repository tunnels, the PWR

type of used fuel is typically packed into a waste package (or canister) with the dimensions of about 1 m in diameter and about 4 m long. This is dictated by the length of individual PWR fuel elements and the number of fuel elements per waste package. 4 PWR elements per waste package are commonly adopted for bentonite-backfilled repositories in various host rocks, including crystalline and clay (e.g. Swedish and Finish, Swiss, and Spanish proposed repository designs). Moreover, the emplacement tunnels may be typically up to 1 km long. The basic material properties used in this initial simulation are presented in Table 4.4.5-1.

Table 4.4.8-1. Some basic THM rock properties for a repository hosted in clay stone.

Parameter	Value
Bulk Density, [kg/m^3]	2400
Matrix Porosity [-]	0.15
Young's Modulus, [GPa]	5
Poisson's ratio, [-]	0.3
Specific heat, [J/kg·°C]	900
Thermal conductivity, [W/m·°C]	2.2
Thermal expansion coefficient, [°C^{-1}]	1.0×10^{-5}
Permeability, [m^2]	5.0×10^{-20}
Biot's effective stress parameter	1.0
Van Genuchten water retension parameter, m	0.41
Van Genuchten water retension parameter, P_0 [MPa]	48

The thermal decay curves for a 10 PWR element waste package was scaled down by multiplying by 4/10 to obtain the decay curve for a 4 PWR element waste package that would match the adopted repository design. This leads to an initial thermal power of 3144 W per waste package. Assuming a waste deposition after 60 years of interim storage, the heat power has decayed to 1818 Watts per waste package. With the assumption of the 50 m tunnel spacing and 500 m emplacement depth, the average thermal power per meter drift may be scaled by adjusting the spacing between individual waste packages along the tunnel. Using model calibration and a maximum temperature kept below 100°C, we adopted an average thermal power of 200 W per meter drift. This would mean that if the individual waste packages are 4 m long, the spacing would be 4 m. Alternatively, for 3 PWR elements per waste package the spacing would be 2 m. For the adopted average thermal conductivity of the rock (2.2 W/m°C), an average thermal power of 200 W per meter drift seems to be the upper practical limit for this type of repository design.

Figure 4.4.7-5 presents the model dimensions and the heat decay curve for these simulations. Note that in comparison to the earlier simulation test shown in Figure 4.4.7-1, the initial thermal power per meter drift is lower and the tunnel spacing is larger. This

is a result of the relatively lower thermal conductivity adopted in this case, which corresponds to an average thermal conductivity for Opalinus Clay (Gens et al. 2007).

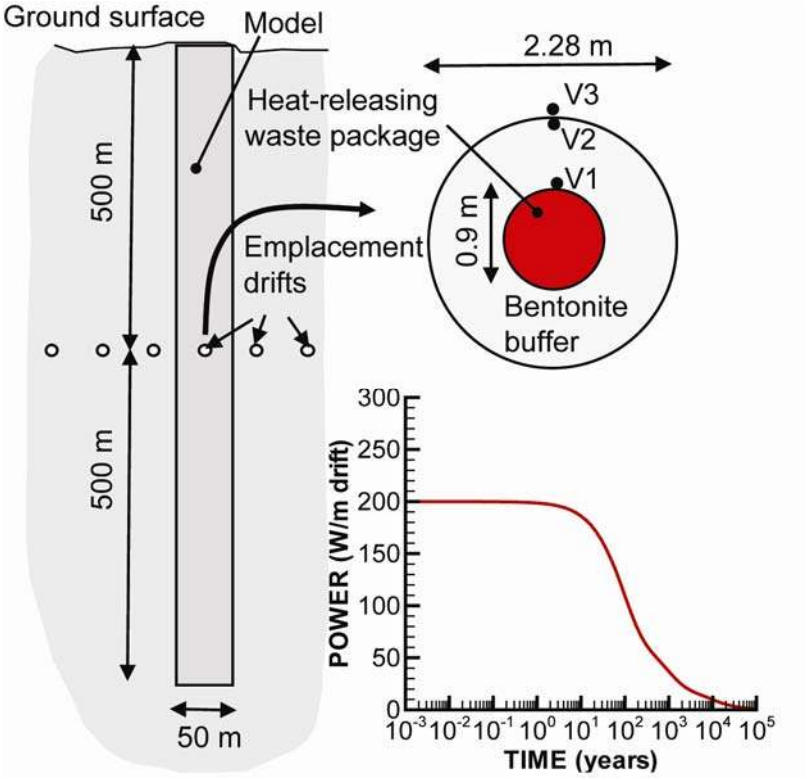

Figure 4.4.7-5. Model domain for a repository hosted in clay stone.

4.4.8.2 Modeling Sequence, Boundary and Initial Conditions

Figure 4.4.8-1 presents the detailed modeling sequence, boundary and initial conditions for the coupled THM simulation. The initial conditions for the rock mass are established at the pre-excavation stage (Figure 4.4.8-1a). The initial stress was defined as $\sigma_h = \sigma_H = \sigma_v = 2400 \cdot 9.81 \cdot D$ where D is elevation relative to ground surface (D = z – 500 and tensile stress is positive). The vertical thermal gradient is assumed to be 30°C/km with a fixed average temperature of 10°C on the ground surface and a fixed temperature of 40 °C at the bottom boundary. The groundwater table is assumed to be located at the ground surface where the pressure is fixed to 0.1 MPa (atmospheric). At the bottom of the model the fluid pressure is set to 9 MPa, which slightly less then hydrostatic. The excavation sequence can be simulated in a one-step steady state calculation with the elements in the drift removed and constant temperature 25°C and pressure of 0.1 MPa at the drift boundary (Figure 4.4.8-1b). After the steady state excavation simulation is completed, the waste canister, bentonite buffer and back-fill are installed instantaneously and the post-closure simulation can start (Figure 4.4.8-1c and 4.4.8-1d).

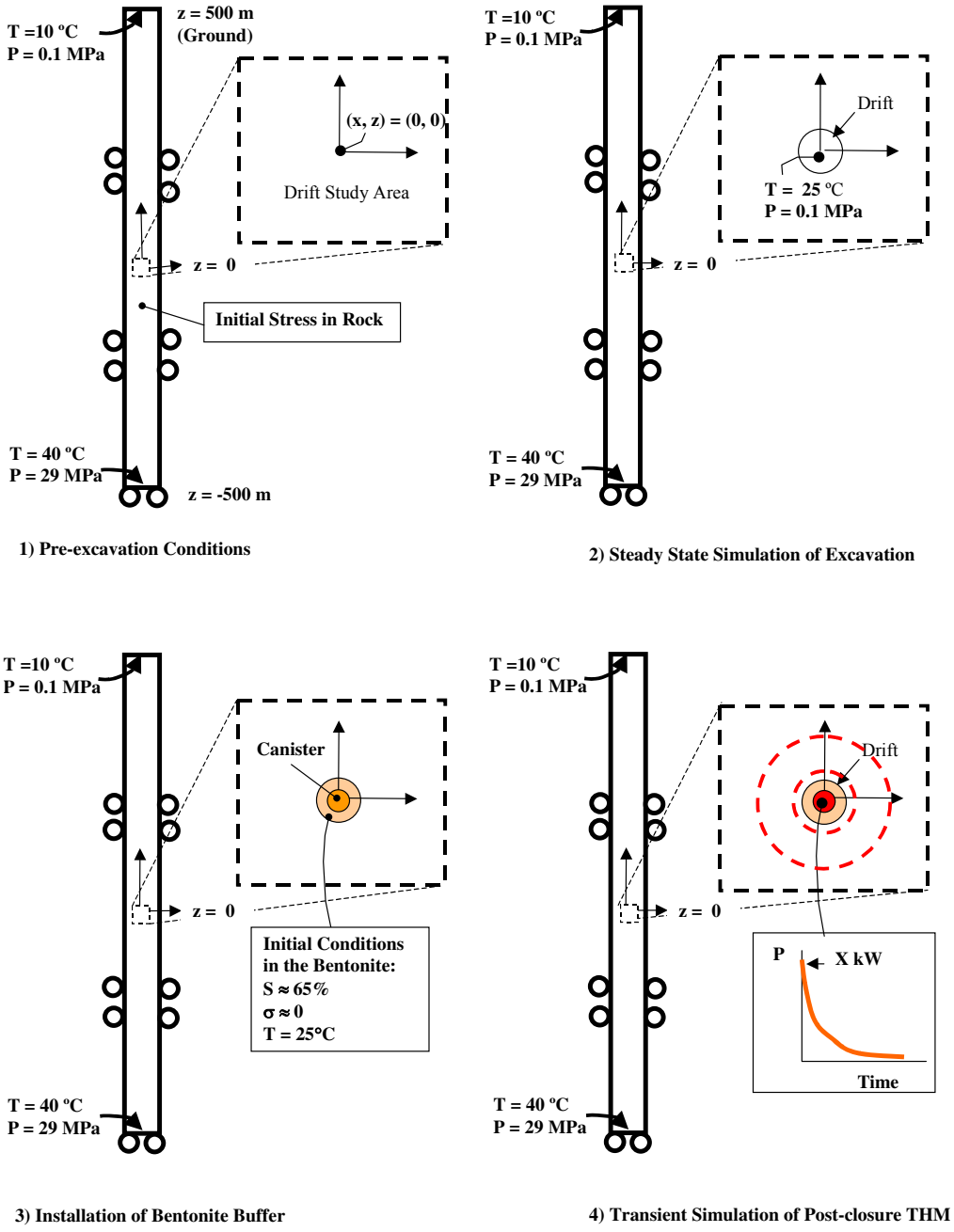

Figure 4.4.8-1. Modeling sequence, boundary and initial conditions.

4.4.8.3 Basic THM simulation results

Figure 4.4.8-2 presents the calculated evolution of temperature, saturation, fluid pressure, and stress within the buffer. The temperature peaks at about 95°C, which is below the 100°C maximum temperature criterion. The resaturation of the buffer is delayed as a result of the low rock permeability and a slight desaturation of the rock can be observed in Figure 4.4.8-2b. The fluid pressure indicates a strong coupling to the temperature field, and as a result of the low rock permeability a significant thermal pressurization occurs

(Figure 4.4.8-2c). This increase in fluid pressure has a direct impact on the stress evolution in the buffer (Figure 4.4.8-2d). Thus, in this case we observe strong interaction between the host rock coupled processes and the THM evolution of the buffer. The results presented are valid for an average permeability representative of 5e-20 m^2. If the permeability is lower, a much stronger thermal pressurization can occur. Figure 4.4.8-3 shows the evolution of stress, bulk modulus and porosity in the buffer. A quite uniform porosity is achieved in the buffer.

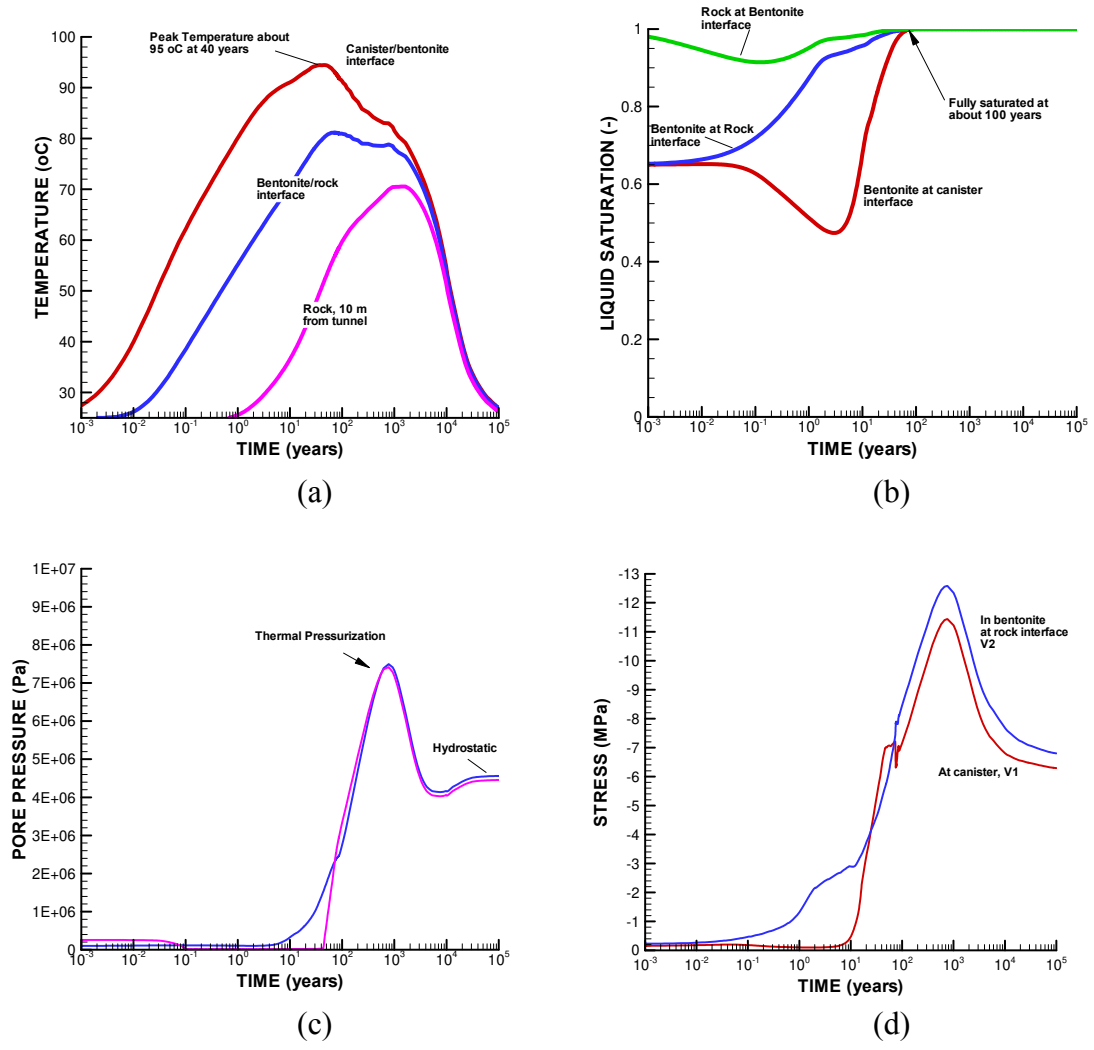

Figure 4.4.8-2. Simulated evolution of THM processes in the buffer: (a) temperature at V1, V3, and V6 (b) liquid saturation at V1, (c) fluid pressure at V3, and (d) total radial stress (σ_x) at V1 and V2.

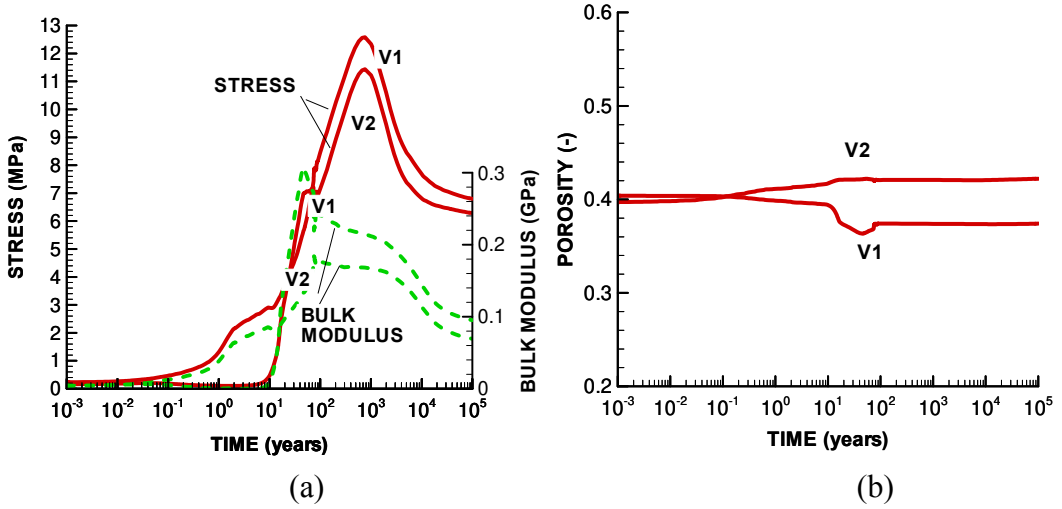

Figure 4.4.8-3. Simulated evolution of THM processes in the buffer when using the BBM: (a) tangential stress and bulk modulus, and (b) porosity for point V1 and V2 located within the buffer.

4.4.8.4 Summary of THM EBS Research and Next Step

A thermo-elasto-plastic constitutive model based on the Barcelona Basic Model (BBM) for mechanical behavior of unsaturated soils has been implemented into TOUGH-FLAC. The model has been tested using a number of simulation examples, both with regard to its implementation using the FLAC^{3D} user defined model capability and with regard to modeling of suction-induced swelling in TOUGH-FLAC. The test simulations included comparison to both independent calculation results and experimental data from bentonite-sand mixtures considered for use in back-fill and protective buffers around disposed spent nuclear fuel in geological nuclear waste repositories. Excellent agreement was achieved between TOUGH-FLAC modeling results and independent analytical and numerical simulation results, which where in satisfactory agreement with experimental data Moreover, the TOUGH-FLAC with BBM was also tested on a full-scale nuclear waste repository problem involving the interaction of multiple components (buffer, canister, rock) over a 100,000 year simulation time. The simulation indicated complex geomechanical behavior of the bentonite backfill, including a nonuniform distribution of buffer porosity and density that could not be captured in an alternative, simplified linear-elastic swelling model. The thermo-elasto-plastic BBM implemented into TOUGH-FLAC is now fully operational and ready to be applied to nuclear waste disposal and other scientific and engineering problems related to the geomechanical behavior of unsaturated soils.

We also conducted initial simulation studies of coupled THM processes in the EBS and host rock for high-level radioactive waste repository in clay formations. This study highlight the important interactions between the buffer and the host rock, in particular regarding the potential for desaturation of the rock and thermal pressurization which can have a significant impact of the coupled THM evolution in the EBS.

Future work is proposed to include an extension of the current BBM implementation in TOUGH-FLAC to more complete modeling of expansive clays, including double-

structured behavior. In such an approach, the material consists of two structural levels: a microstructure in which interactions occur at particle level and a macrostructure that accounts for the overall arrangement of the material comprising aggregates and macropores (Gens et al. 2006, Sánchez et al., 2005, Gens and Alonso, 1992).

4.4.8.5 Coupled TM Processes in Salt

So far, coupled processes described here pertain to clay media. Salt repositories also need to be considered for potential HLW disposal given the isolating characteristics of the salt medium and its mechanical properties. SNL has a long history of research on salt repositories and in the development of models and tools to describe the thermo-mechanical behavior of salt (Munson and Dawson, 1979, 1982; Hansen, 2003; Park et al., 2005; Stone et al., 2010). Recently, Stone et al. (2010) utilized the SIERRA Mechanics code suite to model TM coupled processes in salt. SIERRA Mechanics is part of a concerted development of computational multi-physics tools on sophisticated massively-paralell computer platforms. The TM coupling in SIERRA Mechanics is accomplished by two codes: Aria (Navier-Stokes, energy transport equations) and Adagio (coupled solid mechanics). The main advantages of this coupled TM treatment are the use of sophisticated computational algorithms to solve highly non-linear problems and the ability for scalable implementation in massively parallel computer systems (Stone et al., 2010). Such implementation may be necessary for repository scale calculations needing, for example, accurate representation of the geometry of disposal galleries. The work of Stone et al. (2010) reports 3-D coupled TM calculations for a generic salt repository involving HLW disposal. The results of this study are very encouraging in providing (1) a comparison of results between constitutive models such as multi-mechanism deformation and power law creep for salt mechanics and (2) accurate calculations of the time needed for tunnel and alcove closure as a function of heat load. This approach not only offers a multi-physics capability to analyze coupled processes but also the computational framework that could include probabilistic methods to evaluate the effects of heterogeneities and parameter uncertainty that are inherently important to the evaluation and performance assessment of nuclear waste repository concepts. Future modeling work at SNL is envisioned in order to expand this modeling activity on TM coupled processes on salt using this computational approach.

Some knowledge gaps related to salt repository environments include:

- Brine migration
- Vapor phase and moisture transport
- Buoyancy effects
- Drift stability as a result of HLW heat generation
- Radiolysis and gas generation
- Radionuclide transport and solubility in concentrated brines

Some of these knowledge gaps can be initially evaluated using modeling approaches but these mainly fall in the realm of field- and laboratroy-scale research programs.

4.5 Simulation of Transport Experiments using Diffuse Layer and Ion Equilibrium Approaches

A summary of the new diffuse layer capabilities within CrunchFlow was presented at the Chemistry Workshop of the EBS task force in Speyer, Germany held June 30 and July 1, 2010. In attendance were representatives from the University of Bern in Switzerland, SKB in Sweden, the Clay Technology group in Sweden, the French geological survey (BRGM), and Spain, along with a single representative from Lawrence Berkeley National Laboratory. In addition, the group heard a concise presentation on the ionic equilibrium approach to modeling diffusive transport through compacted bentonite from Martin Birgersson of Clay Technology. The approach of Birgersson and Karnland (2009) consists of considering the diffusive transport as driven by chemical potential rather than concentration gradients. Concentration is discontinuous between the bulk water and the bentonite interlayers where the electrical double layers balancing mineral surface charge overlap. In contrast, the chemical potential based on the assumption of ionic equilibrium (essentially a Donnan equilibrium approach) is continuous and can be used to explain the rates of diffusive transfer. The Birgersson and Karnland approach turned out to be equivalent to consideration of transport within a single domain (no bulk water) consisting of overlapping double layers, and can in fact be modeled with the capabilities in CrunchFlow by setting the bulk water porosity to zero (or a very small number).

Based primarily on these two presentations (from Steefel and Birgersson), the group decided to pursue testing of the diffuse layer and ionic equilibrium approaches. Two benchmark data sets are to be prepared to which modeling can be applied using alternate porosity concepts (multi-porous, including DDL, and ion-equilibrium):

(1) Data set from advective-diffusive multi-component column experiment (Fernandez-Mäder).

(2) A select number of diffusion experiments (PSI & Clay Technology), including some data sets with measured associated swelling pressures (Birgersson). It is proposed that interested teams can test/apply their models to these data sets.

First opportunity to report and discuss results is the upcoming EBS-TF Meeting in Prague, November 2-3, 2010. There is also potential interest by external scientists to have access to such a benchmark (e.g., Ulrich Mayer, UBC [Vancouver CA], connected via NWMO; Tony Appelo, who participated in the Task Force previously).

In addition, the Chemistry group decided that it would be advantageous to couple the Donnan equilibrium (or ionic equilibrium) calculations with calculations of swelling pressure. A preliminary version of this will be attempted in CrunchFlow in the coming year.

4.6 Knowledge Gaps and R&D Plan

4.6.1 Knowledge Gaps

The technical issues outlined below describe critical knowledge gaps that point to R&D needs. An integrated research plan in these areas would involve detailed process-oriented

studies including coupled-processes simulation tools, laboratory experiments, and in-situ tests. The latter will not be conducted soon in the U.S., but several major experiments with bentonite have been or will be conducted internationally. Examples are the Canister Retrieval Tests (CRT), Thermal bentonite test (TBT), and the to-be-conducted Bentonite-Rock Interaction Experiment (BRIE). Participation in the analysis, interpretation and modeling of such tests would be very helpful. Some of the data may be found from the published literature or open company reports, while others may be available only through participation in international cooperative projects. Such participation, however, is an effective way to be positioned at the forefront of the state of science in this field.

1. Studies of bentonite hydration to include new processes not included in conventional formulation of THM models. These processes include thermo-osmosis, microstructure evolution, existence of different states of water in the bentonite, and existence of a threshold hydraulic gradient for water flow.
2. Studies of THM behavior of bentonite pellets and pellet mixtures, and irreversible swelling or compression of bentonite in large gap fillings. This is related to homogenization of the bentonite density in the EBS. Bentonite blocks, pellets, and gaps need to be homogenized to about the same density (heterogeneity to be limited) for bentonite to serve as an effective isolation barrier to radionuclide leakage.
3. Studies of piping and erosion of bentonite. The loss of mass into flowing water needs to be limited. It is further complicated by the localized feature of flow from the host rock. We need to develop conceptual models and computer codes for these processes, as well as experimental data to verify our understanding.
4. Studies of radionuclide transport through bentonite interlayer porosity. By comparing the topics discussed in the Literature Review and the existing capabilities for modeling of diffusive transport in compacted bentonite, it is clear that a capability for modeling transport through montmorillonite interlayer porosity needs to be developed. In addition, almost no validation of the models has been carried out to date, so this is an important activity that requires effort in the relatively near term.
5. Studies of swelling and self-sealing. While it is well known that swelling and self-sealing exist in both clay buffer materials and clay host rock, well established model methodologies to deal with these important phenomena and their relations to reactive transport are still lacking in the literature.
6. Studies of gas generation and its modeling. Due to canister corrosion, gas is generated and flows through EBS (including bentonite) to natural systems (host rock). Gas generation and flow have an important impact on mechanical, chemical, and hydraulic processes in the EBS. [Note that gas flow is relatively sensitive to small-scale heterogeneity.] Although some studies on this topic are available, significant uncertainty remains in this area, in part because models for gas generation and corrosion are de-coupled from models for near-field and natural systems behavior. Gas pressure and migration may result in preferential pathways for gas flow and radionuclides that partition into the gas phase. Preferential gas flow along higher-permeability pathways through the EBS could result in fast gas-phase transport to more permeable formations external to the host rock or even the ground surface. Gas flow will also lead to aqueous phase displacement and aqueous radionuclide

transport. Potential cycling of gas flow and rewetting of the bentonite could result in greater aqueous radionuclide transport than possible from a simple single-displacement process.

7. Studies considering explicit interactions between host rock and EBS and between different EBS components. Most previous studies have been focused on detailed understanding/prediction of one or only a few EBS components, while interactions between other components are disregarded or highly simplified (such as waste form interaction with corrosion products and buffer materials). Inclusion of these interactions between different EBS components makes the coupled processes models more complicated, but at the same time more reliable and usually less conservative. At this point, we are lacking the capability to investigate the interplay between the different components and their interactions via mechanistic process coupling. This interplay may have an important impact on radionuclide release from the EBS.
8. Studies of chemical/mineralogical changes in bentonite. A variety of aqueous chemical and mineralogical changes, including illitization, Na/Ca exchange, reactions with alkaline waters from cementitious materials, reactions with corrosion products, and secondary mineral precipitation affect mineral volume and mechanical characteristics. The potential for induration of the bentonite through these changes and fracturing caused by changes in mineral volumes, thermal expansion/contraction, volume changes associated with changes in pore-water composition, and volume changes caused by mineral transformations need to be evaluated as part of the chemical/mineralogical evolution of the bentonite. The impact on development of preferential flow and transport channels over long time periods needs to be addressed. (Gaucher et al. 2004).
9. Studies of glass dissolution mechanisms. Evidence indicates that glass dissolution is affected by the presence of bentonite. However, the effects are a complex balance between the dissolved silica concentrations and the solubility limits in the presence of clay. The controls that lead to either a decrease in dissolution rates or continued high dissolution rates in the presence of clays need to be investigated. (Houseworth 2010, Section 2.5; Lemmens 2001)
10. Studies of radionuclide sorption on bentonite for varying conditions, including temperature, pH, Eh, mineral phase (e.g., illitization), and Na/Ca exchange. Numerous observations of sorption indicate varying levels of sensitivity to temperature, pore-water and mineral compositions, depending on radionuclide species. The effects of iron corrosion products on bentonite include increased pH and precipitation of magnetite, which can lead to stronger sorption in the backfill. The large number of potential combinations of conditions and radionuclides means that generating empirical sorption results to cover all potential combinations of conditions and radionuclides is impractical. Therefore, a modeling approach is needed. For this to be successful, thermodynamic databases need to be expanded so that predictions of radionuclide sorption can be made over the range of conditions that may occur. (Houseworth 2010, Section 2.8; Sabodina et al. 2006; Khan 2002; Donat et al. 2005; Samper et al. 2008).
11. Further integration of THM & C models for simulating THMC coupled processes. Significant chemical-mechanical couplings for bentonite mean that the traditional separation of THM and THC coupled processes in most existing software may not be

adequate. Given the compatibilities of their software structure, integration of TOUGHREACT with TOUGH-FLAC as a fully-coupled THMC software code is one avenue to consider in attaining this goal.

12. Analysis of recent field data from major bentonite experiments. Examples are the Canister Retrieval Tests (CRT), Thermal Bentonite Test (TBT), and the to-be-conducted Bentonite-Rock Interaction Experiment (BRIE). Some of the data may be found from the published literature or open company reports, while others may be available only through participation in international cooperative projects. Such participation, however, is an effective way to be positioned at the forefront of the state of science in this field.

4.7 Research & Development Plans for the EBS

The R&D plans to address the technical issues identified above are divided into near-term (FY11) plans and longer-term plans.

4.7.1 Near-Term R&D Plan

Near-term R&D plans refer to activities that could start in the next fiscal year.

4.7.1.1 Transport Through Compacted Bentonite

Compacted bentonite has been proposed as backfill material in many international repository programs because of its very low permeability and its strong sorptive properties, both of which will limit the release of radionuclides. For undisturbed conditions, the very low permeability of the compacted bentonite implies that transport of radionuclides away from the waste forms will be almost exclusively by molecular diffusion, with effective diffusivities far below that in water. In much of the compacted bentonite, the pores are so small (<1 nanometer) that the electrical double layers balancing the charge of the bentonite (typically negative at circumneutral pH) overlap, thus potentially excluding anions altogether, or creating a deficiency of them within the diffuse electrical double layer balancing the surface mineral charge. Near-term tasks are:

1. Develop software for representing diffusion through interlayer porosity. This effort will involve 1) algorithm development, and 2) verification of the numerical approach through analytical solutions where available, and 3) validation against laboratory experiments.
2. Validate explicit Diffuse Double Layer model using laboratory experiments involving tracer diffusion through bentonite.

4.7.1.2 Bentonite Erosion in a Fractured Host Rock

Where flowing fractures contact the compacted bentonite surrounding a waste package, a variety of phenomena will occur including swelling of the clay, chemical reaction between solutes in the groundwater and the clay, and clay erosion due to chemical and physical forces on the clay at these locations. Erosion of the bentonite will reduce the storage security of the disposed waste, and this behavior needs to be well understood if this option is selected. Near-term tasks are:

1. A complete literature review will be performed to gather relevant information on the erosion of bentonite in repository-relevant conditions. The results will guide the subsequent work, as needed.
2. Using the literature review, a selected number of tests will be performed examining compacted bentonite erosion. The tests will examine the ionic strength of the groundwater, the chemical composition (relative concentration of monovalent and polyvalent ions), and pH. The tests will require that simple test cells to be designed and constructed.

4.7.1.3 Expansive Double-Structure Clay Model for Bentonite

The long-term chemical and mechanical stability of protective bentonite buffers and tunnel backfill are a key issues in the long-term performance of backfilled, multiple barrier nuclear waste repositories. For example, a certain swelling pressure should be maintained to keep the buffer homogenous, to prevent canister sinking, to prevent adverse effects of external rock shear movements, to limit colloid transport, and to prevent the buffer from being a preferred pathway of radionuclide transport. However, various thermal and chemical conditions can, over time, lead to a loss of swelling pressure. The near-term task is to implement and test the double structure elasto-plastic formulation in TOUGH-FLAC.

4.7.2 Longer-Term R&D Plan

Longer-term R&D plans are for activities that require some prerequisite activities to complete or additional plan development.

4.7.2.1 Transport through Compacted Bentonite

Two complementary sets experiments on bentonite are proposed to test the theory of double-layer diffusion and to develop effective diffusion properties. Tracer diffusion experiments will be set up to investigate and quantify the diffusion properties of the bentonite. Two complementary experiment techniques will be used to quantify the diffusivity of tracer solutes through the studied materials. First, the conventional through-diffusion experiment setup will be used together with wet chemistry analysis to determine the effective diffusion coefficient of tracer solutes of both anionic and cationic form through bentonite. As a second method, synchrotron radiation based X-ray fluorescence (XRF) and X-ray absorption mapping techniques will also be used to directly monitor the diffusion fronts of tracer solutes in the clays and clay-rich rock. In this approach, samples with the diffused tracer solutes are irradiated with high energy of synchrotron X-rays. The spatial distributions of tracer solutes inside the host rock materials are mapped according to their corresponding X-ray fluorescence or X-ray absorption signals at a given experimental time intervals, thereby providing the temporal and spatial data of trace diffusion fronts. The diffusion samples will be scanned periodically to monitor the progress of tracer diffusion fronts and the data obtained will be used to directly calculate the corresponding tracer diffusion coefficients. The tracer experimental data will be used to further develop and validate the models developed for diffusion through nanopores in compacted bentonite.

4.7.2.2 Bentonite Erosion in a Fractured Host Rock

A series of short duration hydrological tests will be performed using specific chemistries identified in FY11 tasks. These tests will consider flow interaction geometry specifically

(currently unclear from the literature, but important for modeling) and provide data useful for process modeling. Erosion rates will primarily be measured by quantifying eroded bentonite, however, the locations and mechanisms of erosion will also be considered.

The short-duration hydrological tests will measure erosion primarily using small scale measurements. A remaining question is if the compacted bentonite is eroded from a fracture and erosion continues into the backfill region, how does the erosion continue? Long-term tests (several months duration) will be performed to examine continued erosion within the backfill. Multiple arrangements of fracture and backfill will be considered, with those likely to provide the best results tested. Conceptual models will be proposed and evaluated so that the results are applicable to extension by numerical modeling.

4.7.2.3 Expansive Double-Structure Clay Model for Bentonite

The implementation of a double-structure model for bentonite, implemented in TOUGH-FLAC during FY11 is then implemented in TOUGHREACT within the framework of electro-chemical processes, including the electric double layer effects. The modified TOUGHREACT will then be compared with results from independent model calculations and experimental data to demonstrate code capability. After verifying the model, additional simulations will be performed to investigate long-term behavior of a hypothetical bentonite-backfilled repository subject to THMC processes.

4.7.2.4 Additional Longer-term R&D

As outlined in Section 4.6.1, a number of additional R&D topics remain to be investigated beyond those with specific plans given in Sections 4.7.1 and 4.7.2. In particular, specific plans need to be developed to address items 1 and 5 through 10 in Section 4.6.1.

5. Summary and FEPs Crosswalk

5.1 Summary

Bentonite and bentonite-sand mixtures have been found to have favorable properties for use as a backfill/buffer material for nuclear waste repositories. This report focuses on analyses of bentonite as a component of the EBS. Specific analyses presented here highlight progress made in areas of THM coupled processes models and reactive transport models for bentonite. A literature review provided in this report and Features, Events, and Processes (FEP) analyses reported separately (Houseworth 2010) document several more technical areas that may require additional research and development.

THMC Processes in Benonite

A literature review highlights the key issues concerning THMC processes in bentonite as well as information on important on-going research activities in international programs. Key issues include bentonite hydration mechanisms, bentonite homogenization, piping and erosion, mineral dissolution and precipitation, Na/Ca exchange and illitization of smectites. The on-going research activities in international programs provides opportunities for testing for bentonite homogenization in the SKB test, Bentonite Rock Interaction Experiment (BRIE), at the Äspö Hard Rock Laboratory URL and THMC

processes for the near field and EBS in the SCK-CEN test, TIMODAZ, being conducted in clay formations at the Belgian, Swiss, and French URLs.

There are several software codes available for analyzing THM processes in geologic media. The TOUGH-FLAC and ROCMAS codes were reviewed in detail for this report. The code TOUGH-FLAC uses a continuum method to represent fractures and couples thermal-hydrologic modeling using TOUGH with geomechanical modeling using FLAC to address THM processes. The current version of TOUGH-FLAC includes the recently developed BBM, a geomechanical constitutive relationship for thermo-elastoplastic behavior that is observed in bentonite. The code ROCMAS provides a discrete fracture representation for THM process including single-phase unsaturated flow. ROCMAS has several options for geomechanical constitutive relationships but currently does not include the BBM**.** The ROCMAS code and TOUGH-FLAC are two different types of simulators that complement each other, have been extensively applied, and yet have the flexibilities for modifications and future improvements.

The implementation of the BBM constitutive relationship in TOUGH-FLAC reported here is a major improvement for modeling of EBS bentonite. The BBM is the most advanced and accepted constitutive model used for modeling of bentonite-buffer behavior in the various European and Japanese nuclear waste programs. The implementation of the BBM in TOUGH-FLAC was shown to give results in excellent agreement with independent analytical and numerical simulation results, and was found to be in reasonable agreement with experimental data. The TOUGH-FLAC with BBM was also tested on a full-scale nuclear waste repository problem involving the interaction of multiple components (buffer, canister, rock) over a 100,000 year simulation time. The simulation indicated complex geomechanical behavior of the bentonite backfill, including a nonuniform distribution of buffer porosity and density that could not be captured in an alternative, simplified linear-elastic swelling model. Simulation studies were also performed to investigate coupled THM processes in the EBS in a low-permeability clay host rock. This study highlight the important interactions between the buffer and the host rock, in particular regarding the potential for desaturation of the rock and thermal pressurization, which can have a significant impact of the coupled THM evolution in the EBS.

Reactive-Diffusive Transport in Bentonite

A review of reactive-diffusive transport phenomena in bentonite highlights the important differences between diffusion in macroporous materials and nanoporous materials. Nanoporous materials contain a significant fraction of pore spaces with dimensions on the order of a nanometer, whereas macroporous materials are dominated by pore spaces dimensions much larger than a nanometer. The main differences in transport behavioar between these two categories of materials result from electrochemical interactions that become significant when the pore size approaches the thickness of the electric double layer. This is particularly important for compacted bentonite because of the large proportion of pore space that is within the nanometer scale. Diffusive transport is therefore connected with (1) the degree of compaction that influences the ionic structure of the clay interlayer and electric double layer, (2) the ionic strength that influences the electric double layer size, and (3) the interaction of chemical species between the macropores and the electric double layer. Current diffusive-reactive transport modeling is limited by the assumption of equilibrium between the macropores and the electric double layer.

Modeling tools for reactive-diffusive transport in the EBS include the software codes CruchFlow and TOUGHREACT. CrunchFlow is capable of modeling solute partitioning into an explicit diffuse double layer and associated diffusion within this layer, but does not account for diffusion into the clay interlayers. This is done using a charge balance equation for the diffuse layer balancing the mineral surface charge present in the Stern Layer and an equilibrium model relating chemical exchange between the double layer and macropore water. TOUGHREACT is a comprehensive non-isothermal multi-component reactive fluid flow and geochemical transport simulator. Aqueous complexation, acid-base, redox, gas dissolution/exsolution, and cation exchange are considered under the local equilibrium assumption. Mineral dissolution and precipitation can proceed either subject to local equilibrium or kinetic conditions. Linear adsorption and decay can be included. The chemical-hydrological couplings between mineral dissolution/precipitation and fluid flow are included through the treatment of temporal changes in porosity, permeability, and unsaturated hydrologic properties. Transport of aqueous and gaseous species by advection and molecular diffusion are considered in both liquid and gas phases.

Two modeling approaches have been proposed for reactive-diffusive transport through bentonite at the recent Chemistry Workshop of the EBS task force in Speyer, Germany held June 30 and July 1, 2010. These are the multi-porous, diffuse double layer approach and the ion-equilibrium approach. Two benchmark data sets are to be prepared to which modeling can be applied using the alternate concepts. The data sets will be generated from (1) advective-diffusive multi-component column experiments and; (2) diffusion experiments, including some measurements of associated swelling pressures.

5.2 Crosswalk between this Report and FEPs

The following table 5.2-1 (next page) identifies work done in this report with the used fuel disposition (UFD) FEPs (Houseworth 2010) associated with the EBS.

Table 5.2-1. FEPs Crosswalk

UFD FEP number	UFD FEP name	Report Sections	Information Provided
2.1.04.01	Evolution and Degradation of Backfill	2 through 5	Detailed treatment of THM modeling, general review of THMC processes.
2.1.08.01	Flow Through the EBS	2 through 5	See FEP 2.1.08.03.
2.1.08.03	Flow in Backfill	2 through 5	Detailed treatment of THM modeling, general review of THMC processes.
2.1.08.06	Alteration and Evolution of EBS Flow Pathways	2 through 5	Detailed treatment of THM modeling, general review of THMC processes.
2.1.09.05	Chemical Interaction of Water with Corrosion Products	5	Brief identification of issues
2.1.09.51	Advection of Dissolved Radionuclides in EBS	2 through 5	Closely related to flow and degradation of backfill
2.1.09.52	Diffusion of Dissolved Radionuclides in EBS	2 through 5	Detailed treatment of coupled process effects on diffusion
2.1.09.53	Sorption of Dissolved Radionuclides in EBS	5	Brief identification of issues
2.1.11.03	Effects of Backfill on EBS Thermal Environment	2 through 5	Detailed treatment of THM modeling.
2.1.11.04	Effects of Drift Collapse on EBS Thermal Environment	None	Generally considered not applicable if backfill is used.
2.1.11.08	Thermal-Mechanical Effects on Backfill	2 through 5	Detailed treatment of THM modeling.
2.1.11.10	Thermal Effects on Flow in EBS	2 through 5	Detailed treatment of THM modeling.
2.1.11.11	Thermally-Driven Flow (Convection) in EBS	2 through 5	Detailed treatment of THM modeling.
2.1.11.12	Thermally-Driven Buoyant Flow / Heat Pipes in EBS	None	Generally considered not applicable for sub-boiling conditions.
2.1.12.01	Gas Generation in EBS	2 and 5	General review of issues
2.1.12.02	Effects of Gas on Flow Through the EBS	2 and 5	General review of issues
2.1.12.03	Gas Transport in EBS	2 and 5	General review of issues

5.3 References

Alonso E.E., Gens A, Josa A. (1990) "A constitutive model for partially saturated soils." *Geotechnique*, 40, 405–430.

Alonso E.E., Alcoverro, J., et al. (26 co-authors) (2005) "The FEBEX benchmark test. Case definition and comparison of modelling approaches." *Int. J. Rock Mech. Min. Sci.*, 42, 611-638.

Appelo, C.A.J. and Wersin, P. (2007) "Multicomponent diffusion modeling in clay systems with application to the diffusion of tritium, iodide, and sodium in Opalinus" *Clay. Environ. Sci. Technol.*, 41, 5002-5007.

Appelo, C.A.J., Vinsot, A., Mettler, S. and Wechner, S. (2008) "Obtaining the porewater composition of a clay rock by modeling the in- and out-diffusion of anions and cations from an in-situ experiment." *J. Contam. Hydrol.*, 101, 67-76.

Appelo, C.A.J., and Postma, D., *Geochemistry, groundwater and pollution*, Rotterdam, The Netherlands, Balkema, 536 pp. (1993)

Bazer-Bachi, F., M. Descostes, E. Tevissen, P. Meier, B. Grenut, M-O. Simonnot and M. Sardin (2007) "Characterization of sulphate sorption on Callovo-Oxfordian argillitby batch, column and through-diffusion experiments." *Physics and Chemistry of the Earth*, 32, 552–558.

Biot, M.A. (1941) "General theory of three dimensional consolidation." *J. Applied Physics*, 12, 155–164.

Bourg, I.C., Bourg, A.C.M., Sposito, G. (2003) "Modeling diffusion and adsorption in compacted bentonite: a critical review." *J. Contam. Hydrol.* **61**, 293–302.

Bourg, I.C., Sposito, G., Bourg A.C.M. (2006) "Tracer diffusion in compacted, water-saturated bentonite." *Clays Clay Mine*r., 54, 363–374.

Bourg, I.C., Sposito, G., Bourg, A.C.M. (2007) "Modeling cation diffusion in compacted water-saturated sodium bentonite at low ionic strength." *Environ. Sci. Technol.*, 41, 8118–8122.

Bower, K.M. and Zyvoloski, G. (1997) "A numerical model for thermo-hydro-mechanical coupling in fractured rock." *Int. J. Rock Mech. Min. Sci. & Geomech. Abstr*., 34, 1201–1211.

Börgesson, L., ABAQUS. In Stephansson, O., Jing, L., and Tsang, C.-F. eds., *Coupled Thermo-hydro-mechanical Processes of Fractured Media*. Developments in Geotechnical Engineering, Elsevier, 79, 565–570. (1996)

Chatterji, S. (2004) "Ionic diffusion through thick matrices of charged particles." *J. Colloid Interface Sci*., 269, 186–191.

Dobson, P.F., T.J. Kneafsey, E.L. Sonnenthal, N.F. Spycher, and J.A. Apps, (2003) "Experimental and numerical simulation of dissolution and precipitation: Implications for fracture sealing at Yucca Mountain, Nevada." *Journal of Contaminant Hydrology*, 62-63, 459-476.

Davis J.A. and Kent D.B. (1990) "Surface complexation modeling in aqueous geochemistry." *Reviews inMineralogy and Geochemistry*, Mineralogical Society of America, 23, 177-260.

Donat, R.; Akdogan, A.; Erdem, E.; Cetisli, H. (2005) "Thermodynamics of Pb^{2+} and Ni^{2+} Adsorption onto Natural Bentonite from Aqueous Solutions." *Journal of Colloid and Interface Science*, 286, 43-52.

Dueck, A. (2007) "Results from suction controlled laboratory tests on unsaturated bentonite – Verification of a model." In: Schanz, T. (Ed.) *Experimental Unsaturated Soil Mechanics*, Springer Proceedings in Physics, 112, 329–335.

Dzombak, D.A and Morel, F.M.M., *Surface Complexation Modeling: Hydrous Ferric Oxide*, Wiley Interscience, New York, 393 pp. (1990)

Eriksen, T.E., Jansson, M., Molera, M. (1999) "Sorption effects on cation diffusion in compacted bentonite." *Engineering Geology*, 54, 231-236.

Gaucher, E.C.; Blanc, P.; Matray, J-M.; Michau, N. (2004) "Modeling Diffusion of an Alkaline Plume in a Clay Barrier." *Applied Geochemistry*, 19, 1505–1515.

Gaucher, E. P. Blanc, F. Barot, G. Braibant, S. Buschaert, C. Crouzet, A. Gautier, J.P. Girard, E. Jacquot, A. Lassin, G. Negrel, C. Tournassat, A. Vinsot and S. Altmann, (2006) "Modeling the porewater chemistry of the Callovo-Oxfordian formation at a regional scale." *C. R. Geosci.*, 338 (12–13), 917–930.

Gens, A. (1995) "Constitutive Laws", In: Gens, A., Jouanna, P., Schrefler, B.A. (Eds.) *Modern Issues in Non-saturated Soils*. Springer-Verlag, Wien, New York, 129–158.

Gens, A, Alonso, E.E. (1992) "A framework for the behaviour of unsaturated expansive clays." *Canadian Geotechnical Journal*, 29, 1013–1032.

Gens, A., Garcia-Molina, A.J., Olivella, S., Alonso, E.E. and Huertas, F. (1998) "Analysis of a full scale *in situ* test simulating repository conditions." *Int. J. Numer. Anal. Meth. Geomech*., 22, 515–548.

Gens A., Sanchez M., Do L., Guimaraes N., Alonso E., Lloret A., Olivella S., Villar M.V., Huertas F. (2009) "A full-scale in situ heating test for high-level nuclear waste disposal: observations, analysis and interpretation." *Geotechnique*, 59, 1–23.

Gens, A., Vaunat, J., Garitte, B., and Wileveau, Y. (2007) "In situ behaviour of a stiff layered clay subject to thermal loading: observations and interpretation." *Geotechnique*, 57(2), 207–228.

Gens, A., Sánchez, M., Sheng, D. (2006) "On constitutive modelling of unsaturated soils." *Acta Geotechnica*, 1, 137–147.

Giambalvo, E.R., Steefel, C.I., Fisher, A.T., Rosenberg, N.D., and Wheat, C.G. (2002) "Effect of fluid sediment reaction on hydrothermal fluxes of major elements, eastern flank of the Juan de Fuca Ridge." *Geochimica et. Cosmochimica Acta*, 66, 1739-1757.

Gonçalvès, I., Rousseau-Gueutin, P., Revil, A. (2007) "Introducing interacting diffuse layers in TLM calculations: a reappraisal of the influence of the pore size on the swelling pressure and the osmotic efficiency of compacted bentonites." *J. Colloid Interface Sci.* 316**,** 92–99.

Guvanasen, V. and Chan, T. (1995) "A new three-dimensional finite-element analysis of hysteresis thermohydromechanical deformation of fractured rock mass with dilatance in fractures." *Proceedings of the 2nd Conference on Mechanics of Jointed and Faulted Rocks*, Vienna, Austria, April 10–14, 347–442.

Hansen, F.D. "The Disturbed Rock Zone at the Waste Isolation Pilot Plant." SAND2003-3407 Report, Sandia National Laboratories, Albuquerque, NM. (2003)

Houseworth, J.E. "The DOE Used Fuel Disposition Campaign Features, Events, and Processes (FEP) Evaluation Report for Bentonite/Clay/Shale Systems." DOE Used Fuel Disposition Campaign, Lawrence Berkeley National Laboratory. (2010)

Israelsson, J.I., (1996a) "Short description of FLAC version 3.2." In Stephansson, O., Jing, L., and Tsang, C.-F. editors. *Coupled Thermo-hydro-mechanical Processes of Fractured Media*. Developments in Geotechnical Engineering, Elsevier, 79, 513–522.

Israelsson, J.I., (1996b) "Short description of UDEC and 3DEC." In Stephansson, O., Jing, L., and Tsang, C.-F. editors. *Coupled Thermo-hydro-mechanical Processes of Fractured Media*. Developments in Geotechnical Engineering, Elsevier, 79, 523–528.

Itasca Consulting Group, FLAC3D, Fast Lagrangian Analysis of Continua in 3 Dimensions, Version 4.0, Minneapolis, Minnesota, Itasca Consulting Group. (2009)

Jougnot, D., Revil, A., and Leroy, P. (2009) "Diffusion of ionic tracers in the Callovo-Oxfordian clay-rock using the Donnan equilibrium model and the formation factor." *Geochimica et Cosmochimica Acta*, 73, 2712-2726.

Khan, S.A. (2002) "Sorption of Long-Lived Radionuclides Cesium-134, Strontium-85 and Cobalt-60 on Bentonite." *Journal of Radionanalytical and Nuclear Chemistry*, 258(1), 3-6.

Kim, H., Suk, T., Park, S., and Lee, C. (1993) "Diffusivities for ions through compacted Na bentonite with varying dry bulk density." *Waste Managament,* 13, 303–308.

Kohl, T. and Hopkirk, R.J. (1995) "The finite element program "FRACTure" for the simulation of Hot Dry Rock reservoir behavior." *Geothermics*, 24, 345–359.

Kolditz O., Bauer S., Beinhorn M., de Jonge J., Kalbacher T., McDermott C., Wang W., Xie M., Kaiser R., Kohlmeier M. "ROCKFLOW – Theory and Users Manual, Release 3.9." Groundwater Group, Center for Applied Geosciences, University of Tübingen, and Institute of Fluid Mechanics, University of Hannover. (2003)

Koutsabeloulis, N.C. and Hope, S.A. (1998) "Coupled stress/fluid/thermal multi-phase reservoir simulation studies incorporating rock mechanics." *Proceedings of SPE/ISRM EUROCK-98 symposium*, Norway, 449–454.

Kozaki, T., Fujishima, A., Saito, N., Sato, S. and Ohashi, H. (1998) "Self-diffusion of sodium ions in compacted sodium montmorillonite." *Nuclear Technology*, 121, 63-68.

Kozaki, T., Liu, J. and Sato, S. (2008) "Diffusion mechanism of sodium ions in compacted montmorillonite under different NaCl concentration." *Physics and Chemistry of the Earth*, 33, 957-961.

Kristensson O., Åkesson M. (2008a) "Mechanical modeling of MX-80 – Quick tools for BBM parameter analysis." *Physics and Chemistry of the Earth*, 33, S508–S515.

Kristensson, O., Åkesson, M. (2008b) "Mechanical modeling of MX-80 – Quick tools for BBM parameter analysis." *Physics and Chemistry of the Earth*, 33, S508–S515.

Kristensson O., Åkesson M. (2008c) "Mechanical modeling of MX-80 – Development of constitutive laws." *Physics and Chemistry of the Earth*, 33, S504–S507.

Lasaga, A. C. (1984) "Chemical kinetics of water-rock interactions." *J. Geophys. Res*., 89, 4009-4025.

Lemmens, K. (2001) "The Effect of Clay on the Dissolution of Nuclear Waste Glass", *Journal of Nuclear Materials*, 298, 11-18.

Leroy, P. and A. Revil, (2004) "A triple-layer model of the surface electrochemical properties of clay minerals." *J. Colloid Interface Sci.*, 270 (2), 371–380.

Leroy, P., Revil, A., and Coelho, D. (2006) "Diffusion of ionic species in bentonite." *J. Colloid Interface Sci.* 296 (1), 248–255.

Leroy P., Revil A., Altmann S., Tournassat C. (2007) "Modeling the composition of a pore water in a clay-rock geological formation (Callovo-Oxfordian, France)." *Geochimica Cosmochimica Acta*, 71(5), 1087-1097.

Lichtner, P. C. (1996) "Continuum formulation of multicomponent-multiphase reactive transport." in Lichtner, P. C., Steefel, C. I., and Oelkers, E. H. (eds.), *Reactive transport in porous media*, Reviews in Mineralogy, Mineral Society of America, 34, 1-79.

Lichtner, P. C. (1988) "The quasi-stationary state approximation to coupled mass transport and fluid-rock interaction in a porous medium." *Geochim. Cosmochim. Acta*, 52, 143-165.

Liu, H.H., Rutqvist, J., Berryman, J.C. (2009) "On the relationship between stress and elastic strain for porous and fractured rock." *Int J Rock Mech & Min Sci*, 46, 289–296.

Liu Q., Zhang C., Liu X. „A practical method for coupled THM simulations of the Yucca Mountain and FEBEX case samples for task D of the DECOVALEX-THMC Project." Proceeding of the GEOPROC2006 International symposium: 2nd International Conference on Coupled Thermo-hydro-mechanical-chemical processes in Geosystems and Engineering, HoHai University, Nanjing, China, May 22–25, 2006, 220–225, HoHai University. (2006)

Madsen, F.T. (1998) "Clay mineralogical investigations related to nuclear waste disposal." Clay Miner. 33, 109-129.

Melkior, T., D. Mourzagh, S. Yahiaoui, D. Thoby, J.C. Alberto, C. Brouard and N. Michau (2004) "Diffusion of an alkaline fluid through clayey barriers and its effect on the diffusion properties of some chemical species." *Appl. Clay Sci.* 26, 99–107.

Melkior, T., S. Yahiaoui, D. Thoby, S. Motellier and V. Barthes (2007) "Diffusion coefficients of alkaline cations in Bure mudrock." *Physics and Chemistry of the Earth*, 32, 453–462.

Molera, M., Eriksen, T. (2002) "Diffusion of $^{22}Na^{+}$, $^{85}Sr^{2+}$, $^{134}Cs^{+}$ and $^{57}Co^{2+}$ in bentonite clay compacted to different densities: experiments and modeling." *Radiochimica Acta*, 90, 753-760.

Munson, D.E. and P.R. Dawson., Constitutive model for the low temperature creep of salt (with application to WIPP). Albuquerque, NM: Sandia National Laboratories. SAND79-1853. 1979.

Munson, D.E. and P.R. Dawson. "A transient creep model for salt during stress loading and unloading." Sandia National Laboratories, Albuquerque, SAND82-0962 Report. (1982)

Muurinen, A., Karnland, O. and Lehikoinen, J. (2007) "Effect of homogenization on the microstructure and exclusion of chloride in compacted bentonite." *Physics and Chemistry of the Earth*, 32, 485-490.

Muurinen, A., Penttilä-Hiltunen, P. and Uusheimo, K. (1998) "Diffusion of chloride and uranium in compacted sodium bentonite." In: W. Lutze and R.C. Erwing, Editors, *Scientific Basis of Nuclear waste Management XII*, Materials Research Society, Pittsburg, PA, 743-748.

Muurinen A. "Diffusion of anions and cations in compacted sodium bentonite." *VTT Publication* 168, Espoo Technical Centre, Finland. (1994)

Nguyen, T.S. (1996) "Description of the computer code FRACON." In Stephansson, O., Jing, L., and Tsang, C.-F. editors. *Coupled Thermo-hydro-mechanical Processes of Fractured Media*. Developments in Geotechnical Engineering, Elsevier, 79, 539–544.

Noorishad, J., Tsang, C.-F. and Witherspoon, P.A. (1984) "Coupled thermal-hydraulic-mechanical phenomena in saturated fractured porous rocks: numerical approach." *J. Geophys. Res.*, 89, 10365–10373.

Noorishad, J., and Tsang, C.-F. (1996) "ROCMAS-simulator: A Thermohydromechanical Computer Code." In Stephansson, O., Jing, L., and Tsang, C.-F. editors. *Coupled Thermo-hydro-mechanical Processes of Fractured Media*. Developments in Geotechnical Engineering, Elsevier, 79, 551–558.

Nordstrom, D. K., and Muñoz, J. L. *Geochemical Thermodynamics*, The Benjamin/Cummings Pub. Co., Menlo Park, California, 477 pp. (1986)

Ochs, M., B. Lothenbach, H. Wanner, H. Sato and M. Yui, (2001) "An integrated sorption–diffusion model for the calculation of consistent distribution and diffusion coefficients in compacted bentonite." *J. Contam. Hydrol.* 47, 283–296.

OECD, "Engineering barrier systems and the safety of deep geological repositories (State-of-the-art Report)", *Nuclear Energy Agency (NEA), Organisation for Economic Cooperation and Development (OECD)*, ISBN 92-64-18498-8. (2003)

Olivella, S., Carrera, J., Gens, A. and Alonso, E.E. (1994) "Nonisothermal multiphase flow of brine and gas through saline media." *Transport in Porous Media*, 15, 271–293.

Ohnishi, Y. and Kobayashi, A., "THAMES". In Stephansson, O., Jing, L., and Tsang, C.-F. editors. *Coupled Thermo-hydro-mechanical Processes of Fractured Media*. Developments in Geotechnical Engineering, Elsevier, 79, 545–549. (1996)

Palandri, J., and Kharaka, Y. K. "A compilation of rate parameters of water-mineral interaction kinetics for application to geochemical modeling." US Geol. Surv. Open File Report 2004-1068, 64 pp. (2004)

Park, B.Y., Hansen, F.D. and Lee, M.Y. (2005) "Numerical Simulation of the Disturbed Rock Zone around Underground Openings in Rock Salt." *Paper presented at the ARMA Meeting 2005*; ARMA/USRMS 05-805.

Philip, J.R. and de Vries, D.A. (1957) "Moisture movement in porous material under temperature gradients." *EOS Trans*., American Geophysical Union (AGU), 38, 222–232.

Pine, R.J. and Cundall, P.A. (1985) "Application of the fluid rock interaction program (FRIP) to the modeling of hot dry rock geothermal energy systems." In Stephansson, O., editor. *Proceedings of the International Symposium on Fundamentals of Rock Joints*, Björkliden, Sweden, 293–302.

Pruess, K., Oldenburg, C.M., and Moridis, G.M. "TOUGH2 User's Guide Version 2." Lawrence Berkeley National Laboratory, Report LBNL-43134. (November 1999)

Pruess, K. "TOUGH2: A general numerical simulator for multiphase fluid and heat flow." Lawrence Berkeley Laboratory, Report LBL-29400, Berkeley, California. (1991)

Pruess, K. "TOUGH user's guide." *Nuclear Regulatory Commission*, report NUREG/CR-4645 (also Lawrence Berkeley Laboratory Report LBL-20700, Berkeley, California). (1987)

Pusch, R. "The microstructure of MX-80 clay with respect to its bulk physical properties under different environmental conditions." *Swedish Nuclear Waste Management Co. (SKB)*, Technical Report TR-01-08, 111 pp. (2001)

Raffensperger, J. P. (1996) "Numerical simulation of sedimentary basin-scale hydrochemical processes." In *Advances in Porous Media*, Corapcioglu, Y. C., (ed.), Amsterdam, The Netherlands, Elsevier Science, 440 pp.

Revil, A. and Leroy, P. (2004) "Governing equations for ionic transport in porous shales." *J. Geophys. Res.* **109**, B03208.

Revil, A. and Jougnot, D. (2008) "Diffusion of ions in unsaturated porous materials." *Colloid Interface Sci.* **319** (1), 226–235.

Romero E., Alonso E.E, Knobelsdorf J. Laboratory tests on compacted bentonite-sand material for the GMT emplacement project. *University of Catalonia, NAGRA NPB 02-05*. p. 68. (2002)

Roscoe, K.H., Burland, J.B. (1968) "On the generalized stress-strain behaviour of the `wet' clay." In: Heyman, J., Leckic, F.A. (Eds.), *Engineering Plasticity*, Cambridge University Press, Cambridge, 535–609.

Rutqvist J. (2010) "Status of the TOUGH-FLAC simulator and recent applications related to coupled fluid flow and crustal deformations." *Computers and Geosciences* (in press).

Rutqvist J., Börgesson L., Chijimatsu M., Hernelind J., Jing L., Kobayashi A. and Nguyen S. (2009a) "Modeling of damage, permeability changes and pressure responses during excavation of the TSX tunnel in granitic rock at URL, Canada." *Environmental Geology*, 57, 1263–1274.

Rutqvist J., Bäckström A., Chijimatsu M., Feng X-T, Pan P-Z., Hudson J, Jing L., Kobayashi A., Koyama T., Lee H-S, Huang X-H, Rinne M. and Shen B. (2009b) "Multiple-Code Simulation Study of the Long-term EDZ Evolution of Geological Nuclear Waste Repositories." *Environmental Geology*, 57, 1313–1324.

Rutqvist, J., Ijiri, Y., and Yamamoto, H. (2009c) "Implementing the Barcelona Basic Model into TOUGH-FLAC for analysis of geomechanical behavior of unsaturated soils." *Proceedings of the TOUGH symposium 2009*, Lawrence Berkeley National Laboratory, Berkeley, Sept 14–16.

Rutqvist, J., Barr, D., Birkholzer, J.T., Fujisaki, K., Kolditz, O., Liu, Q.-S., Fujita, T., Wang, W., Zhang, C.-Y. (2009d) "A comparative simulation study of coupled THM processes and their effect on fractured rock permeability around nuclear waste repositories." *Environmental Geology*, 57, 1347–1360.

Rutqvist J. and Moridis G.J. (2009) "Numerical Studies on the Geomechanical Stability of Hydrate-Bearing Sediments." *Society of Petroleum Engineers SPE Journal*, SPE-126129, 14, 267-282.

Rutqvist J, Freifeld B, Min K-B, Elsworth D, Tsang, Y. (2008a) "Analysis of thermally induced changes in fractured rock permeability during eight years of heating and cooling at the Yucca Mountain Drift Scale Test." *Int J Rock Mech & Min Sci*, 45, 1373–1389.

Rutqvist, J, Barr, D., Birkholzer, J.T., Chijimatsu, M., Kolditz, O., Liu, Q., Oda, Y., Wang, W., Zhang, C. (2008b) "Results from an international simulation study on coupled thermal, hydrological, and mechanical (THM) processes near geological nuclear waste repositories." *Nuclear Technology*, 163, 101–109.

Rutqvist J. and Tsang C.-F. "Review of SKB's Work on Coupled THM Processes Within SR-Can: External review contribution in support of SKI's and SSI's review of SR-Can." *Swedish Nuclear Power Inspectorate (SKI)*, Technical Report 2008:08. (2008)

Rutqvist, J., Tsang, C.-F. (2002) "A study of caprock hydromechanical changes associated with CO_2-injection into a brine formation." *Environmental Geology*, 42, 296-305.

Rutqvist, J., Chijimatsu, M., Jing, L., De Jonge, J., Kohlmeier, M., Millard, A., Nguyen, T.S., Rejeb, A., Souley, M., Sugita, Y., Tsang, C.F. (2005) "Numerical study of the THM effects on the near-field safety of a hypothetical nuclear waste repository – BMT1 of the DECOVALEX III project. Part 3: Effects of THM coupling in fractured rock." *Int. J. Rock Mech. Min. Sci.*, 42, 745–755.

Rutqvist, J., Tsang, C.-F. "A fully coupled three-dimensional THM analysis of the FEBEX in situ test with the ROCMAS code: prediction of THM behavior in a bentonite barrier, In: Stephansson." O., Hudson, J.A., Jing, L., (Eds.) *Coupled T-H-M-C Processes in Geo-Systems: Fundamentals, Modelling, Experiments and Applications*. Elsevier Geo-Engineering Book Series, Oxford, p. 143–148. (2004)

Rutqvist J., Y.-S. Wu, C.-F. Tsang, and G. Bodvarsson (2002) "A Modeling Approach for Analysis of Coupled Multiphase Fluid Flow, Heat Transfer, and Deformation in Fractured Porous Rock." *Int. J. Rock Mech. Min. Sci.* 39, 429-442.

Rutqvist J., Börgesson L., Chijimatsu M., Nguyen T. S., Jing L., Noorishad J., and Tsang C.-F. (2001) "Coupled Thermo-hydro-mechanical Analysis of a Heater Test in Fractured Rock and Bentonite at Kamaishi Mine – Comparison of Field Results to Predictions of Four Finite Element Codes*." Int. J. Rock Mech. Min. Sci.* 38, 129-142.

Sabodina, M.N.; Kalmykov, S.N.; Sapozhnikov, Yu. A.; Zakharova, E.V. (2006) "Neptunium, Plutonium, and ^{137}Cs Sorption by Bentonite Clays and their Speciation in Pore Waters." *Journal of Radioanalytical and Nuclear Chemistry*, 270(2), 349-355.

Samper, J.; Lu, C., Montenegro, L. (2008) "Reactive Transport Model of Interactions of Corrosion Products and Bentonite." *Physics and Chemistry of the Earth*, 33, S306–S316.

Sánchez, M., Gens, A., Guimarães, L. do N., Olivella, S. A (2005) "Double structure generalized plasticity model for expansive materials." *Int J Numer Anal Methods Geomech*, 29, 751–787.

Sato, H., Yui, M., and Yoshikawa H., (1995) "Diffusion behavior for Se and Zr in bentonite." *Mater. Res. Soc. Symp. Proc.* **353**, 269–276.

Settari, A., and Mourits, F.M. (1998) "A Coupled reservoir and Geomechanical Simulation System." *SPE Journal*, 27(9), SPE paper 50939, 219-226.

Slider, H. C. "Practical petroleum reservoir engineering methods, An Energy Conservation Science." Tulsa, Oklahoma, Petroleum Publishing Company. (1976)

Sonnenthal, E. Chapter 5 in: Birkholzer, J. Rutqvist, E. Sonnenthal, and Barr, D. "Long-Term Permeability/Porosity Changes in the EDZ and Near Field due to THM and THC Processes in Volcanic and Crystalline-Bentonite Systems." *DECOVALEX-THMC Project Task D Final Report*. (2008)

Steefel, C.I., K. Maher, (2009) "Fluid-rock interaction: A reactive transport approach." *Reviews in Mineralogy and Geochemistry*, **70**: 485-532.

Steefel, C. I., and Lasaga, A. C. (1994) "A coupled model for transport of multiple chemical species and kinetic precipitation/dissolution reactions with applications to reactive flow in single phase hydrothermal system." *Am. J. Sci.*, 294, p. 529-592.

Steefel, C. I., and MacQuarrie, K. T. B. (1996) "Approaches to modeling of reactive transport in porous media," In Lichtner, P. C., Steefel, C. I., and Oelkers, E. H. (eds.), Reactive transport in porous media, *Reviews in Mineralogy*, Mineral Society of America, v. 34, p. 83-129, 1996.

Stone, C.M., Holland, J.F., Bean, J.E., and Arguello, J.G. (2010) "Coupled Thermal Mechanical Analyses of a Generic Salt Repository for High Level Waste." *Paper presented at the ARMA Meeting 2010*. ARMA 10-180.

Stumm, W. Chemistry of the Solid Water Interface: Processes at the Mineral Water Particle Water Interface in Natural Systems, John Wiley & Sons, 428 p. (1992)

Swenson, D.V., DuTeau, R. and Sprecker, T. A (1997) "coupled model of fluid flow in jointed rock applied to simulation of a hot dry rock reservoir." *Int. J. Rock Mech. Min. Sci. & Geomech. Abstr.*, 34, Paper 308.

Thomas, H.R. and Sansom, M.B. (1995) "Fully coupled analaysis of heat, moisture, and air transfer in unsaturated soil." *J. Engng. Mech.*, ASCE, 121, 392–405.

van Genuchten, MT. (1980) "A closed-form equation for predicting the hydraulic conductivity of unsaturated soils." *Soil Sciences Society of America Journal*, 44, 892–898.

Verma, A., Pruess, K. (1988) "Thermohydrologic Conditions and Silica Redistribution Near High-Level Nuclear Wastes Emplaced in Saturated Geological Formations." *J. Geophysical Res.*, 93(B2), 1159-1173.

Walter, A.L., Frind, E.O., Blowes, D.W., Ptacek, C.J., Molson, J.W. (1994) "Modeling of multicomponent reactive transport in groundwater, 1, Model development and evaluation." *Water Resour. Res.*, 30 (11), 3137-3148.

Wang, W., Rutqvist, J., Görke, U.-J., Birkholzer, J.T., Kolditz, O. (2010) "Non isothermal flow in low permeable porous media: A comparison of Richards' and two-phase flow approaches." *Environmental Earth Sciences*, (in press).

Wersin, P., Curti, E., Appelo, C.A.J. (2004) "Modelling bentonite-water interactions at high solid/liquid ratios: swelling and diffuse double layer effects." *Appl. Clay Sci.*, 26, 249-257.

Wolery, T. J. "EQ3/6: Software package for geochemical modeling of aqueous systems: Package overview and installation guide (version 8.0)." Lawrence Livermore National Laboratory Report UCRL-MA-110662 PT I, Livermore, California. (1992)

Xu, T., and Pruess, K. (1998) "Coupled modeling of nonisothermal multiphase flow, solute transport andreactive chemistry in porous and fractured media: 1. Model development and validation." Lawrence Berkeley National Laboratory Report LBNL-42050, Berkeley, California, 38 pp., 1998.

Xu, T., and Pruess, K. (2001) "Modeling multiphase fluid flow and reactive geochemical transport in variably saturated fractured rocks: 1. Methodology." *Am. J. Sci.*, 301, 16-33.

Xu, T., Sonnenthal E., Spycher, N., Pruess, K. "TOUGHREACT User's guide: A simulation program for nonisothermal multiphase reactive geochemical transport in variably saturated geologic media." Lawrence Berkeley National Laboratory Report LBNL-55460-2008. (2008)

Yeh, G. T., and Tripathi, V. S. (1991) "A model for simulating transport of reactive multispecies components: model development and demonstration." *Water Resour. Res.*, 27, 3075-3094.

5.4 Key References for THMC Processes in EBS-Bentonite

General:

Åkesson, M. (2010) "Summary Report of Bentonite Working Group." *Proceedings of European Commission THERESA-TIMODAZ Coupled THMC Conference*, Luxembourg, September 29-October 1, 2009. To be published by European Commission, 2010.

Alonso, E.E. and Ledesma, A (2005). Advances in Understanding Engineered clay barriers. A.A. Balkema Publishers, Leiden, 583 p., 2005.

Birgersson, M., Börgesson, L., Hedström, M., Karnland, O. and Nilsson, U. (2009) "Bentonite Erosion, final report from Clay Technology." *Swedish Nuclear Fuel and Waste Management Co. (SKB)*, Stockholm, Technical report TR-09-34. (2009)

Bock, C.D., Bosgiraud, J-M., Weber, H., Rothfuches, T., Verstricht, J., Breen, B., and Johnson, M. (2008). Achievements of the ESDRED Project in Buffer Construction Technology, Proceedings of EURADWASTE '08 Conference, Luxembourg, October 20-22, 2008.

Börgesson, L., Hernelind, J. "Coupled thermo-hydro-mechanical calculations of the water saturation phase of a KBS-3 deposition hole." *Swedish Nuclear Fuel and Waste Management Co. (SKB)*, Stockholm, Technical Report TR-99-41. (1999)

Chijimatsu, M., Börgensson L., Fujita T., Jussila P., Nguyen, S., Rutquist, J., and Ling, L. (2009) "Model development and calibrataion for the coupled thermal, hydraulic and mechanical phenomena of the bentonite." *Environmental Geology*, 57, 1255-1261.

EC (2007) "EURATOM FP6 Research Projects and Training Activities (2007) Project Synopses." Published by the European Commission, Directorate-general for Research Communication Unit, Volume III, EUR 22385.

EC (2010) *Proceedings of European Commission THERESA-TIMODAZ Coupled THMC Conference*, Luxembourg, September 29-October 1, 2009. To be published by European Commission, 2010.

Gatabin C., Billaud P., (2005) "Bentonite THM mock-up experiments." Sensors data report, CEA, France.

Nguyen, T.S., Börgesson, L., Chijimatsu, M., Hernelind, J., Jing, L., Kobayashi, A. and Rutqvist, J. (2009) "A Case Study on the influence of THM coupling on the near field safety of a spent fuel repository in sparsely fractured granite." *Environmental Geology*, 57, 1239-1254.

Pusch, R. (2006) "The performance of clay barriers in Repositories for high-level radioactive waste." *Nuclear Engineering and Technology*, 38(6), 483-488.

Pusch R. and Yong, R. "Microstructure of Smectite clays and engineering performance." Taylor & Francis, London and New York. (ISBNIO:0-415-36863-4). (2006)

Rothfuchs, T. Joclewer, N. and Zhang, C-L. (2007) "Self-sealing Barriers of Clay (Mineral Mixtures – the SB-project at the Mont Terri Rock Laboratory." *Physics and Chemistry of the Earth*, Parts A/B/C, 32(1-7), 106-115.

Swedish Nuclear Fuel and Waste Management Company (SKB) "Äspö Hard Rock Laboratory, Annual Report." *Swedish Nuclear Waste Management Co. (SKB),* Technical Report TR-09-10, Stockholm, Sweden. (2009)

Tsang, C.F., Stephansson, O., Jing, L., Kautsky, F. (2009) "DECOVALEX project: from 1992 to 2007." *Environmental Geology*, 57(6), 1221-1237.

Tsang C.F., Åkesson M, Barnichon J-D., Jing L., Li X. L., and Schulze O. (2010) "A Combined Review of Key Issues Related to Coupled THMC Processes in the Near-field of Radioactive Waste Repositories in Salt, Clays and Bentonite-Crystalline Rock Systems." *Proceedings of European Commission THERESA-TIMODAZ Coupled THMC Conference*, Luxembourg, September 29-October 1, 2009. To be published by European Commission, 2010.

THMC Processes in Bentonite:

Birgersson M, Åkesson M, Hökmark H, (2008) "Gas intrusion in saturated bentonite – A thermodynamic approach." *Physics and Chemistry of the Earth*, 33, 248-251.

Castellanos, E., Villar, M.V., Romero, E., Lloret, A., Gens, A. (2008) "Chemical impact on the hydro-mechanical behaviour of high-density FEBEX bentonite." *Physics and Chemistry of the Earth*, 33, S516-S526.

Dueck, A. (2008) "Laboratory results from hydro-mechanical tests on a water unsaturated bentonite." *Engineering Geology*, 97(1-2), 15-24.

Dueck, A. and Börgesson, L. (2007) "Model suggested for an important part of the hydro-mechanical behaviour of a water unsaturated bentonite." *Engineering Geology*, 92(3-4), 160-169.

Lloret, A., Villar, M.V., Sanchez, M., Gens, A., Pintado, X,, Alosnso, E.E. (2003) "Mechanical behaviour of a heavily compacted bentonite under high suction changes." *Géotechnique*, 53, 27-40.

Romero, E., Gens, A., Lloret, A. (2003) "Suction effects on a compacted clay under non-isothermal conditions." *Géotechnique*, 53, 65-81

Sánchez, M., Gens, A., Guimaraes, L. do N., Olivella, S (2005). "A double generalized plasticity model for expansive materials". *Int J Numer Anal Methods Geomech*, 29, 751-787.

Schanz, T., Tripathy, S. (2009) "Swelling pressure of a divalent-rich bentonite: Diffuse double-layer theory revisited", *Water Resourses Res*, 45, Art. Number: W00C12.

Sánchez, M., A Gens, LJDN Guimarães, Olivella, S. (2005) "A double structure generalized plasticity model for expansive materials." *Int J Numer Anal Methods Geomech*, 29, 751-787.

Thomas, H.R., Siddiqua, S., Seetharam, S. (2009) "Inclusion of higher temperature effects in a soil behaviour model", *Géotechnique*, 59(3), 279-282

Thomas, H., and Vardon P. (2010) "The TH(C)M behaviour of highly-compacted bentonite clay related to high-level nuclear waste disposal – some recent developments." *Proceedings of EC-Timodaz-Theresa THMC Conference, 29 Sept-01 Oct 2009*, to be published, European Commission, 2010.

Tong F. G., Jing L, Zimmerman R. W. (2009) "An effective thermal conductivity model of geological porous media for coupled thermo-hydro-mechanical systems with multiphase flow." *Int. J. Rock Mech. Min. Sci.*, 46, 1358-1369.

Tripathy, S., Schanz, T., (2007), "Compressibility behaviour of clays at very large pressures", *Canadian Geotechnical Journal*, 44, p355-362.

Tripathy, S., Subba Rao, K.S., (2009), "Cyclic swell-shrink behaviour of a compacted expansive soil", *Geotechnical and Geological Engineering*, 27 (1), p89-103.

Zheng, L. and J. Samper (2008) "Coupled THMC model of FEBEX mock-up test." *Physics and Chemistry of the Earth*, 33, S486–S498.

Zheng, L., J. Samper, L. Montenegro, A. M. Fernández. (2010) "A coupled THMC model of a heating and hydration laboratory experiment in unsaturated compacted FEBEX bentonite." *Journal of Hydrology*, 386(1-4), 80-94.

THM numerical models:

Chen Y., Zhou C., Jing L. "Modelling coupled THM processes of geological porous media with multiphase flow: Theory and validation against laboratory and field scale experiments." *Computers and Geotechnics*, 36, 1308–1329.

Cleall, P.J., Thomas, H.R., Melhuish, T.A., Owen, D.H. (2006) "Use of parallel computing and visualisation techniques in the simulation of large scale geoenvironmental engineering problems." *Future Generation Computer Systems*, 22, 460-467.

Kimura, M., Nakama, S., Suzuki, H., Fugita, T. (2010) "Development of Prototype Numerical model on the coupled thermo-Hydro-Mechanical-chemical processes in the near-field of a high-level radioactive waste repository." *Proceedings of EC-Timodaz-Theresa THMC Conference, 29 Sept-01 Oct 2009*, to be published, European Commission, 2010.

Sánchez, M., Gens, A., Guimarães, L., Olivella, S. (2008). "Implementation algorithm of a generalised plasticity model for swelling clays". *Computers and Geotechnics*, 35 (6), 860-871.

Seetharam, S.C., Thomas, H.R., Cleall, P. (2007) "Coupled thermo/hydro/ chemical/mechanical model for unsaturated soils – numerical algorithm." *International Journal for Numerical Methods in Engineering*, 70(12), 1490-1511.

Thomas, H.R., Yang, H.T., He, Y., Cleall, P.J. (2003) "A multi-level parallelised substructuring frontal solution for coupled thermo/hydro/mechanical problems in unsaturated soil". *Int J Numer Anal Methods Geomech*, 27, 951-965.

Tong F.G., Jing L., Zimmerman R. W. (2010) "A fully coupled thermo-hydro-mechanical model for simulating multiphase flow, deformation and heat transfer in buffer material and rock masses." *Int. J. Rock Mech. Min. Sci.*, 47(2), 205-217.

Vardon, P.J., Cleall, P.J., Thomas, H.R., Philip, R.N., Banicescu, I. (2009) "Three-dimensional field-scale coupled Thermo-Hydro-Mechanical modelling: a parallel computing implementation." *Submitted by invitation for publication in the special issue of the ASCE International Journal of Geomechanics, Environmental Geotechnology*: Contemporary Issues.

Wang W, Kosakowski G, Kolditz O. (2009) "A parallel finite element scheme for thermo-hydro-mechanical (THM) coupled problems in porous media." *Comput Geosci*, 35(8), 1631-1641.

Wang W, Kolditz O. (2007) "Object-oriented finite element analysis of thermo-hydro-mechanical (THM) problems in porous media." *Int J Numer Methods Eng,* 69(1), 162-201.

Xie M, Agus S, Schanz T, Kolditz O. (2004) "An upscaling method and numerical modelling of swelling/shrinking processes in compacted bentonite/sand mixtures." *Int J Numer Anal Methods Geomech*, 28, 1479-1502.

Chemistry:

Birgersson, M. and Karnland, O. (2009) "Ion equilibrium between montmorillonite interlayer space and an external solution – Consequences for diffusional transport." *Geochimica et Cosmochimica Acta*, 73(7), 1908-1923.

Cleall, P.J., Seetharam, S.C., Thomas, H.R. (2007) "On the inclusion of some aspects of chemical behaviour of an unsaturated soil in thermo/hydro/mechanical models: Part 1, Model development." *American Society of Civil Engineers Journal of Engineering Mechanics*, 133(3), 338-347.

Cleall, P.J., Seetharam, S.C., Thomas, H.R. (2007) "On the inclusion of some aspects of chemical behaviour of an unsaturated soil in thermo/hydro/mechanical models: Part II, Application: transport of soluble salts in a compacted bentonite", *ASCE Journal of Engineering Mechanics*, 133(3), 348-356.

Guimaraes, L. do N., Gens, A., Olivella, S. (2007) "Coupled thermo-hydro-mechanical and chemical analysis of expansive clay subjected to heating and hydration." *Transport in porous media*, 66, 341-372.

Guimaraes, L. do N., Gens, A., Sánchez, M., Olivella, S. (2006) "THM and reactive transport of expansive clay barrier." *Communications in Numerical Methods in Engineering*, 22, 849-859.

Li, Y., Cleall, P.J., Thomas, H.R., (2009) "Multi-dimensional chemo-osmotic consolidation of clays." Submitted to *Computers and Geotechnics*.

Mata, C., Guimaraes, L. do N., Ledesma, A., Gens, A., Olivella, S. (2005) "A hydro-geochemical analysis of the saturation process with salt water of a bentonite crushed granite rock mixture in an engineered nuclear barrier." *Engineering Geology*, 81, 227-245.

Musso, G., Romero, E., Gens, A., Castellanos, E. (2003) "The role of structure in the chemically induced deformations of FEBEX bentonite." *Applied Clay Science*, 23, 229-237.

Seetharam, S.C., Cleall, P.J., Thomas, H.R. (2006) "Modelling some aspects of ion migration in a compacted bentonitic clay." *Engineering Geology*, 85, 221-228.

Seetharam, S.C., Thomas, H.R., Vardon, P.J. (2009) "Non-isothermal multi-component reactive transport model for unsaturated soil." *Submitted by invitation for publication in the special issue of the ASCE International Journal of Geomechanics, Environmental Geotechnology*: Contemporary Issues.

Xie M., Bauer S., Kolditz O., Nowak T., Shao H. (2006) "Numerical simulation of reactive processes in an experiment with partially saturated bentonite." *J Contam Hydrol*, Vol. 3, 122-147.

Experiments and their Modelling:

Alonso EE, Alcoverro J, Coste F, Malinsky L, Merrien-Soukatchoff V, Kadiri I, Nowak T, Shao H, Nguyen TS, Selvadurai APS, Armand G, Sobolik SR, Itamura M, Stone CM, Webb SW, Rejeb A, Tijani M, Maouche Z, Kobayashi A, Kurikami H, Ito A, Sugita Y, Chijimatsu M, Börgesson L, Hernelind J, Rutqvist J, Tsang CF, Jussila P. (2005) "The FEBEX benchmark test: case definition and comparison of modelling approaches." *Int J Rock Mech Min Sci*, 42(5-6), 611-638.

Cho, W-J., Lee, J-O., and Kwon, S. (2010) "Simulation of Thermo-hydro-mechanical process in the engineered barrier system of a high-level waste repository." *Proceedings of EC-Timodaz-Theresa THMC Conference*, 29 Sept-01 Oct 2009, to be published, European Commission.

Cleall, P.J., Melhuish, T.A. Thomas, H.R., (2006), "Modelling of the three-dimensional behaviour of a prototype nuclear waste repository", *Engineering Geology*, 85, p212-220.

Dixon, D., Lundin, C., Örtendahl, E., Hedin, M and Ramqvist, G. "Deep repository-engineeering barrier systems. Half-scale tests to examine water uptake by bentonite pellets in a block-bentonite backfill system". *Swedish Nuclear Waste Management Co. (SKB)*, Report R-08-132. (2008)

Gens A., Sánchez, M., Guimarães, L. do N., Alonso, E.E., Lloret, A., Olivella, S., Villar, M.V., Huertas, F. (2009). "A full-scale in situ heating test for high-level nuclear waste disposal: observations, analysis and interpretation". *Geotechnique*, 59, 377-399.

Herklotz, M., Jobmann, M., and Yildizdag, K. (2010) "Investigation on the TH-behaviour of a heated bentonite barrier by measurements and numerical calculations." *Proceedings of EC-Timodaz-Theresa THMC Conference*, 29 Sept-01 Oct 2009, to be published, European Commission, 2010.

Millard, A., Slimane, K.B., and Barnichon J.D. (2010) "Preliminary investigation of the Canister Retrieval Test, Influence of the flow parameters on the THM behaviour (1020)." *Proceedings of EC-Timodaz-Theresa THMC Conference*, 29 Sept-01 Oct 2009, to be published, European Commission.

Thomas, H.R., Cleall, P.J., Chandler, N., Dixon, D., Mitchell, H.P. (2003) "Water infiltration into a large scale in-situ experiment in an underground research laboratory – physical measurements and numerical simulation." *Géotechnique*, 53(2), 207-224.

Thomas, H.R., Cleall, P.J., Dixon, D., Mitchell, H. (2009) "The coupled thermal-hydraulic-mechanical behaviour of a large scale in-situ heating experiment." *Géotechnique*, 59(4), 401-413.

Van Geet, M.m Volckaert, G., Bastiens, W., Maes, N., Weetjens, E., Sillen, X., Vallejan, B., Gens, A. (2007) "Efficiency of a borehole seal by means of pre-compacted bentonite blocks." *Physics and Chemistry of the Earth*, 32, 123-134.

Vaunat, J., A., Gens, A. (2005) "Analysis of the hydration of a bentonite seal in a deep radioactive waste repository." *Engineering Geology*, 81, 317-328.

Villar M.V., Sánchez, M., Gens, A. (2008) "Behaviour of a bentonite barrier in the laboratory: Experimental results up to 8 years and numerical simulation". *Physics and Chemistry of the Earth*, 33, S476-S485.

Zandarin, M.T., Olivella, S., Gens, A. and Alonso, E. (2010) "A 1-D thermo-hydro-mechanical model of the middle section of the Canister Retrieval Test." *Proceedings of EC-Timodaz-Theresa THMC Conference*, 29 Sept-01 Oct 2009, to be published, European Commission, 2010.

DISPOSAL SYSTEMS EVALUATION FRAMEWORK (DSEF) AND THERMAL ANALYSIS

6. Disposal Systems Evaluation Framework (DSEF) and Thermal Analysis

6.1 Introduction

The Disposal Systems Evaluation Framework (DSEF) is intended to be a flexible systematic analysis and knowledge-management framework for evaluation of disposal system options for a wide range of potential future nuclear fuel cycles and used fuel disposition alternatives. This knowledge-management framework will also serve as a valuable communication tool for the community of producers and users of knowledge. The capability to solicit feedback from users is essential; such feedback can, in turn, be used to improve the structuring of information and the manner in which it is presented. Hence, an iterative process is envisioned wherein the DSEF will evolve into a powerful, objective tool supporting decision making.

The DSEF can (1) facilitate integration of UFD campaign process and system models and data, (2) enhance the UFD campaign to interface with other FC-R&D elements, and (3) provide rapid response capability to address information requests from DOE Management or other organizations.

The development of EBS concepts and evaluation of their performance relies on many aspects of the disposal system such as site characteristics and waste form. These aspects of the disposal system can be designated as "knowledge items" that also include EBS properties, EBS performance, and site-specific data among others (Japan Nuclear Cycle Development Institute, 2005). Integration and organization of this knowledge is crucial to the examination of EBS concepts. Some of these "knowledge items" such as waste forms and related categories will be discussed in the following sections. Another important aspect of the EBS evaluation is the analysis of heat transport in the host disposal environment along with the baseline for thermal load of the EBS components and natural barriers. Section 4.4 describes the development of the Thermal Analysis Toolkit to conduct this type of analysis.

6.2 Overview of the DSEF

The DSEF will use a logical process for developing one or more disposal-system concepts (also referred to as repository system in this report) for any given waste form and geologic setting combination. The following text and subsequent sections provide a description of the planned DSEF approach within the EBS evaluation activity.

In the Features, Events, and Processes (FEPs) group of work packages, there are seven categories of waste forms and eight categories of geologic setting being studied. Each of these categories could be subdivided as studies become more detailed:

- Waste Forms:
    - Once-Through Used Fuel: This includes the following subcategories:
        - Commercial Spent Nuclear Fuel (CSNF)-nominal burnup: Uranium (U) and mixed oxide MOX).
        - CSNF-high burnup (U and MOX, >50% burnup without reprocessing, such as in some fusion-fission hybrids).

        - High Temperature Gas Reactor (HTGR) fuel - TRISO/graphite: Large volume, low volumetric heat, and burnup higher than Light Water Reactors LWRs.
        - DOE Spent Nuclear Fuel (DOE SNF): U metal from N-reactor, and carbides and oxides.
    - Borosilicate Glass: This includes the following subcategories:
        - Current borosilicate glass: Includes processing chemicals from original separations, with U/Pu removed, but minor actinides and Cs/Sr remaining.
        - Potential borosilicate glass: No minor actinides and/or no Cs/Sr; Mo may be removed to increase glass loading of radionuclides; it has a lower volumetric heat rate.
    - Glass Ceramic: This is glass-bonded sodalite from Echem processing of EBR-II, and from potential future Echem processing of oxide fuels.
    - Metal Alloy: This includes the following subcategories:
        - Metal alloy from Echem: Includes cladding as well as noble metals that did not dissolve in the Echem dissolution
        - Metal alloy from aqueous reprocessing: Includes undissolved solids and transition metal fission products.
    - Advanced Ceramic: An advanced waste form that includes iodine volatilized during chopping, which is then gettered during head-end processing of used fuels.
    - Lower Than High Level Waste (LTHLW): Includes Classes A, B, and C, as well as Greater Than Class C (GTCC).
    - Other: Examples include radionuclides removed from other waste forms (e.g., Cs/Sr, I, C), as well as new waste forms such as a salt waste form.
- Examples of Disposal-System Environments:
    - Surface storage: at reactor sites, or at off-reactor and/or centralized sites.
    - Near surface: e.g., LLW disposal sites such as trenches, shallow landfill burial.
    - Mined hard rock, Unsaturated Zone (UZ): e.g., tuff or granite
    - Mined salt
    - Mined clay or shale
    - Deep Borehole: crystalline rock.

The DSEF encompasses several decision-support analysis categories (note that the framework can provide links to the corresponding analysis toolkits):

- High-level simulator of waste-isolation performance of the disposal system. This is not a Total System Performance Assessment (TSPA), which will be developed separately. This tool looks at waste hazard durations, regulatory requirements, and existing performance assessments to give a very high-level rough estimate of performance

- Sorter of disposal-system attributes (pros and cons). It is anticipated that the DSEF will be exercised for multiple disposal-system concepts for many of the combinations of waste forms and disposal-system environments listed above. Thus, a compilation of pros and cons for each situation will aid in grouping and contrasting various options.
- High-level estimator of disposal-system cost. This will use high-level estimating tools benchmarked to existing detailed cost estimates or actual costs.
- High-level thermal-analysis toolkit to assess geometric requirements (footprint, drift and waste-package spacing) for the disposal system, based on specified thermal criteria (e.g., limits on peak temperatures of engineered components and the near-field). Once a geologic setting and waste form are selected for evaluation, thermal analysis is key to defining potential disposal-system layouts (single level, multi-level, in-drift, horizontal borehole, vertical borehole, deep borehole from the surface, etc.) and EBS concepts (capillary barrier, clay barrier, etc.). Early attention will be focused on the thermal tools.
- High-level assessment of overall system impacts of a disposal concept. The disposal system is one component of the overall fuel cycle. As such, it must interface with other components that may influence the disposal-system design requirements. One goal of the DSEF is to integrate with higher-level systems analysis tools being used and developed in the FC-R&D arena (see below).

The DSEF will also establish a UFD campaign knowledge management system to organize high-level information, data, and assumptions, thereby facilitating consistency in high-level system simulation and economic analyses. This system will likely be housed with the INL-based documentation system. Attention will be given to lessons learned from the systems used at the Waste Isolation Pilot Plant (WIPP) and the Yucca Mountain Project (YMP). Where reference material from other programs (e.g., international) is used or cited, the knowledge-management system will import the reference material directly or refer to it in bibliography form. Alternative data sets (e.g., from other programs) will also be utilized to evaluate their influence on DSEF analyses for given waste form and disposal-system combinations. The knowledge-management system can also be used to maintain the results of DSEF realizations, enabling the comparison and ranking of various waste-form/disposal-system-environment/disposal-system-design options. Finally, the UFDC knowledge-management system will be able to provide a compendium of "templates" that can be utilized, in a labor-efficient fashion, to build parallel DSEF analyses (e.g., "one offs").

The DSEF is being implemented in two parts. One part is a Microsoft Excel workbook with multiple sheets. This workbook is designed to be logical and user friendly, such that anyone within the UFD campaign can use it as a guide to develop repository conceptual designs, and disposal-system design that respect thermal, geometric, and other constraints. The other part is a Microsoft Access relational database file that will be centrally maintained to document the ensemble of conceptual designs developed with individual implementations of the Excel workbook.

The DSEF Excel workbook includes sheets for waste form, environment, geometric constraints, engineered barrier system (EBS) design, thermal, performance assessment (PA), materials, cost, and fuel cycle system impacts. Each of these sheets will guide the

user through the process of developing internally consistent design options, and documenting the thought process. The sheets will interact with each other to transfer information and identify inconsistencies to the user. In some cases, the sheets will be stand-alone, and in other cases (such as PA), the sheets will refer the user to another tool, with the user being responsible to transfer summary results into the DSEF sheet. Finally, the DSEF includes three top-level sheets: inputs & results, interface parameters, and knowledge management (i.e. references to reports, models, and publications such as the degradation mode surveys discussed below). These sheets will enable the user to see the overall picture on only a few summary sheets, but develop the design option systematically using the detailed sheets.

The DSEF Access relational database file will collect the key inputs, results, and interface parameters from each Excel workbook implementation. The power of a relational database will then be available to sort and organize groups of designs, and to answer queries about what evaluations have been done in the UFD campaign.

As an initial step in identifying candidate engineered-materials for this range of waste forms and environments, LLNL is reviewing the material science literature. A logical place to start is the degradation mode surveys historically performed for the unsaturated tuff environment of Yucca Mountain.

In later stages, it will utilize software developed in the field of knowledge engineering and knowledge-management systems (Umeki et al. 2009). At certain points in the logical process, the DSEF software will point the evaluator to other software tools to do analyses needed to move the process forward. In the development of the DSEF, we will be mindful to make it no more complex than necessary to evaluate the system being considered. The DSEF will organize and document the work such that multiple realizations for different combinations can be compared and contrasted.

6.2.1 Waste Form

The DSEF team will develop a catalog of potential waste forms, and will assemble information about waste form and waste package combinations. Waste form parameters include heat/volume ratio, heat/mass ratio, and waste density, as well as the mass and half-lives of the radionuclides in the waste. ANL and LLNL will jointly assemble the information.

This information will interface with the Systems Analysis Campaign “VISION” model of nuclear fuel cycles and material flows, the Separations and Waste Forms Campaign waste stream and waste form descriptions, as well as the Waste Form, EBS, Natural Systems and FEPS work packages in the UFD campaign.

6.2.2 Geologic Setting

The DSEF team will determine geologic parameters (such as thermal conductivity) for the disposal-system setting that are needed to calculate thermal performance. These parameters will be used to determine (see Appendix A) whether a disposal-system concept provides sufficient heat removal to respect temperature limits of the waste form, EBS components, and near-field. The DSEF team will assemble other geologic parameters for each disposal-system setting, which are needed for a rough estimate of disposal-system performance. These parameters include porosity, permeability, and rock composition.

6.2.3 Disposal-System Concept and the EBS

A number of options for disposal-system concept will be considered, including surface storage (prior to disposal, or in some cases, until a short-lived waste form has decayed), near-surface burial (for low hazard, short-lived waste), single or multi-level geologic mined systems, and deep boreholes. EBS emplacement options include large waste packages in drifts, horizontal or vertical borehole emplacement from drifts, and deep boreholes. The barrier options in the EBS include the waste form, cladding, barriers internal to the waste package, the waste package itself, capillary barriers, drip shields, backfill, buffer materials, sorptive materials, and seals above deep boreholes. Further, the size of the waste package (capacity) and the spacing (between waste packages and between drifts or deep boreholes) are a key factor to meeting thermal limits.

The combination of waste form parameters and geologic setting parameters will be used to compile a set of disposal-system design options for that waste form and geologic setting combination. Each option of the set will be treated as a separate realization of the DSEF.

LLNL will develop a thermal-analysis toolkit to perform this evaluation, in a labor- and computationally-efficient fashion, for various geologic media, during FY10 and will refine and apply the tool in FY11. Options that will be evaluated include a simplification of the YMP multiscale model (discretized), the YMP waste emplacement flexibility model (uses analytic solutions to simplified geometries), and the model developed by ANL for GNEP and AFCI. LLNL and Ted Bauer of ANL will develop the thermal toolkit. Initial thoughts on the thermal toolkit are included as Appendix A, below.

The results of the thermal analysis will determine the required disposal-system (e.g., repository) footprint for that waste form (type and quantity) and geologic setting. In turn, the disposal-system footprint and design provide much of the information needed for a high-level cost estimate. LLNL, ANL, and SNL will develop the concepts.

A catalog of candidate materials for the engineered barriers will be developed by LLNL. Metals will be evaluated based on an extension of the LLNL Degradation Mode Surveys developed for Yucca Mountain. Other barrier materials (clay, backfill, etc.) will initially use information developed in other repository programs worldwide.

6.2.4 Cost and Performance

Costs of WIPP and cost estimates of YMP will be used to envelop a high-level cost estimate for the barriers and for disposal-system construction, for each option evaluated. LLNL and SNL will develop the cost-estimation component of the DSEF.

An initial selection of included FEPs will be determined from the UFD FEP work package list. The FEP list will be the basis of a preliminary high-level model to be developed jointly by ANL and LLNL. This model will be an extension of models developed by ANL for GNEP, ASCI, and other FC-R&D programs during the last several years. The model will consider natural and human-caused initiating events appropriate for the geologic setting. The FEPs will be selected by LLNL, SNL, and ANL.

The DSEF team will identify the key impacts of the disposal-system concept on the pre-disposal waste management system, using tools developed by the Systems Analysis Campaign. LLNL will study the uncertainty quantification tools from the following

programs: Stockpile Stewardship, NIF, Climate, ASCEM, etc. for their applicability to the DSEF. This will be accomplished by the middle of FY11.

6.2.5 Siting Criteria

The result of the above steps will be a preliminary set of siting criteria for this geologic setting, waste form, and disposal-system concept. These can be used to iterate through the process with more specific geologic setting information based on generic application of the siting criteria. Here, we define generic as distinguishing between major categories of the same medium, without specifying any particular geographic location.

For a generic disposal-system setting, the ensemble of DSEF evaluations will identify the envelope of waste-form options that could be potentially accommodated. Equally important, the evaluations will identify the envelope of waste-form options that could not be potentially accommodated, by the combination of geologic setting, and disposal-system concept.

6.2.6 Metrics

Metrics to be considered during the thought process include cost, performance, and licensability. Pre-disposal system impacts will include:

- Flexibility with respect to future changes in waste streams.
- Range of potential waste forms that could use the disposal-system concept, and geologic setting, evaluated for a single waste form.

6.3 Interface Between DSEF and Fuel Cycle Systems Models

In addition to providing a framework to organize and integrate disposal-system information within the UFDC, the DSEF should also provide a working interface with other parts of the program, and with the rest of the nuclear energy production system. A primary interface is with the Systems Analysis models for static and dynamic nuclear energy systems (VISION, SLAM, and the hierarchy of model that support them). These models gather mass flow and waste stream information from other elements of the nuclear fuel cycle (fuel fabrication, reactors, separations and waste forms, etc.) for any given nuclear energy system scenario. This provides an avenue for DSEF to receive comprehensive and internally consistent waste stream information for a given nuclear energy scenario. DSEF can then provide feedback to the system and economics models on disposal implications such as storage requirements, disposal alternatives and disposal-system (e.g., repository) size and performance parameters. With a working lineage to the broader system models, DSEF will provide a functional ‘back end’ capability to evaluate the wide range of disposition alternatives currently under consideration.

DSEF will replace the constrained “YM-like” repository parametric analysis that has been a useful working model for disposal impacts in prior FC-R&D systems analyses. With the broad range of fuel cycle options, and wide variety of disposal pathways alternatives, a simple parametric model is no longer adequate.

A starting list of potential exchange parameters between DSEF and VISION/SLAM include:

Inputs from Systems to DSEF:

- Waste stream partitions (and alternatives) and normalized mass flows
- Radionuclide content
- Waste forms, characteristics, and alternatives
- Timing relationships

Feedback from DSEF to Systems:

- Waste categorization and potential disposition pathways
- Storage requirements/characteristics
- Disposal alternatives
- Disposal-system characteristics: footprint, drift length, package count,
- Isolation performance factors

A conceptual mapping of DSEF onto the evolving Systems Model hierarchy is shown in Figure 7.3-1. Details of the interface will develop as both DSEF and SLAM evolve.

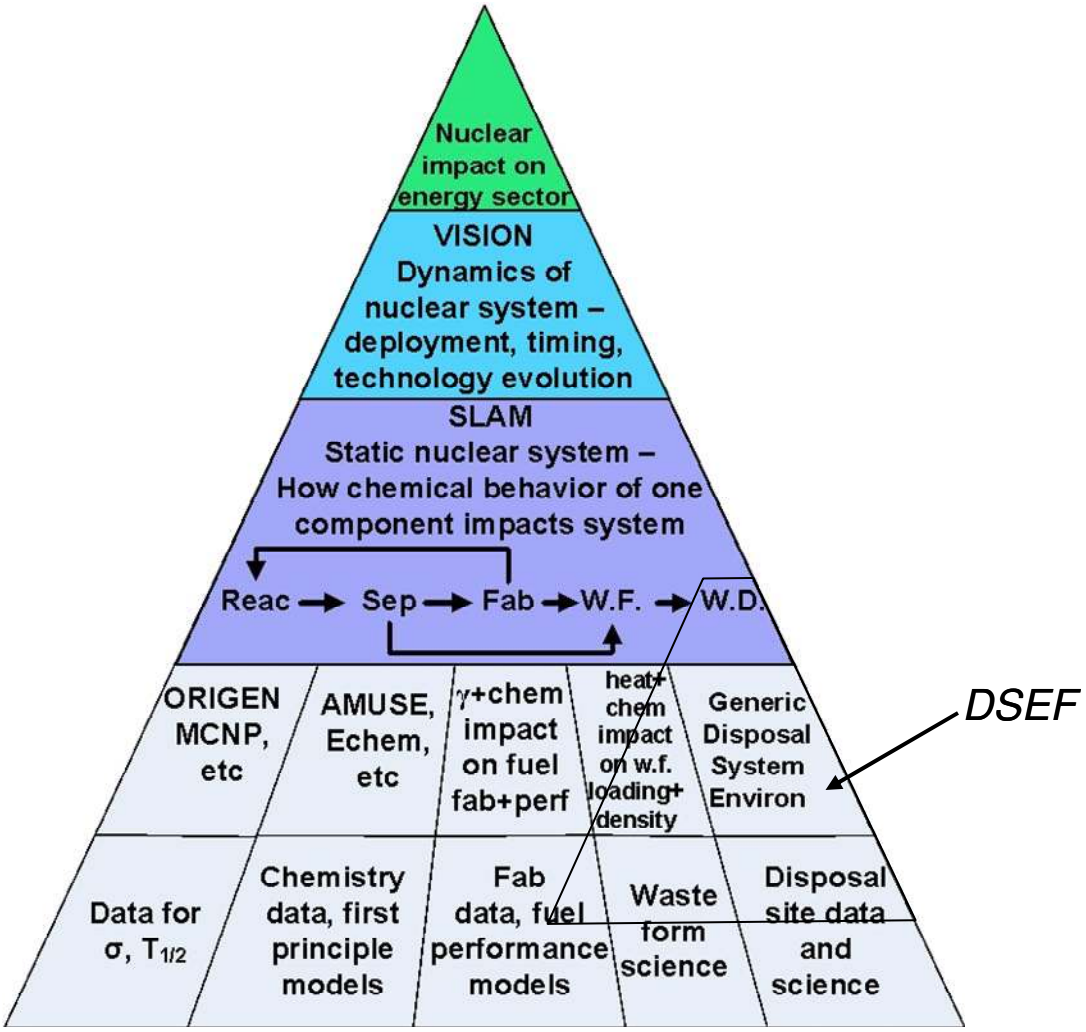

Figure 7.3-1. The Systems Model hierarchy and data interface with the DSEF.

6.4 Thermal Analysis Toolkit

A key aspect of evaluating potential used-fuel-disposition (UFD) alternatives is determining space requirements for the engineered barrier system (EBS). While much of the application of this tool will be for geologic disposal systems, it is also intended to address a broader range of disposal-system concepts, such as shallow burial systems and surface-storage facilities. The primary physical constraint in determining the space requirement for a given quantity and type of used fuel is heat dissipation in the host environment, in conjunction with the thermal criteria of the EBS components and natural barriers. Typically, thermal criteria are expressed as temperature limits; however, they may also include temporal and spatial temperature gradients, if those gradients can be steep enough to lead to phenomena detrimental to barrier performance. Heat dissipation primarily depends on the heat source (time dependent, for the used fuel per unit mass or volume), the geometry of the EBS, and the thermal conductivity of the EBS components (e.g., backfill) and host rock. EBS geometry covers a wide range of possibilities, from the simplest geometries, such as the diameter and spacing of deep disposal boreholes, to very complex geometries, such as level spacing; drift diameter, length, and spacing;

borehole diameter, length, and spacing; and waste-package diameter and length. If thermal criteria are achieved with margin for a UFD/EBS alternative, it is possible to decrease spacing between the relevant EBS components (e.g., boreholes, emplacement drifts, emplacement boreholes, etc.), which increases the areal density of the used fuel, and is equivalent to reducing the disposal-system space requirements.

The Thermal Analysis Toolkit is designed to be a flexible, computationally- and labor-efficient software package to conduct thermal analyses for a wide range of potential UFD/EBS alternatives. In its initial stage of development, one option for this toolkit is to use the thermal-conduction version of the NUFT code (Nitao, 1998), a catalog of EBS concepts, a catalog of thermal properties for the engineered and natural barriers, and a catalog of heat-generation histories for UFD alternatives. Another option is to use analytical solution approaches developed in the YMP and elsewhere. Protocols will be established for the importing and reviewing of thermal property and UFD heat-generation-history data. Users will be given the option of specifying their own thermal-property and heat-generation-history input data; however, the preferred approach is to utilize data that has a confirmed pedigree. Within the available range of EBS concepts, the user will be able to specify EBS geometric parameters, such as drift diameter and spacing (both vertical and horizontal), borehole diameter and spacing, etc. Users will initially be given the option of developing additional EBS concepts by utilizing an existing template from the EBS-concept catalog and making revisions specific to the new EBS concept. In a later stage of development, a more flexible mesh-generation capability may be available to facilitate generating new EBS concepts.

The first generation version of the Thermal Analysis Tool will apply the conservative assumption that heat flow in the EBS is dominated by thermal conduction. For geologic disposal, this assumption is reasonably conservative, since convection tends to dissipate temperature buildup, and thermal radiation tends to smooth out variations in the EBS between hotter and cooler regions. The first generation version will focus on geologic disposal. For surface-storage and near-surface burial facilities, it will be necessary to address atmospheric convection, using appropriately selected values of the heat-transfer coefficient, as well as a reasonable means to represent thermal radiation. The first generation version will also assume lateral and longitudinal symmetry, which is to say that lateral and longitudinal heat loss at the edges of the disposal system (e.g., repository edges) is negligible. Thus, this tool will be applicable to the center of the disposal system where temperatures and temperature gradients are highest. The benefit of assuming lateral and longitudinal symmetry is that the 3-D model of the disposal system can be of a representative region, which is infinitely repeated in the plan view.

If necessary, future generations of the Thermal Analysis Tool could address the influence of thermal convection in a fashion similar to that applied in the Multiscale Thermohydrologic Model (Buscheck et al. 2006). Application of the Multiscale Thermohydrologic Model methodology also allows for relaxing the assumption about lateral and longitudinal symmetry.

The NUFT option for the first generation version of the Thermal Analysis Toolkit will consist of three software modules:

1. **Thermal-Analysis Pre-Processor**: This script (possibly written in MATLAB) reads in (1) the user-selected EBS concept from the EBS-Concept catalog, (2) the user-specified geometric parameters for the EBS concept of interest, and (3) the user-selected

thermal properties from the Thermal-Property catalog or user-specified thermal properties, and generates the input file for the thermal-analysis simulator (e.g., NUFT code, SINDA/G).

2. **Thermal-Analysis Simulator**: Utilizing the thermal-conduction version of the NUFT code and an input file generated by the thermal-analysis pre-processor, this simulator generates temperature output wherever thermal criteria are specified (e.g., waste-package surface).

3. **Thermal-Analysis Post-Processor**: Applying user-specified thermal criteria, this processor determines whether (or when and where) thermal criteria are exceeded. It can also report by how much margin thermal criteria are met for a UFD/EBS-concept combination, which is useful in developing more space-efficient dimensions for that UFD/EBS-concept combination.

6.5 Review of Degradation Mode Surveys

These degradation mode surveys were documented (e.g. Farmer et al., 1988a,b, Gdowski et al., 1988a,b and Bullen et al., 1988) for waste package candidate materials to be used at Yucca Mountain, including three austenitic alloys (304L, 316L and Alloy 825) and three copper alloys (CDA 102, CDA 613 and CDA 715) used in the nuclear industry and marine environments, respectively. The work contains information on phase stability, environmental effects of a repository, general corrosion, localized corrosion, stress corrosion cracking, hydride cracking, microbially-influenced corrosion and internal corrosion of candidate high-level radioactive waste (HLRW) package materials. Key features described in the degradation mode surveys are summarized below.

Elevated chromium, copper and nickel in steels typically yield superior corrosion resistance. The formation of a 1–5 nm Cr_2O_7 layer on the surface of candidate austenitic alloys provides good protection from general corrosion and oxidation.

Table 1. Approximate general corrosion rates, μm/year (Gdowski et al., 1988a).

Environment / Alloy	304	316	825	CDA102	CDA613	CDA715
Atmospheric/Marine	<0.15	<0.01	<0.15	<1	<1	<1
Aqueous/Seawater	25			30	5	11
Hot Water (50, 80, 100°C)	<0.3	<0.3	<0.3			
Steam (100, 150°C)	<0.1	<0.1	<0.1			
Superheated Steam (566, 631°C)	7					
Water vapor (95°C) with gamma irradiation				4	2	6

Gamma irradiation of liquid films on candidate waste package material produces several oxidizing and reducing species by radiolysis that may increase intergranular stress

corrosion cracking (IGSCC) in some sensitized alloys. It is assumed that nuclear waste package contents will not generate significant neutron flux.

Radiolysis of moist air and surface films causes hydrogen generation. Hydrogen has the potential to alter the metallurgical behavior of the container material, and it is important to examine the hydrogen diffusivity and solubility in such materials. For example, hydrogen solubility in 304 stainless steel (SS) ranges from ~100 – 300 ppm (at 25 – 275^{o}C). Low concentrations of hydrogen (~30 appm) have been shown to degrade primarily the ductility of the material hence making alloys more brittle.

Hydrogen embrittlement (HE) susceptibility appears to be related to the austenite-to-martensite transformation, with martensite being more susceptible to HE. No consensus is reported on the HE mechanism in austenitic steels. Furthermore, Gdowski and Bullen (1988b) states that there is a definite lack of literature on the effects of hydrogen in Alloy 825. Alloys with low carbon content (<0.03% such as 304L, 316L and <0.05% such as Alloy 825) have enhanced resistance to sensitization (which may translate into higher HE resistance) versus their higher carbon equivalent alloys (e.g. 304 and 316). However, literature suggests (Gdowski et al. 1988b) HE *does* occur in 304L, 316L and Alloy 825. More recent Yucca Mountain-related work on HE will be reviewed in a subsequent UFD-EBS milestone.

Pitting resistance is typically higher in Alloy 825 than 304 or 316 steels, largely due to the increased Mo content in the alloy. Localized corrosion decreases with larger molybdenum additions.

The presence of certain microbial colonies on the surface of the waste package can lead to pitting corrosion. Reducing bacteria form hydrogen compounds (such as hydrogen sulfide), while oxidizing bacteria can in some cases oxidize elements of steel (such as iron), causing rust. Microenvironments can persist between the microbial colony and the material surface, preventing repassivation, concentrating pH effects, or accelerating hydrogen corrosion effects. MIC has been observed in 304L and 316L, but no catastrophic MIC was observed in Alloy 825.

Stress corrosion cracking (SCC) appears under a very specific combination of conditions, namely material susceptibility, tensile stress and aggressive environment. SCC of 304L and 316L U-bend samples has been observed in high chloride environments at elevated temperature. Resistance to SCC is largely due to higher nickel additions.

Welds can also affect the properties and behavior of the materials. For austenitic steels, problems include weld-induced sensitization, hot cracking, sigma-phase formation, and corrosion of the weld filler metal. Of concern are resistance to corrosion, hot cracking and formation of intermetallic phases. Heat affected zones (HAZ) of welds can be affected by the precipitation of $Cr_{23}C_6$. Both 304L and 316L have low carbon content, minimizing the formation of the carbide, while 825 contains titanium which preferentially forms carbides. When the compositions of 304L and 316L are adjusted to include 5% ferrite structure, impurities in the alloy are attracted to the ferrite and segregated from the grain boundary, thus preventing grain boundary cracking. Additionally, during the welding of 304L and 316L, a brittle sigma-phase can form. In Alloy 825, ferrite inclusion is not possible, so Alloy 625 is used as a weld-filler. The use of a different material for weld-filler can lead to the formation of a duplex microstructure containing

both austenite (gamma-phase) and ferrite (alpha-phase). Literature on weld cracking of Alloy 825 is very limited.

During heat treatments such as welding (550 – 800°C), Cr-rich carbides precipitate along grain boundaries, causing Cr-depletion in the surrounding area to a level below the 13 – 15% required for passivation. Lower temperature sensitization (LTS, ~400°C) observed over longer periods of time could also be problematic, possibly for 304L and 316L, although high-nickel alloys may not be subject to LTS. However, there was no experimental evidence of a reduction in corrosion resistance due to LTS at the time of the degradation mode surveys of Farmer et al. (1988a).

After the degradation mode surveys were completed, the Yucca Mountain Program favored more corrosion-resistant alloys (i.e. progressing from Alloy 825 to 625 and then to Alloy 22, C-22). A literature search of Ni-Cr-Mo alloy degradation has been performed. The results are currently being reviewed and will be reported in a subsequent UFD-EBS milestone.

Additionally, a review of phase stability in Ni-Cr-Mo alloys, particularly relating to modeling using Calphad methodology (Turchi et al., 2006) showed evidence of fcc matrix, long range order (LRO, Pt_2Mo-type) formation of the oP6 phase, Frank-Kasper phases (P and σ), carbides and silicides. The work also showed that the low Cr content excluded the formation of the sigma phase in alloy C-4. Similarly, the low Cr and Mo content in alloy C-276 significantly reduced the formation of the sigma phase and prevented the formation of the oP6 phase.

Understanding the kinetics of phase transformations is also important. Experimental work (Torres, 2003) provides evidence of phase transformations in Alloy 22, and concludes that in reality such phase transformations occur at a slower rate than predicted. The work by Turchi et al. (2007) suggests that the Ni_2Cr-type LRO transformation in Alloy 22 is slow enough such that it is not a concern for repository conditions (<200°C for 100,000 years).

The above material summarizes a lengthier summary of these references; that summary is included as appendices A through C. Work continues on library literature searches for the period between the degradation mode survey work by Farmer et al (1988a,b) and Gdowski et al. (1988a,b) and present, as well as a review of the international literature for the range of geologic environments that have been investigated. Full references are given in the appendix sections, following.

Appendix A – Includes reviews of the degradation mode surveys plus additional information regarding phase transformation and kinetics.

Appendix B – Contains definitions of waste characteristics and waste environment.

Appendix C – Contains mechanical properties of several austenitic steels at room temperature.

6.6 References

Angel, T. "Formation of Martensite in Austenitic Stainless Steels: Effects of Deformation, Temperature, and Composition', J. of the Iron and Steel Institute 177, 165. (1954)

Asphahani, A. I. and Uhlig, H.H. "Stress Corrosion Cracking of 4140 High Strength Steel in Aqueous Solutions", Journal of the Electrochemical Society 122(2), 174. (1975)

Asphahani, A. I. "Localized Corrosion of High Performance Alloys", Materials Performance 19, 8, 9-21. (August 1980)

Bain, E. C., Abron, R. H., Rutherford, J. J. B. "The Nature and Prevention of Intergranular Corrosion in Austenitic Stainless Steels", Trans. Amer. Soc. for Steel Treating 21, 481. (1933)

Briant, C. L. "Hydrogen assisted cracking of austenitic SS", Hydrogen Effects in Metals, Eds. I. M. Bernstein, A. W. Thompson, The Metallurgical Society AIME, 527. (1981)

Bullen, D. B., Gdowski, G. E., "Phase Stability – Vol. 1", UCID-21362 Vol. 1. (August 1988)

Bullen, D. B. and Gdowski, G. E. "Survey of Degradation Modes of Candidate Materials for High-Level Radioactive-Waste Disposal Containers, Volume 1 – Phase Stability", LLNL-UCID-21362-Vol.1 (1988)

Buscheck, T.A., Y. Sun, and Y. Hao. "Multiscale Thermohydrologic Model Supporting the License Application for the Yucca Mountain Repository," American Nuclear Society, La Grange Park, IL, Proceedings 2006 International High-Level Radioactive Waste Management Conference. (April 30 – May 4, 2006)

Copson, H. R. "Physical Metallurgy of Stress Corrosion Fracture", Interscience, 247. (1959)

DeLong, W. T. "A Modified Phase Diagram of Stainless Steel Weld Metals", Metal Progress 77 (2), 98-100. (1960)

Japan Nuclear Cycle Development Institute 2005, "H17: Development and management of the technical knowledge base for the geological disposal of HLW, Knowledge Management Report", September, 100 pp. (2005)

Farmer, J. C., McCright, R. D., Kass, J. N. "Survey of Degradation Modes of candidate Materials for High-Level Radioactive-Waste Disposal Containers- Vol. 3 Overview", UCID-21362 Overview. (June 1988a)

Farmer, J. C., Van Konynenburg, R. A., McCright, R. D., Bullen, D. B. "Survey of Degradation Modes of candidate Materials for High-Level Radioactive-Waste Disposal Containers- Vol. 3 Localized Corrosion and Stress Corrosion Cracking of Austenitic Alloys", UCID-21362 Vol. 3. (April 1988b)

Furuya, T., Fukuzuka, T., Fujiwara, K., Tomari, H. "Gamma-Ray Irradiation Effects on Stress Corrosion Cracking of Alloys for a High Level Liquid Waste Package", R-D Kobe Sielosho Gijutsu Hokoku, Vol. 33, No. 1, pp. 43-46. (January 1983)

Gdowski, G. E., Bullen, D. B. “Oxidation and Corrosion – Vol.2”, UCID-21362 Vol. 2. (1988a)

Gdowski, G. E., Bullen, D. B. "Effects of Hydrogen in Austenitic and Copper-Based Alloys – Vol. 6", UCID-21362 Vol. 2. (August 1988b)

Gdowski, G. E. “Survey of Degradation Modes of Four Nickel-Chromium-Molybdenum Alloys”, UCRL-ID-108330. (March 1991)

Graver, D. L. "Hydrogen Permeation and Embrittlement of Some Nickel Alloys", Corrosion of Nickel-Based Alloys, American Society for Metals, Metals Park, Ohio, 79-85. (1984)

Holzworth, M. L. "Hydrogen Embrittlement of Type 304L SS", Corrosion 25, No. 3, 107. (1969)

Karmazin, L., Krejc´I, J., Zeman, J. “Gamma-Phase and Ni2Cr-Type Long-Range Order in Ni-Rich Ni-Cr-Mo Alloys”, Mater. Sci. Eng. A183, 103-109. (1994)

Marshall, P. Austenitic Stainless Steels, Elsevier Publishers, London (1984)

Nitao, J. J. “Reference Manual for the NUFT Flow and Transport Code, Version 2.0”, UCRL-MA-130651. Lawrence Livermore National Laboratory, Livermore, CA. (1998)

Perng, T. P., Altstetter, C. J. “Effects of Deformation on Hydrogen Permeation in Austenitic Stainless Steels”, Acta Mat. 34, 1771. (1986)

Pope, D. H. “Microbiologically influenced corrosion in the nuclear power industry: Case histories, Methods of detection, control and prevention”, Proceedings of the 3rd Int. Symp. On Environmental Degradation of Materials in Nuclear Power Systems – Water Reactors, Traverse City, Michigan, August 30 to September 1987, The Metallurgical Society. (1988)

Povich, M. J. “Low Temperature Sensitization of Type 304 SS”, Corrosion 34, No.2, 60. (1978)

Scarberry, R. C. Hibner, E. L., Crum, J. R. (1979) “Assessment of Pitting-Potential Measurements in Severely Corrosive Environments”, Paper Number 245, Corrosion 79, Atlanta, Georgia, March 12-16, National Association of Corrosion Engineers, Katy, Texas.

Shen, T. H. “X-ray Microanalysis of Precipitates in Alloy C-22”, LLNL Technical Memorandum, March 20, 2000 (unpublished).

Strum, M. J., Weiss, H., Farmer, J. C., Bullen, D. B. “Survey of Degradation Modes of candidate Materials for High-Level Radioactive-Waste Disposal Containers- Vol. 7 Weldability of Austenitic Alloys”, UCID-21362 Vol. 7. (June 1988)

Torres, S.; LLNL private communication (April 2003).

Turchi, P. E. A. Kaufman, L., Liu, Z-K, “Modeling of Ni-Cr-Mo Based Alloys: Part I - Phase Stability”, Computer Coupling of Phase Diagrams and Thermochemistry 30 (2006) 70.

Turchi, P. E. A. Kaufman, L., Liu, Z-K. “Modeling of Ni-Cr-Mo Based Alloys: Part II – Kinetics”, Computer Coupling of Phase Diagrams and Thermochemistry 31, 237. (2007)

Umeki, H., K. Hioki, H. Takase, and I. G. McKinley, "Overview of the JAEA KMS (Knowledge Management System) Supporting Implementation and Regulation of Geological Disposal in Japan", Proc. ICEM'09: 12th International Conference on Environmental and Radioactive Waste Management, October 11-15, Liverpool, UK, ICEM2009-16354. (2009)

Weiner, L. C. "Kinetics and Mechanism of Hydrogen Attack of Steel", Corrosion 17, No.3, 137. (1961)

6.7 Appendix A

One task of the Yucca Mountain Site Characterization Project (YMP) was to select a material from which to fabricate high-level radioactive-waste (HLRW) containers for the potential repository. In this appendix, we briefly summarize the results of a survey study performed in 1988 (Farmer et al., 1988a) for candidate materials considered for the conceptual design (CD) of the HLRW containers of the YMP Site Characterization Plan (SCP).

In 1988 the review was conducted on YMP SCP degradation due to

- General Corrosion of Waste Packages
- Microbially Influenced Corrosion (MIC) of Waste Packages
- Stress Corrosion Cracking (SCC) of Waste Packages
- Localized Corrosion of Waste Packages
- Corrosion in Welds
- Hydride Cracking of Waste Packages
- Internal Corrosion of Waste Packages Prior to Breach

All these degradation mechanisms except microbiological corrosion were included in the survey study.

Waste Repository Requirements

Containers must maintain mechanical integrity for 50 years, and complete containment of the waste for 300 to 1000 years. Heat generation leads to container peak temperature of ~250^{o}C, decaying to 150^{o}C after 100 years.

Candidate Materials

Three austenitic alloys (304 L, 316 L and Alloy 825) and three copper alloys (CDA 102, CDA613 and CDA715) were selected in the 1988 survey (Farmer et al., 1988a), see Table A1a and Table A1b, respectively. The 3 austenitic alloys are used in the nuclear industry. The three copper alloys are used in marine environments.

Table A1a: Chemical composition of austenitic candidate alloys (Farmer et al., 1988a).

Element	304L	316L	Alloy 825
C	0.03 max	0.03 max	0.05 max
Mn	2.00 max	2.00 max	1.0 max
Si	1.00 max	1.00 max	0.5 max
Cr	18.0 - 20.0	16.0 - 18.0	19.5 - 23.5
Ni	8.0 - 12.0	10.0 - 14.0	38.0 – 46.0
P	0.045 max	0.045 max	-
S	0.03 max	0.03 max	0.03 max
Cu	-	-	1.5 – 3.0
Ti	-	-	0.6 – 1.2
N	0.10	0.10	-
Mo	-	2.0 – 3.0	3.0
Fe	Bal.	Bal.	Bal.

Table A1b: Chemical composition of Cu-based candidate alloys (Farmer et al., 1988a).

Alloy	Cu	Ni	Al	Mn	Sn	Fe	Zn	Other
CDA102	99.95	-	-	-	-	-	<0.001	Pb<0.001 Cd<0.001 S<0.0018 Hg<0.0001 P<0.003
CDA613	90.82	0.05	6.75	0.16	0.20	2.46	0.01	Pb<0.01 Co<0.01
CDA715	69.18	29.60	-	0.51	-	0.53	0.07	Pb 0.01 P 0.002 C 0.04 S 0.01

Note the presence of high Cr content in the austenitic candidate alloys. At least 12% (w/w) Cr is necessary for the formation of a protective Cr-oxide film. Control of the C content reduces the precipitation of Cr-rich $M_{23}C_6$ carbides at the grain boundary (GB), namely the "sensitization" of the material. Addition of Ti eliminates this problem in Alloy 825. In other words, the addition of Ti stabilizes Alloy 825 against sensitization (see next section). Also, note the addition of Mo in 316L SS and Alloy 825 for pitting resistance in aqueous corrosion applications. The presence of Cu in Alloy 825 grants resistance to sulfuric acid.

Oxidation and Corrosion

General corrosion and oxidation is reviewed in (Gdowski and Bullen, 1988a). The authors conclude that the formation of thin uniform Cr-oxide (Cr_2O_7) layers (10-50 Å thick) on the surface provides the exceptional resistance of the candidate austenitic alloys to general corrosion and oxidation.

- Atmospheric corrosion rates of 304 (similar to 304L) and Alloy 825 in marine atmospheres are low (below ~0.15 μm/y) with 316 (similar to 316L) ranked as the best material with atmospheric corrosion rate in marine atmosphere below ~0.01 μm/y.
- Aqueous corrosion rate of 304 in seawater (Panama Canal) is large (~25 μm/y), ~7 μm/y in superheated steam (566 and 621°C); this might limit the container lifetime in such environments.
- The austenitic candidate alloys will be resistant to general corrosion and oxidation in hot water and steam. Aqueous corrosion rates of 304L, 316L and Alloy 825 are all below ~0.3 μm/y in hot water (50, 80, 100°C) and below ~0.1 μm/y in steam (100 and 150°C).

Similar analysis is performed (Gdowski and Bullen, 1988a) for Cu-based alloys. CDA 613 shows the best corrosion resistance to general corrosion and oxidation. The authors note that atmospheric and aqueous corrosion are the least significant modes of degradation; i.e. other corrosion mechanisms are expected to be life limiting (see next section).

- Atmospheric corrosion rates of CDA 102, CDA 613 and CDA 715 in marine atmosphere are below ~1 μm/y
- Aqueous corrosion rates of CDA 102 and CDA 715 in seawater immersion are large (~30 μm/y and ~11 μm/y). CDA 613 is the best (corrosion rate ~5 μm/y).
- General corrosion rates of CDA 102 and CDA 715 under gamma irradiation in air nearly saturated with water vapor (moist air) at 95°C are large (~4 and 6 μm/y, respectively). Again CDA 613 is the best (corrosion rate ~2 μm/y).

Environmental Effects in the Repository

Nuclear waste containers will be exposed to high gamma radiation. It is assumed that the container surface might be covered by a thin liquid (water) layer, which is irradiated by γ-photons from the decay of radionuclides in the waste. Section 7 of the degradation mode survey (Farmer et al., 1988b Vol.3) gives a summary on the effect of γ radiation on stress corrosion cracking of sensitized 304 SS and Alloy 825. In general, γ irradiation of aqueous solutions produces several oxidizing and reducing species by radiolysis. Irradiation of liquid water by γ rays produces, ionic, free radicals and molecular products that are very chemically reactive, i.e. radical products (H^+, OH^-,e^-_{aq},, HO_2) and molecular products H_2O_2, and H_2. The literature survey shows that γ radiation increases the intergranular stress corrosion cracking (IGSCC) susceptibility of sensitized 304 SS in high temperature oxygenated pure water. Experiments performed by Furuya et al. (Furuya et al, 1985) in boiling deionized water (100°C) show that γ irradiation (γ flux ~1.1 x 107 R/h) promotes IGSCC in sensitized 304 SS, see Fig. A1. He also reports that Alloy 825 exhibited no SCC with or without γ irradiation. From the work of Furuya et al. (1985) we conclude that Alloy 825 shows no change in its resistance to SCC in the presence of γ irradiation. Note that the conclusions are still open for 304 SS since the

literature survey shows contradictory results for sensitized 304 SS; i.e. other authors found a beneficial effect of γ irradiation on 304 SS.

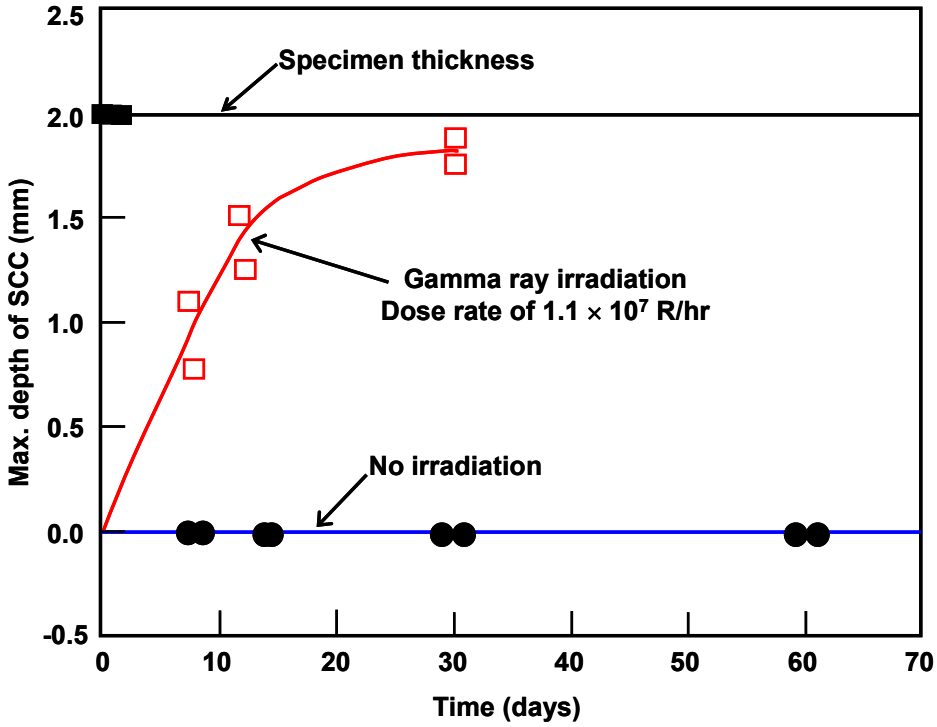

Figure A1: γ irradiation promotes an increase in the IGSCC susceptibility of sensitized 304 SS (after Furuya et al., 1985; see also Farmer et al., 1988b).

The effect of fast (E > 1 MeV) neutron irradiation followed by high gamma irradiation on SCC of 304 SS has been studied by several authors but is not reported here since it is assumed that nuclear-waste containers will not be subjected to significant neutron flux.

Biological Corrosion (MIC) of Candidate Materials

Biological corrosion cannot be ruled out, even in the unfavorable environment near the waste package that includes high temperature, high γ-dose, and dryness. The bacteria *Gallionella* and *Sphaerotilis* most commonly cause MIC in SS. MIC has been found in 304L and 316L SS (Pope, 1987); especially on welds. No catastrophic MIC has been reported for Alloy 825.

Stress Corrosion Cracking (SCC)

SCC is a type of localized corrosion characterized by fine cracks, which can propagate quite rapidly leading to failure of the component and potentially the associated structure. SCC appears under a very specific combination of three conditions:

1. The use of materials that are susceptible to SCC
2. Tensile stress, either from structural loading or present as residual stresses from forming or welding operations during manufacture and installation; and
3. The presence of a specific aggressive environment.

These conditions were met for 304L (9% Ni, w/w) and 316L (12% Ni, w/w) U-bend specimens immersed in 0.8% NaCl and HCl (pH 2.2) at 141°C where SCC was observed after 30 days exposure (Asphahani, 1975). No SCC was observed in Alloy 825 with higher Ni content (43%, w/w). Higher resistance to SCC is linked to higher Ni content as shown in Fig. A2 where several Fe-Cr-Ni wires were exposed to a boiling 42% $MgCl_2$ solution. Alloys with more that 45-50% Ni (w/w) showed higher resistance to chloride cracking.

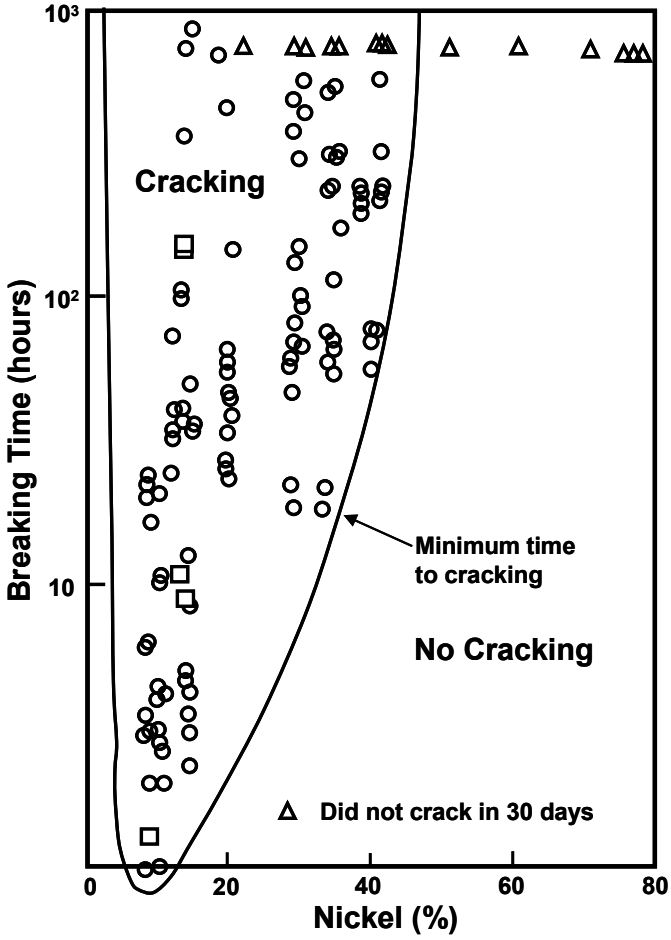

Figure A2: Susceptibility to SCC is higher for alloys with low Ni content (after Copson, 1959; see also Farmer et al., 1988b).

As discussed in Gdowski (1991), the high Ni and Mo contents in Alloy C-276 (and other alloys such as Alloy G) is suggested as the reason for its exceptional resistance to SCC in acidic NaCl, and in boiling 42% $MgCl_2$ solutions.

Pitting Resistance

Resistance to pitting is quantified as the difference E_c-E_{corr}, where E_c is the pitting potential and E_{corr} is the corrosion potential. The more positive the difference E_c-E_{corr} is, the more resistant the alloy is to pitting. Pitting of 304, 316 SS and Alloy 825 was studied in two different substitute ocean water environments at T = 80°C: 1) deaerated and 2) SO_2-saturated, using immersion tests, slow-scan (0.6 V/h) and fast scan (50 V/h) potentiodynamic techniques (Scarberry et al, 1979). These experiments show that Alloy 825 is the most resistant to pitting, see as an example Table A2 and Fig. A3 with results obtained using the slow-scan technique for the pitting potential, E_c, corrosion potential, E_{corr}, and resistance to pitting defined as E_c-E_{corr} in the SO_2-saturated seawater.

Table A2: Pitting potential E_c, corrosion potential E_{corr} and resistance to pitting given in units of E_c-E_{corr} for 304 SS, 361 SS, and Alloy 825 immersed in SO_2-saturated seawater at T = 80°C (after Scarberry et al, 1979).

Alloy	Test	E_c (mV)	E_{corr} (mV)	$E_c - E_{corr}$ (mV)	Immersion Test
304	SS	-268	-80 to -10	-148 to -258	Pitted
316	SS	-60	-140 to -80	20 to -80	Pitted
825	SS	70	-100 to -60	170 to 110	Pitted

Values reported in Table A2 appear in Fig. A3 for 304, 316, and 825 in the SO_2-saturated seawater case, showing that Alloy 825 has the largest difference E_c-E_{corr} = 140 mV, SCE and therefore the highest pitting resistance (see green bars).

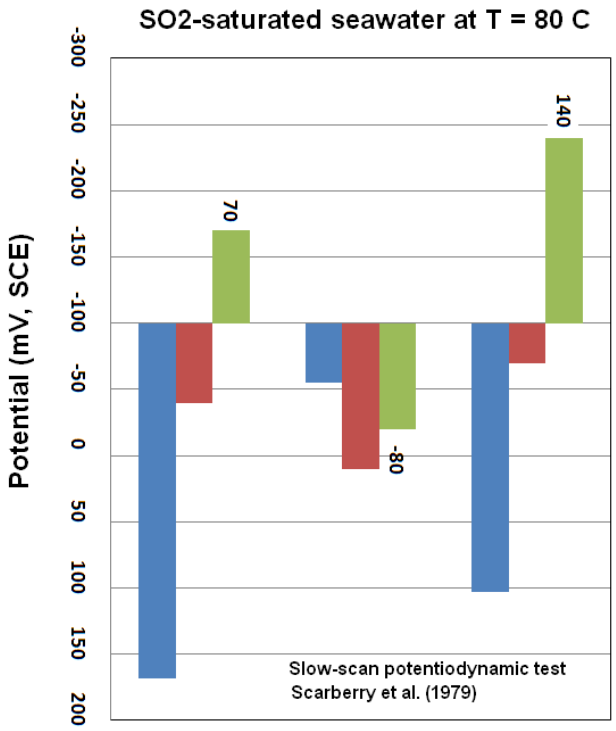

	Ec	Ecorr	Ec - Ecorr
Alloy 825	70	-80	140
316 SS	-60	-110	-30
304 SS	-268	-45	-203

Figure A3: Pitting potential E_c, corrosion potential E_{corr} and resistance to pitting given in units of E_c-E_{corr} for 304 SS, 361 SS, and Alloy 825 immersed in SO_2-saturated seawater at T = 80°C (Scarberry et al, 1979).

Effect of Mo Content on Pitting

Resistance to pitting corrosion is improved with increasing Mo content in the alloy. Note that 304 SS has no Mo, and both 316L and Alloy 825 have low Mo content (2- 3% Mo and 3% Mo (w/w), respectively). It is important to mention that other alloys with higher Mo content, like Alloys C-276, C-4, C-22, and Alloy 625 (16%, 14 - 17%, 12.5 - 14.5%, 9% w/w, respectively) are discussed in (Gdowski, 1991). An example of this behavior is given by Asphahani who conducted constant potential tests for 316 SS, Alloy 825, C-276, and Alloy 625 in a 3.8% $FeCl_3$ solution at 70°C (Asphahani, 1980). Figure A4 shows that localized corrosion decreases with larger Mo additions.

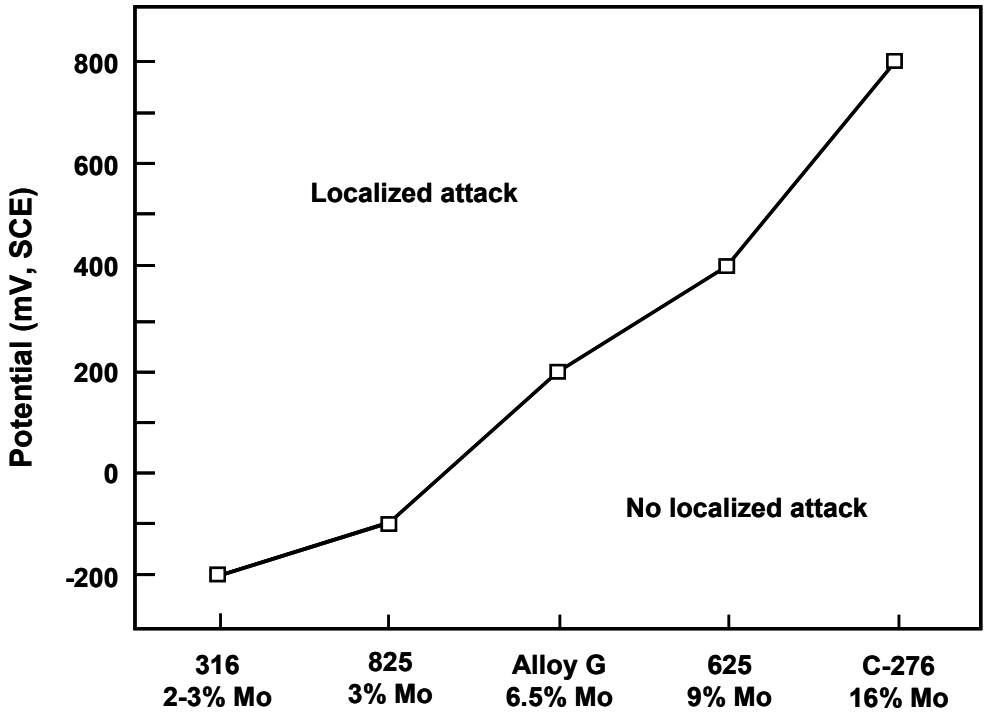

Figure A4: Localized corrosion decreases with larger Mo additions in constant potential tests performed for 316 SS, Alloy 825, C-276, and Alloy 625 in 3.8% $FeCl_3$ at 70°C (after Asphahani, 1980; see Farmer et al. 1988b).

Corrosion resistance of welded austenitic alloys

Welding problems that are specific to the candidate austenitic steels 304L, 316L, and Alloy 825 for HLRW are listed below (Taken from "Overview – Survey of Degradation Modes of Candidate Materials for HLRW Disposal Containers" (Farmer et al., 1988a):

General Comments on Welding

In the report "Fusion Welding" it is assumed that heating of the surfaces to be joined to $T > T_m$ and if necessary addition of weld filler metal.

Different zones are defined in a weld. Important to the discussion are FZ and HAZ. FZ corresponds to the fusion zone consisting of filler metal diluted by the surrounding base metal. There is a zone that follows the FZ where a partially melted zone exists. Beyond this region we find the HAZ, where all microstructural changes are restricted to the solid state.

The welding process is intrinsically linked to melting and re-solidification that translates into compositional and microstructural changes of the bulk metal. Examples of compositional changes are: 1) oxygen pick up during the welding and 2) solidification segregation. Oxygen pick up is reduced using, for example protective inert gas shielding atmospheres. Compositional segregation is responsible for hot cracking. It is generally accepted that the presence of ferrite in the weld metal helps prevent hot cracking.

Weld-Induced Sensitization

Heat affected zones (HAZ) of welds could be affected by $Cr_{23}C_6$ carbide precipitation. All 3 steels, i.e. 304L, 316L and Alloy 825, have chemical compositions that minimize sensitization. Type L steels (304L and 316L) have specific low carbon content (C < 0.03% w/w max.) in their chemical composition and Alloy 825 has Ti which promotes the formation of Ti carbides reducing the loss of Cr.

Sigma-Phase Formation and Corrosion of Weld Filler Metal

Phase stability of the weld metal is also important. The brittle sigma-phase has been found to form during welding of 304L and 316L. Alloy 825 will be stable but welding with Alloy 625, as filler, could lead to a duplex microstructure with coexisting austenite (γ) and ferrite (α).

It is very important to note that the available literature on weld cracking of Alloy 825 is very limited.

More details on the degradation consequences of welded austenitic steels are found in Volume 7: "Weldability of Austenitic Steels" (Strum, 1988). The author's survey underlines three areas of concern for the welded austenitic steels candidates, i.e.:

1) Resistance to corrosion
2) Hot cracking
3) Formation of intermetallic phases

Hot Cracking

In Volume 7 (Strum, 1988), four stages in hot cracking of stainless steels are mentioned:

1) Dendrite formation: solid dispersed in liquid in a continuous way – no crack possible
2) Interlocked dendrites: liquid circulating between dendrites – cracks refilled and healed
3) Critical solidification range: liquid volumes lack interconnections – cracks cannot be filled
4) Liquid completely solidifies – no cracking occurs

Several theories try to explain the reason why ferrite reduces or eliminates hot cracking. Ferrite is believed to act as an impurity sink that prevents GB cracking due to segregation of impurities. The weld metal compositions in both 304L and 316L are adjusted so as to assure a content of ~5% ferrite. This is not possible in Alloy 825 since it is purely austenitic. To prevent hot cracking in Alloy 825, a weld filler of a different composition is used (Alloy 625). The *DeLong* diagram (DeLong, 1960) shown in Fig. A5 is an example that shows the work reported in the literature to help design a fusion zone (FZ) in a weld with a given content of ferrite.

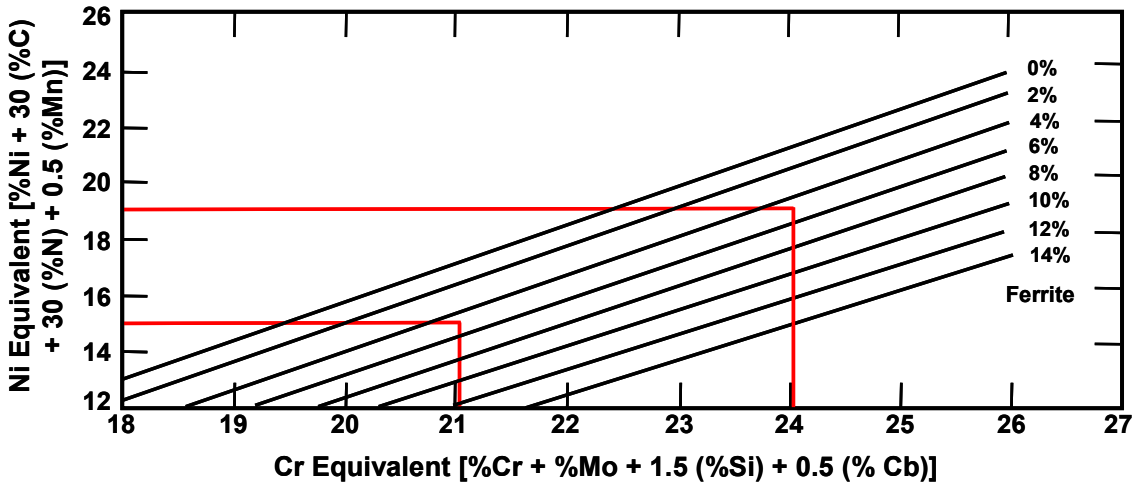

Figure A5: DeLong diagram (DeLong, 1960; see also Strum, 1988) defines weld chemical composition to obtain different amount of ferrite. Red lines indicate that Cr equivalent values needed to retain 5% ferrite in a typical 316L weld.

Equivalent compositional values are reported in Fig. A5. An example for 316L follows with:

Ni equivalent = Ni + 30 C + 30 N +0.5 Mn = 10 + 30 * 0.03 + 0.5 *2 = 14.9 ~ 15

where Cr, Mo, Si, and C_b (see Fig. A5) are the element chemical composition in wt% (w/w). Red lines in the graph indicate typical Ni equivalent values for 316L equal to 19 and 15, for 316L containing 10% (w/w) or 14% (w/w), respectively and those of the corresponding Cr equivalent needed to obtain a weld that retains 5% ferrite.

It is important to note that a survey (Strum, 1988) on weld cracking of Alloy 825, mentions that Alloy 825 is known to hot crack and adds that no published data is available in the literature on hot cracking effects in Alloy 825. The authors (Strum, 1988) recommend studies to be performed to get a full understanding of hot cracking causes in Alloy 825. They also suggest *friction welding* as a possible means of joining that does not involve melting.

Corrosion of welds in austenitic steel candidates

Sensitization is the most common cause of weld-related intergranular corrosion in austenitic alloys. Sensitization is the precipitation of metal carbides, $M_{23}C_6$ usually Cr carbides, on the GB which mirrors a depletion of Cr in the region near the GB with a deleterious impact on the materials corrosion resistance. Among the theories that attempt to explain intergranular corrosion of sensitized austenitic steels we should consider the "Cr depletion theory" from (Bain, 1933). The theory assumes:

1) Cr in the bulk material (13 - 15%, w/w) is sufficient to provide a protective passive film
2) Cr in the region near to a carbide precipitate has a Cr content lower than that required for passivation.

Precipitation of Cr-rich carbides occurs during sensitization heat treatments. $M_{23}C_6$ carbide precipitation in welds takes place in the temperature range of 550°C to 800°C. (Note: the M in $M_{23}C_6$ can be Cr or Fe or Mo). $M_{23}C_6$ carbides have a tendency to

precipitate along GB. Precipitation of $Cr_{23}C_6$ carbides at GB is at the origin of the Cr-depletion of the surrounding area, to a point that is below the critical level needed for passivation, as shown in Fig. A6, see also Povich (1978):

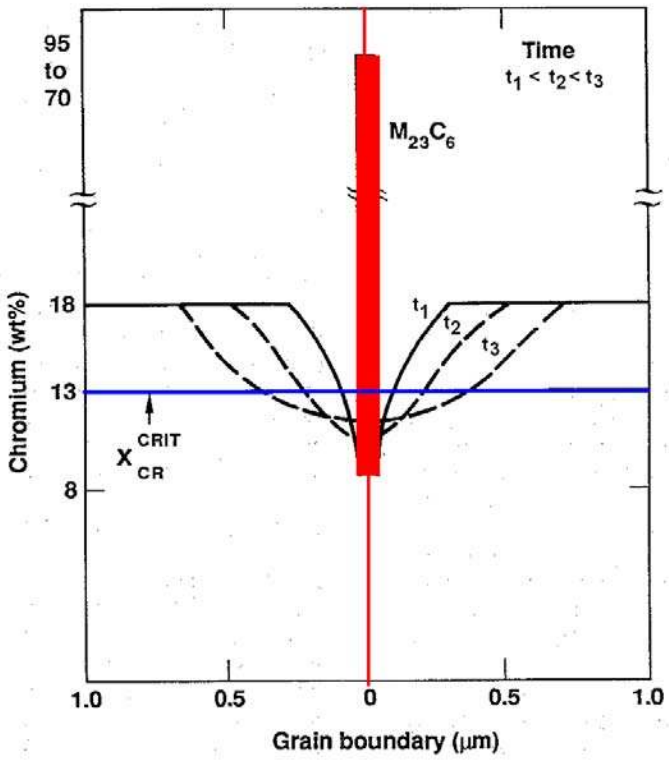

Figure A6: Cr content along the GB region is schematically represented at different times (t1 < t2 < t3), underlying the fact that the region depleted in Cr is growing as a function of time (after Povich, 1978; see also Strum, 1988). A Cr concentration of ~13% (w/w) is assumed to be the critical Cr concentration needed for passivation to occur (indicated by the blue line).

Long Storage Times and Low-Temperature Sensitization (LTS)

Low-temperature sensitization was of major interest to the Nevada Nuclear Waste Storage Investigations (NNSWI) Project. Both 304L and 316L are reported to be susceptible of LTS. LTS is a nucleation and growth phenomenon, where carbides nucleate during the sensitization heat treatment and then grow while exposed to temperatures T ~400^{o}C for long time. Significant increase in GB carbides size in a SS weld is found after 10 days LTS at 400^{o}C, see Fig. A7 (Povich, 1978).

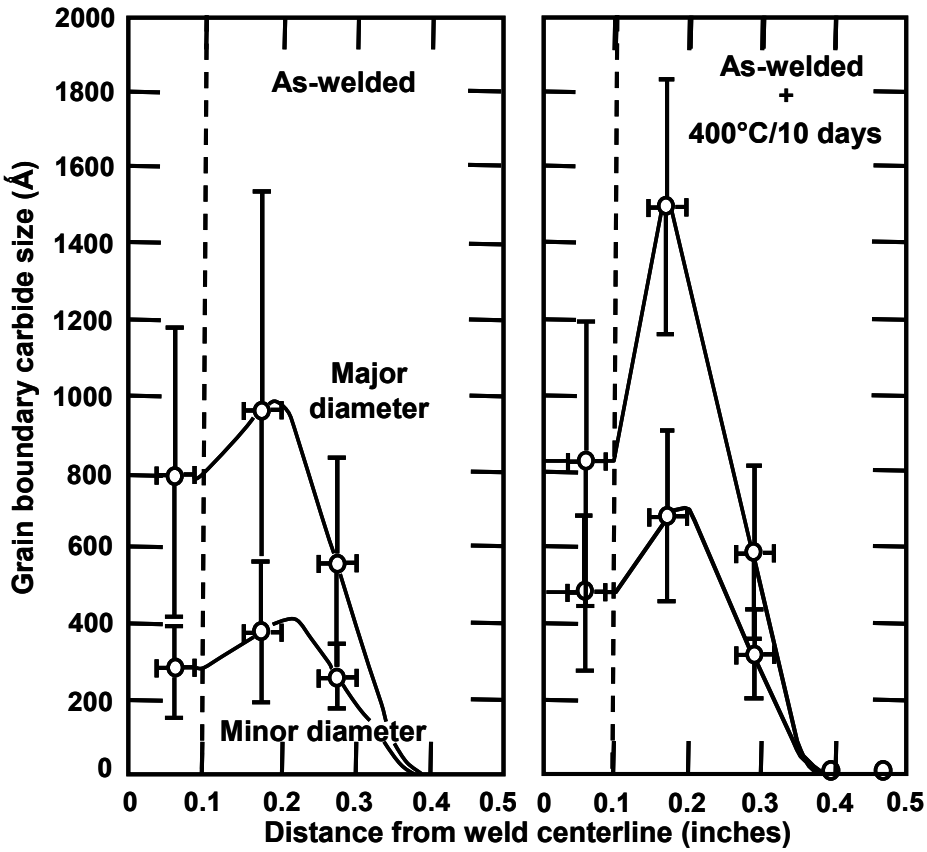

Figure A7: Consequences of Low-temperature sensitization (LTS) on the carbide size; (left) before LTS heat treatment, (right) after LTS heat treatment at 400°C for 10 days (after Povich, 1978).

Difficulties in the evaluation of the consequences of LTS are linked to the short-term exposures and the prediction of long-term growth. Also, the authors underline that there is data on the loss of corrosion resistance due to LTS in 304L SS. No data is available for 316L. Even less information is available on LTS of Alloy 825; it would appear, however, that the high-nickel alloys are not subject to LTS.

Hydrogen Embrittlement in Austenitic Steels

No consensus is reported in the literature survey (Farmer et al. 1988a, Gdowski and Bullen, 1988b) on the hydrogen embrittlement (HE) mechanism in austenitic steels. Experiments in the literature survey (Gdowski and Bullen, 1988b) show that hydrogen embrittlement occurs in the three candidate austenitic steels: 304L, 316L and Alloy 825. It is important to note that there is a [quote] “definite lack of literature” on the effects of hydrogen in Alloy 825.

Hydrogen Embrittlement Effects

Hydrogen and other corrosive species have been shown to cause sensitized alloys to stress corrode more easily than the unsensitized alloys. Alloys with low carbon content, such as 304L (C = 0.03% w/w max), 316L (C = 0.03% w/w max) and Alloy 825 (C =

0.05% w/w max) have enhanced resistance to sensitization that should be reflected in higher HE resistance. Briant (1981) suggests that resistance to HE in austenitic steels is linked to martensitic formation. In 1954, Angel defines the temperature for inducing austenite to martensite transformation, M_d, in terms of the elemental composition of the alloy given by Angel (1954):

$$M_d\,(C) = 413 - 462\,(C+N) - 9.2\,Si - 8.1\,Mn - 13.7\,Cr - 9.5\,Ni - 18.5\,Mo$$

According to this, 316L SS with a low M_d should be a more stable alloy against martensite transformation, more stable than 304L SS and Alloy 825, and therefore more resistant to HE.

Degradation of Mechanical Properties Due to Hydrogen Embrittlement

Low concentrations of H (~30 appm) have been shown to degrade primarily the ductility of the material, i.e. the material becomes more brittle; shown in Fig. A8 by a reduction in the elongation (Graver, 1984). The degradation of elongation is larger in 304 SS (red line) than in 316 SS (blue line) or Alloy 825 (black line). In the experiment, H was cathodically charged for periods of 2 to 32 days.

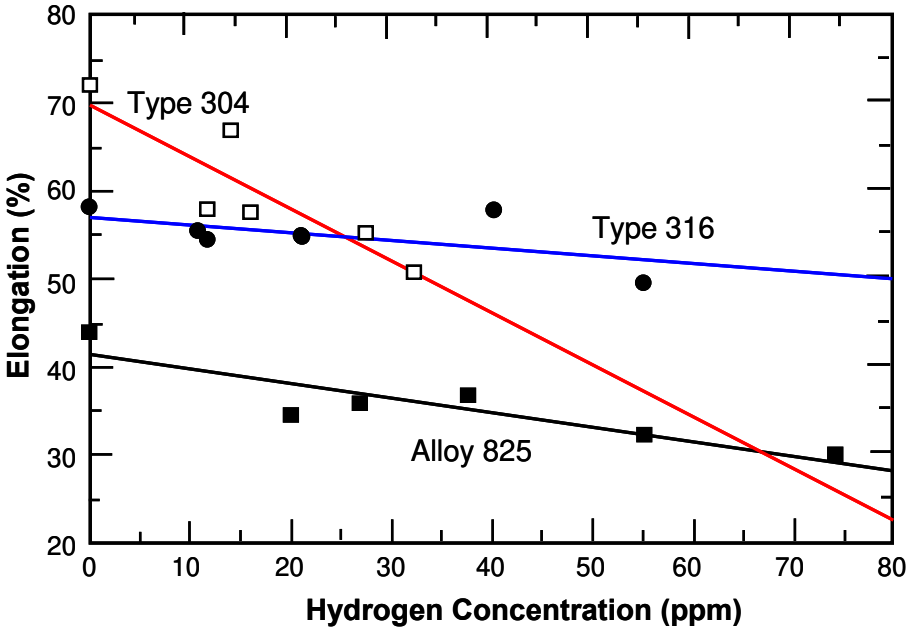

Figure A8: Large reduction in elongation in 304 SS is found at relative low (~30 appm) amounts of hydrogen (red line). 316 SS (blue) and Alloy 825 (black) have a similar dependence, with absolute values always lower for Alloy 825 than for 316 SS (after Graver, 1984).

Yield strength (YS) and tensile strength (UTS) also show degradation as a function of H concentration in both 304 SS and 316 SS as shown in Fig. A9.

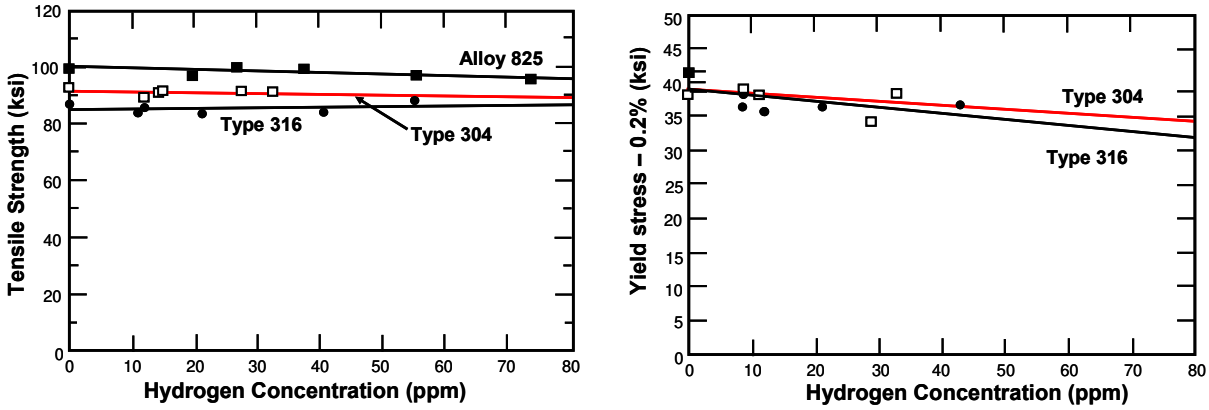

Figure A9: Degradation of mechanical properties induced by hydrogen charging in: a) UTS in 304 SS, 316 SS and Alloy 825 (left) and b) 0.2%YS in 304SS and 316 SS (right) (after Graver, 1984; see also Gdowski and Bullen, 1988).

It has been shown experimentally that 304L steel loss of elongation is recovered after aging at 100°C. This is shown in Fig. A10, where the percent-elongation is reported as a function of aging time.

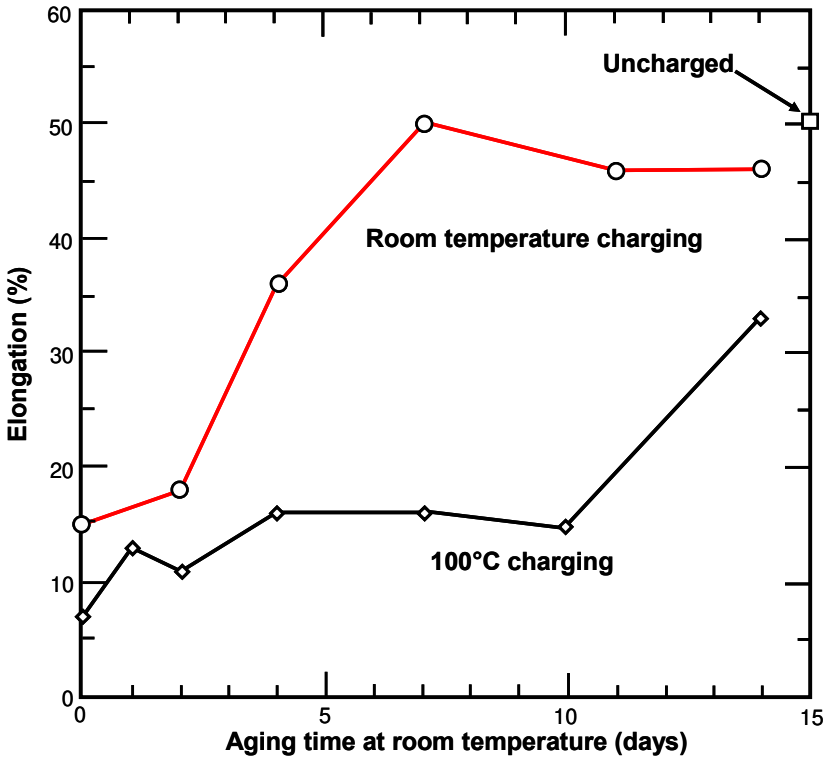

Figure A10: Loss of ductility is recovered after aging at 100°C in both 304L SS specimens (after Holzworth, 1969; Gdowski and Bullen, 1988), a) specimen charged with H at RT (red line) and b) specimen charged with H at 100°C (black line).

In the experiment shown above (Holzworth, 1969), the steel was first charged at two temperatures (RT and 100°C) and then the percent elongation was measured as a function of aging time (days). The charging with H was performed in a non-hydrogen atmosphere, i.e. charging conditions 1N H_2SO_2 and 0.1 A/cm^2. Both specimens show

elongation recover after aging for 15 days. A specimen charged at RT shows a faster recovery than a specimen charged at 100°C. A specimen not charged with H shows ~50% elongation after aged for 15 days at 100°C. The specimen charged at RT reaches ~47% elongation after 15 days as compared to ~32% for the specimen charged at 100°C.

It is important to examine hydrogen diffusivity (D) and solubility (S) in these materials. Note that no properties are reported in the degradation mode survey for Alloy 825 diffusivity or solubility – they are assumed to be those of nickel in the discussion. Also, no data for 316 SS diffusivity or solubility was reported. D and S for 316 SS are assumed to be similar to that of 304 SS for which data is available (Perng, 1986) that shows low diffusivity and low solubility of hydrogen in this steel. At temperatures relevant to repository environment, D and S are small in magnitude, e.g. at T = 25°C. Hydrogen diffusivity in 304 SS is $D = 4 \times 10^{-12}$ cm^2/s, while at T =275°C diffusivity reaches $D = 7 \times 10^{-8}$ cm^2/s. Both diffusivity and solubility in 304 SS increase as temperature increases (Arrhenius behavior). Hydrogen solubility in 304 SS is ~100 – 300 ppm for the same temperature range.

Phase Stability

Alloy 825 (*Incoloy*) is an austenitic Ni-Fe-Cr alloy with additions of Mo, Cu, and Ti. Alloy 825 phase stability is better than that of 304L and 316L SS (Bullen, 1988). Figure A11 shows that 304L and 316L SS are closer to the α+γ phase region while Alloy 825 is well within the γ-phase (Marshall, 1984; Bullen and Gdowski, 1988).

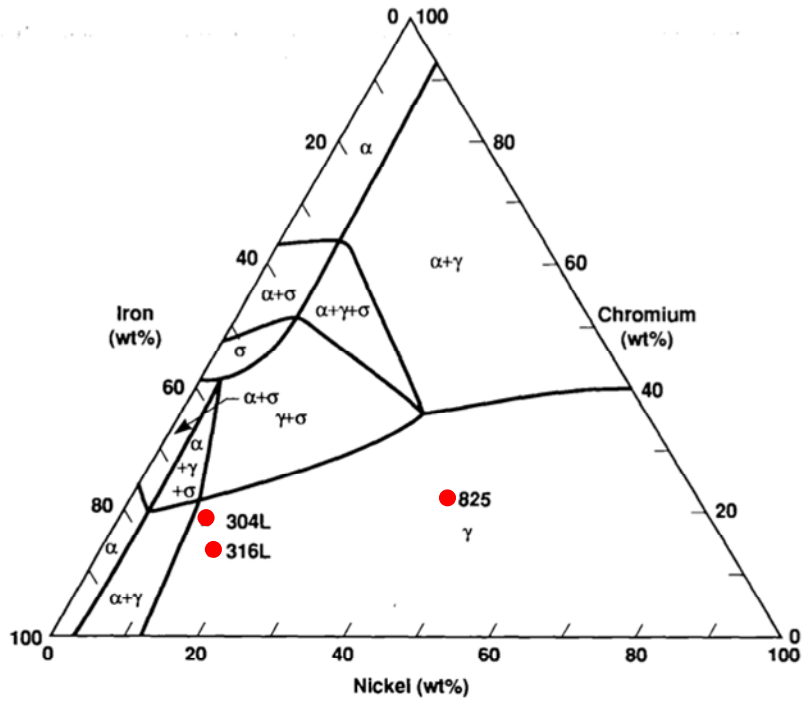

Figure A11: Fe-Cr-Ni equilibrium phase diagram at 650°C. Note: red stars help locate 304L, 316L and Alloy 825 (after Marshall, 1984; Bullen and Gdowski, 1988).

Martensitic transformations have not been observed in Alloy 825. Martensitic transformations occur in 304L and 316L SS. Also, the sigma-phase has been observed in 316L promoted by the presence of Si. The formation of a sigma-phase can result in

significant degradation of the 316L mechanical properties. Also, GB attack could result from the $M_{23}C_6$ carbide precipitation in both 316L and 304L SS.

A heat treatment is proposed that enhances Alloy 825 resistance to sensitization. Sensitization involves the precipitation of Cr-rich $M_{23}C_6$ carbides at the GB that in turn causes a depletion of Cr in the adjacent region. Since Cr is responsible for the corrosion resistance of these alloys via the formation of thin uniform Cr-oxide layers on the surface, the loss of Cr in the matrix translates into localized intergranular attack that can occur when the material is exposed to corrosive service conditions. A stabilization heat treatment (annealing at 970°C to 925°C for 1 hr) enhances Alloy 825's resistance to sensitization. Alloy 825 contains Ti, which is a strong 'getter' of carbon. Ti removes the carbon from solution and prevents alloy additions (such as Cr) from forming carbides. The heat treatment is specified to ensure that Ti has consumed the carbon.

Among the copper alloys, CDA 102 (OFHC Cu) is ranked as the one with the best phase stability followed by CDA 715 and CDA 613. CDA 102 is a single-phase material (CDA 102 is essentially pure Cu). CDA 715 (Cu with 30% Ni, w/w) and CDA 613 (Cu with 6.8% Al, w/w) are solution-hardened materials that offer improved mechanical and corrosion performance. The review study performed in 1988 (Farmer et al., 1988a) shows that these materials would remain single-phased to at least 300°C, see the case of CDA 613 in Fig. A12.

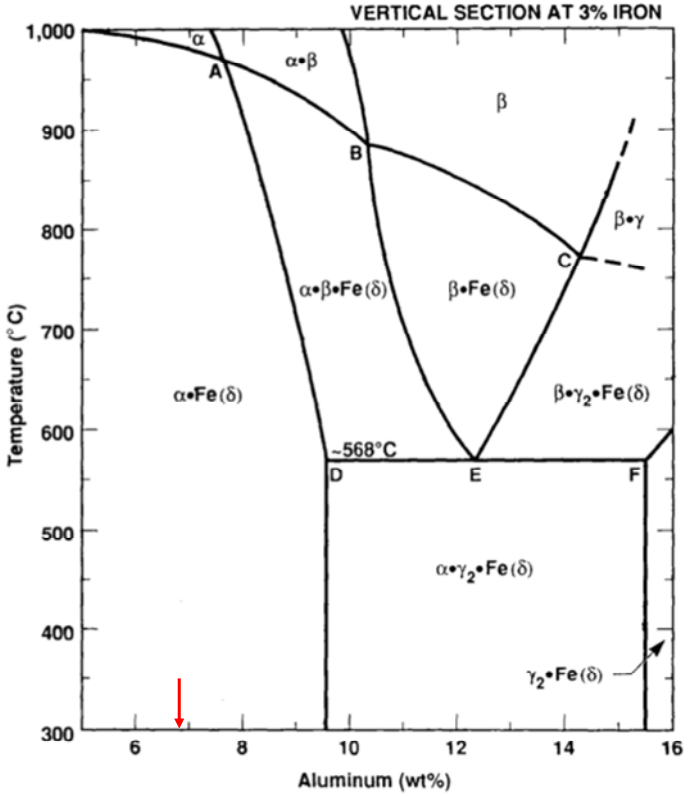

Figure A12: Cu-Al-3%Fe phase diagram showing that CDA 613 with a composition of Cu (6.8% Al, w/w – red arrow) is single-phased (α-phase) with iron precipitates [Fe(δ)] (after West , 1982; Farmer et al., 1988a; Bullen and Gdowski, 1988).

Migration and precipitation of Fe in CDA 715 and CDA 613 and of Sn in CDA 613 may cause material degradation. Precipitates of Fe in CDA 613 may grow in size over extended periods of time. Also, it is believed that Fe_3Al is formed in CDA 613, which would mean that Fe diffusion would be less than that of free Fe in Cu.

Phase stability in Ni-Cr-Mo alloys

Using Calphad methodology, property diagrams were calculated for several Ni-Cr-Mo based alloys at their nominal alloy compositions (Turchi et al., 2006). These diagrams display the phase fraction of each stable phase as a function of temperature. These alloys (at equilibrium at low temperature) exhibit part of the fcc matrix, long-range order (LRO) of Pt_2Mo-type indicated by the formation of oP6 phase, complex Frank-Kasper phases (P and σ phases), carbides and silicides at low phase fraction. Figure A13 shows this happening in C-4 and C-276 Alloys and Fig. A15 below shows similar findings in C-22. (Note that the authors also show that W has a positive effect of destabilizing the oP6 phase).

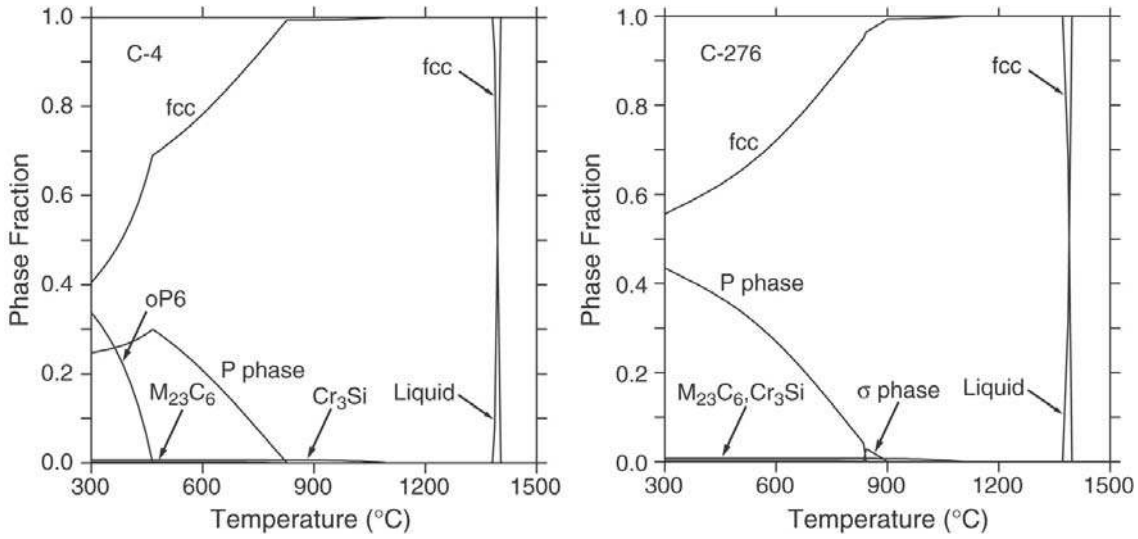

Figure A13: Phase fraction diagram for a) C-4 (left) and C-276 alloys (right) indicating that at equilibrium and at low temperatures oP6 LRO phase, P and sigma phases are present (after Turchi et al., 2006).

C-4

In the case of Alloy C-4, Turchi (2006) shows that the main phases forming, besides the fcc matrix, are the P- and oP6-phases, and at very low phase fraction the $M_{23}C_6$ and the A15 Cr_3Si-type phases; see Fig. A13a (left). The relatively low content in Cr in this alloy excludes the formation of the σ-phase.

C-276

In the case of Alloy C-276, as in the case of alloy C-4, Turchi (2006) shows that the low content in Cr and Mo significantly reduces the formation of the σ-phase and prevents the formation of the oP6-phase; see Fig. A13b (right). Because of the presence of C and Si, the A15 of Cr_3Si-type and $M_{23}C_6$ are found in this alloy as in the C-4 alloy.

Alloy C-22

Turchi (2006) discusses a comparison of predicted results and experimental findings for Alloy 22.

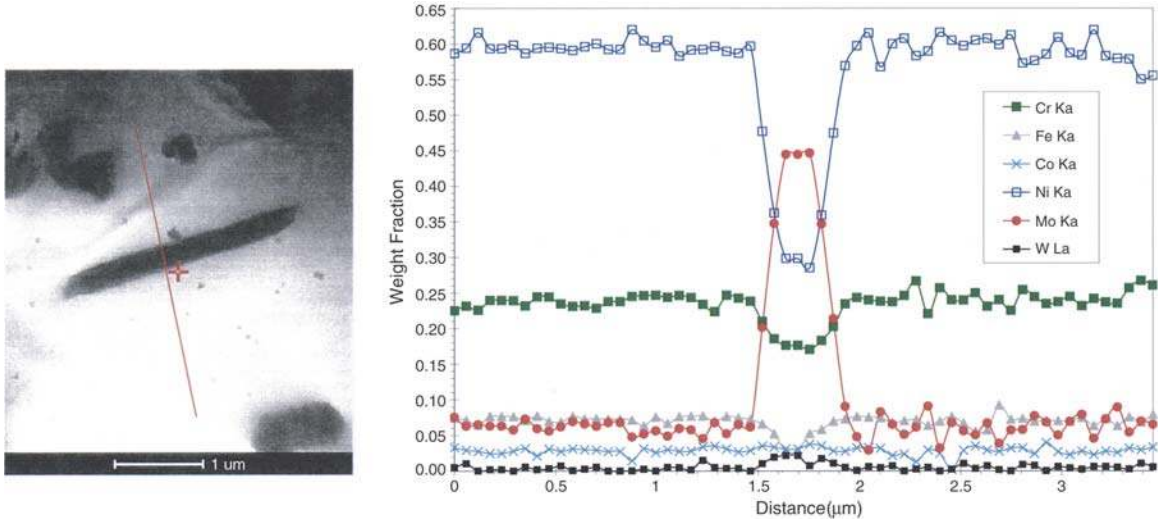

Figure A14: Platelet of P-phase precipitate in Alloy 22 annealed for 22 h at 704°C a) Micrograph (left) and b) EDX Experiment (right) (Shen, 2000).

The authors report a micrograph (see Fig. A14a, left) that shows a platelet of P-phase precipitate in a fcc matrix of Alloy C-22 annealed at 704°C for 22 hours (Shen, 2000). EDX spectroscopy experiment across the red straight line in the micrograph shows a decrease in Ni content in the platelet (open blue squares in the weight fraction vs. distance plot in Fig. A14b, right), increase in Mo content (red circles) in the platelet. Also they report some evidence of decrease in Cr (green line) and Fe (open triangles) and a slight increase in W (small black solid squares at the bottom of the plot). There is no evidence of solute depletion in the zone surrounding the platelet.

Property diagrams derived for Alloy 22 using *Calphad* methodology are shown in Fig. A15. The diagram on the left corresponds to phase fraction as a function of temperature; with the straight line in the figures indicating the annealing temperature in the experiment, i.e. T =704°C. The diagram shows that at this temperature P-phase forms in the alloy with a phase fraction of ~20%.

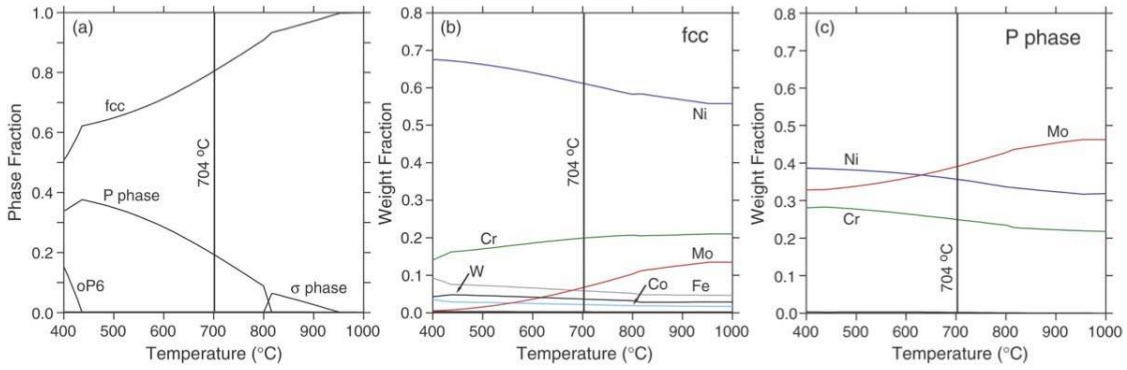

Figure A15: Phase fraction diagram for Alloy 22 as a function of temperature (left). Weight fractions of elements in Alloy 22 as a function of temperature (b) in fcc phase (center) and b) in P phase (right) (after Turchi et al., 2006).

Also shown in Figure A15 are the weight fractions for Alloy 22 in fcc phase (center) and in P phase (right). These diagrams indicate that in the fcc phase at T =704°C, the composition of the alloy is that of the starting fcc condition while in the P phase, there is a larger weight fraction of Mo than Ni and Cr indicating a fair agreement with the experimental evidence.

Kinetics of Phase Transformations in Ni-Cr-Mo Alloys

The ordering transformation that takes place in these Ni–Cr–Mo based alloys has been linked to an increased susceptibility to SCC and hydrogen embrittlement. In 2007, the kinetics of phase transformations in Ni-Cr-Mo alloys was investigated (Turchi et al., 2007) aimed at predicting the rate at which LRO is occurring in Alloy 22 under repository conditions. The authors conclude that the diffusion kinetics in the temperature range where the formation of the LRO phase of Ni_2Cr-type occurs is extremely slow. It is therefore very unlikely that the ordered phase will form under repository conditions, i.e., below 200°C, even for as long as 100,000 years.

Using the *Calphad*/*Dictra* methodology, the authors determine the kinetics of transformation in Alloy 22 from a fcc matrix to the oP6-ordered phase, fcc to P, and fcc to σ-phase, see Fig. A16. The temperature-time transformation (TTT) diagram shows the critical order–disorder temperature is 596°C (left), the transformation temperature is about 836°C and 727°C for P- and σ-phase, respectively.

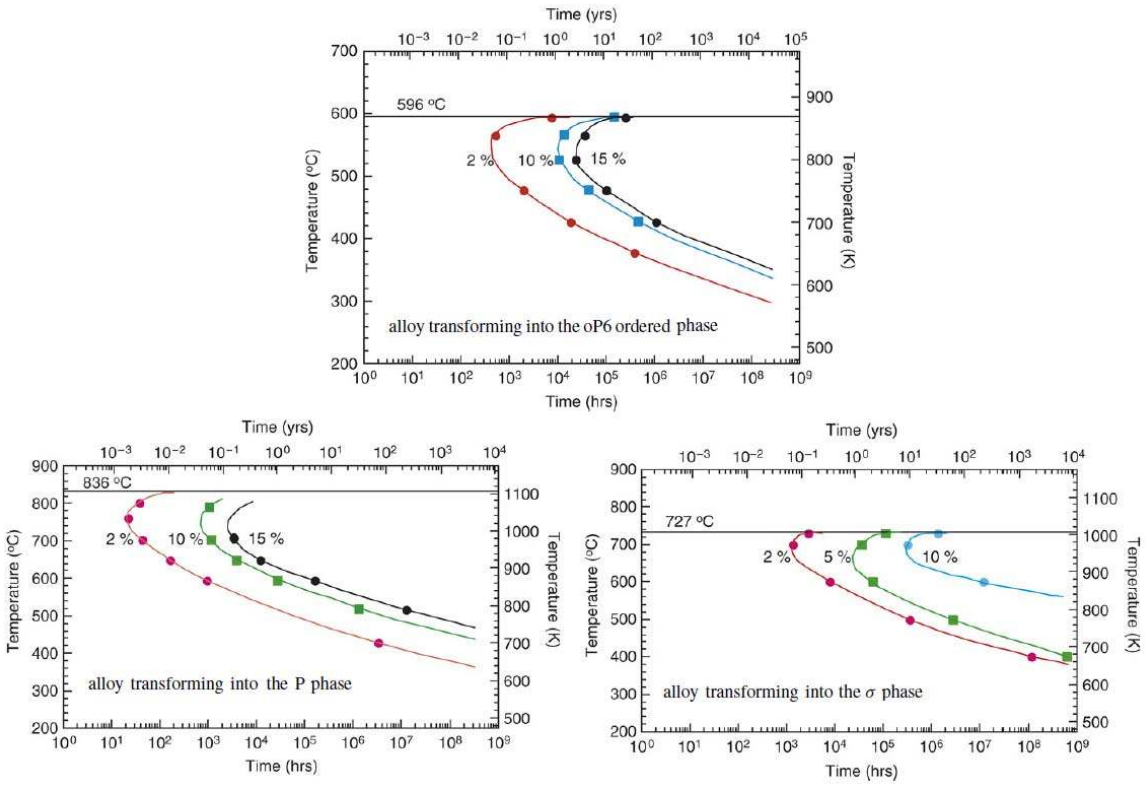

Figure A16: Kinetics of transformations from fcc to oP6-phase (top) and from fcc to P (bottom left) and from fcc to σ-phase (bottom right) in Alloy 22 (after Turchi et al., 2006).

Simulation results and volume-fraction measurements (Torres, 2003) are shown in Fig. A17 at two temperatures T = 700°C and T =750°C. Simulations and measurements show agreement and indicate that the phase transformation occurs in reality at a slower pace than predicted.

Also, experimental findings from Karmazin (1994) indicated in Fig. A18 by blue squares and results predicted with *Dictra* for a Ni-Cr binary alloy (blue circles corresponding to the label 10% Ni_2Cr) are shown together with isothermal TTT diagrams for Alloy 22 transformation in P-phase (black lines) and qualitative observations performed at LLNL (Torres, 2003), see labels on GB coverage, LRO and bulk precipitation. Again good compatibility was found between experiments and predictions.

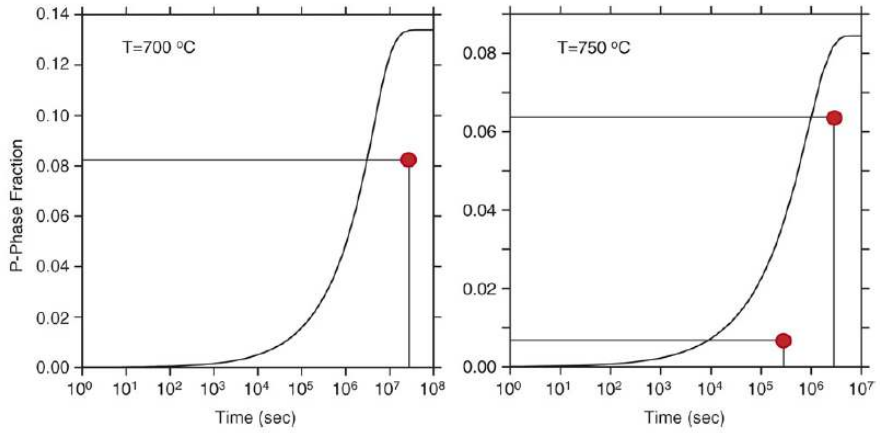

Figure A17: Volume fraction measurements of fcc to P transformation in Alloys 22 (Torres 2003) as compared to predicted results (after Turchi et al., 2007)

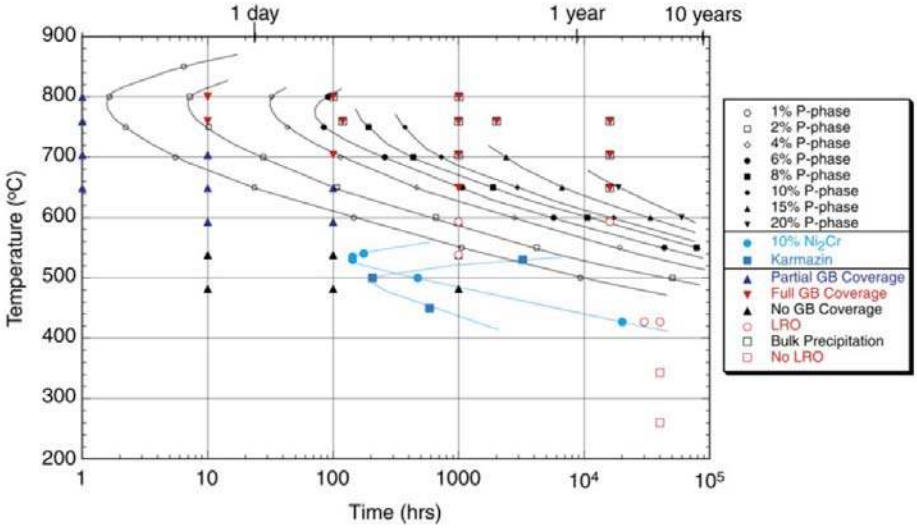

Figure A18: Isothermal TTT diagram a) calculated for a binary Ni–Cr alloy with a 10% transformation of the fcc matrix in the oP6-ordered phase of Ni_2Cr-type; see lower curves describing the prediction (blue circles) and the results extracted from the experimental work of Karmazin (blue squares) (after Karmazin et al., 1994) and b) calculated for a fcc-based matrix of a surrogate of Alloy 22 transforming into the P-phase (black lines), with transformation from 1% (open circles) to 20% (down triangles).

6.8 Appendix B

Waste Package Design Criteria and Waste Environment at Yucca Mountain

When the degradation mode surveys were written in the late 1980's, a HLRW container was required to maintain mechanical integrity for ~50 years after emplacement to allow retrieval in the pre-closure phase of repository operation. Waste packages were required to provide complete containment for a period of ~300 to 1,000 years. However, with the evolution of 10CFR60 [1] to 10CFR 63 [2], specific requirements for barriers, including waste package post-closure performance, were replaced with requirements for a combination of natural and engineered barriers, and with overall performance of the repository being subject to quantitative requirements. As part of repository development, DOE designed the waste packages for extremely long term performance, hundreds of thousands of years in the repository environment.

After a few years in the repository, containers will face T_{max} ~250^{o}C, and high γ-radiation. Such γ-radiation will promote radiolytic decomposition of the moist air near the container surfaces. Hydrogen has the potential to alter the metallurgical behavior of the container material. (Note: After ~100 years, the temperature of the container decays to ~150^{o}C).

[1] DOE 10 CFR Part 60: Disposal of High-Level Radioactive Wastes in Geologic Repositories.

[2] DOE 10 CFR Part 63: Disposal of High-Level Radioactive Wastes in Geologic Repositories at Yucca Mountain, NV.

6.9 Appendix C

Mechanical Properties of Several Austenitic Steels at Room Temperature

Table C1: Mechanical properties of the candidate austenitic alloys at room temperature [1,2]

Material	UTS [MPa]	0.2%YS [MPa]	Elongation [%]
304 SS	655	241	65
316 SS	586	255	65
Alloy 825	693	301	43

[1] Metals Handbook, Volume 2, Properties and Selection: Nonferrous Alloys and Pure Metals, 9th ed. American Society for Metals, Metals Park, Ohio, 237. (1979)

[2] Source Book on Industrial Alloy and Engineering Data, American Society for Metals, Metals Park, Ohio, 185-207, 219-223. (1978)

7. Distribution List

1	MS0836	H. K. Moffat	1516
1	MS0372	J. G. 'Lupe' Arguello Jr.	1525
1	MS0748	Jon C. Helton	1545
1	MS0888	D. G. Enos	1825
1	MS1033	Cliff Hansen	6112
1	MS0736	Evaristo (Tito) Bonano	6220
1	MS0779	M. D. Siegel	6222
1	MS0779	Yifeng Wang	6222
8	MS0779	Carlos F. Jové Colón	6222
1	MS0779	Kevin McMahon	6222
1	MS1369	Ernest Hardin	6224
1	MS1369	Geoffrey A. Freeze	6224
1	MS1369	Peter N. Swift	6224
1	MS1370	Robert J. MacKinnon	6224
1	MS1369	Joon Lee	6224
1	MS1369	Paul Mariner	6224
1	MS1369	C. R. Bryan	6225
1	MS1369	Bill W. Arnold	6225
1	MS1369	Teklu Hadgu	6225
1	MS0744	I. Khalil	6233
1	MS0747	Ken B. Sorenson	6223
1	MS0718	Ruth F. Weiner	6231
1	MS0754	Patrick V. Brady	6910
1	MS0751	Frank Hansen	6914
1	MS0751	Thomas Dewers	6914
1	MS0754	James L. Krumhansl	6915
1	MS0754	Mark Rigali	6915
1	MS0899	Technical Library	9536 (electronic copy)